May - August 1996
Volume II Number II

ISSN 0859 144X

THE ASEAN JOURNAL OF RADIOLOGY

Published by The Radiological Society and the College of Radiologists of Thailand, Bangkok, Thailand

Supported through an educational grant from

BRACCO
INTERNATIONAL

Have you really considered the importance of open MRI on patient comfort?

- for your patients who will return to you?
- for your technicians, who will improve throughput?
- for your radiologists, who will not have to read patient movement artifacts?
- for your administrator, who will see better return on investment?

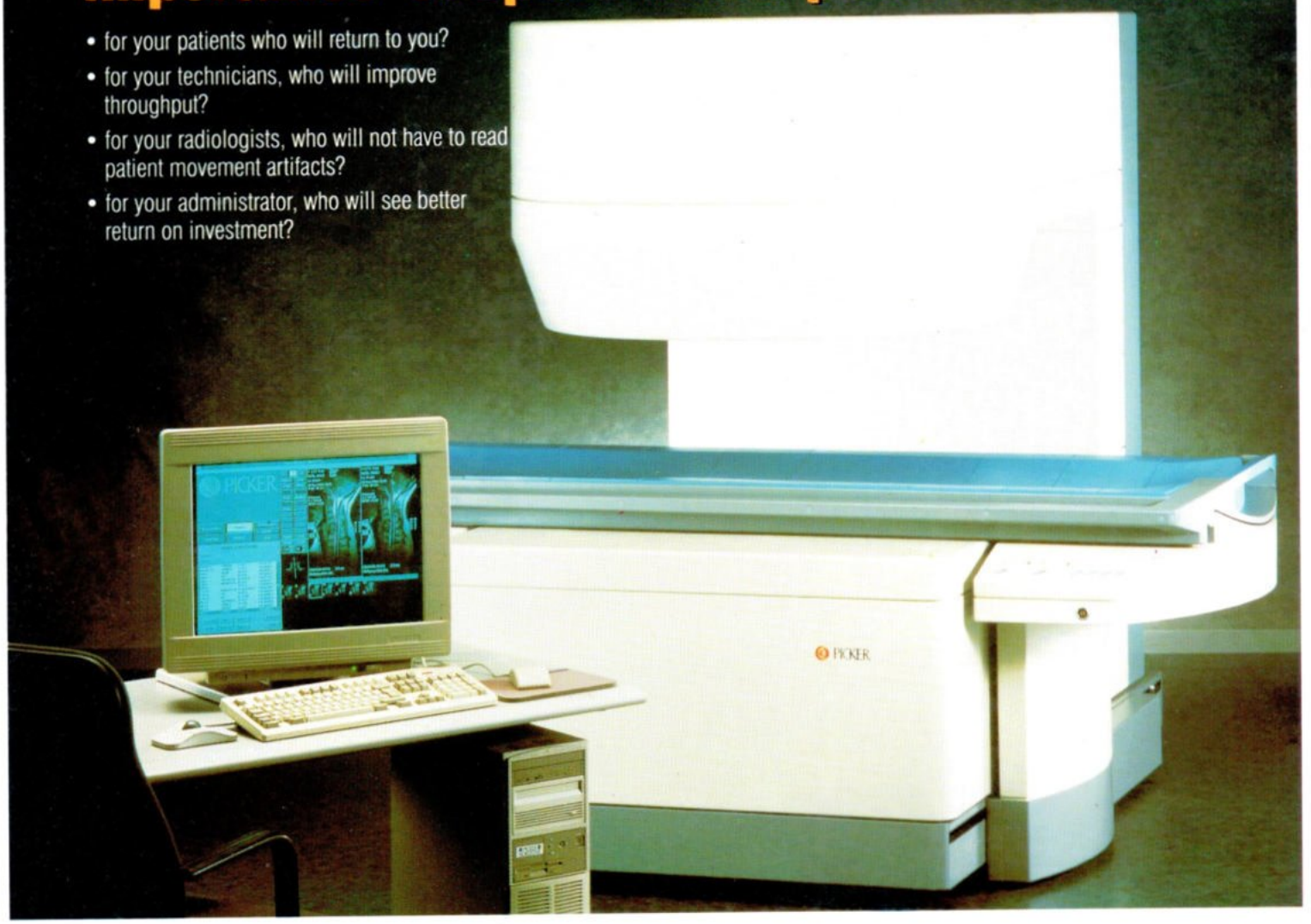

The new OUTLOOK™ in MRI...

Picker's new, really open, state-of-the-art, whole body MRI scanner.

Features include: 46 cm free vertical opening, freedom of patient handling in horizontal plane, easy access to the patient, CP phased array coils, powerful and fast gradients, high quality MR angio with MT, integrated MPR and MIP, and very fast 233 MHz Digital AlphaStation™ 400 console. The most modern open MRI scanner available.

OUTLOOK™ is Picker's newest addition to its impressive line of MRI scanners.
For more information, please contact your nearest Picker representative.

PICKER

Picker International, Inc.
World Headquarters
595 Miner Road
Cleveland, Ohio 44143
U.S.A.
Tel: 1-216-473-3000
Fax:1-216-473-2413

Picker International, France
GEC S.A.
2, rue Henri Bergson
92600 Asnières
France
Tel: 33-1-46-13-52-54
Fax:33-1-47-33-11-31

Picker International GmbH
Robert-Bosch-Strasse 11
6238 Hofheim 4 Wallau
Germany
Tel: 49-6122-9140
Fax: 49-6122-8536

Picker International Canada, Inc.
7956 Torbram Road
Brampton, Ontario L6T 5A2
Canada
Tel: 1-950-791-1494
Fax: 1-950-791-7297

Picker International, Inc.
Room 1303
C C Wu Building
302-308 Hennessy Road
G.P.O. Box 15
Wanchai, Hong Kong
Tel: 852-892-1238
Fax: 852-838-4302

Picker International Latin America
110 Merrick Way
Suite 3A
Coral Gables, Florida,
33134 U.S.A.
Tel: 1-305-444-9993
Fax: 1-305-445-0545

Picker International GmbH
Moseliggasse 1
4th floor. A-1232 Vienna
Austria
Tel: (43) 1-66107
Fax: (43) 1-6610760

Picker International Ltd.
Kemble House
Kemble Street
London, WC2B 4 AJ
England
Tel: +44-71-489-4044
Fax: +44-71-489-4043

Picker Singapore
101 Thomson Road,
#10-01 United Square,
Singapore 1130
Tel. (65) 250-9866
Fax. (65) 254-0020

Picker International GmbH
European/Middle
East Distribution,
Headquarters
Robert-Bosch-Str. 11.
65719 Hofheim
Tel: +49-6122-9140
Fax: +49-6122-914-460

Picker Italia SpA
Vicolo Carloni, 4
I-22055 Merate (Lecco)
Tel: (39)39-9901169
Fax: (39)39-9901016

040398

May - August 1996

Volume II Number II

ISSN 0859 144X

THE ASEAN JOURNAL OF RADIOLOGY

Published by The Radiological Society and the College of Radiologists of Thailand, Bangkok, Thailand

Supported through an educational grant from

BRACCO INTERNATIONAL

1. The AAR Journal of Radiology publishes the papers on Radiological Sciences, such as research work, review articles, case reports, innovations in Medical Sciences related to all branches of Radiology, and letters to the editor. The aforementioned materials can be written in English only.

2. The authors have to submit 2 copies of the manuscript and a diskette: **to Prof. Dr. Kawee Tungsubutra,** 318 Kaweevej Hospital, Tarksin Road, Dhonburi, Bangkok 10600, Thailand.
or to the Associate Editors at the Radiological Society of Malaysia, Indonesia, Phillippine, Singapore and Brunei. The names and addresses of the Associate Editors in each country were published in the front page of this Journal.

3. The original copy to be submitted must be typed in a double space on one side of the page of 8″ × 11″ paper.

4. The format of the article must include:

a. Title page and address of the author (s)

b. Abstract

c. Introduction (Background)

d. Material and Method

e. Results and discussion (Tables and Illustrations)

f. Acknowledgement (if any)

g. References (Follow the Vancouver style developed by ICMJE)

5. We will provide 25 copies of reprints for the author (s) who submit (s) and article for publication in the AAR Journal.

6. The illustrations and tables must be clearly prepared with legends in English as they are the art works to be reproduced.

7. The authors are responsible for the contents of the article as to its facts and findings.

8. Ethics.

Paper reporting studies which might be interpreted as human experimentation (e.g. controlled trials) should conform to the standards of the Declaration of Helsinki (see British Medical Journal 1964:2:177) and should indicate that approval that such studies may proceed has been granted by the local or hospital Ethics Committee.

When reporting experiments on animals indicate whether the institution's or the National Research Council's guide for, or any national law on, the care and use of laboratory animals was followed.

Message from

Prof. Dr. Kawee Tungsubutra

Editor-in-Chief, The Asean Journal of Radiology.

This is the second number of Volume II of the Asean Journal of Radiology. (Asean J.R.) In this issue we have a variety of articles in Diagnostic Radiology : Ultrasound, C.T., MR., Spiral C.T. and Interventional Radiology. A case report of Menkes Syndrome which is a rarity in Thailand has been presented in this issue. Radiotherapy and Radiation Physics articles were also published in this Volume II , No II. We have articles from Singapore, Malaysia, Thailand. I would like to invite and encourage writers from Philippines and Indonesia to present their papers to furnish the Asean Journal of Radiology so that it is really the Journal written by the Asean !

Kawee Tungsubutra

THE ASEAN JOURNAL OF RADIOLOGY

Volume II Number II May-August 1996

CONTENTS

Volume II Number II May-August 1996

CONTENTS

Pictorial Essay

MAMMOGRAPHIC FEATURES OF TYPICAL BENIGN CALCIFICATIONS

Malai MUTTARAK,M.D.
Ladda CHALOEYKITTI,BSc.

Calcifications in the breast are important because they may be the first and only sign of breast carcinoma. However, the great majority of calcifications found on mammograms are associated with benign disease. Careful analysis of size, shape, number, density and distribution of calcifications can help in differential diagnosis of benign from malignant calcifications. The purpose of this paper is to present a variety of a typical mammographic benign calcifications in order to avoid unneccessary biopsy of these calcifications.

VASCULAR CALCIFICATIONS

Vascular calcifications (Fig.1A,B) typically appear as linear, parallel calcifications along the vessel walls, producing a "railroad track" configuration when well developed. Differentiation from fine linear malignant calcification may be a problem when arterial calcifications are in the very early forming.

CALCIFIED FIBROADENOMA

Fibroadenomas are the most common breast masses seen in women younger than 35 years of age. Calcificatons occur when they undergo degeneration. Early calcification in a fibroadenoma frequently occurs at the periphery of the mass (Fig.2). By the time, calcifications in fibroadenoma become larger and more extensive. Finally, the soft tissue masses are no longer appearent, leaving only typical large coarse "popcorn-like" calcifications (Fig.3-5).

SECRETORY DISEASE

Secretory disease, or ductal ectasia or plasma cell mastitis, occurs most often in perimenopausal or postmenopausal women. They are frequently bilateral. The cause of duct ectasia is uncertain but may be related to the accumulation of thickened secretion within the ducts that eventually lead to dilatation and rupture of the duct walls. The calcifications associated with this condition may be intraductal, in the wall of the duct, or periductal, and the morphology depends on the location (Fig.6,7). Those occur in the duct lumens appear as smoothly marginated solid cores that are longer and wider than the casting malignant calcifications. Calcifications within the walls or periductal present as hollow cylinders.

MILK OF CALCIUM IN CYSTS

In cystic hyperplasia, milk of calcium may be secreted into the fluid showing the characteristic mammographic appearance as smudge like densities on the craniocaudal view and calcium-fluid level when the breast is imaged in the upright projection with a lateral beam (Fig.8,9). These calcifications behave similary to the sediment at the bottom of a cup of tea, resulting in their designation as teacup calcifications. Its recognition is important because this lesion has no known malignant potential and biopsy is unnecessary.

EGGSHELL OR RIM CALCIFICATIONS

These calcifications are frequently seen in the walls of tiny cysts and may also occur in cases of fat necrosis secondary to blunt trauma, surgical incision, or radiation therapy. The calcifications may be very thin, 1 mm. or less or have thicker walls (Fig.10).

Department of Radiology, Faculty of Medicine, Chiang Mai University, Chiang Mai THAILAND

DERMAL CALCIFICATIONS

Dermal calcifications are usually related to a chronic inflammatory process such as folliculitis and are often located in sebaceous glands (Fig.11). Typically, they are very well defined margins and a central lucency, regional or diffuse distribution. Obtaining tangential views to the area of concern will proved that calcifications are actually within the skin. Other skin lesions that may calcify include nevi, hemangiomas, skin tags and dystrophic calcifications associated with scarring.

FOREIGN-BODY INJECTION GRANULOMAS

Patients who have had silicone or paraffin injections for augmentation of the breasts several years ago are found to have very dense breasts with multiple nodules. On mammogram, calcified granulomas are round or ring like appearance similar to those of fat necrosis. Siliconomas (Fig.12A,B) trend to be larger in size than paraffinomas (Fig.12C) but the mammographic features of all such lesions are both characteristic and clearly benign.

SUMMARY

Calcifications occur in the breast are frequently associated with benign disease. However, mammographically detected calcifications are frequently the only sign of breast cancer. While some benign calcifications cannot be distiguished from those of malignancy and biopsy is usually needed to confirm the diagnosis. There are many typically benign calcifications that radiologists should be familiar with in order to avoid suggestion biopsy of these calcifications.

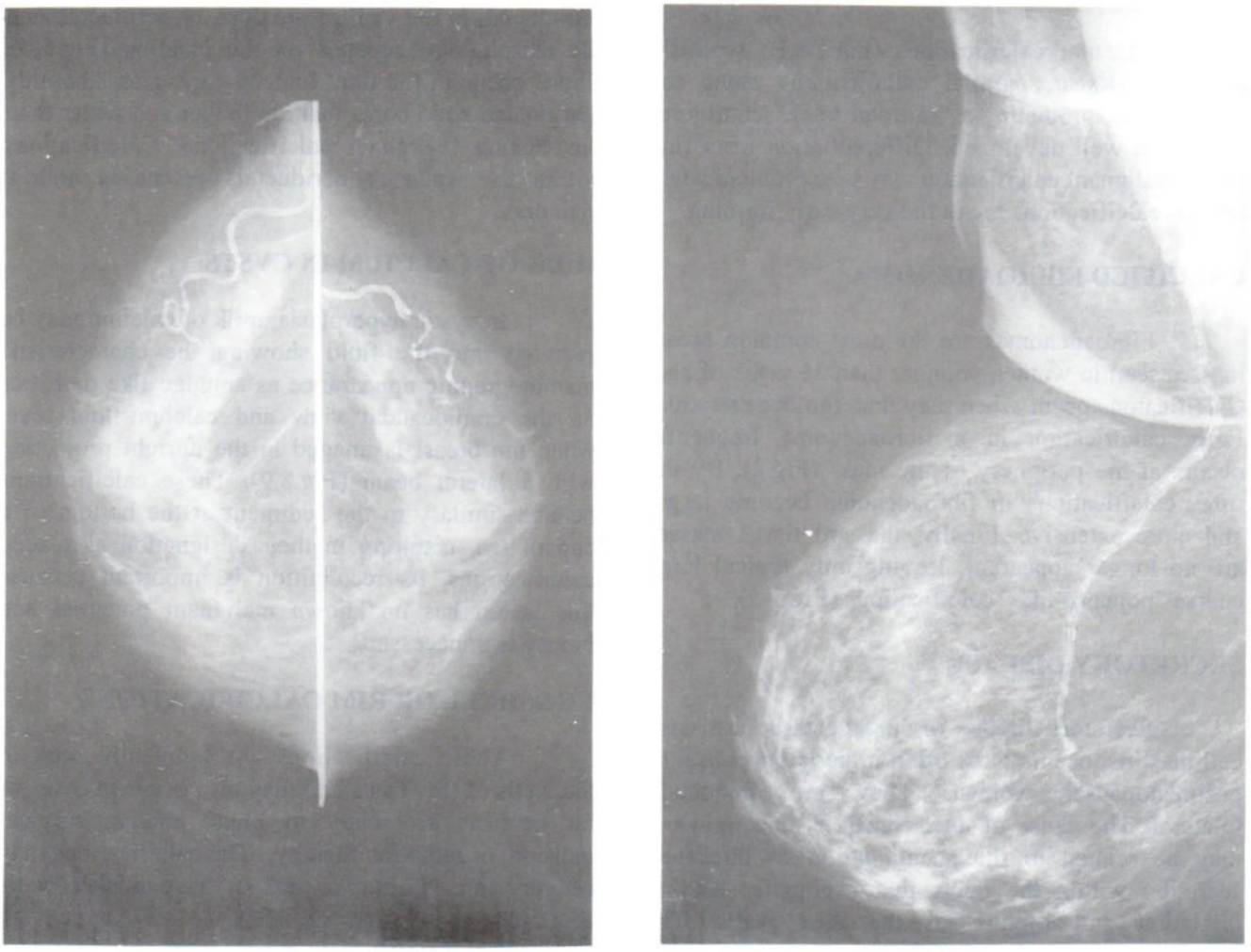

Fig.1 A,B. Mammograms demonstrate typical "railroad track" appearance of vascular calcifications.

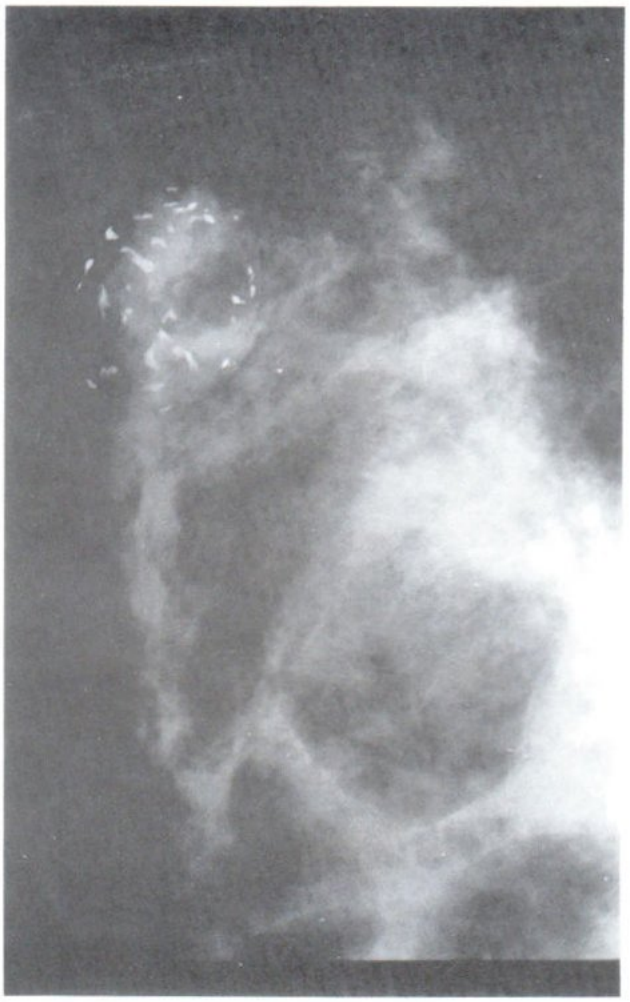

Fig.2 Demonstrating early peripheral calcification in a well circumscribed fibroadenoma.

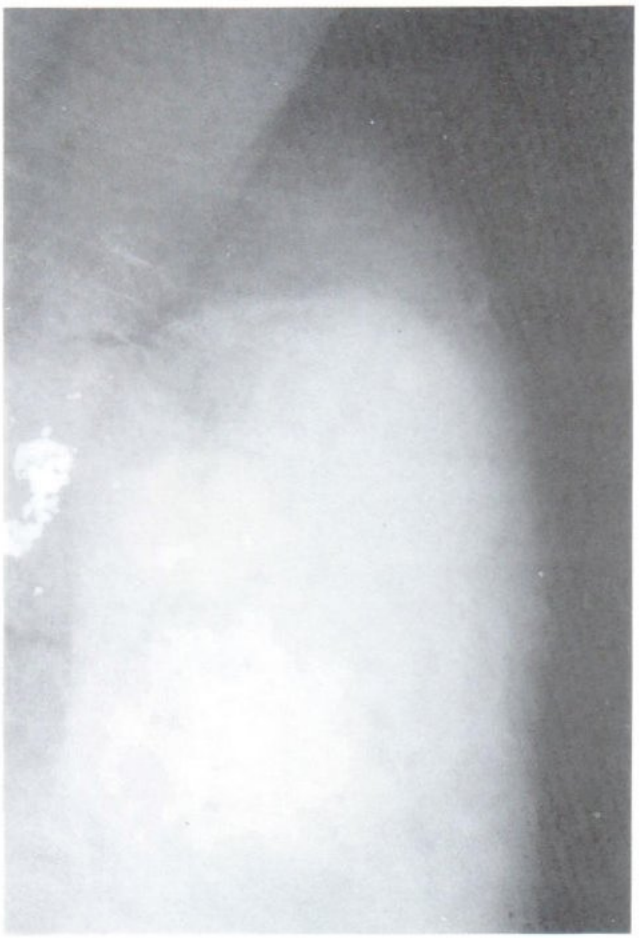

Fig.3 Left mediolateral oblique view. The breast is very dense with a large well define mass and very coarse, dense calcifications. Excisional biopsy revealed fibroadenoma with calcification.

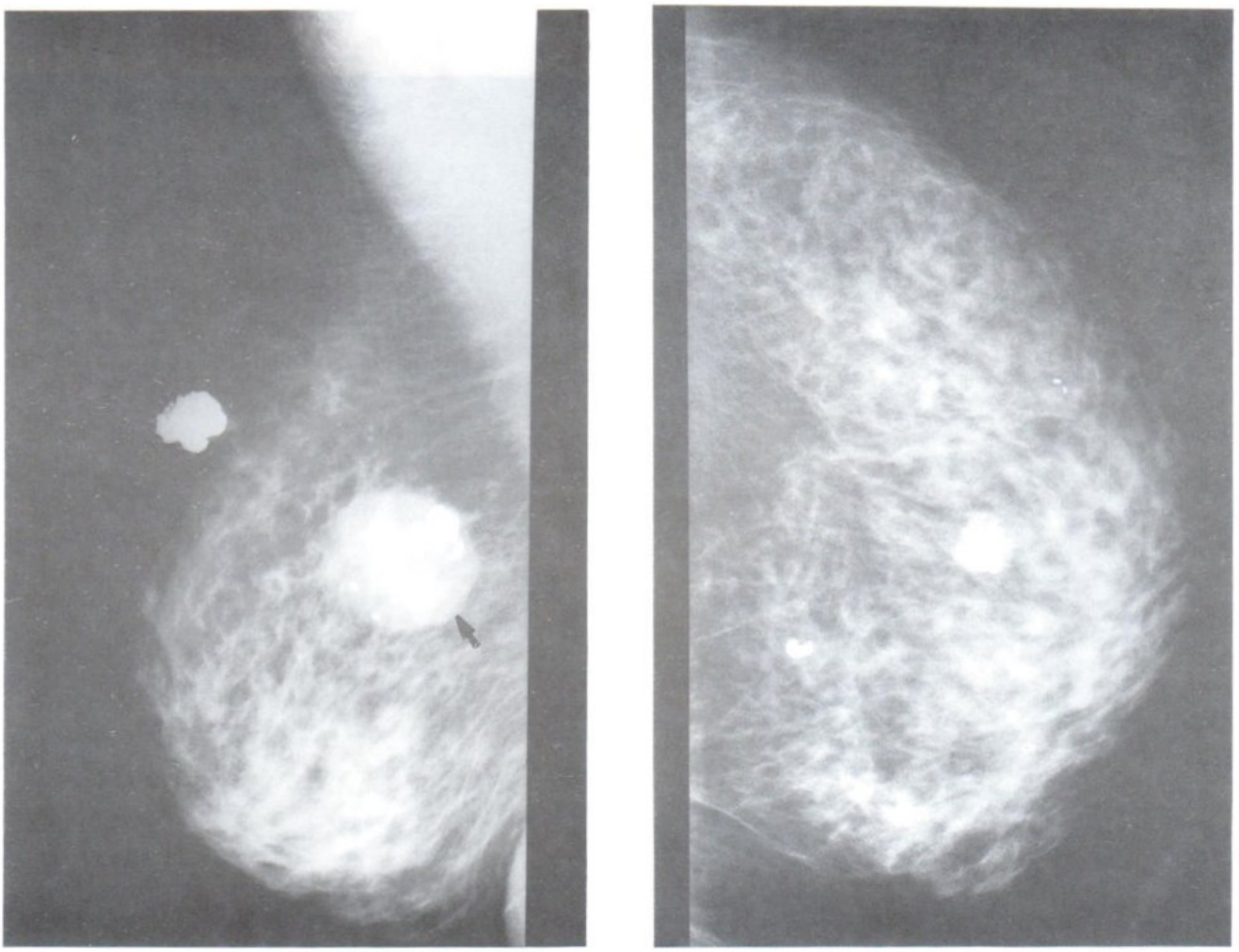

Fig.4 A,B. Mammograms show bilateral calcified fibroadenomas with typical "popcorn" calcifications. The residual soft tissue mass is visible for the largest lesion (arrow).

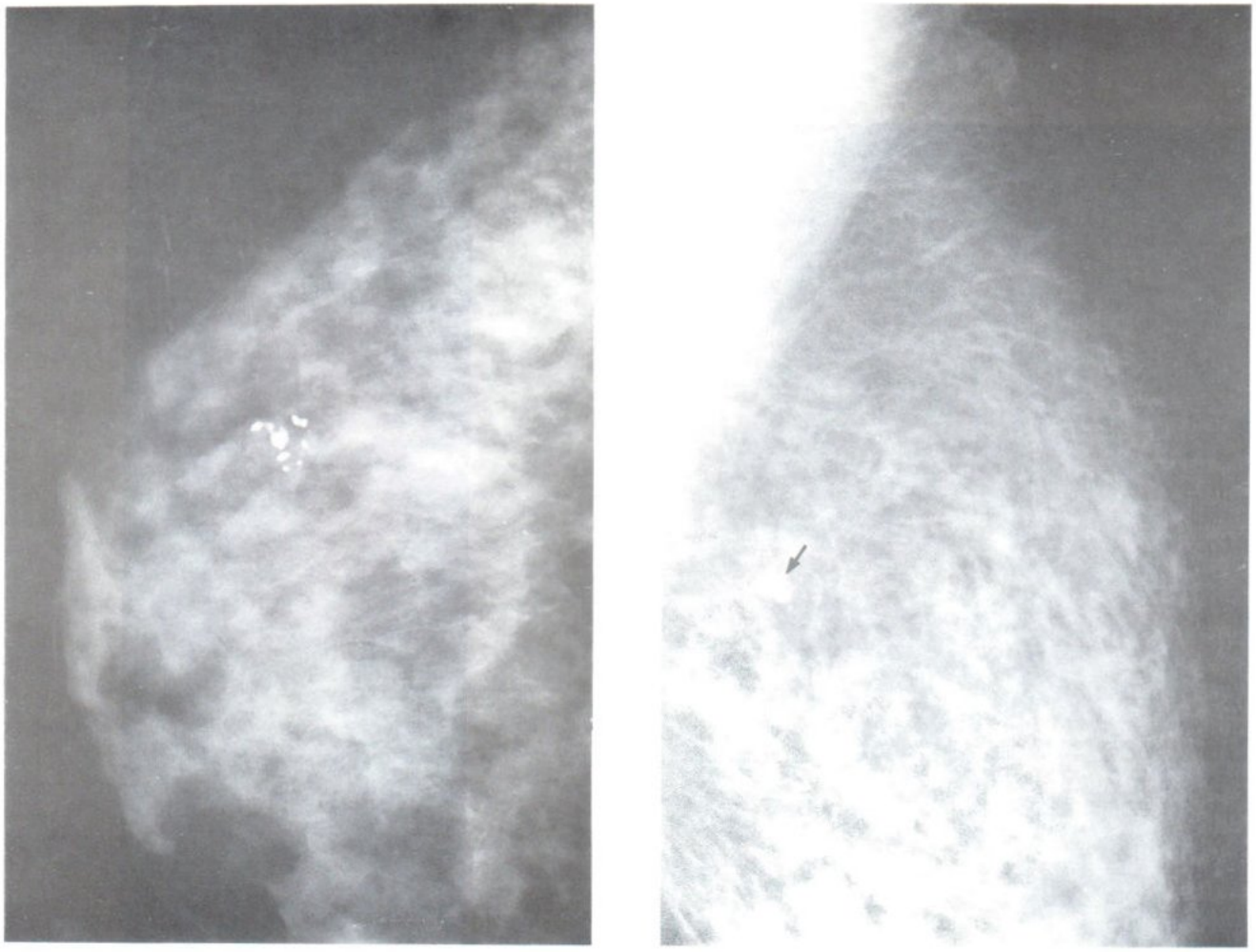

Fig.5 A,B. Mammograms demonstrate coarse calcified degenerating fibroadenoma with regression of soft tissue component.

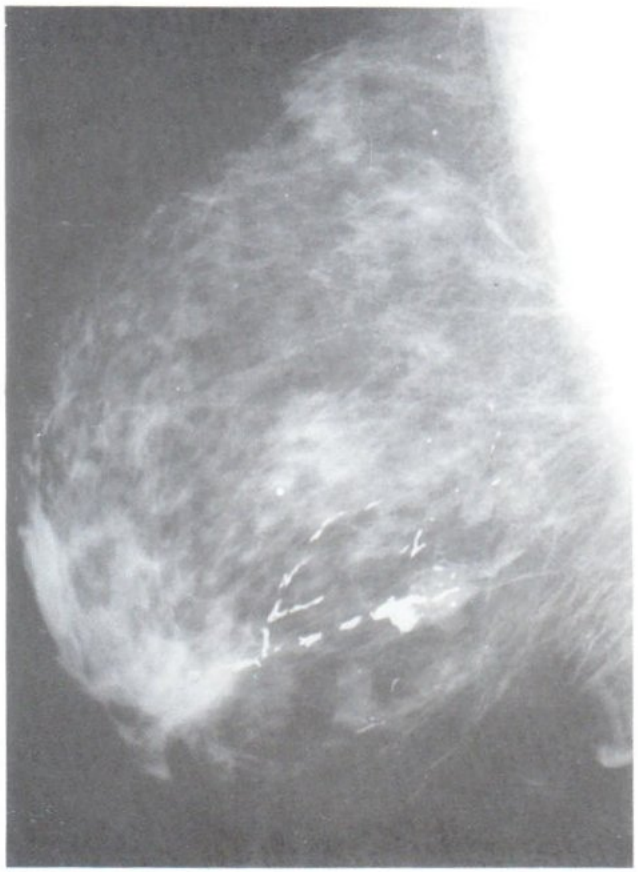

Fig.6 Mammogram discloses large rod- like calcification in duct lumens, secondary to secretory disease.

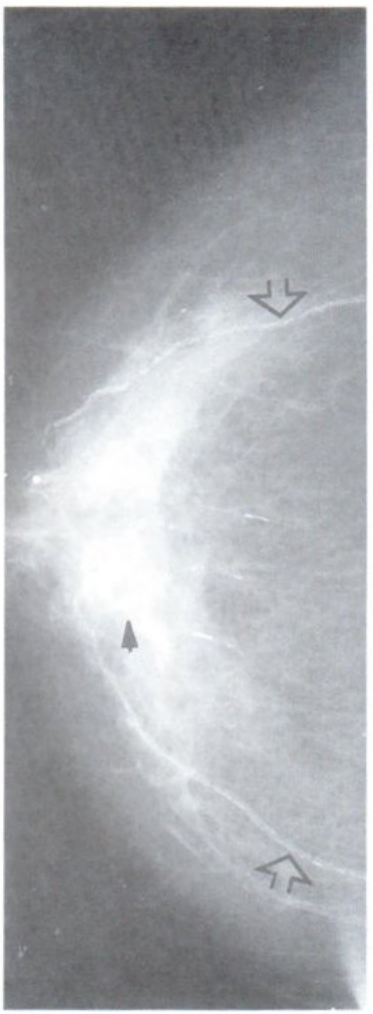

Fig.7 Mammogram shows three types of typical benign calcification. Radilroad track appearance of arterial calcification (arrow) eggshell calcification of fat necrosis or cyst (arrow head) and rod - like ductal calcifications oriented toward the nipple.

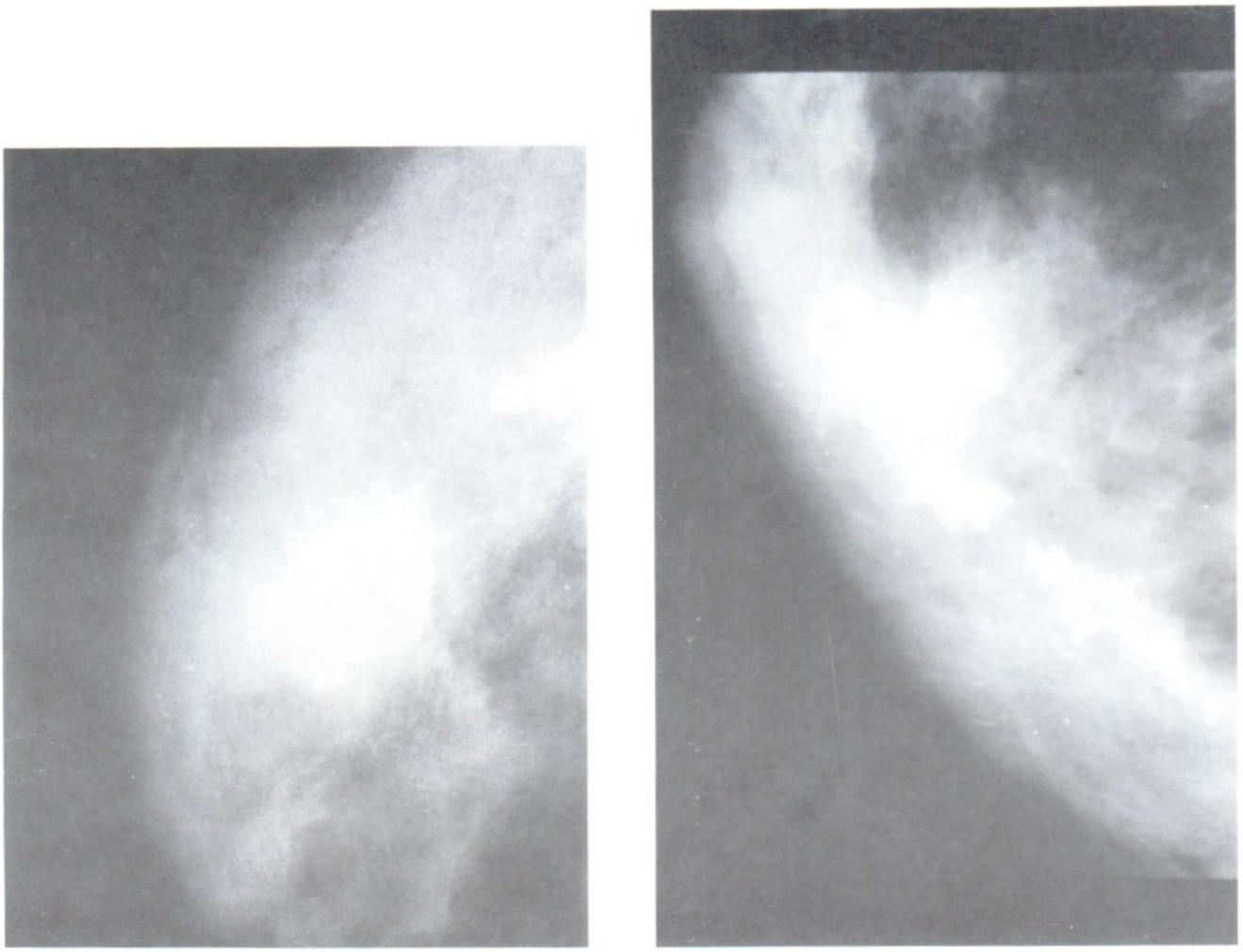

Fig.8 A. Craniocaudal view demonstrates multiple round calcifications. B.Mediolateral oblique view shows milk of calcium sediments in the dependent portion of cysts.

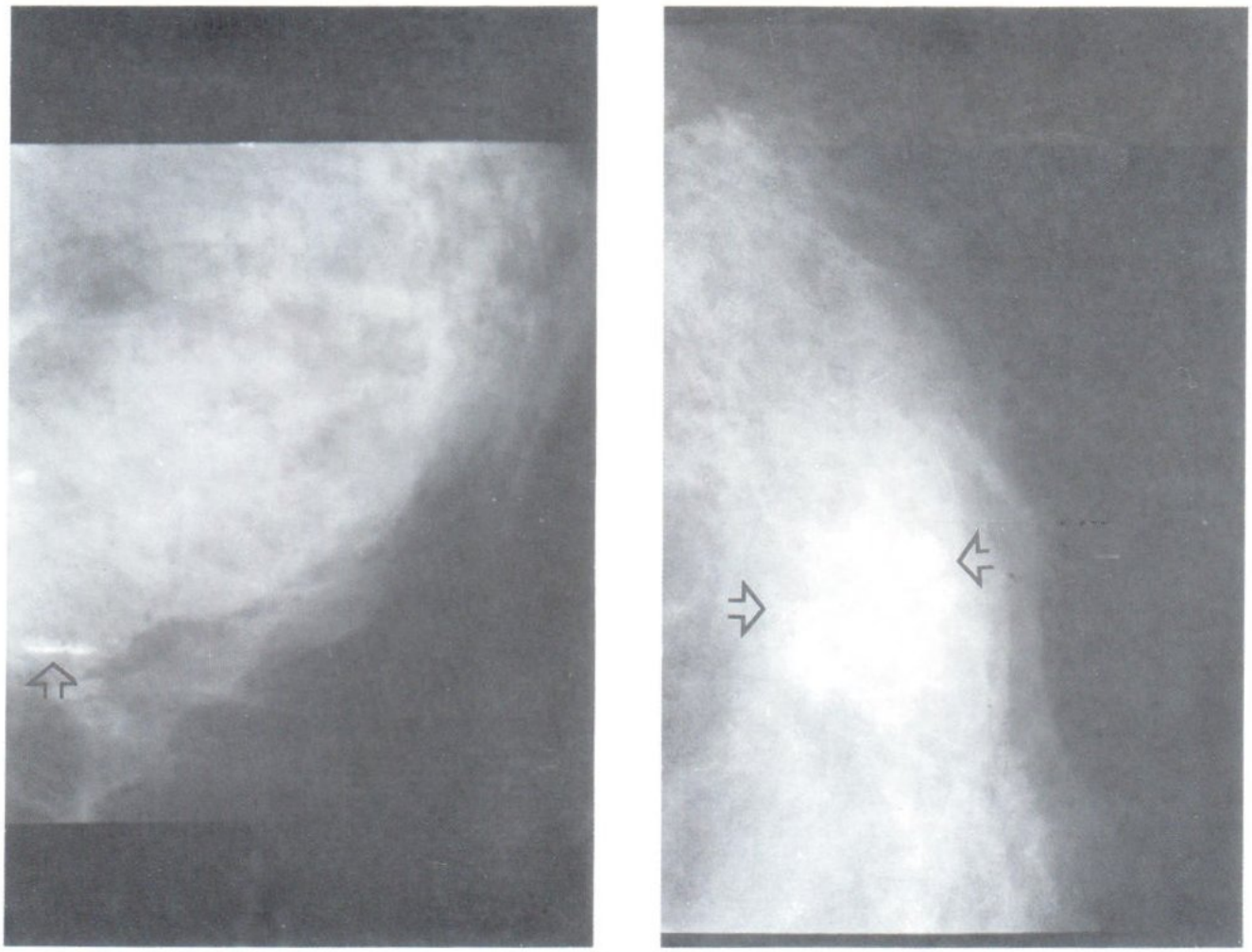

Fig.9 Milk of calcium. Multiple well defined particles sediment in lower most portion of a large cyst to form a horizontal pattern (arrow) on MLO view (A) and round pattern (arrow) on CC view (B).

A

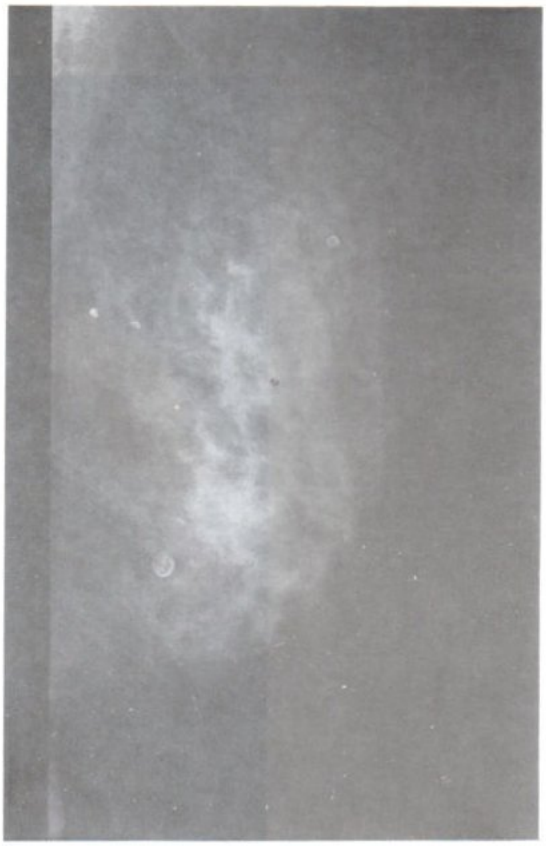

B

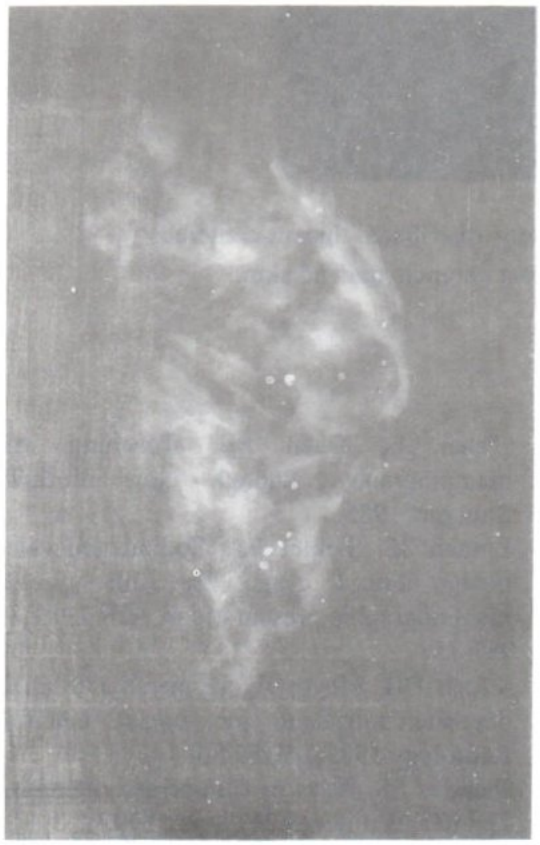

C

D

Fig.10 A-D. Mammograms show multiple small and large eggshell or rim calcifications.

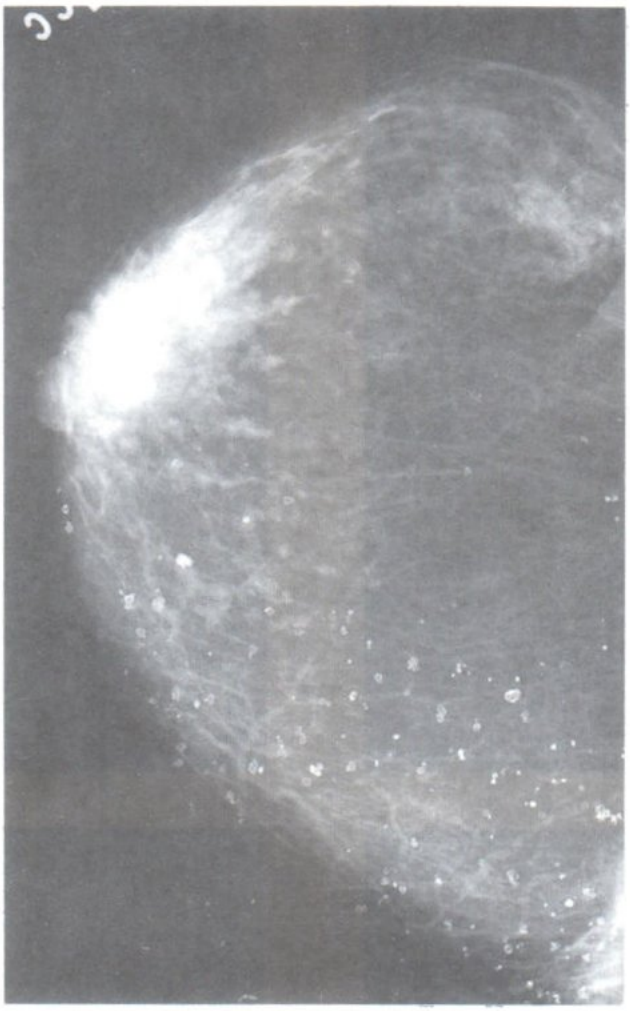

Fig.11 Craniocaudal view shows diffusely distributed lucent-centered calcifications overlying both breast parenchyma and skin.

REFERENCES:

1. Paredes ES, Abbitt PL, Tabbarah S, et al, Mammographic and histologic correlations of microcalcification. Radiographics 1990;10:577-89
2. Sickles EA. Breast calcifications: Mammographic evaluation. Radiology 1986;160:289-93.
3. Kopans DB. Discriminating analysis uncovers breast lesions. Diagnostic Imaging 1991; September: 94-100
4. Bassett LW. Mammographic analysis of calcifications. Radiol Clin North Am 1992;30:93-105.
5. Tabar L, Dean PB. Teaching atlas of mammography. 2nd.ed. New York:Thieme-Stuttgart:1985.
6. Linden SS, Sickles EA. Sedimented calcium in benign breast cysts: The full spectrum of mammographic presentations. AJR 1989;152: 967-71.
7. Kopan DB, Meyer JE, Homer MJ et al. Dermal deposite mistaken for breast calcifications. Radiology 1983;149:592-4
8. Paredes ES. Atlas of film-screen mammography. 2nd ED. William & Wilkins , 1992
9. Homer MJ, Cooper AG, Pile-Spellman ER. Milk of calcium in breast microcysts:Manifestation as a solitary focal disease. AJR 1988;150:789-90.

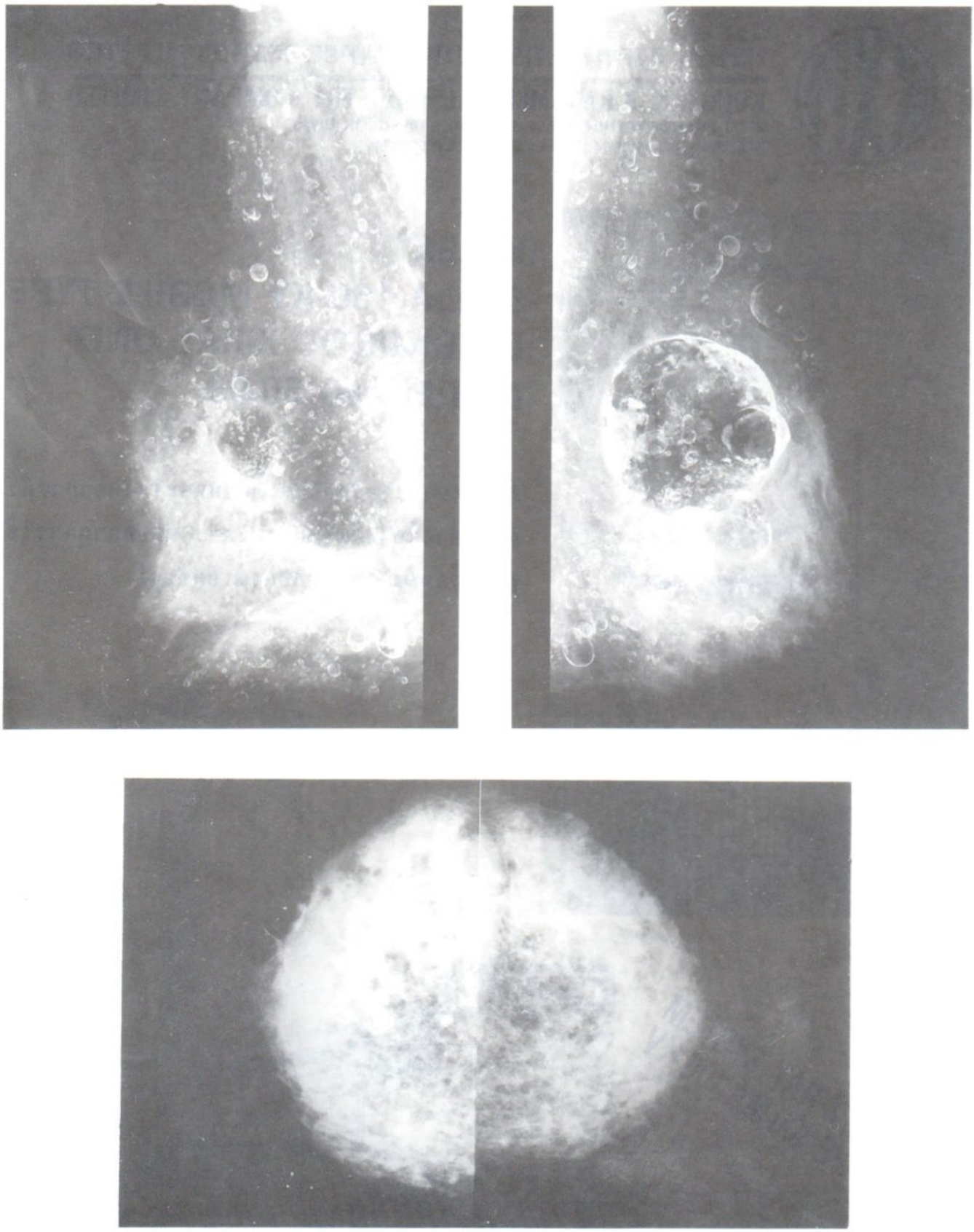

Fig.12 A,B,C. Foreign-body-injection granulomas. A,B. Siliconomas are large and rim calcification, C.paraffinomas, appearing as much smaller nodules.

บริษัท คงศักดิ์เอ็กซเรย์การแพทย์อุตสาหกรรม จำกัด
KONGSAK X-RAY MEDICAL INDUSTRY COMPANY LIMITED
212/1 PHAHONYOTHIN SOI 55 BANGKHEN BANGKOK 10220
TEL. 5213214, 5511794 CABLE: KELEX FAX: 5523744

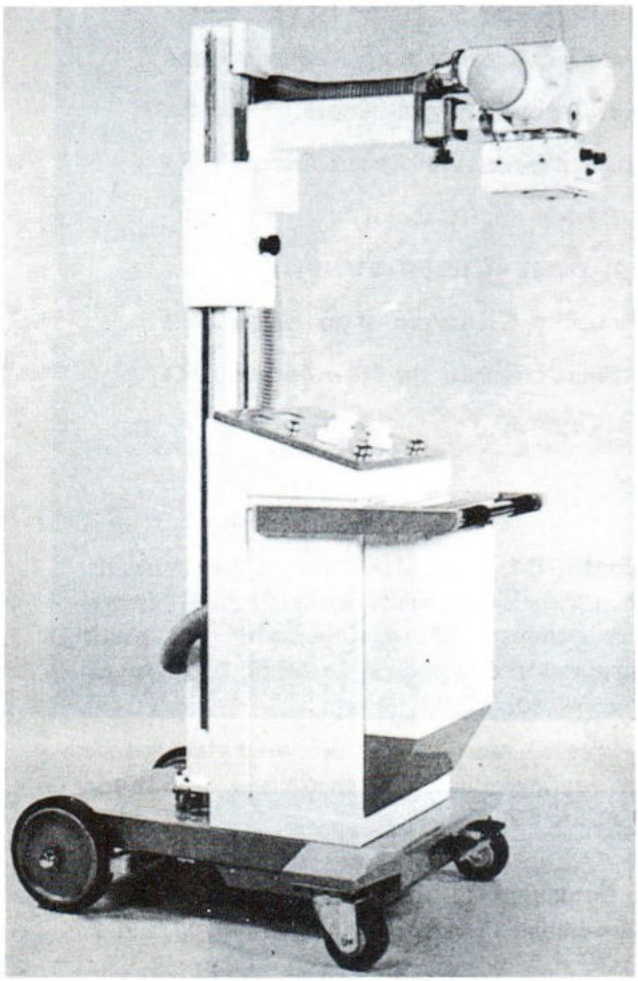

KELEX
50 mA 100 KV MOBILE TYPE DIAGNOSTIC X-RAY UNIT MODEL MD 50-99

- # เหมาะสำหรับคลินิคเอกชนและโรงพยาบาลทั่วไป
- # มีช่างผู้ชำนาญให้การบริการ ตลอดอายุการใช้งาน
- # พร้อมทั้งจำหน่ายอุปกรณ์เอ็กซเรย์

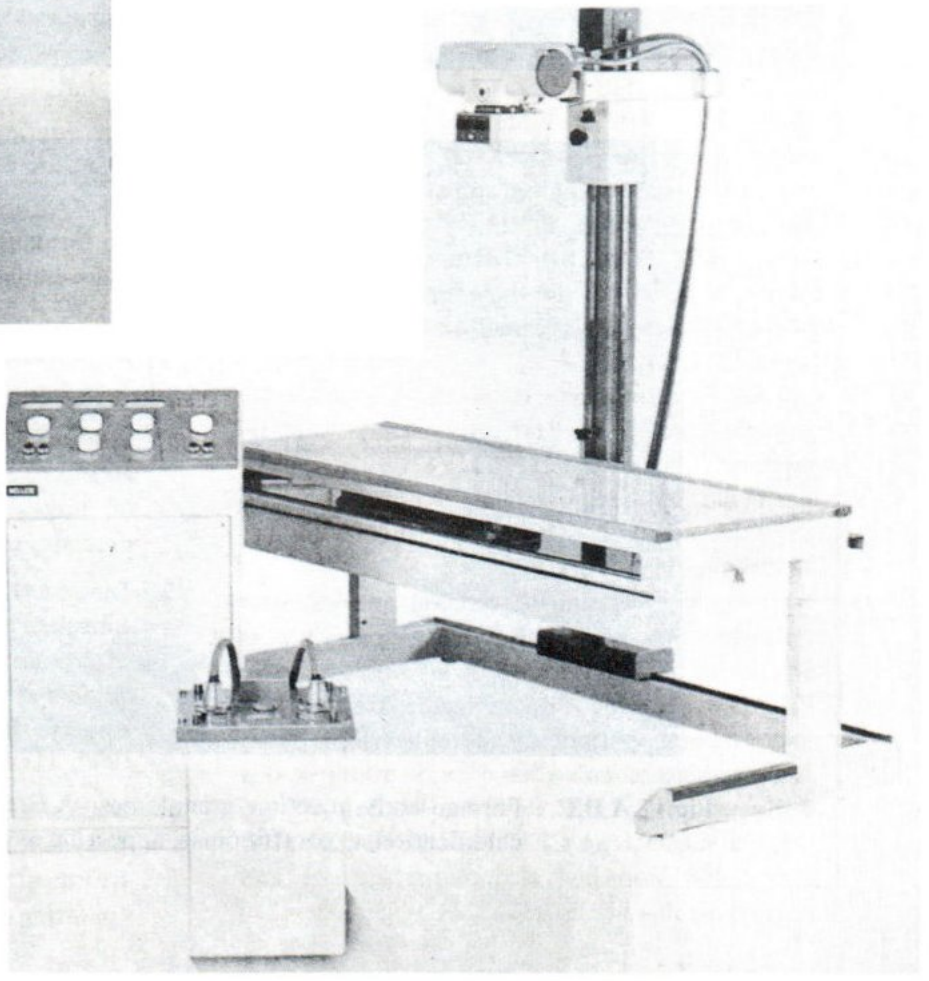

KELEX
MD 100-99 X-RAY SYSTEM
FULL WAVE 100 MA 100 KV

BILATERAL PLEURAL EFFUSION IN PARAGONIMIASIS A CASE REPORT

Jaturat KANPITTAYA, M.D.*
Jamaree TEERATAKULPISARN, M.D.**
Chusak KUPTARNOND, M.D.***
Smarn TESANA, M.Sc.****
Eimorn MAIRIANG, M.D.*

ABSTRACT

A 14-year-old boy was admitted with chest pain, low grade fever and a productive cough for about 2 months. The chest film showed bilateral pleural effusion. The Significant laboratory finding was eosinophilia, 22% in peripheral blood and 49% in pleural fluid. The images of ultrasonogram and computed tomography revealed unexplained exudative bilateral pleural effusion, bizarre appearance and a questionable moving organism. Finally the operation was done and a living parasite of Paragonimus heterotremus was found.

Keywords : Paragonimus, pleural effusion, eosinophilia, ultrasonogram, computed tomography

INTRODUCTION

Paragonimiasis is a parasitic disease caused by the trematode, Paragonimus. sp. Human infection occurs by ingestion of raw or incompletely cooked freshwater crab or crayfish infected with the metacercaria. Paragonimiasis is endemic in certain areas of East and Southeast Asia. Several case reports of paragonimiasis in Indo-Chinese refugees in North America have been published. The first reported case in Thailand was a patient from Lomsak district, Petchabun province (Promas, 1928). Six species of Paragonimus have been reported in Thailand. P. heterotremus has been postulated to be the main cause of human paragonimiasis in Thailand. There are two form of Paragonimiasis, pulmonary and ectopic. Pleural lesions are uncommon. A case of pleural paragonimus is reported.

CASE REPORT

A 14-year-old boy from Petchabun province of Thailand complaining of persistent chest pain and a productive cough for about 2 months. This was the third hospital admission. Physical examination and chest radiograph confirmed bilateral pleural effusion. Head and neck examination revealed no adenopathy. No evidence of subcutaneous swelling. The white cell count was 7,500 with 22% eosinophil ; hemoglobin was 13.4 g/100 ml, and the hematocrit was 40%. Stool examination was negative for parasite. Pleural fluid analysis was compatible with an exudative fluid with 49% eosinophil; the sediment consisted of neutrophils, lymphocytes and histiocytes. Chest x-ray showed bilateral pleural effusion (Fig. 1). Additional imaging of ultrasonogram and computed tomography

* Department of Radiology
** Department of Pediatric
*** Department of Surgery
**** Department of Parasitology
Srinagarind Hospital, Khon Kaen 40002, Thailand.

showed bizarre appearance of pleural fluid containing folded strings like echos (Fig. 2, 3). Due to unresolving of bilateral pleural effusion, finally an operation was performed. The operative findings revealed bilateral turbid yellow fluid 500 cc on the left and 300 cc on the right with fibrinous exudative material. One living adult worm of paragonimus was found on the left side. Both fluid and fibrinous exudative material were surrounded by thickened pseudocyst wall completely. This pseudocyst located in subpulmonic space (Fig 4).

The surgeon removed the parasite, and cyst wall completely to encourage lung expansion. After the operation, the patient recovered unevenfully. The patient received combine medical treatment of praziquantel 25 mg/kg/dose for 3 days.

DISCUSSION

Paragonimiasis is endemic in Asia (China, Korea, Taiwan, Japan and Thailand), Africa and South America. There is a high rate of infection following ingestion of contaminated water or raw crab or crayfish infected with metacercaria. The cyst wall of the metacercaria is digested by the host and the larvae penetrates the intestine, ingesting host tissue as it passes through the peritoneal cavity, diaphragm and pleura into the lungs over a period of approximately four weeks. The larvae develop to be adult flukes in cystic cavities formed around the flukes within the lungs.

The characteristics of clinical manifestations are chronic cough and hemoptysis although the patients are still healthy and without debility.

The diagnosis of paragonimiasis is made either by detecting eggs in the sputum, stool, fluid from bronchoscopic lavage, or biopsy specimens, or by a positive anti-Paragonimus antibody test (detection band of 31.5 kDa antigenic component, ELISA with sensitivity and specificity about 100% and 99% respectively). Egg detection rates have been reported to be 28-38%. Otherwise high level of gamma globulin can be used in diagnosis of Paragonimus.

No specific change in radiological finding is observed. The appearance of pulmonary lesions on radiographs varies with the stage of infection and the surrounding tissue reaction. During the process of pleural penetration by juvenile worms, pleural effusion or pneumothorax is seen, and during the process of larval migration within the lung, patchy migrating air-space consolidation appears. The initial finding is patchy air-space consolidation due to hemorrhagic pneumonia caused by the migrating worm. At this stage, pleural effusion or pneumothorax is frequently seen. The cyst form is supposed to be ischemic infarction after obstruction of an arteriole or a vein by a worm or by eggs. Peripheral linear shadow 2-4 mm thick and 3-4 cm long extending from the pleural surface suggest worm migration tracks or peripheral atelectasis caused by obstruction of small airways by the worm. Such linear opacities are most commonly and clearly seen in patients with pleural effusion.

The prevalence of pleural effusion in patients with pleuropulmonary paragonimiasis varies from 2.9-54%. Chest x-ray was found to be normal in 7% (Benjapong 1984) to 14% (Walker 1955). The tomographic study showed lung lesion in 100% (Benjapong 1984). Change of pulmonary lesions and unexplained bilateral pleural effusions were findings suggestive of paragonimiasis, especially in endemic areas.

ACKNOWLEDGMENT

Thanks to Mr E. W. Renton for preparation of the manuscript.

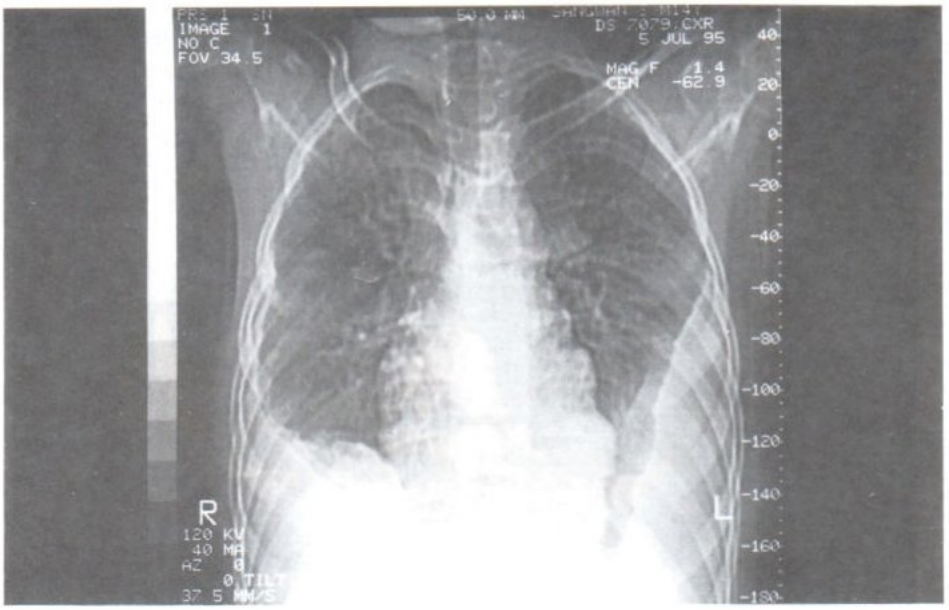

Fig. 1 Chest radiograph shows bilateral pleural effusion

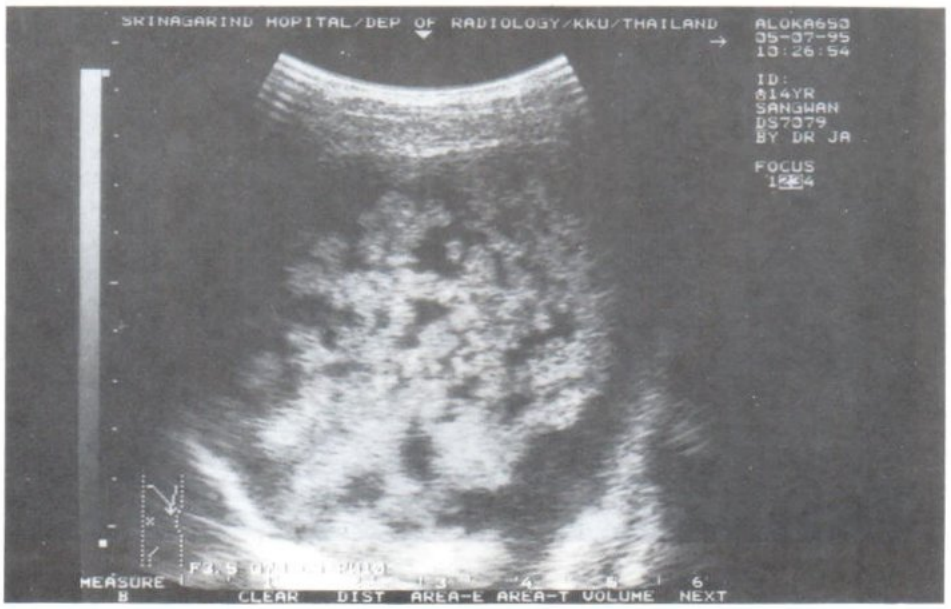

Fig 2 Ultrasonograms demonstrate floating echo bands within pleural fluid

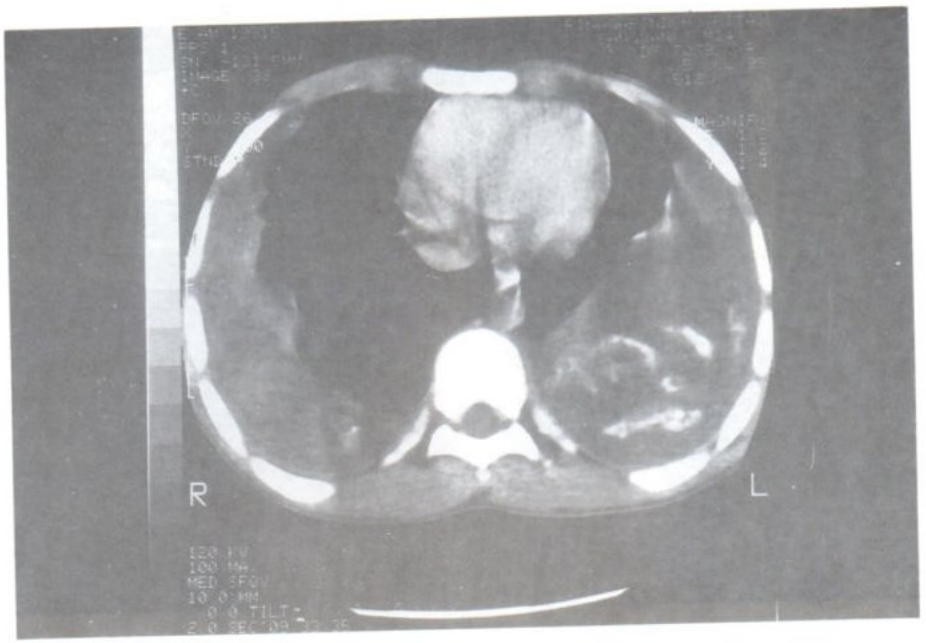

a

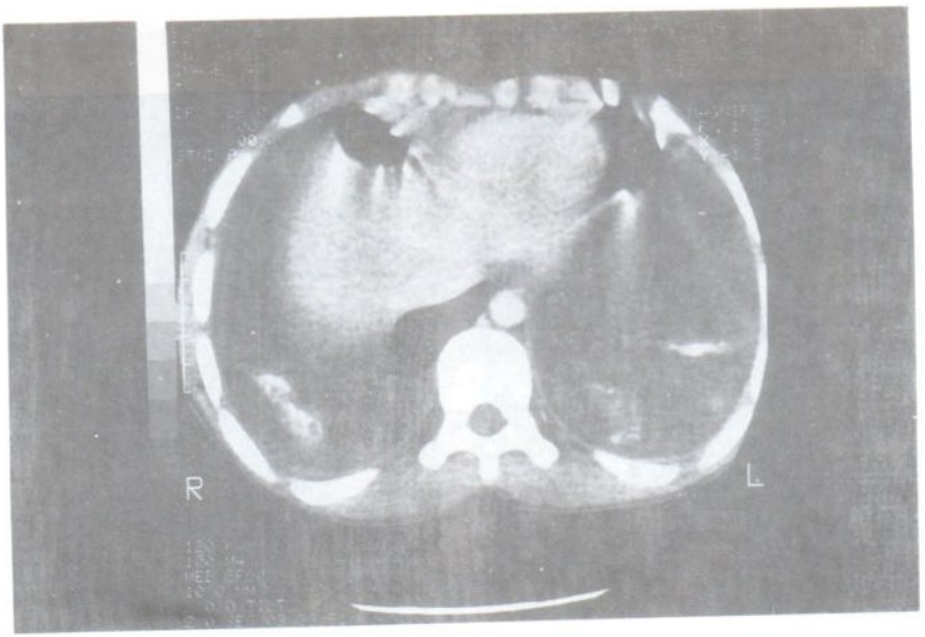

b

Fig. 3 a,b CT scan shows high attenuation bands in bilateral pleural fluid.

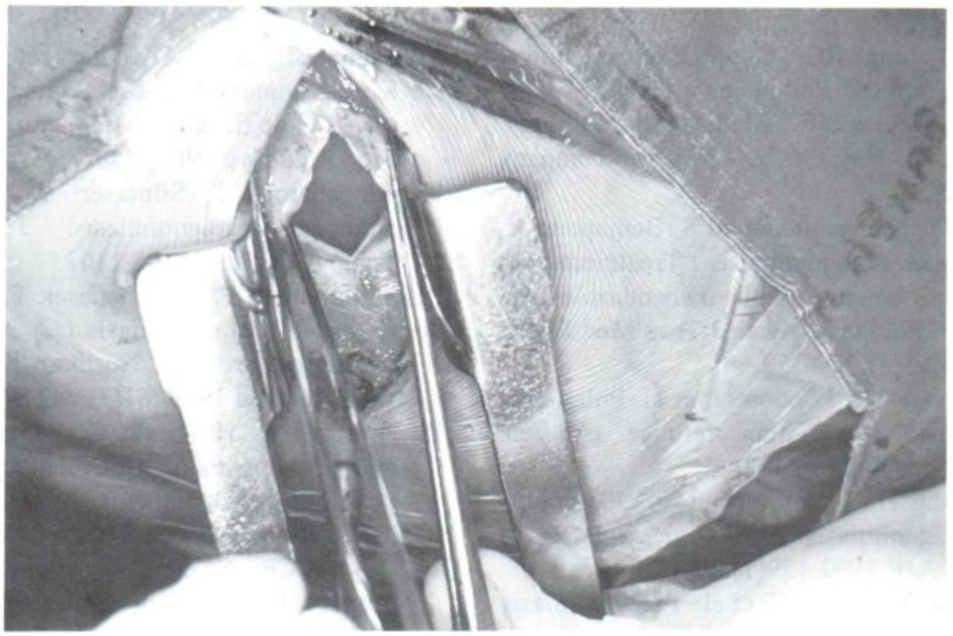

a

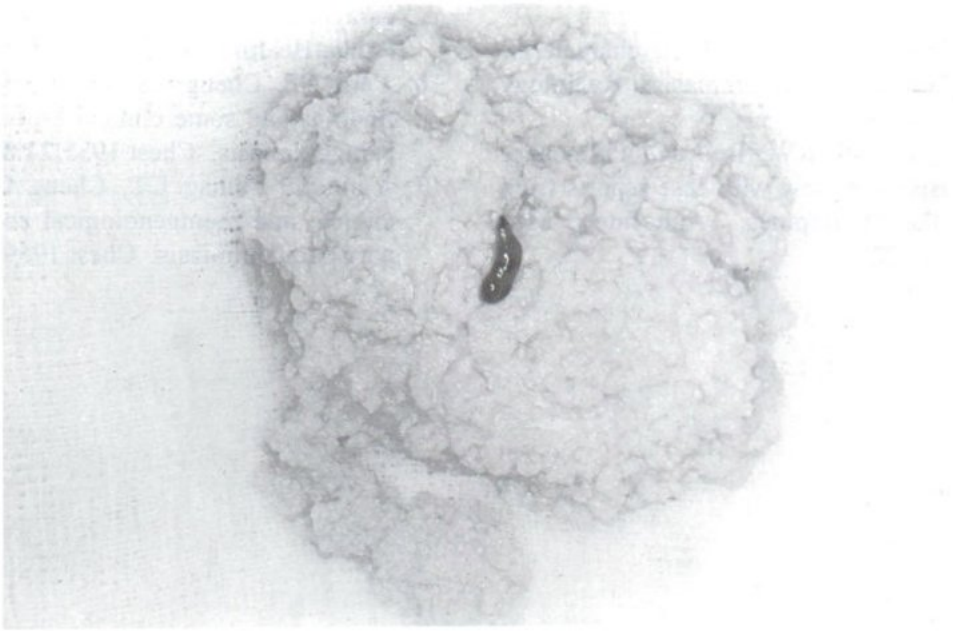

b

Fig 4 a. Subpulmonic pseudocyst on the left side containing turbid yellow fluid.

b. Adult worm of paragonimus lying on plenty of yellowish fibrinous exudative material

REFERENCES

1. Beaver PC, Jung RC, Cupp EW. Clinical parasitology 9 th ed. Philadelphia 1984;464-470
2. Beck JW., Davies JE. Medical parasitology. second ed. The C.V. Mosby company 1976;150-152
3. Benjapong W, Naeypatimanond S, Benjapong K, et al. Study on paragonimiasis : Treatment with mebendazole, emetine with mebendazole and praziquantel. Southeast Asian J Trop Med Public Health 1984;15(3):354-359
4. Burton K, Yogev R, London N, et al. Pulmonary paragonimiasis in Laotian refugee children. Pediatrics 1982;70:246-248
5. Im JG, Whang HY, Kim WS, et al. Pleuropulmonary paragonimiasis: Radiologic findings in 71 patients. AJR 1992;159(1):39-43
6. Johnson JR, Falk A, lber C, et al. Paragonimiasis in the United States: A report of nine cases in Hmong immigrants. Chest 1982;82:168-171
7. Johnson RJ, Johnson JR. Paragonimiasis in Indochinese refugees. Am Rev Respir Dis 1983;128:534-538
8. Miller FL, Walker R. The roentgen characteristics of pulmonary paragonimiasis. Radiology 1955;65:231-235
9. Roque FT, Ludwick RW, Bell JC. Pulmonary paragonimiasis: A review with case reports from Korea and the Phillippines. Ann Intern Med 1953;38:1206-1221
10. Sadun EH, Buck AA. Paragonimiasis in South Korea: immunodiagnosis, epidemiologic,clinical, roentgenologic and therapeutic studies. Am J Trop Med Hyg 1960;9:562-569
11. Singcharoen T, Silprasert W. CT findings in pulmonary paragonimiasis. J Comput Assist Tomogr 1987;11:1101-1102
12. Sutthipunthu P, Songthanasak T, Kamboonruang C, et al. Paragonimiasis : A case report from Chiang Rai province, Northern Thailand. J. Med. Ass. Thailand 1978 ;61(7) : 427-433
13. Suwanik R, Harinsuta C. Pulmonary paragonimiasis: An evaluation of roentgen findings in 38 positive sputum patients in an endemic area in Thailand. AJR 1959; 81:236-244
14. Taylor CR, Swett HA. Pulmonary paragonimiasis in Laotian refugees. Radiology 1982;143:411-412
15. Wongkham C, Maleewong W, Intapan P, et al. Partially purified antigens of Paragonimus heterotre-mus for serodiagnosis of human paragonimiasis. Southeast Asian J Trop Med Public Health 1994;25(1):176-180
16. Yang SP, Cheng CS, Ghen KM. Chest x-ray findings and some clinical aspects in pulmonary paragonimiasis. Chest 1955;27:88-95
17. Yang SP Hunag CT, Cheng CS, et al. The clinical and roentgenological courses of pulmonary paragonimiasis. Chest 1959;36:494-508

ISOLATED POSTERIOR CRUCIATE LIGAMENT INJURY: MR DIAGNOSIS

Weawdao TECHAWATTANAKUL[1], Pimjai SIRIWONGPAIRAT[1],
Suvipaporn SIRIPORNPITAK[1], Janjira JATCHAVALA[1], Patchrin PEKANAN[1].

ABSTRACT

MRI findings in a case of isolated avulsion of posterior cruciate ligament (PCL) was described. They were seen as separation of the tibial insertion of the PCL with hypersignal lesions on T_1WI between the tibia and the avulsed fragment. The anatomy and mechanism of PCL injury was reviewed.

INTRODUCTION

MRI is now the examination of choice in noninvasive diagnosis of knee ligament injuries. The evaluation of the menisci and the anterior cruciate ligament (ACL) was widely established (5), in contrast to the evaluation of the posterior cruciate ligament (PCL) (1-2) PCL injury is uncommon and occurs either as intrasubstance tears or avulsion from the site of origin or insertion. In this report, we present a case of an isolated avulsion of the PCL, describing the MR appearance and discuss anatomy and mechanism of PCL injury.

CASE REPORT

In August 1995, a 40 year old man was sent to the Ramathibodi Hospital for an MRI study of the knee. He injured his left knee 3 weeks ago. Initial physical examination of the left knee revealed an intact neurovascular status, but the ligamentous stability of the knee could not be determined. A lateral radiograph of the knee showed an avulsion fracture at the posterior aspect of proximal tibia suggesting associated posterior cruciate ligament (PCL) insufficiency (Fig. 1). MR imaging of the left knee showed the site of impact fracture of the tibia (Fig. 2) and the avulsed fragment at the tibial insertion of the PCL (Fig. 3). The collateral and anterior cruciate ligaments, the menisci and the capsule were normal.

DISCUSSION

Injury of the PCL occurs in about 2%-23% of all knee ligament injuries, and in 30% of these cases, the PCL injury is isolated (2). However, the actual incidence may be greater because many injuries remain clinically undetected (4). Because clinical evaluation can often be difficult or misleading, the diagnosis of a PCL tear can be missed. The PCL may be difficult to evaluate at arthroscopy when the ACL is intact and usually connot be directly seen by the surgeon from the anterior approch unless the ACL is torn. An intact menisco femoral ligament of Humphry can simulate an intact PCL during arthroscopy even if the PCL is ruptured. Thus, an isolated tear of the PCL may not be confirmed at arthroscopic evaluation even when suspected clinically on the knee of posterior

[1] Department of Radiology, Ramathibodi Hospital, Rama 6 Street, Bangkok 10400, Thailand.

tibial laxity. MR imaging provides reliable visualization of the PCL and can accurately demonstrate the presence and degree of injury to the PCL as well as associated ligamentous, meniscal and bone abnormalities (1,2).

The PCL is a spirally oriented fiber bundle that courses from the leteral aspect of the medial femoral condyle to its insertion in a depression in the posterior aspect of the intraarticular tibia, approximately 1 cm below the articular surface. The PCL is thicker (thickness 1.3 cm) and stronger than the ACL and has twice the tensile strength of any other knee ligament. The PCL is extrasynovial but intracapsular. It is taut in flexion and becomes predominantly lax in extension, with tension retained in the posterior aspect. The ligament subtends a reticent angle of 30°-45°, depending on the degree of flexion. The PCL serves as the major stabilizing structure in the knee, preventing posterior translation of the tibia on the femur and working in concert with the ACL and collateral ligament to limit rotatory motion.

On MR images, the normal PCL apears as a well defined band of very low signal intensity that courses between the medial femoral condyle and the posterior tibia. In the sagittal plane, the normal PCL is essentially always visualized, appearing near the midline of the joint on two or three consecutive images. In extension, the PCL is lax and describes a thick, gentle arc posteroinferiorly from the femur to the tibia. The meniscofemoral ligaments of Humphry and Wrisberg are often seen immediately adjacent to the PCL as they course from the medial femoral condyle to the posterior horn of the lateral meniscus; they are situated anterior and posterior to the PCL, respectively. On coronal images, the posterior vertical portion of the PCL is seen in the intercondylar notch, adjacent to the lateral aspect of the medial femoral condyle. The ligament curves forward anteriorly, and the horizontal portion appears as a circular or ovoid area of low signal intensity within the intercondylar notch. Axial images are useful in visualizing the vertical portion of the PCL from its tibial insertion to the genu, where it is seen as an ovoid signal void.

Three common mechanisms of the PCL injury are recognized

1. A direct blow to the proximal anterior tibia in a flexed knee, forcefully displacing the tibia posteriorly, and usually resulting in a midsubstance tear of the PCL and often in injury to the posterior joint capsule. This mechanism is often seen in the setting of motor vehicle accidents where impact with the dashboard results in posterior tibial displacement. Alternatively, a fall on a hyperflexed knee can drive the tibia posteriorly, tearing the PCL with posterior tibial displacement, the collateral ligaments usually remain intact. Bone contusion tend to occur at the site of impact between the anterior tibial plateau and the posterior femoral condyle.
2. Hyperextension may cause PCL injury or avulsion of the tibial attachment of the PCL with preservation of the ligamentous substance with continued extension, the ACL may rupture as well. Contusion are often seen in the anterior portion of the tibial articular surface and in the anterior aspect of the femoral condyles
3. Severe abduction or adduction forces associated with rotational forces may rupture the cruciate ligaments after the collateral ligament fail. With valgus stress, in particular, the ACL tends to rupture before the PCL.

Sonin AH. et al. retrospectively reviewed the results of 2,739 consecutive MR imaging examination of the knee performed at Northwestern University Medical School from January 1990 through February 1994. Seventy-one patients (2.6%) met the MR imaging criteria for a partial or complete tear of the PCL. Only five patients (7% of the positive PCL tear) had avulsive injury of the tibial insertion with the PCL apparently intact. Avulsion injuries of the tibial insertion site of the PCL were identified on the basis of focal discontinuity of the tibial articular surface, with a discrete bony fragment attached to an otherwise intact PCL and separated from the remainder of the tibia. Plain lateral radiograph of the knee was required to confirm the presence of an avulsed fragment of bone at the posterior aspect of the knee joint.

If unrecognized, PCL disruption leads to post traumatic osteoarthritis, principally of the medial femorotibial and patello fermoral compartments, resulting from instabilily.

Bone avulsion injuries are treated by reimplantation of the tendon and attached fragment with screw fixation or pull-through suture.

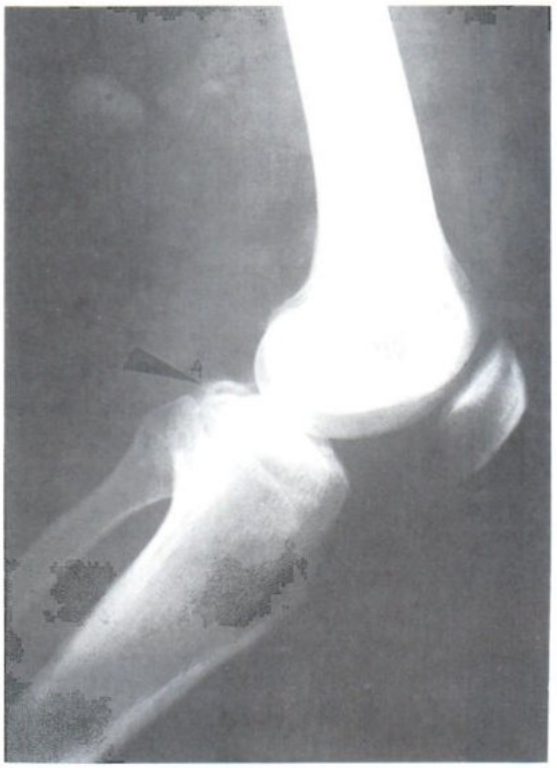

Fig. 1 Lateral radiograph of left knee shows an avulsion fracture (arrow head) at the site of posterior cruciate ligament (PCL) insertion.

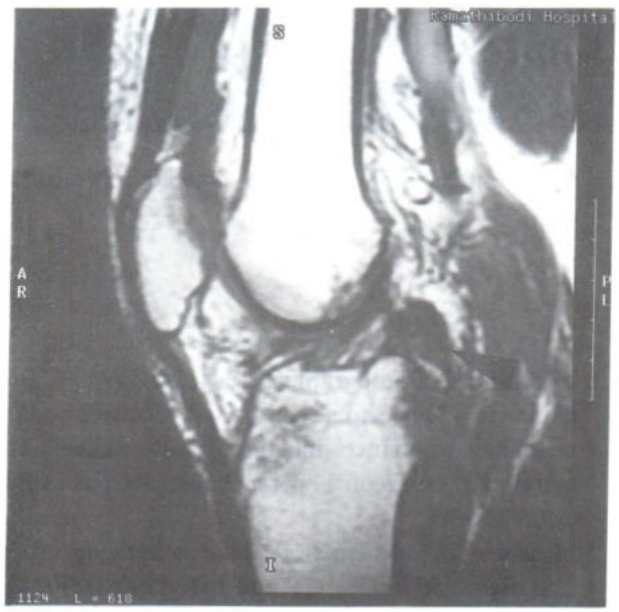

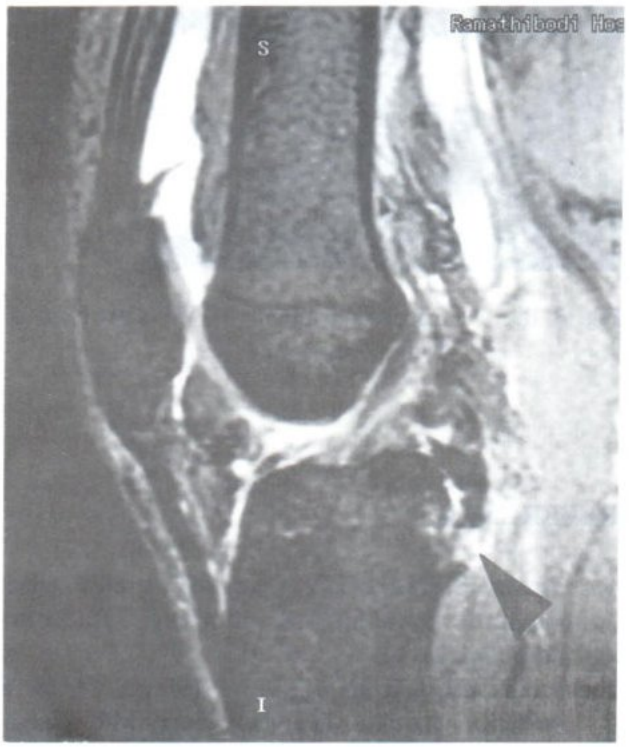

Fig. 2 A. Sagittal T_1 WI shows a low signal intensity area at the site of tibial fracture and the separated PCL.
B. Sagittal T_2WI shows an abnormal high signal intensity between the tibia and avulsed fragment. The PCL itself is intact.

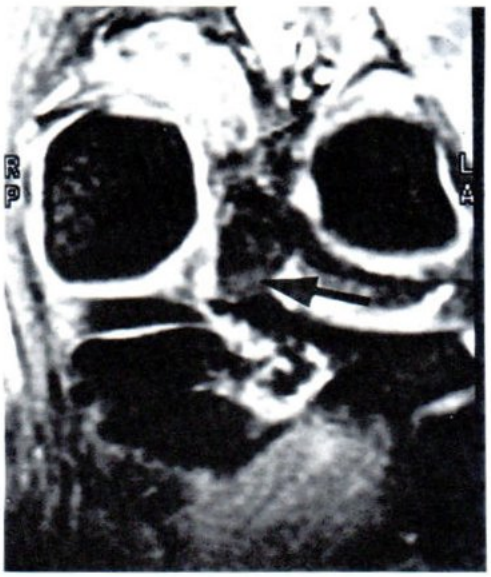

Fig. 3 A. Coronal T_1WI through the posterior knee demonstrates the separated fragment attached to the PCL.

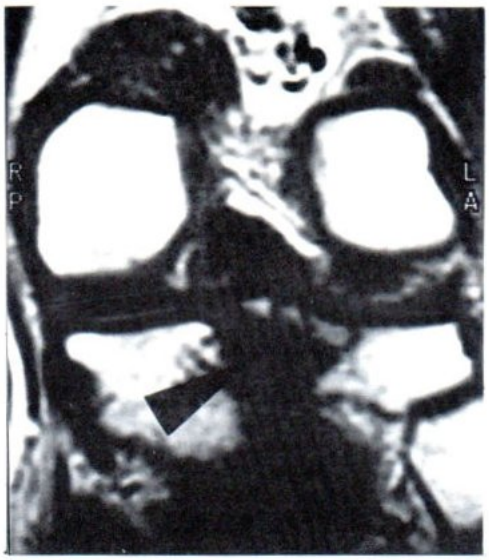

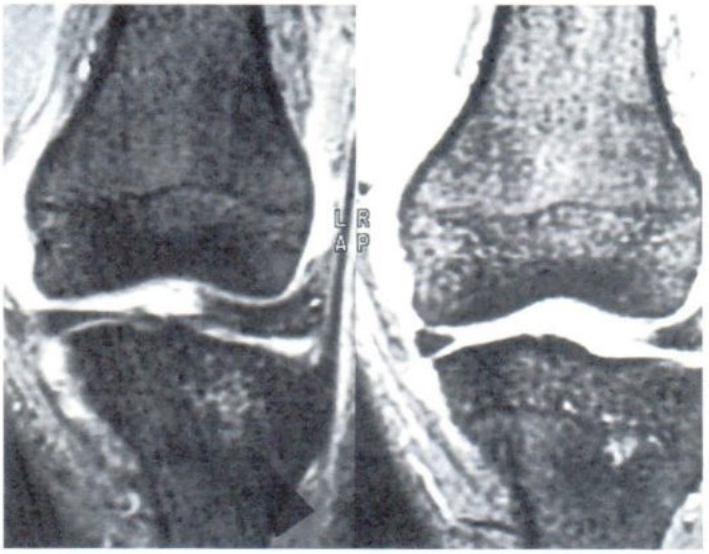

Fig. 3 B. Coronal gradient T_2 WI shows an area of high signal intensity in the tibial plateau representing bone contusion.

REFERENCE

1. Grover JS, Bassett LW, Gross ML, et al. Posterior cruciate ligament:MR imaging. Radiology 1990;174:527-30.
2. Sonin AH, Fitzgeral SW, Friedman H, et al. Posterior cruciate ligament injury:MR imaging diagnosis and patterns of Injury. Radiology 1994;190-455-58.
3. Yu J, Peter Silge C, Sartoris DJ, et al. MR Imaging of injuries of the extensor mechanism of the knee. Radiographics 1994;541-51.
4. Bonamo JJ, Saperstim AL, Contemporary magnetic resonance imaging of the knee: The orthopedic surgeon's perspective. RCNA 1994; 2(3):481-93.
5. Manaster B.J. Magnetic Resonace imaging of the knee:Seminar in US, CT and MR 1990;11:307-26.
6. Sonin AH, Fitzgeral SW, Hoft FL, et al. MR imaging of the posterior cruciate ligament: Normal, abnormal, and associated injury patterns. Radiographic 1995;15:551-61.

THE UNRUPTURED EXTRADURAL INTRACAVERNOUS CAROTID ANEURYSM

Nitat KIATHIRANON[1], Rattana KHUNTIRANON[1],
Upin SANGKUM[2], Anusak LIANGUDOM[3], Patchrin PEKANAN[4].

ABSTRACT

Extradural intracavernous aneurysm of the internal carotid artery was demonstrated in a 48-year old woman who presented with right exophthalmos and total opthalmoplegia. The aneurysm was an unruptured one. Coronal CT scan showed a target sign in the bulging right cavernous sinus. Reports concerning the CT findings of such aneurysm were rare.

INTRODUCTION

Aneurysms that arise from the intracavernous portion of the internal carotid artery may be asymptomatic or may cause dysfunction of the cranial nerves in the cavernous sinus (1,2). Its incidence varied from 5% to 11% (1,3). Bony erosion occurred in about 8% and wall calcification appeared in about one third of them. The internal carotid artery may be displaced or occluded by pressure from the aneurysm. Rupture of one of the these aneurysms into the cavernous sinus may cause a carotid-cavernous sinus fistula. Bilateral aneurysms in this location have been described (1,4).

CASE REPORT

A 48-year-old Thai woman was admitted to Prasat neurologic institute for investigation to find the cause of her right exophthalmos and total ophthalmoplegia which occurred three weeks ago. CNIII, IV, VI and V_1 palsy was noted at physical examination as well as the presence of mild optic disc swelling. Lumbar puncture showed normal findings. CT scan of the brain and orbits and cerebral angiography were performed and illustrated in figure 1-4. At operation an unruptured extradural intracavernous aneurysm of right internal carotid artery was noted and it was clipped successfully.

DISCUSSION

Linsky (4) considered an aneurysm to be intracavernous if it was shown by angiography to arise proximal to the ophthalmic artery. He also included aneurysms at or distal to the ophthalmic artery which found intraoperatively to arise completely within the cavernous sinus.

In published studies, the intracavernous carotid artery aneurysms accounted for 2.5% to 11.5% of all intracranial aneurysms (2,6-9), and were more frequent in female and in older patients, ie, the mean age of patients ranged from 49 to 64 years (10-12), and the female to male ratio ranged from 2:1 to 8:1. Intracavernous carotid artery aneurysms are not likely to rupture and cause subarachnoid hemorrhage. They tend to expand gradually, and symptoms, if they appear, may be caused by mass effect on cranial nerves.

[1] Department of Neuroradiology, Prasat Neurologic Institute, Rajavithi Street, Bangkok 10400, Thailand.
[2] Department of Neuromedicine, Prasat Neurologic Institute.
[3] Department of Neurosurgery, Prasat Neurologic Institute.
[4] Department of Radiology, Ramathibodi Hospital, Bangkok.

They can be classified as traumatic, mycotic or idiopathic. Although occasionally these aneurysms become very large, if they are located wholly within the cavernous sinus, their rupture rate is extremely low. If small intracavernous carotid artery aneurysms rupture, they usually result in a carotid-cavernous fistula (3,14,16,18). The incidence of ruptured aneurysms at the intracavernous portion of the internal carotid artery varies from 0-30% (2,13,14-17).

A previous classification (19,20) related the intracranial internal carotid artery to the anterior clinoid process and separated it into infraclinoid and supraclinoid segments. By inference the infraclinoid segment is extradural. This classification is purely descriptive purposes, but does not distinguish whether a particular aneurysm arises outside or inside the dura. Previous anatomical studies (21-23) have identified the origin of the ophthalmic artery as the point at which the ICA pierces the dura. The ophthalmic origin is intradural in 89% of dissection, lying at the level of penetration of the dura by the ICA in 83%, or within 1 mm distal to this point in 6.5%. In the remaining 11% the artery arises extradurally. Since the ophthalmic artery is clearly visible in most carotid angiograms, its origin serves as a practical landmark of the point at which the ICA becomes intradural. Thus any aneurysm arising from the ICA from a site more than 1 mm proximal to the origin of the ophthalmic artery can reasonably be viewed as extradural (19). Aneurysms arising from this part of the ICA may attain great size, but rarely rupture because their walls are supported by the dura (20).

Not long ago, intracavernous carotid artery aneurysms could be treated only by cervical carotid artery ligation with or without extracranial-intracranial bypass (5,24-26) or by direct surgical repair with cardiac stanstill (27). Acceptable results were obtained by treating cavernous sinus aneurysms with balloon occlusion of the internal carotid artery proximal to the aneurysm (9,28-30) or with balloon embolization of the aneurysm lumen and preservation of the ipsilateral ICA (30). Favorable outcome in patients treated with direct surgical approaches for clipping were also reported (31-35), aneurysmorrhaphy (32-36) or cavernous sinus trapping with saphenous-vein bypass grafting (36-38).

Homogeneously enhanced unilateral bulging of the cavernous sinus is seen in aneurysms of cavernous carotid-ophthalamic artery complex, C-C fistula, meningioma, schwannoma, metastasis (homogenous or perineural) and lymphoma. Angiography is suggested to rule out aneurysm or C-C fistula. A lesion with a homogeneously enhanced center lumen (patent) surrounding hypodense unenhanced area (thrombus) should arouse us to think of an aneurysm as in this presenting case.

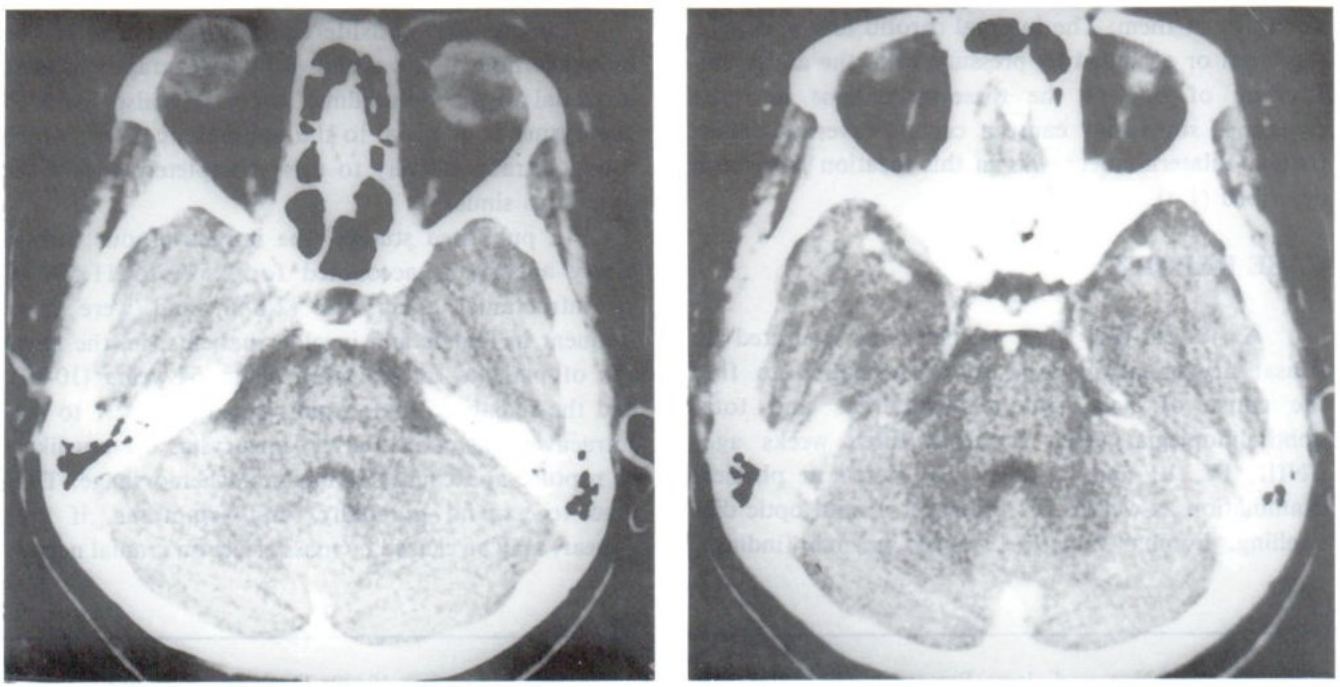

Fig. 1 Pre and post contrast axial CT scan of the brain revealed exophthalmos without bulging of the cavernous sinuses.

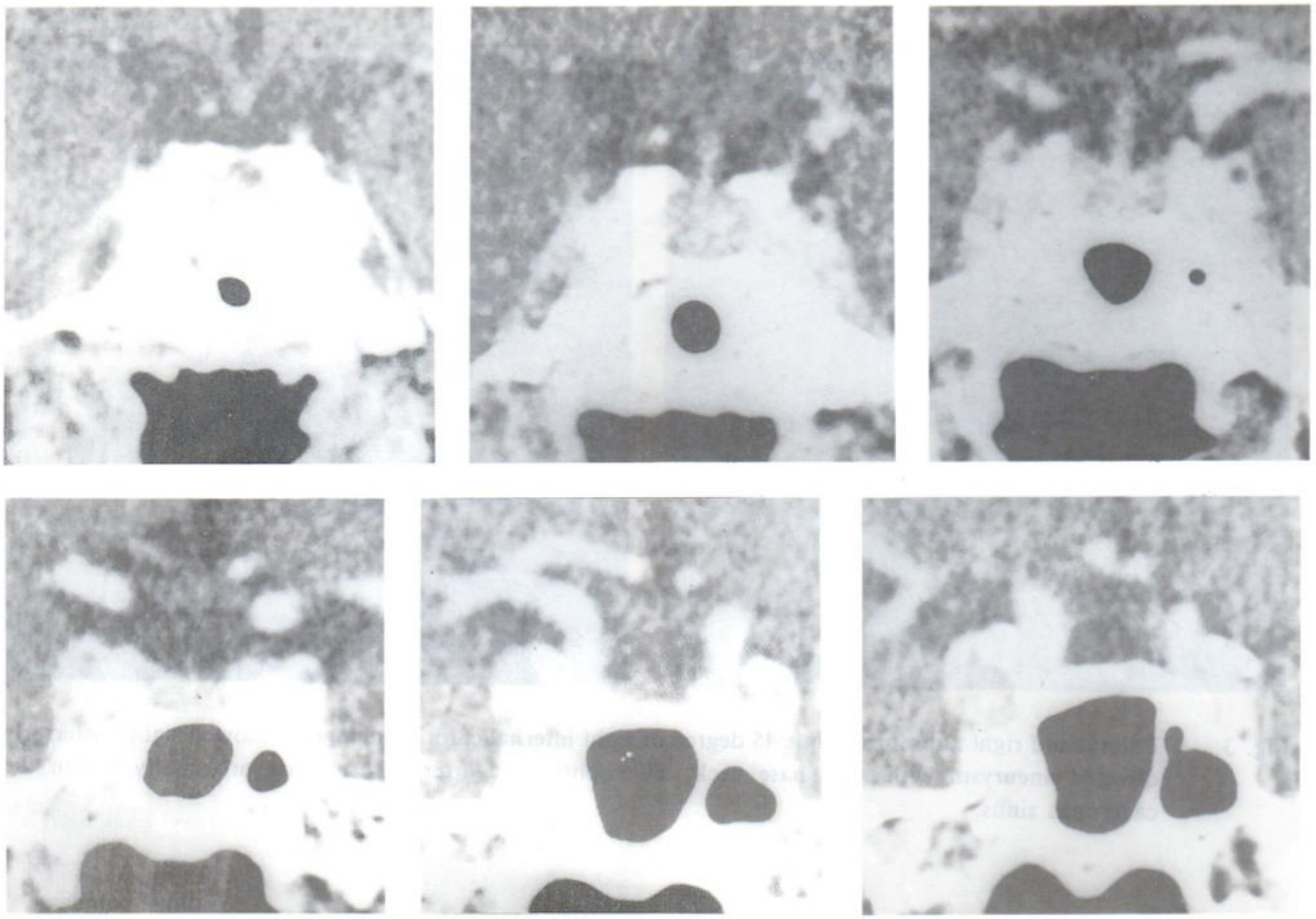

Fig. 2a An outpouching of the right cavernous sinus was noted at coronal enhanced CT scan.

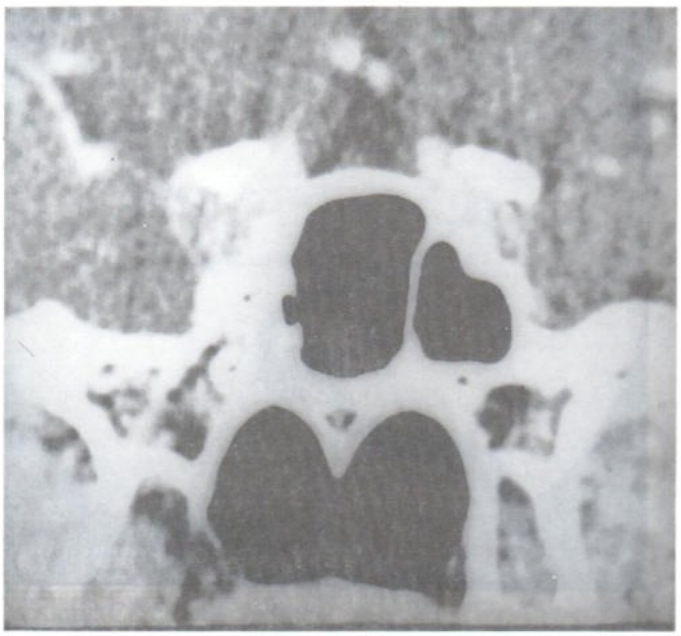

Fig. 2b. A target was seen in the bulging right cavernous sinus. There was no bony erosion or wall calcification

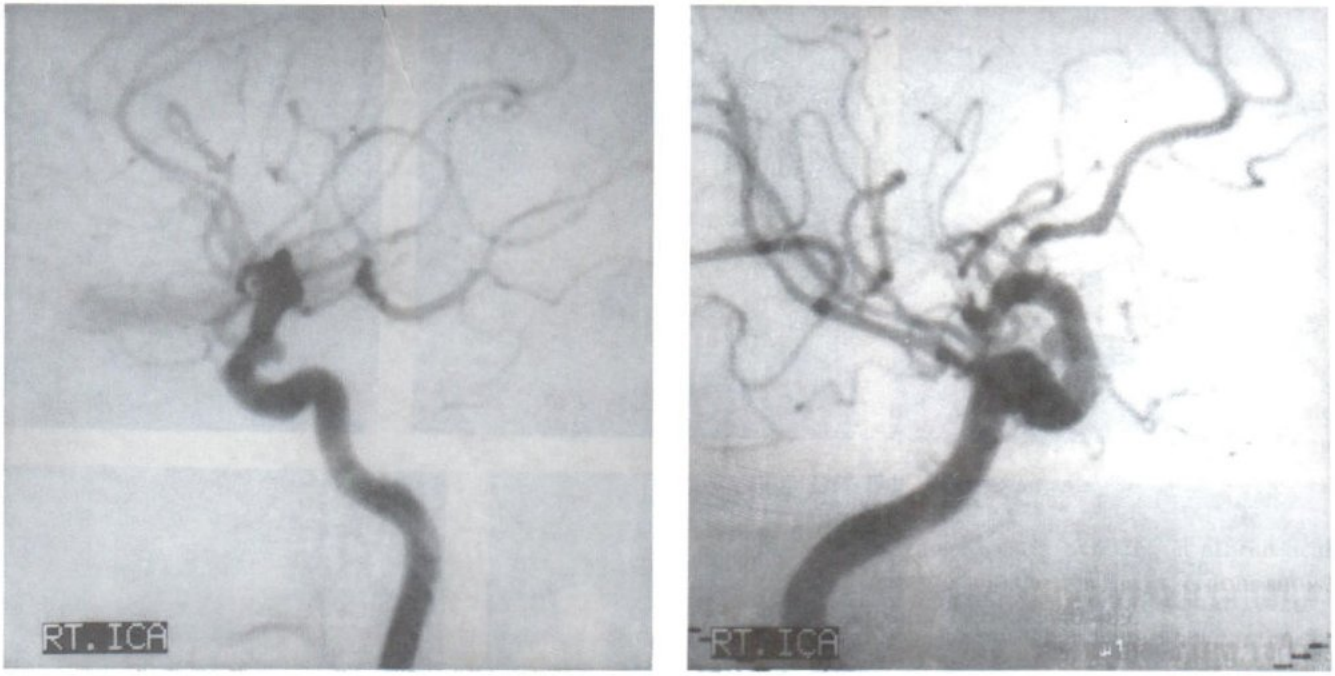

Fig. 3 Lateral and right anterior oblique 45 degree of right internal carotid angiogram showed right posteriorly directed aneurysm with wide base neck. The ophthalmic artery arose more proximally within the cavernous sinus.

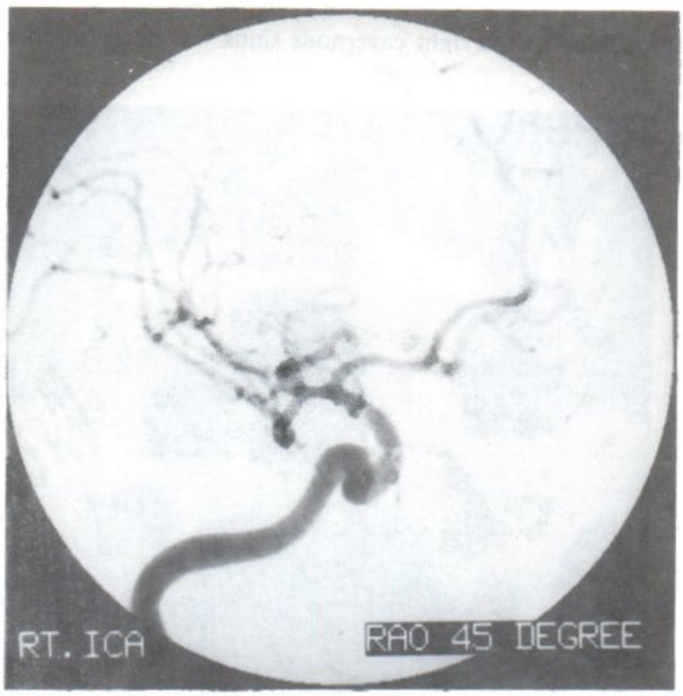

Fig. 4 Ten days-post operative cerebral angiogram showed no narrowing or irregularity of the parent vessel.

REFERENCES

1. Allcock JM. Aneurysms. In:Newton TH, Potts DG., ed Radiology of the skull and brain, St. Louis: CV Mosby, 1974;2451.
2. Barr HWK, Blackwood W. Meadows SP. Intracavernous carotid aneurysms, a clinical pathological report. Brain 1971;94:607-622.
3. Lombardi G, Passerini A, Migliavacca F. Intracavernous aneurysms of the internal carotid artery. Am J Roentgenol Radium Ther Nucl Med 1963;89:361-371.
4. Noterman J, Warszaeski M, Jeanmart L, Brihaye J. Bilateral aneurysm of the internal carotid artery in the cavernous sinus: case report. Neuroradiology 1972;4:63-65.
5. Linsky ME, Sekhar LN, Horton JA, Hirsch WL, Yonas H. Aneurysms of the intracavernous carotid artery: a multidisciplinary approach to treatment. J Neurosurg 1991;75:525-534.
6. Inagawa T. Follow-up study of unruptured aneurysms arising from the C3 and C4 segments of the internal carotid artery. Surg Neurol 1991;36:99-105.
7. Hoddes JE, Fletecher WA, Goodman DF, Hoyt WF. Rupture of cavernous carotid artery aneurysm causing subdural hematoma and death. Case report. J Neurosurg 1988;69:617-9.
8. Pendl G, Vorkapic P, Richling B, Koos WT. Strategies in intracavernous saccular aneurysms. In:Dolenc VV, ed. The cavernous sinus. A multidisciplinary approach to vascular and tumorous lesions. Wien, New York: Springer, 1987:240-51.
9. Scialfa C, Vaghi A, Valsecchi F, Nernardi L, Tonon C. Neuroradiological treatment of carotid and vertebral fistulas and intracavernous aneurysms. Neuroradiology 1982;24:13-25.
10. Ando T, Nakashima T, Shimiqu K, Sakai N, Yamada H. Clinical analysis of large or giant intracavernous aneurysms with reference to long-term results (in Japanese.) Jpn J Stroke 1990;12:185-94.
11. Berenstein A, Ransohoff J, Kupersmith M. Transvascular treatment of giant aneurysms of the cavernous carotid and vertebral arteries: functional investigation and embolization. Surg Neurol 1984;21:3-12.
12. Jefferson G. On the saccular aneurysms of the internal carotid artery in the cavernous sinus. Br J Surg 1938;26:267-302.
13. Linsky ME, Sekhar LN, Hirsch W Jr, Yonas H, Horton JA. Aneurysms of the intracavernous carotid artery:clinical presentation, radiographic features, and pathogenesis. Neurosurgery 1990;26:71-9.
14. Morley TP, Barr HWK. Giant intracranial aneurysms: diagnosis, course, and management. Clin Neurosurg 1969;16:73-94.
15. Whittle IR, Dorsch NW, Besser M. Giant intracranial aneurysms:diagnosis, management, and outcome. Surg Neurol 1984;21:218-30.
16. Jha AN, :Lye RH. Aneurysms of the intracavernous internal carotid artery, outcome following carotid ligation or conservative treatment. In:Proceedings of the international symposium on the cavernous sinus. Ljubjana, Yugoslavia, 1986:413.
17. Dolenc VV, Cerk M, Sustersic J, Pregelj R, Skrap M. Treatment of intracavernous aneurysms of the ICA and CCFs by direct approach. In:Dolenc VV, ed. The cavernous sinus. A multidisciplinary approach to vascular and tumorous lesions. Wien, New York: Springer, 1987:297-310.
18. Obrador S, Gomez-Bueno J, Silvela J. Spontaneous carotid-cavernous fistula produced by ruptured aneurysm of the meningohypophyseal branch of the internal carotid artery. Case report. J Neurosurg 1974;40:539-43.
19. Punt J. Some observations on aneurysms of the proximal internal carotid artery. J Neurosurg 1979;51:151-154.
20. Dilenge D. Feon M: the internal carotid artery, in Newton TH, Potts DG (eds): Radiology of the skull and Brain, Volume II, Book 2. St. Louis: CV Mosby, 1974;pp 1202-1245.
21. Hayreh SS. Arteries of the orbit in the human being. Br J Surg 1963;50:938-953.
22. Hayreh SS, Dass R: The ophthalmic artery. I Origin and intra-cranial and intra-canalicular course. Br J Ophthalmol 1962;46:65-98.
23. Renn WH, Rhoton AL Jr. Microsurgical anatomy of the sellar region. J Neruosurg 1975;43:288-298.
24. Gelber BR, Sundt TM Jr. Treatment of intracavernous and giant carotid aneurysms by combined internal carotid ligation and extra to intracranial bypass. J Neurosurg 1980;52:1-10.
25. Little JR, Rosenfield JV, Awad IA. Internal carotid artery occlusion for cavernous segment aneurysm. Neurosurgery 1989;25:398-404.

26. Silvani V, Rainoldi F, Gaetani P, et al. Combined STA/MCA arterial bypass and gradual internal carotid artery occlusion for treatment of intracavernous and giant carotid artery aneurysms. Acta Neurochiur 1985;78:142-147.
27. Parkinson D. Surgical approach to cavernous sinus aneurysms, in Pia HW, Langmaid C, Zierski I (eds): Cerebral aneurysms. Advances in diagnosis and therapy. Berlin: Springer-Verlag 1979;pp 224-228.
28. Berenstein A, Ransohoff J, Kupersmith M, et al. Transvascular treatment of giant aneurysms of the cavernous carotid and vertebral arteries. Functional investigation and embolization. Surg Neurol 1984;21:3-12.
29. Fox AJ, Vinela F, pelz DM, et al, Use of detachable balloons for proximal artery occlusion in the treatment of unclippable cerebral aneurysms. J Neurosurg 1987;66:40-46.
30. Higashida RT, Halbach VV, Dowd C, et al. Endovascular detachable balloon embolization therapy of cavernous carotid artery aneurysms: results in 87 cases. J Neurosurg 1990;72:857-863.
31. Diaz FG, Ohaegbulam S, Dujovny M, et al. Surgical alternatives in the treatment of cavernous sinus aneurysms. J Neurosurg 1989;71:846-853.
32. Dolenc V. Direct microsurgical repair of intracavernous vascular lesion. J neurosurg 1983;58:824-831.
33. Dolenc V. Surgery of vascular lesions of the cavernous sinus. Clin Neurosurg 1988;36:240-255.
34. Perneczky A, Knosp E, Vorkapic P, et al. Direct surgical approach to infraclinoid aneurysm. Acta Neurochir 1985;76:36-44.
35. Strother Cm, Lunde S, Graves V, et al. Late paraophthalmic aneurysm rupture following endovascular treatment. Case report. J Neurosurg 1989;71:777-780.
36. Sekhar LN, Linskey ME, Sen CN, et al. Surgical management of lesions within the cavernous sinus. Clin Neurosurg 1991;37:440-489.
37. Diaz FG, Ohaegbulam S, Dujovny M, et al. Surgical alternatives in the treatment of cavernous sinus aneurysms. J Neurosurg 1989;71:846-853.
38. Sekhar LN, Sen CN, Jho HD. Saphenous vein graft bypass of the cavernous internal carotid artery. J Neurosurg 1990;35-41.

GIANT SURPRISE! : A GIANT INTRACRANIAL ANEURYSM MIMICKING A MENINGIOMA ON CT

ONG TEONG OON MBBS(MAL) *

GNANA KUMAR FRCR, MMED(RAD) **

ABSTRACT

An adult male presented with symptoms and signs of an intracranial space occupying lesion(SOL). Computed tomography performed revealed an enhancing left parasellar mass which led to the provisional diagnosis of meningioma. However, as a giant aneurysm was considered in the list of differential diagnosis, a 4 vessel cerebral angiogram was done. This revealed a 7cm. giant aneurysm of the left internal carotid artery, and thus illustrates the importance of angiography in the evaluation of enhancing parasellar masses.

Key words : Giant Intracranial Aneurysm, Meningioma, Computed Tomography

INTRODUCTION

In the evaluation of sella and parasellar lesions, computed tomography(CT) scan has long been a recommended imaging modality. It has proved reliable for detecting or ruling out the presence of a mass and in assessing tumour extension (1 & 2). It was also pointed out that angiography is occasionally necessary in some of these cases to rule out an aneurysm before subjecting patients to craniotomy. A few other reports later supported the fact that the differentiation of a giant intracranial aneurysm(GIA) from an intracranial neoplasm can be difficult based on CT findings alone and further evaluation with angiograms should always be considered (3 & 4). We report a patient with GIA of the left internal carotid artery who was diagnosed as a parasellar meningioma on the basis of CT appearences. The diagnosis of a GIA was subsequently confirmed on angiogram.

CASE REPORT

A 42 year old male carpenter presented to the University Hospital with headache and visual abnormality of 4 months' duration. He noted that his headache started in the morning upon awakening and was persistent throughout the day. Over the past 4 months, it had progressively become more severe and was beginning to disturb his daily activities and sleep. At the same time, he also complained of a slowly progressive decrease in visual acuity of his left eye and he could not see things on his far right. He had been well before this and a review of systems revealed no further significant history. On general examination, he was a slightly agitated man who appeared distressed by his headache. Neurological examination showed normal third to twelfth cranial nerves. His muscle power and sensation were also normal. He had visual acuity of 6/6 on the right and

* Medical officer department of Radiology University Hospital

** Lecturer department of Radiology University Hospital

Correspondence : GNANA KUMAR FRCR MMED(RAD) Department of Radiology University Hospital 50603 Kuala Lumpur

6/12 on the left. Both pupils were equal in size and reactive to light and examinations of the fundi were normal. Visual field testing by confrontation revealed a right temporal and a left nasal field defect. Routine blood tests and plain skull radiographs were unremarkable. Pre and post contrast CT scan performed in 5mm contiguous slices of the posterior fossa and 10mm for the rest of the brain on the patient revealed a well-defined extra axial mass in the left parasellar region (figure 1 & 2). It was slightly hyperdense compared to normal brain tissue on pre contrast scans and showed intense homogenous enhancement after intravenous administration of contrast. There was no perifocal oedema, mass effect, calcification or surrounding bony hyperostosis seen. Based on these findings, a provisional diagnosis of left parasellar meningioma was made. Four vessel angiography performed a few days later revealed a 7 cm giant aneurysm arising from the suprasellar portion of the left internal carotid artery (figure 3 & 4). At surgery the aneurysm was noted to have a broad neck beginning at the supraclinoid portion of the internal carotid artery and extending to the anterior cerebral-middle cerebral artery bifurcation. The sac was adherent to the third cranial nerve and the majority of it was not thrombosed. clipping of the aneurysm was done.

DISCUSSION

Giant Intracranial Aneurysms(GIAs) are aneurysms greater than 2.5cm in size (5). They constitute 0.2 to 5% of all intracranial aneurysms and most commonly arise from the internal carotid artery (5 & 6). In contrast to smaller intracranial aneurysms which usually present with subarachnoid haemorrhage, GIAs rarely bleed and often present with symptoms of an expanding mass (5). As a result of compression effects, GIAs in the suprasellar portion of the internal carotid artery are known to cause visual field defects due to the close vicinity of the optic pathways (7,8 & 9). In a patient who presents with neuro-ophthalmological abnormalities, radiological evaluation that follows will usually

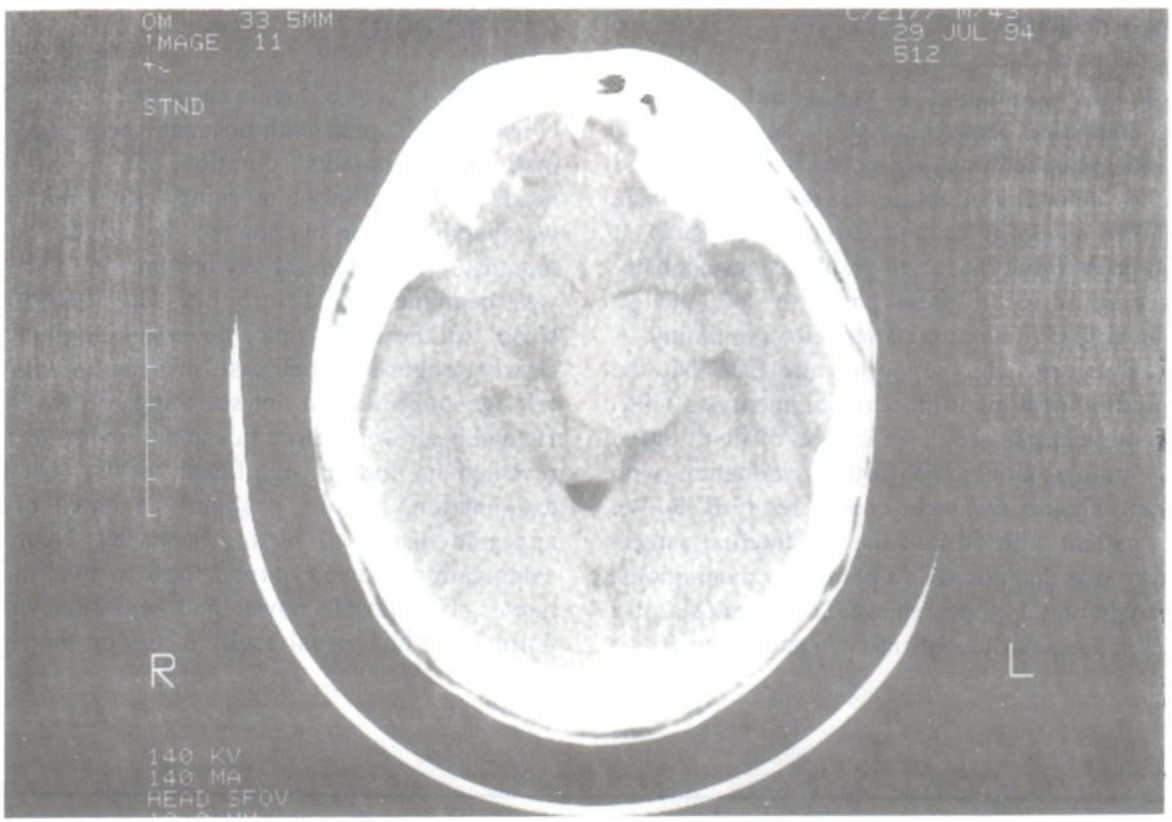

Fig. 1 Pre contrast CT scan of the brain showing a well defined hyperdense mass in the left parasellar region.

include a CT scan of the brain. Owing to its large size, a GIA can be easily seen on CT scan as a space occupying lesion (SOL). In non enhanced scans it appears as a well-circumscribed extra axial mass with density higher than that of the normal brain parenchyma. There should be no surrounding oedema but bony erosion may be present as a result of prolonged pressure. Scan done immediately following intravenous contrast would demonstrate diffuse uniformed enhancement, unless thrombosis is present within the aneurysm (4). In these cases, there may be no enhancement or it may be confined to the periphery,giving rise to the "rim-like" pattern of enhancement.

On CT scanning, non thrombosed GIAs may be confused with intracranial neoplasms such as meningiomas, neurinomas, and gliomas. In the parasellar region, meningiomas are probably the greatest mimic as they exhibit CT features and enhancement characteristics very similar to that of GIAs. They are also not uncommonly found in this location, constituting about 15% of all meningiomas (10). One important feature to look for in differentiating a meningioma from a GIA is the presence of surrounding bony hyperostosis. Some authors have quoted incidence of as hihg as 90% in meningioma, although some are only seen retrospectively (11). Another method of differentiation that has been described is using dynamic sequential scanning following a bolus of intravenous contrast. The density of an aneurysm increases with the circulating contrast medium, then falls, while that of the meningioma rises more gradually as the contrast medium leaks from the capillaries, and it remains dense longer (12).

Magnetic Resonance Imaging (MRI) where available show a complex but characteristic appearence because of the presence of blood in the aneurysm. A flow void is usually present in the centre of the aneurysm on both T1 and T2 weighted sequences. Low signal intensity on all pulse sequences is characteristic for fast or turbulent blood

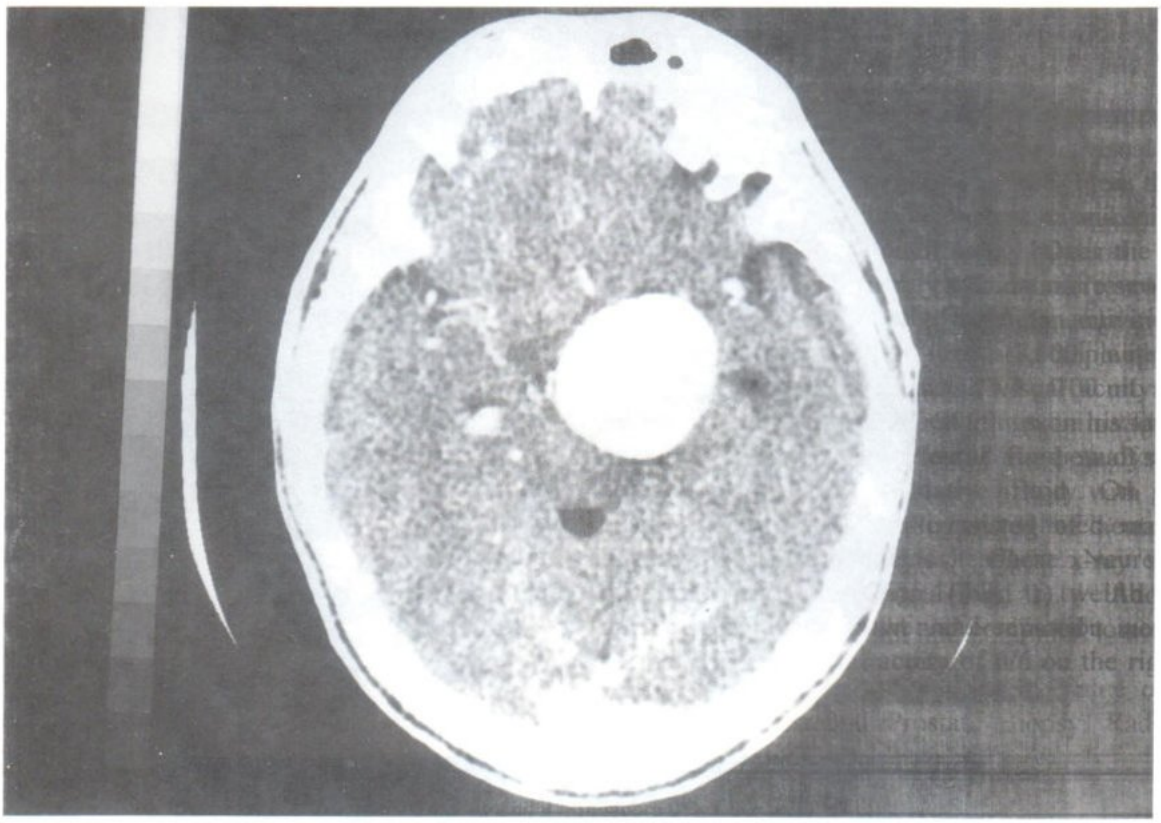

Fig. 2 Following intravenous contrast media, there was intense homogenous enhancement of the mass.

flow and thus allowing for differentiation of an aneurysm and a solid tumour. 2D Time Of Flight (TOF) Magnetic Resonance Angiography and Phase Contrast (PC) techniques are however better for demonstrating the slow flow in the lumen of large aneurysms (13).

However, in the absence of MRI and definite differentiating features previously described, a GIA can easily be mistakenly diagnosed as a meningioma on standard pre and post contrast CT scanning. This case illustrates that angiography continue to have a place in the evaluation of an enhancing parasellar mass and should always be considered so as to avoid an unpleasant giant surprise on the operating table.

REFERENCES

1. Leeds NE, Naidich TP. Computerized tomography in diagnosis of sellar and parasellar lesions. Semin Roentgenol 1977; 12: 121-135
2. Naidich TP, Pinto RS, kushner MJ et al. Evaluation of sellar and parasellar masses by computed tomography. Radiology 1976; 120: 91-99.

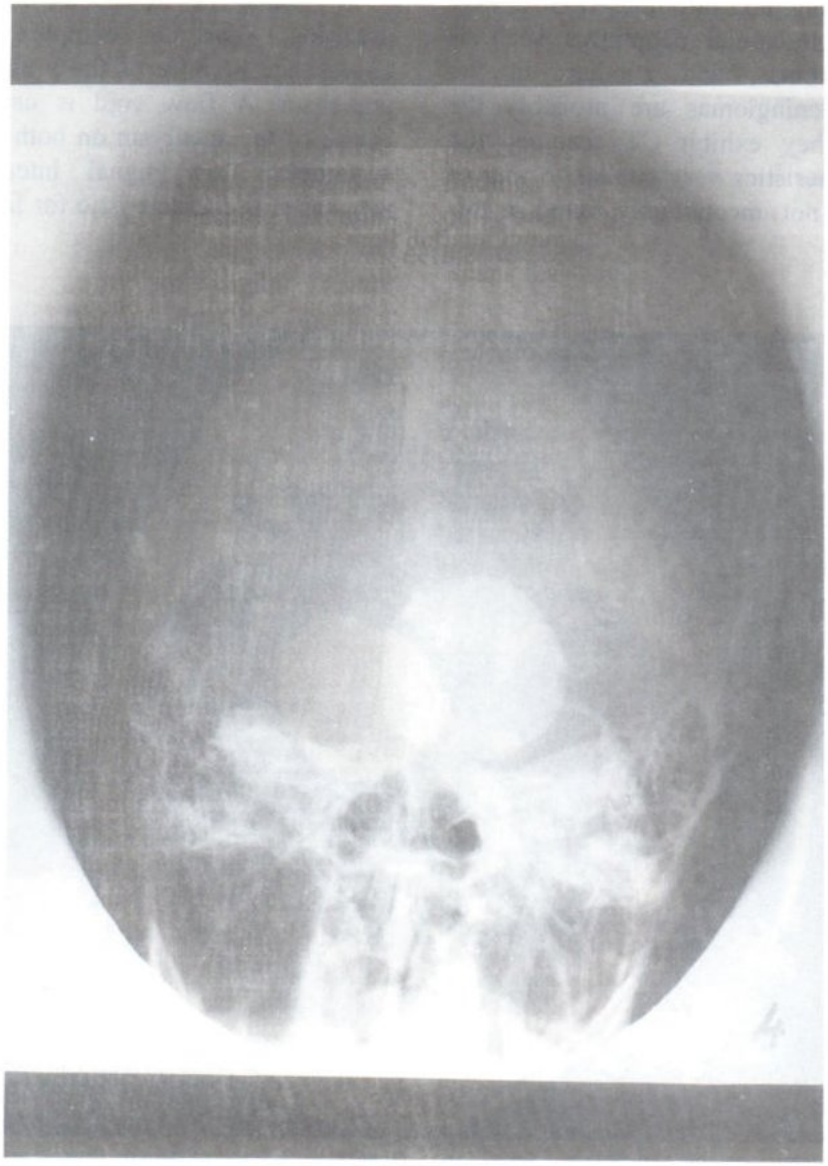

Fig. 3 Towne's view of the left internal carotid angiogram showing a giant aneurysm in the suprasellar portion.

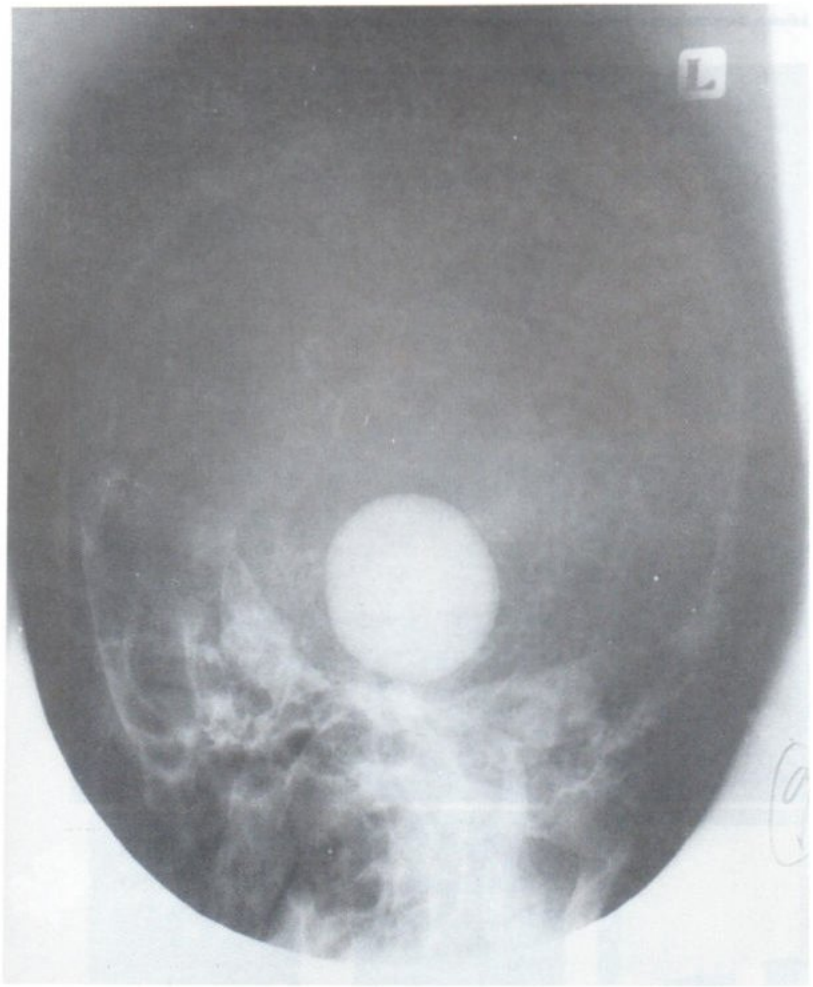

Fig. 4 Oblique view of the giant left internal carotid aneurysm.

3. Byrd SE, Bentson JR, Winter J et al. Giant intracranial aneurysm simulating brain neoplasm on CT. J Comput. Assist Tomogr 1978; 2: 303-307
4. Kokoris N, Rothman LM, Wolintz AH. Computed tomography and angiography in the diagnosis of suprasellar mass lesions. Am. J Ophthalmol 1980; 89: 278-283.
5. Morley TP, Barr HWK. Giant intracranial aneurysms : Diagnosis, course and management. Clin, Neurosurg 1968; 16: 73-94.
6. Sundt TM Jr, Peipgras PG. Surgical approach to giant intracranial aneurysms : Operative experience with 80 cases. J Neurosurg 1979; 51: 731-42.
7. Norwood EG, Kline LB, Chandra-Sekar B. et al. Aneurysmal compression of the anterior visual pathway. Neurology 1986; 36: 1035-41.
8. Berson EL, Freeman MI, Gay AJ. Visual defects in giant suprasellar aneurysms of the internal carotid. Arch Ophthal 1966; 76:52-58.
9. Peiris JB, Russell RWR. Giant aneurysms of the carotid system presenting as visual field defect. J Neurosurg Psychiatry 1980; 43: 1053-64.
10. Hirsh WL, Jr,Roppolo Hmn, Hayman LA et al. Sella and parasellar region : pathology In : Latchaw RE eds. MR and CT imaging of head, neck and spine, 2nd. ed, vol 2. St Louis : Mosby Year Book, 1991 : 683-741.
11. Lane B, Moseley IF, Theron J. Cranial and intracranial pathology (2). In : Grainger RN, Allison DJ Eds. Diagnostic Radiology 2nd. eds. vol 3. Edinburgh : Churchill Livingstone 1992 : 1965-2000
12. Moseley IF, Sutton D, Kendel B et al. Intracranial lesions (2). In : Sutton D. Textbook of radiology and medical imaging. 5th. eds. Vol 2. Edinburgh : Churchill Livingstone 1993 : 1537-1577.
13. Runge VM. MRI of the Brain. Philadelphia : J.B. Lippincott Co. 1994 : 406-407

SHIMADZU

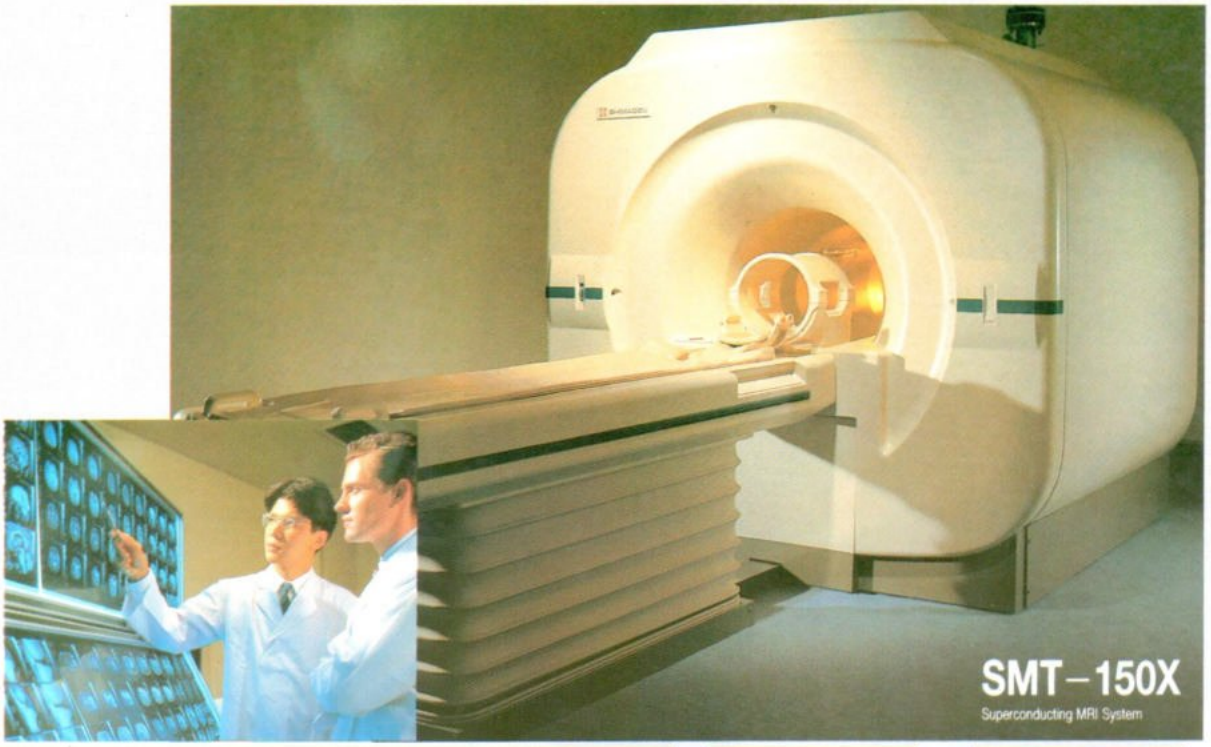

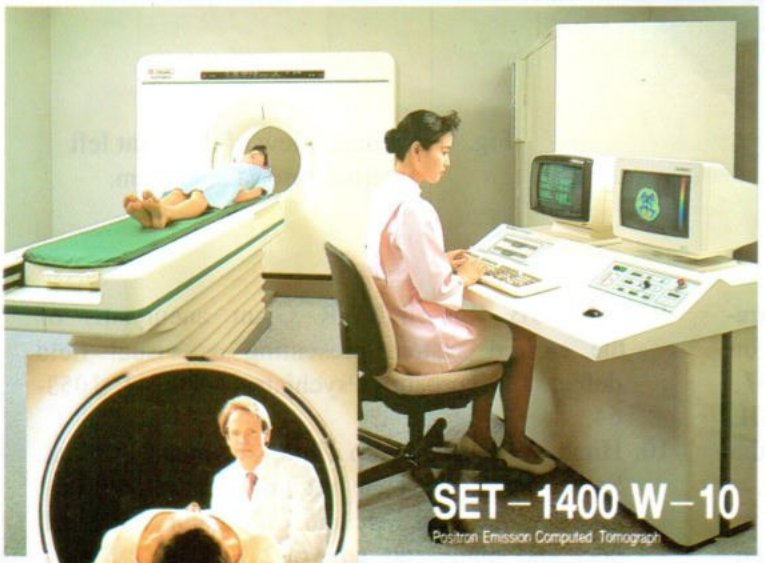

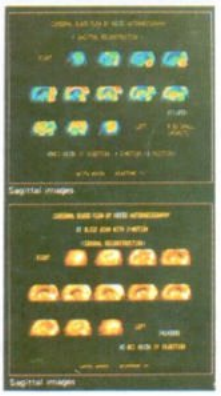

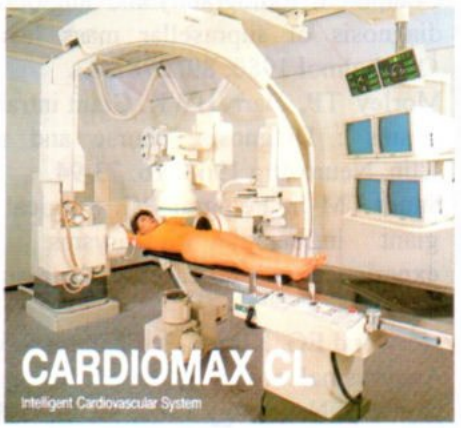

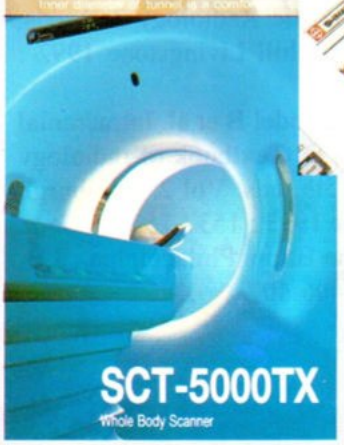

SOLE DISTRIBUTOR :

INTERNATIONAL COSMETICS CO., LTD.

757/10 Soi Pradoo 1, Sathupradit Road, Yannawa, Bangkok. **10120**

Tel. **2949541, 2940294** (Ext. **264, 273**) Telefax : **2949541**

MIDDLE CEREBRAL ARTERY PSEUDOANEURYSM POST GUN-SHOT WOUND

Patchrin PEKANAN[1], Thitiporn RANGSITPOL[1,2], Wiwatana THANOMKIAT[1,3], Sopon KUMPOLPUNTH[1].

ABSTRACT

A pseudoaneurysm of the genu of left middle cerebral artery was demonstrated by i.v. enhanced CT scan and by left carotid angiography after a gun shot wound in a 31 year-old man. The contrast leak was seen at the angiographic injection. The active bleeding was noted in the unenhanced CT brain scan. The traumatic pseudoaneurysm of the middle cerebral artery was considered rare.

INTRODUCTION

Intracranial vascular injury could result in post-traumatic brain infarction, pseudoaneurysm, arteriovenous fistula, and venous thrombosis (1). Intracranial pseudoaneurysm are relatively rare after head injury in adults (1,2). In children, it is reported to account for 11% of all pediatric cases of aneurysm (3). The traumatic pseudoaneurysms have a propensity to hemorrhage. It can develop immediately or over a period of months to years. The most common time for presentation is 2 to 8 weeks after trauma.

CASE REPORT

A 31 year-old male patient was shot at the left part of the head and the bullet came out from his right cheek. The incident occurred on December 24, 1994. The clot was removed from his left cerebral hemisphere at a private hospital. He was referred to the Ramathibodi Hospital on December 27, 1994 with good consciousness. He was confused on that night with right hemiparesis. The consciousness was deteriorated progressively. On January 1, 1995. CT scan was performed and showed a round enhanced focus at the anterior left temporal lobe within the surrounding contusive hematoma (Fig. 1). Left corotid angiography was thus proceeded and showed contrast leakage from left middle cerebral artery at the genu area of this vessel.

Craniotomy was performed but the bleeding could not be controlled and left common carotid artery ligation was performed. A pseudoaneurysm was found at genu of left middle cerebral artery. The patient, however, did not survive.

DISCUSSION

Development of a false saccular aneurysm is usually secondary to a disruption in the continuity of the arterial wall. A periarterial hemorrhage forms and is contained by the fascia. During systole, arterial blood pressure forces blood into the periarterial region. Blood accumulates at the site of the leak until the extra arterial pressure equals the mean arterial pressure. During diastole blood tends to return into the vessel

[1] Department of Radiology, Ramathibodi Hospital, Rama 6 Street, Bangkok 10400, Thailand.
[2] Department of Radiology, Phrapinklao Hospital, Bkk.
[3] Department of Radiology, University of Songklanakarin, Songkla.

lumen. The periarterial hemorrhage clots and then retracts. The center of the clotted hematoma becomes cavitated and thus communicates with the arterial lumen. The fibrotic reaction produced in the surrounding tissues forms a wall of the pseudoaneurysm (6).

On angiography, a traumatic pseudoaneurysm frequently has an irregular contour and a wide or nonexistent aneurysmal neck. This is because the wall of the aneurysm actually represents an encapsulated hematoma in communication with the artery. Occasionally, the adventitia remains intact. Therefore, the wall of the pseudoaneurysm offers little structural support unless it is surrounded by firm structures such as bone, ligaments, or dura. A pseudoaneurysm can spontaneously thrombose and even calcify in the chronic phase. Angiography underestimates the true size of a partially or totally thrombosed aneurysm because it visualizes only the patent lumen. The opacified portion of a partially thrombosed aneurysm can be considerably smaller than the size of the mass that is seen on CT and MR images (1).

Burton (7,8) classified the traumatic aneurysms according to the type of vascular trauma and the type of aneurysm produced, grouped as follows:(a) true aneurysm-partial dilatation resulting from partial disruption of the arterial wall (b) false aneurysm-cavity of an encapsulated hematoma communicating with the lumen of the artery (c) mixed aneurysm-caused by rupture of the true aneurysm giving rise to a secondary false aneurysm.

Post traumatic aneurysms can enlarge rapidly. As in our case, the false aneurysm appeared 7-8 days after trauma. MRI immediately after the shot wound revealed no aneurysm.

The location of a pseudoaneurysm is related to the path of penetrating trauma, the vascular suspensory points of the brain, and vascular contiguity with the edges of the dura (1,4). Although traumatic pseudoaneurysms of the ICA usually involve the cavernous segment, the supraclinoid, intrapetrous, and upper cervical segments can also be affected. A pseudoaneurysm in these locations is frequently associated with an anterior basilar skull fracture. When the common carotid artery or the lower cervical portion of the ICA is injured, the cause in usually a gunshot wound or blunt trauma to the neck (9). Branches of the ACA, especially the callosomarginal and posterior internal frontal arteries, can be injured because of their close relationship to the falx and corpus callosum. More proximally located traumatic pseudoaneurysms of the MCA and PCA are extremely rare (1). Traumatic pseudoaneurysms occasionally involve the peripheral cortical vessels or the meningeal vessels secondary to penetrating trauma or an adjacent skull fracture (7). A MCA pseudoaneurysm has been reported to follow needle puncture aspiration of a subdural hematoma (5). A skull fracture can also result in a pseudoaneurysm of an extracranial vessel, especially the superficial temporal artery.

REFERENCES

1. Gean AD. Imaging of head trauma. New York, Raven Press; 1994.
2. Davis JM, Zimmerman RA. Injury of the carotid and vertebral arteries. Neuroradiology 1983; 25:55-69.
3. Harwood-Nash DC, Fitz CR. Neuroradiology in infants and children. St. Louis, CV Mosby; 1976.
4. Thompson JR, Harwood-Nash DC, Fitz CR. Cerebral aneurysms in children AJR 1973;118:163.
5. Overton MC, Calvin TH Jr. Iatrogenic cerebral cortical aneurysm: case report. J Neurosurg 1966;24:672-675.
6. Davis JM, Zimmerman RA. Injury of the carotid and vertebral arteries. Neuroradiology 1983; 25:55-69.
7. Rumbaugh CL, Bergeron RT, Talalla A. Kurze T. Traumatic aneurysms of the cortical cerebral arteries. Radiology 1970;96:49-54.
8. Burton C, Velasco F, Dorman J. Traumatic aneurysm of a peripheral cerebral artery. Review and case report. J Neurosurg 1968;28:468-474.
9. Mokri B, Piepgras DC, Sundt Tm Jr, Pearson BW. Extracranial internal carotid artery aneurysms. Mayo Clin Proc 1982;57:310-321.

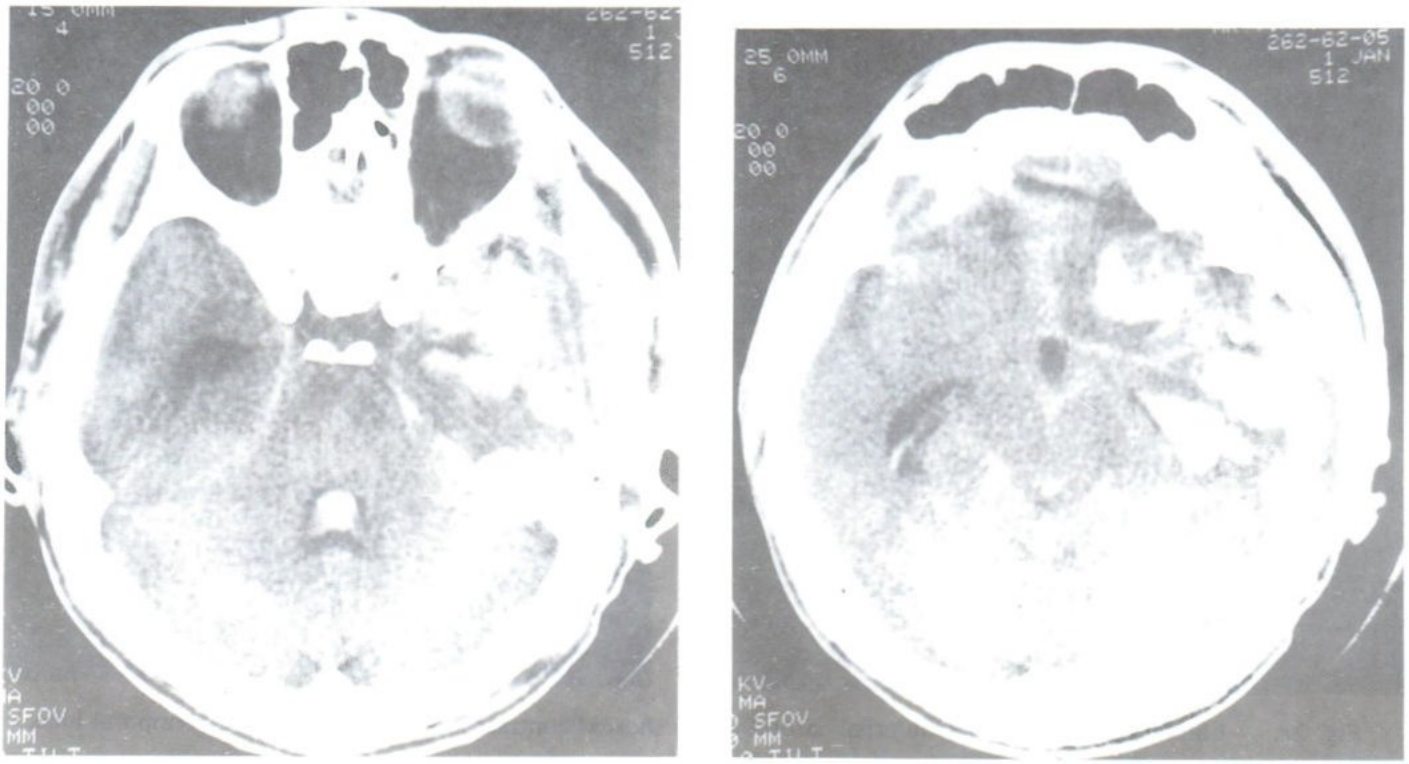

Fig. 1A Non contrast CT scan of the brain showed contusive hematomas at left temporal lobe; a left parietotemporal craniotomy was done.

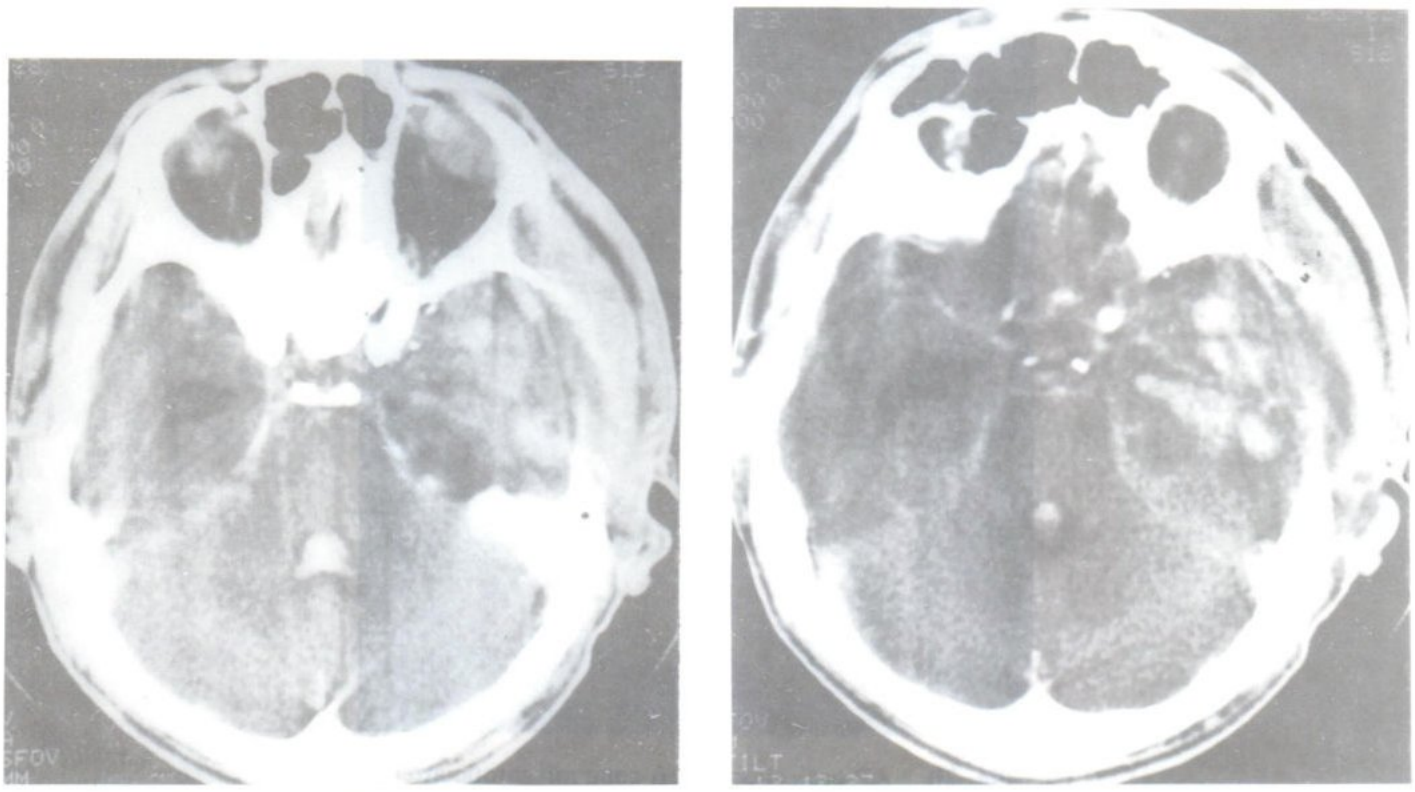

Fig. 1B Post contrast CT scan of the brain showed a nodular enhancement at the mid anterior left temporal lobe.

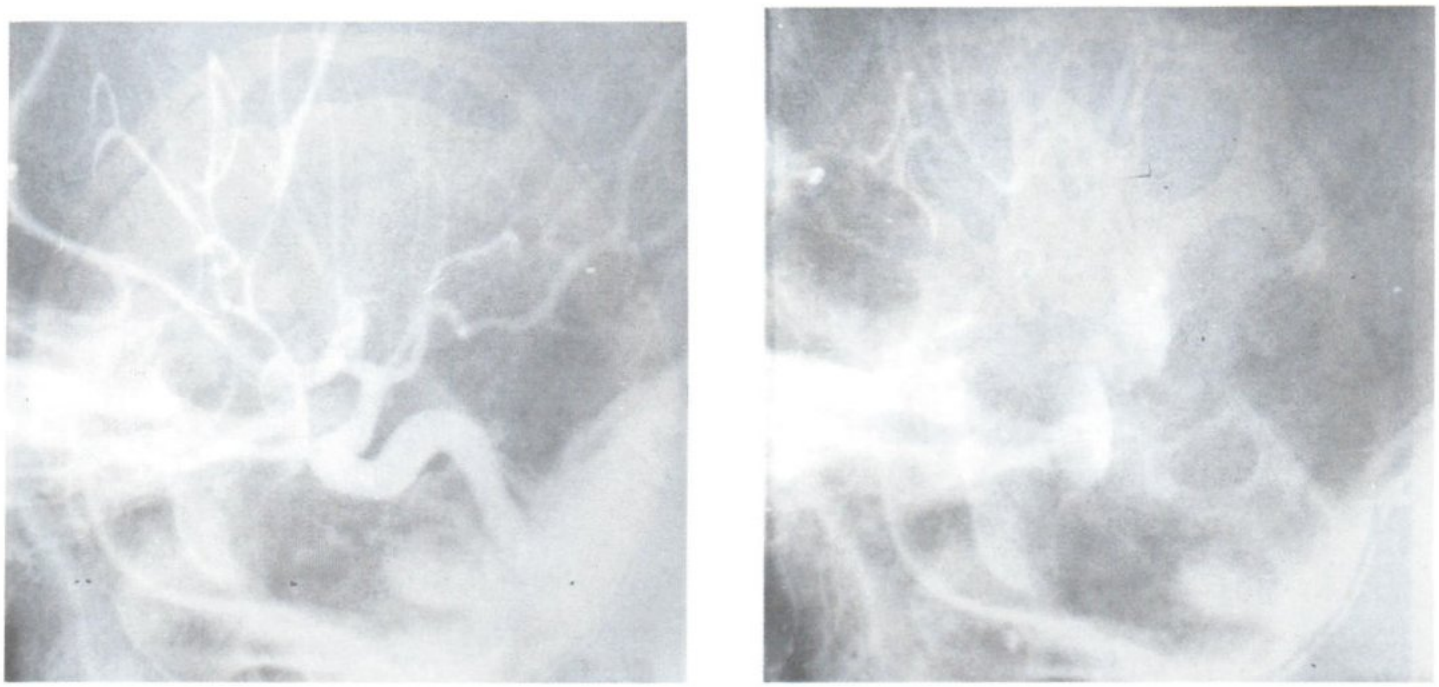

Fig. 2A Lateral projection of left internal carotid artery showed contrast leakage at left anterior temporal lobe.

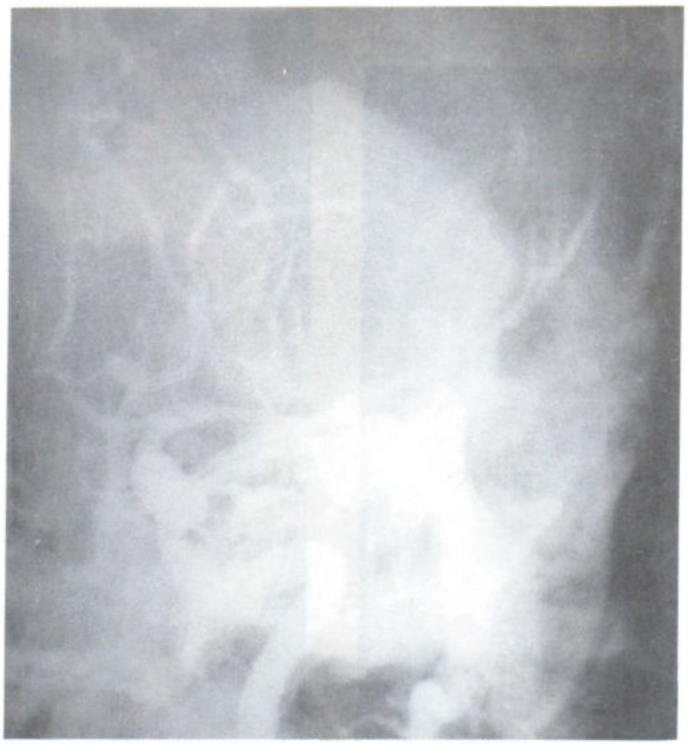

Fig. 2B. AP projection of left common carotic artery injection showed narrowing lumen at around genu portion of left middle cerebral artery.

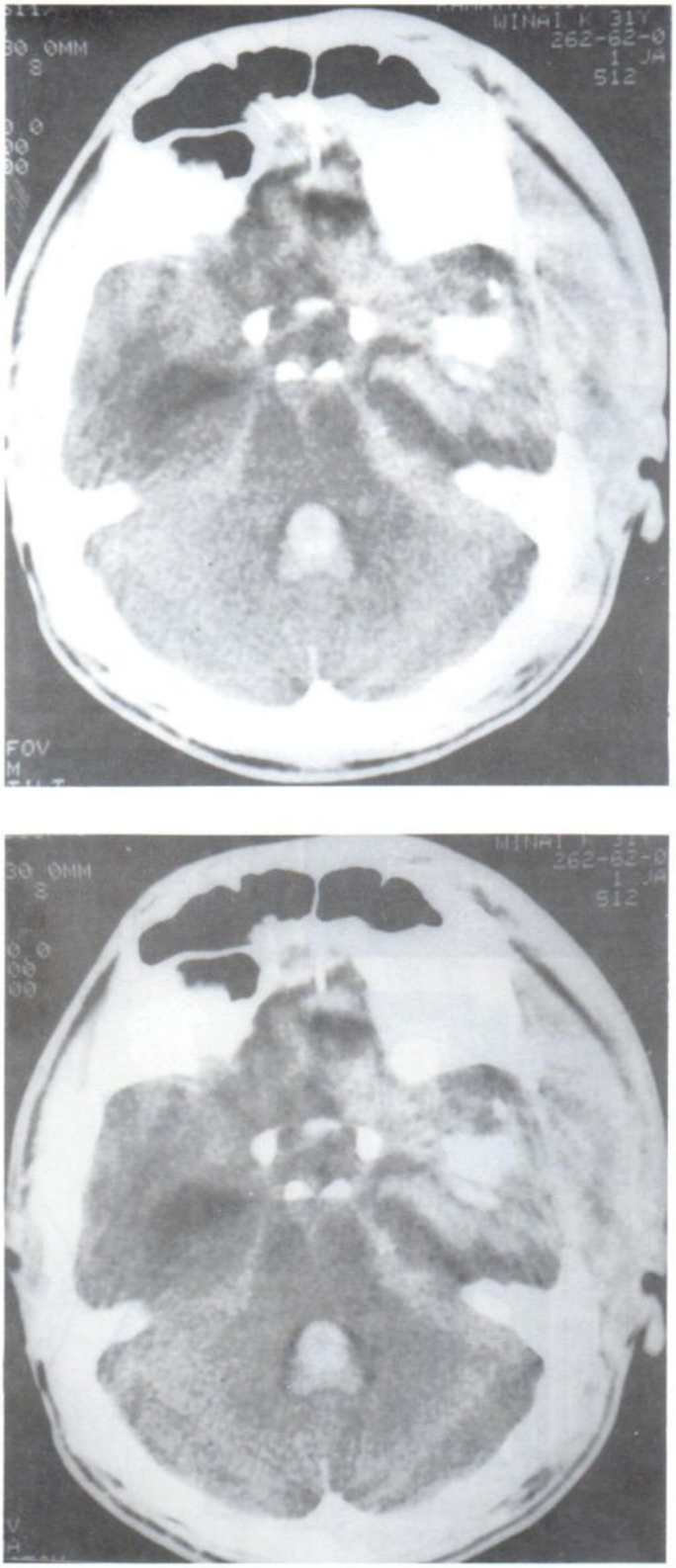

Fig. 2C Dense contrast leakage was shown by post angiographic CT scan at left temporal lobe.

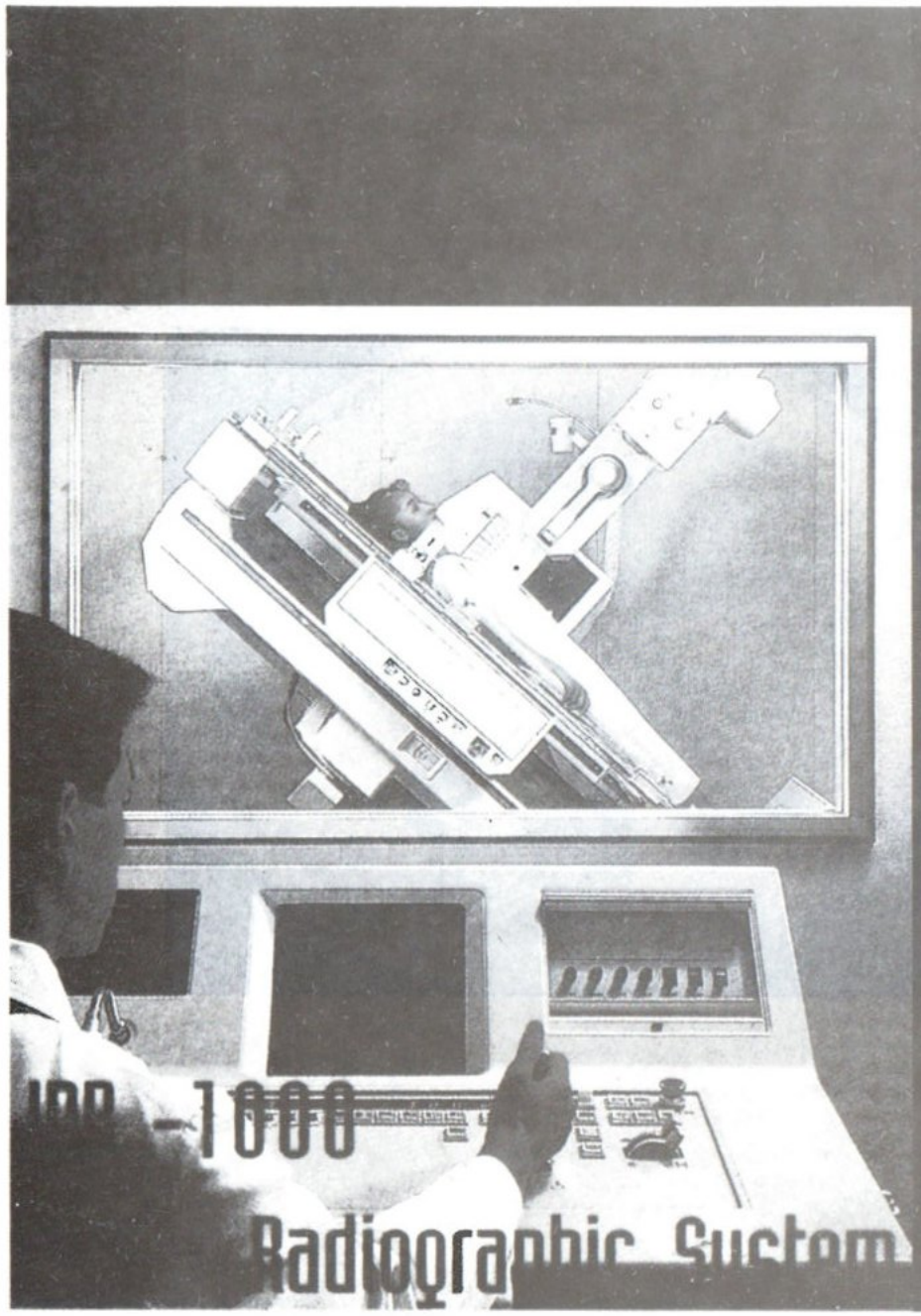

SHIMADZU

INVERTERTYPE Mobile X-ray system

SCT-4800T WHOLE BODY CT SCANNER

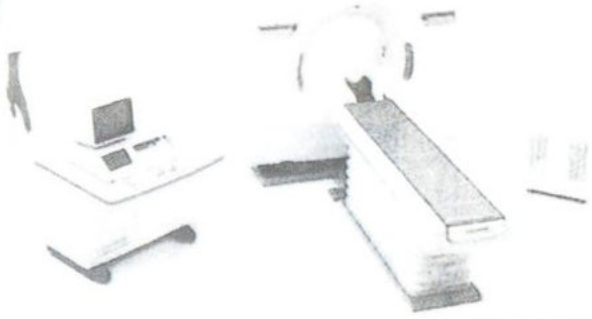

MAGNETIC RESONANCE IMAGING

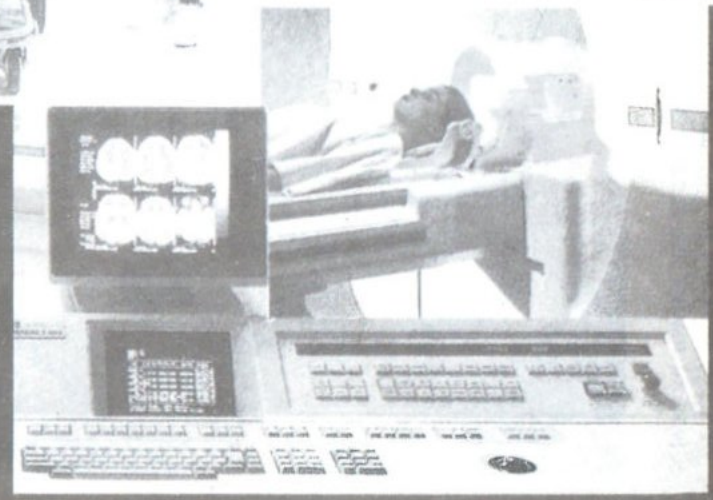

บริษัท รังสิภัณฑ์ จำกัด

RADIOLOGICAL EQUIPMENT CO.,LTD.

170-172/1 (ชั้น 2-3) ถนนบริพัตร ป้อมปราบ กรุงเทพฯ 10100

170-172/1 (Floor 2-3) BORIPHAT ROAD BANGKOK 10100 THAILAND

TEL: 2212386,2237954,2239791,2243402 TELEFAX: (02) 2251657

MENKES SYNDROME

Patchrin PEKANAN, Sirintara PONGPECH, Siriporn THANAMEE

ABSTRACT

Menkes syndrome was reported in a 4-month-old boy. The patient had a seizure problem and recurrent urinary tract infection. His serum copper and cereluplasmin was very low. Imaging study showed bladder diverticuli by voiding cystography, brain atrophy by CT and MRI, bizarre elongation and kinking of the intracranial arteries by MRI and MRA.

INTRODUCTION

Menkes syndrome is a rare x-linked recessive disorder, first described by Menkes et al in 1962 (1,2). The gene defect is located near Xcen. Its synonyms are Kinky hair syndrome, trichopoliodystrophy, steely hair disease and copper transport disease. Clinical manifestations (1) are 1) sparse, stubby, twisted, and fractured hairs; variation in diameter of the hair shaft 2) developmental regression, mental retardation, seizure, ataxia, irritability, hypothermia, intracranial hemorrhage, death in early infancy 3) laboratory findings: low level of copper in plasma, urine, and hair; low level of plasma ceruloplasmin; an increased number of free sulfhydryl groups and decreased number of disulfide bonds in hairs; cultured fibroblasts containing four to six times higher concentrations of copper than control cells; postmortem diagnosis by copper measurement in the muscle tissue (high); copper measurement in the chorionic villi of the affected fetus in the first trimester (high) 4) malabsorption and maldistribution of copper in body organs; 5) other reported abnormalities; cryptorchidism, cataracts, atypical form (hypotonicity, fine myoclonic movements, ataxia, delayed psychomotor development, pili torti, etc.), etc.

Radiologic manifestations (1) include 1) bilateral symmetrical metaphyseal spurring of long bones in infancy 2) flaring of ribs 3) osteoporosis, fracture (s) 4) diaphyseal periosteal reaction of long bones 5) thickening of scapulae and clavicles 6) microcephaly, excessive wormion bones in the posterior fontanelle region 7) computed tomography (CT): progressive development of diffuse cortical brain atrophy, subdural accumulation of fluid, multifocal areas of ischemic infarction 8) widespread arterial changes: narrowing of the lumen, dilatation, tortuosity, elongation 9) cerebral angiogram, CT: loop-the-loop appearance, supernumerary serpentine branches, marked tortuosity 10) other reported abnormalities: hydronephrosis, hydroureter, bladder diverticula, polypoid lesion in the stomach, emphysema, round lumbar and thoracic vertebral bodies, ureteropelvic junction obstruction, vesicoureteral reflux and urinary tract infection.

A case of Menkes syndrome was presented, abnormalities were noted at the urinary tract and brain.

CASE REPORT

A 4-month-old boy admitted to the hospital due to seizure problem. The patient was pre-term-delivered by a Caesarian section with a birth weight of 2600 gram and moderate meconium stain. The Apcar score was 8,8,8 and with respiratory distress. He was noticed to have blond hair at birth though his parents' hair was black. However, he was discharged at that time in a good condition. The HIV Ag was negative and the urine Fecl 3 was also negative. At

Department of Radiology, Ramathibodi Hospital, Rama 6 Steet, Bangkok 10400, Thailand.

this admission, he was found to have kinky hair with coarse and blond color, microphthalmos, high arch palate, stiffy nose, and pectus excavatum. The development was delayed. The serum level of copper and cereluplasmin was very low and measured 2.27 ug/dl (normal 80-150 ug/dl) for the copper and 0.35 mg/dl (normal 20-46 mg/dl) for the cereluplasmin.

Phenobarbital was given to control seizure and copper-sulphate was supplemented. His hair became black and white (Fig. 1).

He was sent to study the urinary tract due to recurrent urinary tract infection. Multiple bladder diverticuli were noted (Fig. 2) without reflux. Skeletal survey showed no abnormality.

Contrast enhancement CT scan of the brain showed cerebral and cerebellar atrophy with lateral and third ventricular dilatation (Fig. 3) MRI of the brain revealed tortuousity of the intracranial vessels, especially at the circle of Willis and both middle cerebral arteries (Fig. 4). MRA of the brain also showed kinking and tortuousity of the intracranial blood vessels (Fig. 5).

DISCUSSION

Menkes' disease is characterized by deficiencies of copper in the liver and serum and more significantly, of a number of specific copper-proteins including cytochrome C oxidase, ceruloplasmin and lysyl oxidase (3). Copper is essential to human life, apparently only as a prosthetic element irreversibly bound to one of about a dozen copper-proteins. Normally there must be available, in vivo, sufficient copper to complete the synthesis of these copper-proteins by incorporation into specific apoproteins. Virtually all disturbances in copper metabolism involve either a deficiency of one or more of these essential copper-proteins, or the presence in tissues and organs of more copper than these apoproteins can bond. Genetic mechanism regulates both the synthesis of specific copper-proteins and the balance of copper.

An abnormality in copper binding or copper utilization which results in enzyme dysfunction is responsible for the neurodegenerative changes and fragmentation of elastic fibers noted in various types of arteries in patients with this condition. No known therapy, including the oral or parenteral administration of copper, can prevent death in the first decade of life.

The cause of the bladder diverticula in children with Menkes disease is not known. The walls of the diverticula of the bladder in a case reported by Harcke (4) were composed almost exclusively of elastic tissue and was considered acquired. Bladder diverticula may be a consequence of an increasing disturbance in innervation of the bladder (4). The diverticula constitute sites of urinary stasis which may lead to infection in our patient.

Widespread arterial tortuosity and variation in lumen size were demonstrated angiographically, in the brain, intraabdominal and peripheral arteries (6). Histologically, fragmentation of the internal elastic lamina and intima thickening were the findings of the most severely affected vessels. This bizarre appearance of the intracranial vessels were previously shown by MRI (6-8) and by MRA (9).

Cerebral atrophy are fairly nonspecific findings that can be seen in numerous conditions. It has been postulated that the cerebral atrophy and myelin deficiency may be the result of the arteriopathy (10).

ACKNOWLEGMENT

We thank the department of pediatrics for allowing us to study the case.

REFERENCES

1. Taybi H, Lachman RS. Radiology of syndromes, metabolic disorders, and skeletal dysplasias. 3rd ed. Year book medical publishers, inc: Chicago, 1990:605-7.
2. Menkes JH, Alter M, Steigleder GK, Weakley DR, Sung JH. A sex linked recessive disorder with growth retardation, peculiar hair, and focal cerebral and cerebellar degeneration. Pediatrics 1962;29:764-79.
3. Berkow R, Fletcher AJ. The merck manual. 16th ed. Merck research laboratories: Rahway, 1992: 977-8.
4. Harcke HT, Capitanio MA, Grover WD, Valdes-Dapena MV. Bladder diverticula and Menkes' syndrome. Radiology 1977;124:459-61.
5. Adams PC, Strand RD, Bresnan MJ, Lucky AW. Kinky Hair syndrome: Serial study of radiological findings with emphasis on the similarity to the battered child syndrome. Radiology 1974;112:401-7.

6. Johnsen DE, Coleman L, Poe L. MR of progressive neurodegenerative change in treated Menkes' kinky hair disease. Neuroradiology 1991;33:181-82.
7. Blaser SI, Berns DH, Ross JS, Lanska MJ, Weissman BM. Serial MR studies in Menkes disease. J Comput Assist Tomogr 1989;13:113-5.
8. Faerber EN, Grover WD, Defiupp GJ, Capitanio MA, Liv TH. Swartz JD. Cerebral MR of Menkes kinky hair disease. AJNR 1989;10:190-2.
9. Jacobs DS, Smith AS, Finelli DA, Lanziert CF, Wiznitzer M. Menkes kinky hair disease: Characteristic MR angiographic findings. AJNR 1993;1160-3.
10. Kendall BE. Disorders of lysosomes, peroxisomes, and mitochondria. AJNR 1992;13:621-53.

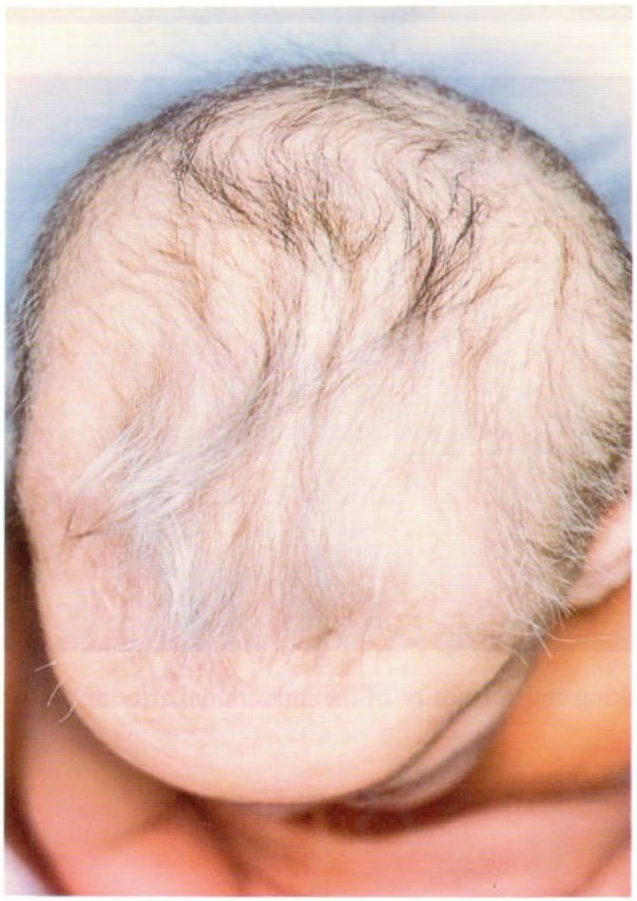

Fig. 1 The coarse hair with black and white colour of the patient was noted.

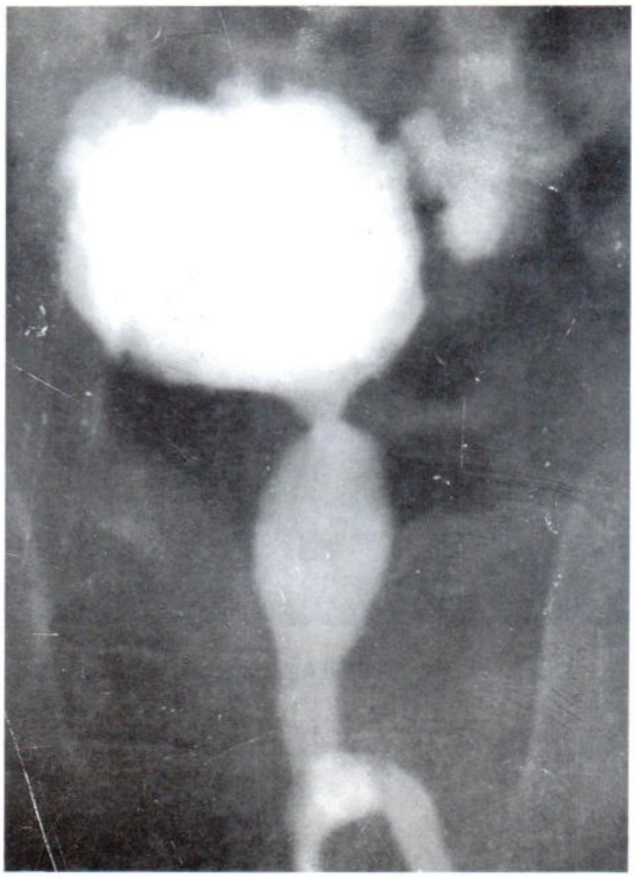

Fig. 2 Urinary bladder diverticuli were shown by voiding cystourethrogram without uretero-vesical reflux.

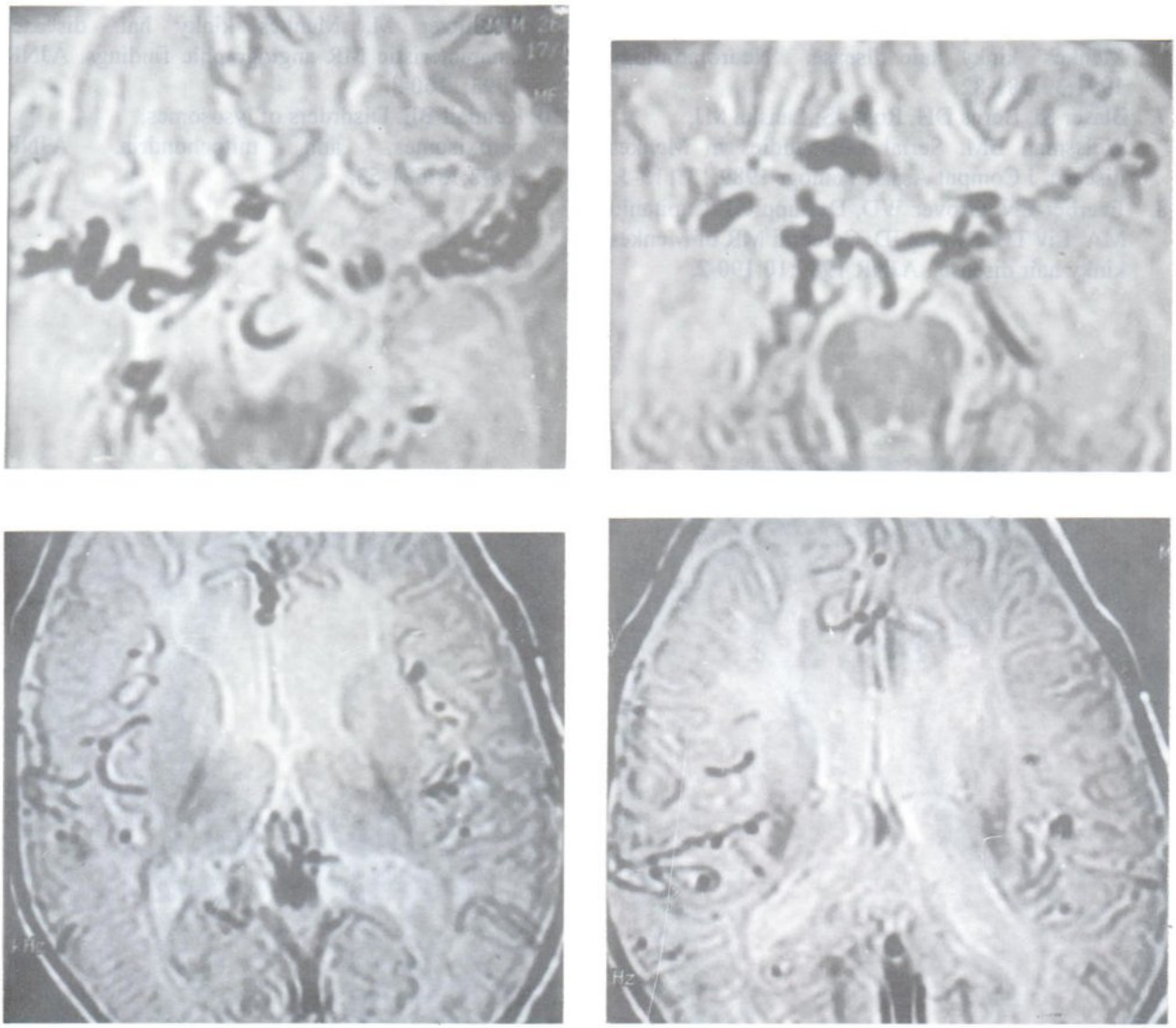

Fig. 3 PD axial MRI images of the brain shows kinking and tortuosity of the intracranial arteries.

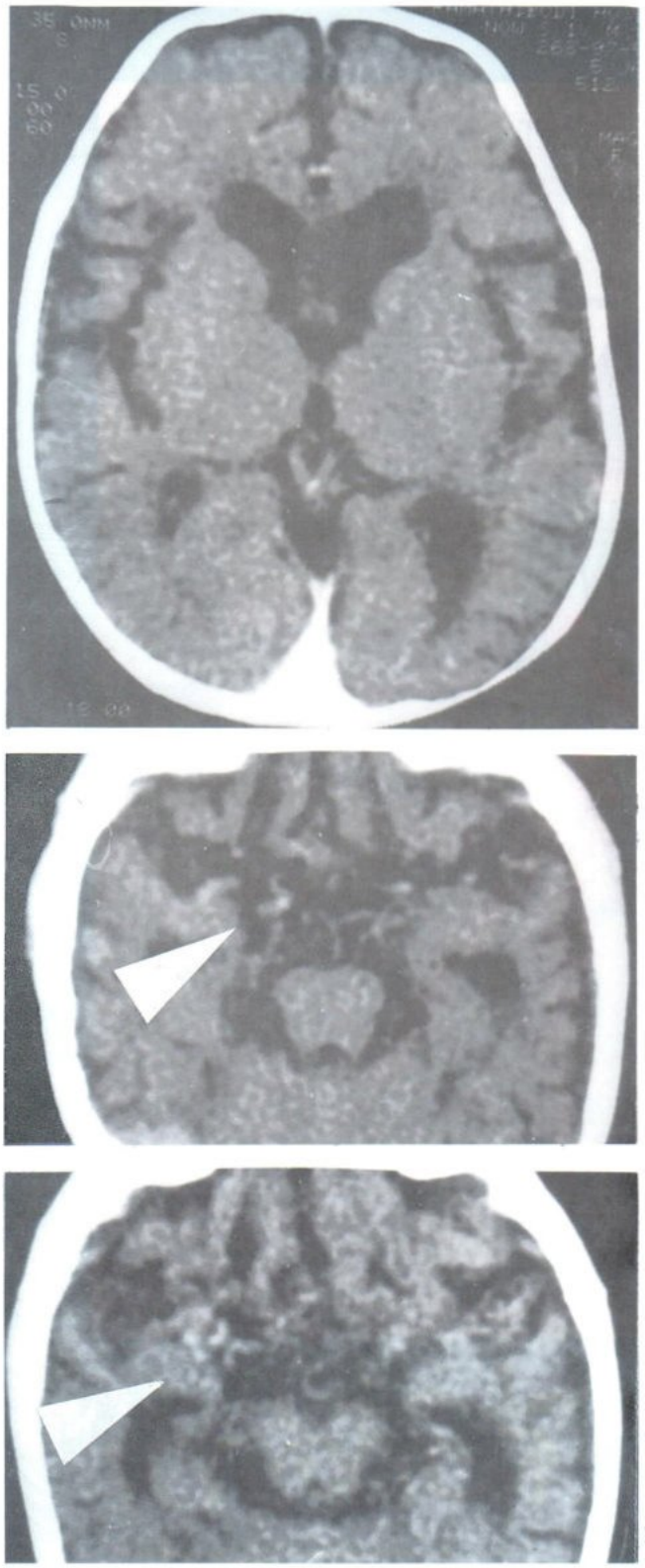

Fig. 4 Enhanced axial CT scan of the brain showed cerebral and cerebellar atrophy with tortuosity of the arteries in the region of the circle of Willis

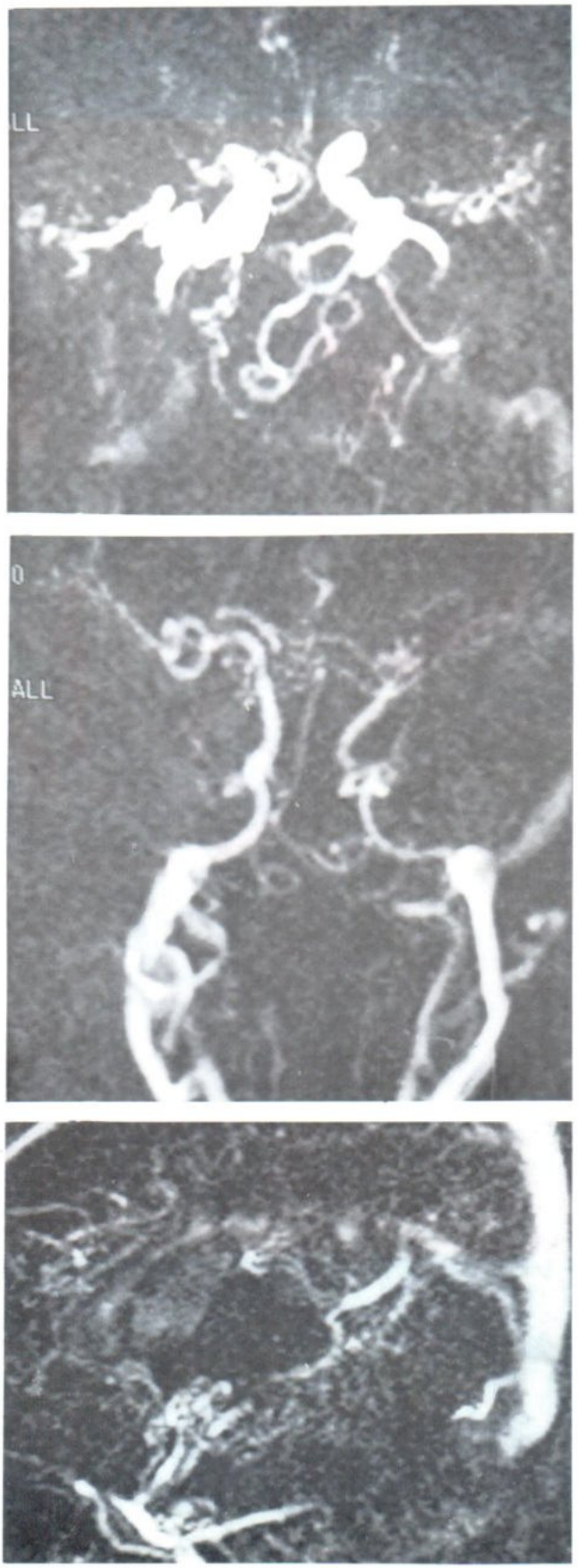

Fig. 5 MRA of the brain in axial, coronal and sagittal views shows loop- the-loop appearance of the intracranial arteries.

Philips Medical Systems

ร่วมสรรค์สิ่งที่ดีกว่า

Let's make things better.

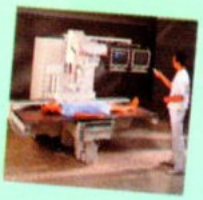

Multi DIAGNOST 3

The Multi DIAGNOST 3 is one of a new generation of remote-controlled systems, complementing the DIAGNOST 93 and DIAGNOST 96. All three systems have an attractive family look. With quality built-in, all were designed to be reliable, easy-to-use, efficient and provide digital image quality second to none.

Philips Medical Systems
Philips Electronics (Thailand) Ltd.
209/2 Sanpavut- Bangna Road Prakanong Bangkok 10260
Tel. (662) 745-4090 Fax. (662) 398-0792

PHILIPS

BONE IMAGING IN BURKITT'S LYMPHOMA

Swee Tian QUEK MBBS (S'pore), FRCR (UK)
Sew Kee CHANG MBBS (Melb), FRCR (UK)

ABSTRACT

Burkitt's Lymphoma is a tumour of B lymphocytes and unlike other lymphomas tend to be extranodal rather than nodal. Most radionuclide imaging of this disease has been with Gallium-67 citrate (Ga-67). Radionuclide bone imaging with Technetium-99 methylene diphosphonate (Tc-99m MDP) reports increased activity in areas of bone involvement with a single report of uptake in metastatic calcification in the lungs and gastric mucosa [1]. We present a case of primary Burkitt's lymphoma of the mandible that shows decreased uptake on a Tc-99m MDP bone scan.

Keywords: Burkitt's lymphoma, radionuclide bone scan.

CASE REPORT

A three year old Indonesian Chinese boy presented with a three-month history of a right mandibular mass. It was non tender with a gradual increase in size over this period. He was otherwise well with no significant past medical or family history. Physical examination revealed right mandibular and inner cheek swelling. There were no teeth loosening, lymphadenopathy or other abnormal findings. Apart from an elevated lactase dehydrogenase (LDH) at 804 (normal:300-700), the other blood results were normal. The anti-EBV VCA/IgG titres were raised at 640 (normal<5). Bone marrow aspirates were normal.

Plain radiographs show mottled small lucencies in the body and ramus of the right mandible (Fig. 1). Contrast-enhanced Computed tomography (CT) revealed a large soft tissue mass on either side of the right mandible obliterating the parapharyngeal space. The right masseter muscle was inseparable from the mass. There was irregularity of the bony cortex but no overt bone destruction (fig. 2). A Magnetic Resonance Imaging (MRI) examination of this region showed a right mandibular mass with the masseter muscle stretched around it (Fig. 3). There was bilateral small cervical lymphadenopathy. In addition there were several small enhancing lesions in the sphenoid bone that were thought to represent other areas of bone involvement. A SPECT Tc-99m MDP bone scan showed decreased uptake of the right mandibular body (Fig. 4). There were no other abnormal areas of activity in the rest of the skeleton. An open biopsy of the tumour was performed. Histopathology revealed a monotonous, diffuse infiltrate of small round cells with a starry-sky appearance consistent with Burkitt's lymphoma.

DISCUSSION

Burkitt's lymphoma has shown an interesting epidemiological pattern. It is endemic in Africa where it represents a common childhood malignancy with the mandible being the site most frequently involved. Non-endemic Burkitt's lymphoma is

Department of Diagnostic Radiology National University Hospital Lower Kent Ridge Road SINGAPORE 119074

Correspondence : Swee Tian QUEK, Department of Diagnostic Radiology, National University Hospital. Lower Kent Ridge Road, SINGAPORE 119074.

uncommon; the terminal ileum, cervical lymph nodes and bone marrow are the most frequently involved sites. The incidence in non-endemic Burkitt's lymphoma in the mandible is 15-18%. Despite this interesting epidemiological difference, the tumour from both the endemic and non-endemic areas shows similar histopathology and responds to the same treatment [2].

Gallium scintigraphy has been found to be useful in the list of investigations in the staging of Burkitt's lymphoma as well as post-chemotherapy assessment [3,4]. Increased gallium uptake is typically seen at sites of tumour involvement and has been shown to be more sensitive than bone scintigraphy and plain radiography. Tc-99m MDP scintigraphy has shown areas of bone involvement in the rest of the skeleton though less sensitive than gallium that also has the advantage of assessing other non-skeletal sites of involvement. Increased uptake of Tc-99m MDP in soft tissues with metastatic calcifications in Burkitt's lymphoma in lungs and stomach has, however, been reported. In our patient, the primary bone lymphoma shows decreased uptake on the bone scan. With the clinical picture of a soft tissue tumour related to bone the differential diagnoses are those of a soft tissue sarcoma, lymphoma and osteomyelitis. Osteomyelitis was excluded based on clinical findings though Burkitt's lymphoma may present with systemic symptoms not unlike osteomyelitis. In any case the bone scan would exclude osteomyelitis as a possibility as typically there would be marked increased activity on the bone scan. A soft tissue sarcoma with bone destruction would also be expected to show increased activity due to bone reactivity to the tumour. This appearance of a "cold" lesion on bone scan with Burkitt's lymphoma has not been previously reported and would suggest that this appearance on a bone scan of a primary mandibular lesion in a child would favour the diagnosis of lymphoma rather than other tumours or infection.

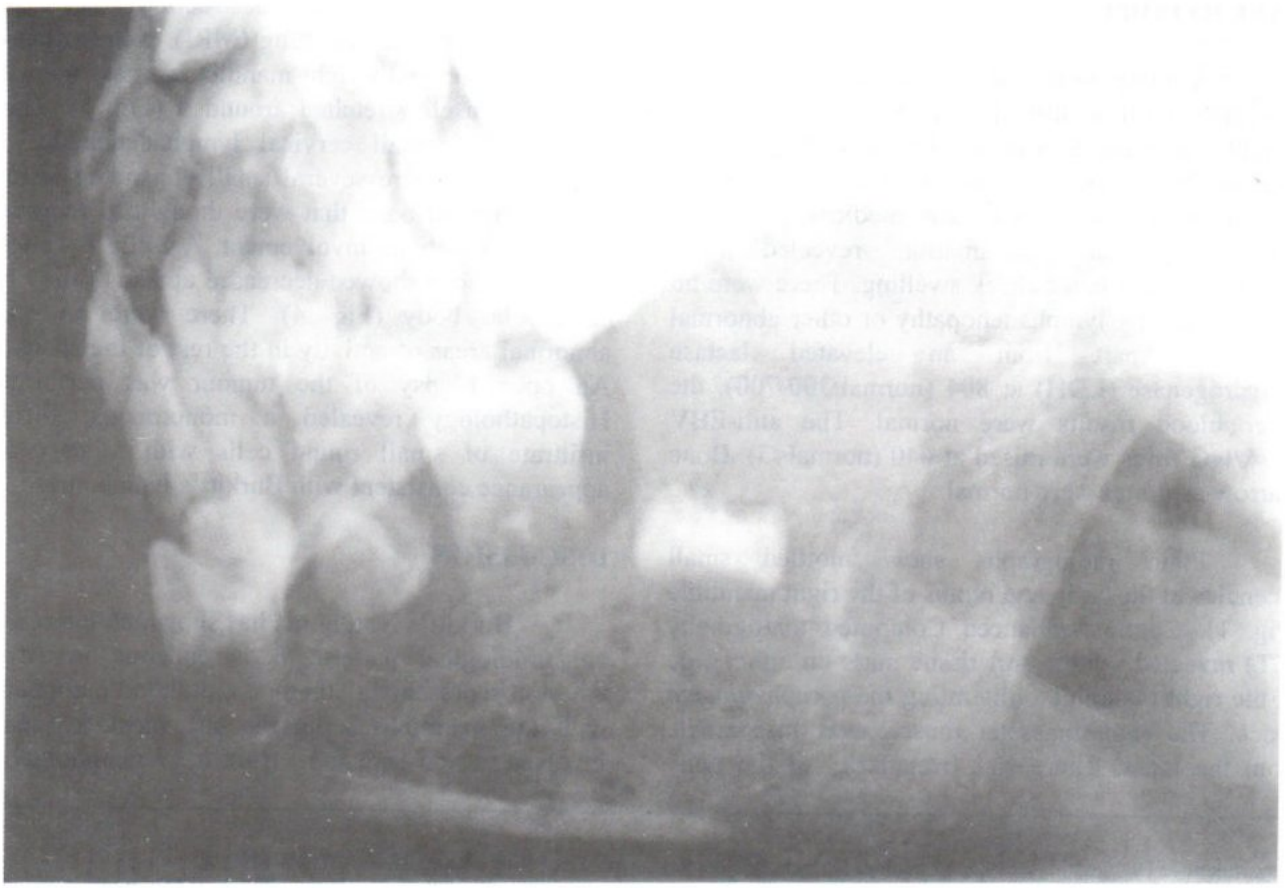

Fig. 1 Radiograph of the right mandible shows multiple lucencies in the body.

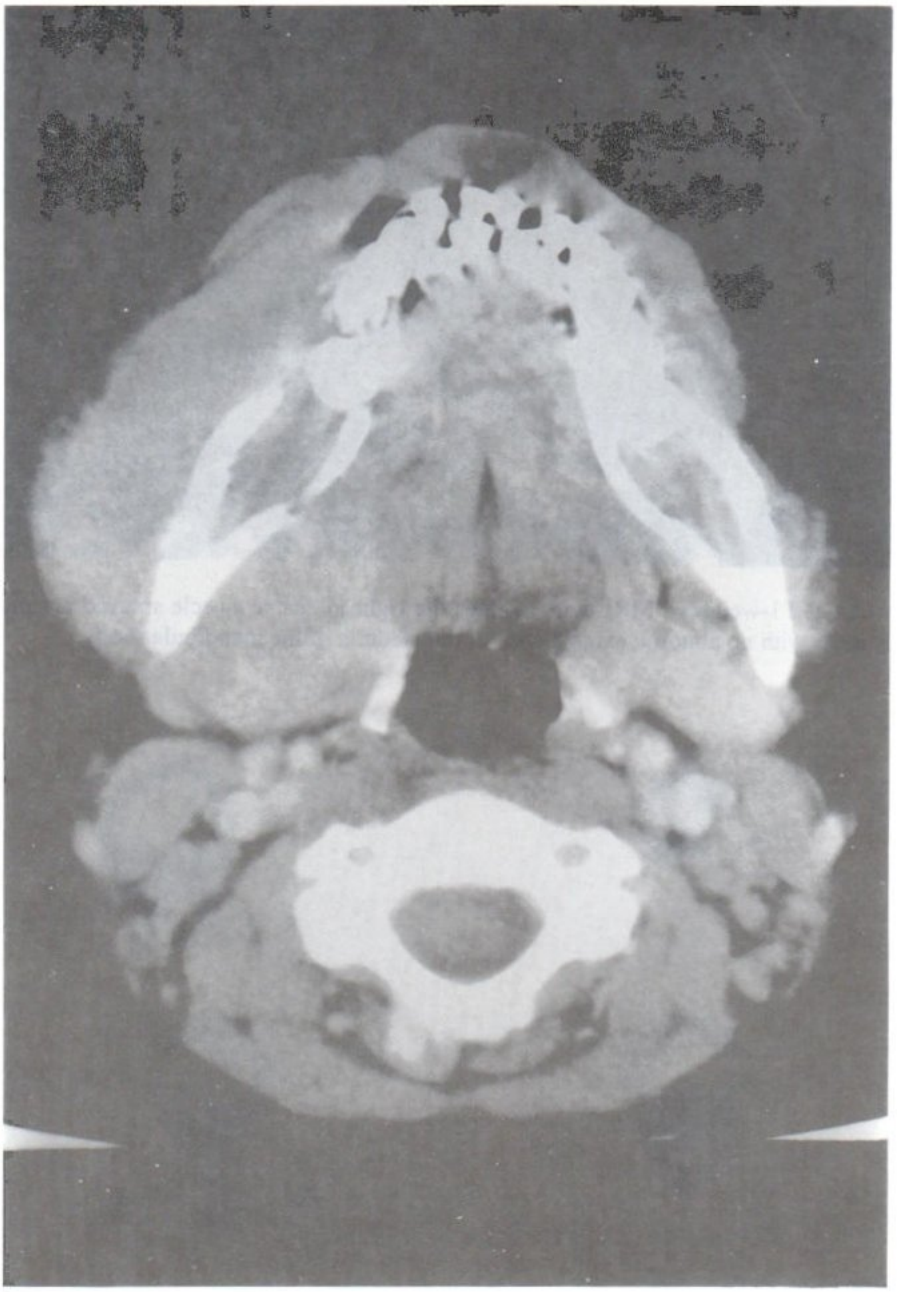

Fig. 2 Contrast-enhanced CT scan shows a soft tissue mass inseparable from the masseter muscle on either side of the right mandible. There is no bony destruction.

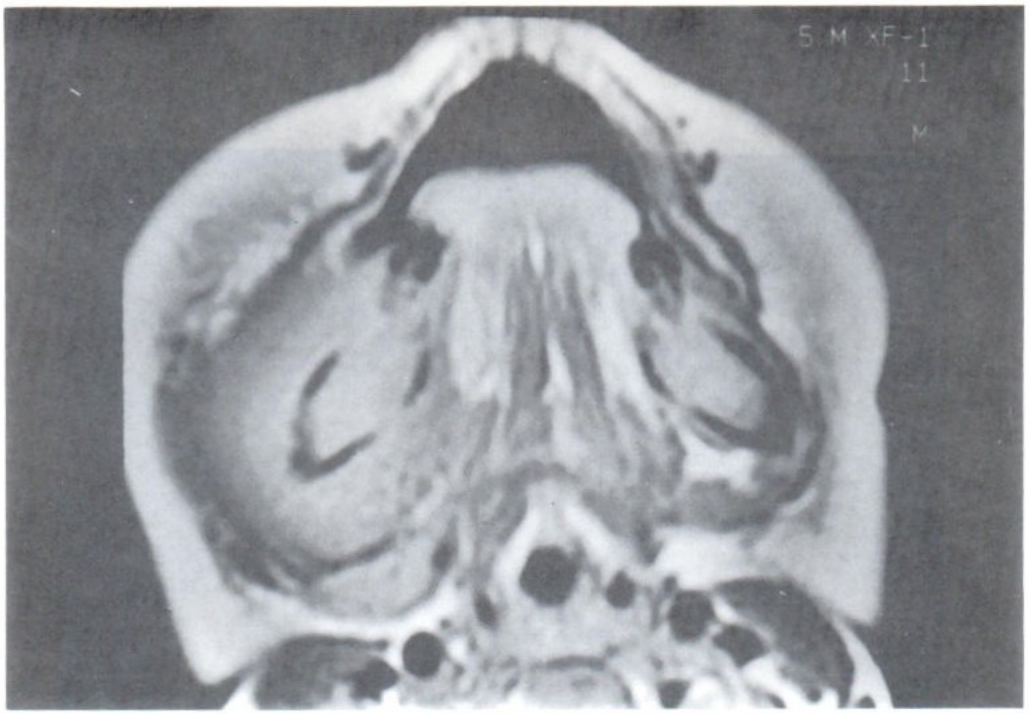

Fig. 3 Axial T1-weighted MRI demonstrates the right masseter muscle splayed around a soft tissue mass with no abnormal signal seen of the medulla of the mandibular body.

Fig. 4 A SPECT Tc-99m MDP bone scan shows abnormal decreased activity of the right mandible.

REFERENCES

1. CAPELLA, J, LECHERE, J, and KRAIEM , A, Metastatic calcifications in Burkitt's lymphoma, J Radiol. 1984;65(8-9):593-596.
2. HUPP, J R, COLLINS, F J V, ROSS, A and MYALL R W T, A Review of Burkitt's Lymphoma : Importance of Radiographic Diagnosis, J Max-fac Surg. 1982:240-245.
3. BAR-SHALOM, R, ISRAEL, O, EPELBAUM, R et al, Gallium-67 Scintigraphy in lymphoma with bone involvement, J Nucl Med., 1995;36(3):446-450.
4. GLASS, R B J, FERNBAVCH, S K, CONWAY, J J, SHKOLNIK, A, Gallium Scintigraphy in American Burkitt Lymphoma: Accurate assessment of tumour load and Prognosis, Am J Roentgenol., 1985;145:671-676.

TRANSRECTAL BIOPSY OF THE PROSTATE GUIDED BY TRANSRECTAL ULTRASOUND IN AN ASEAN POPULATION:CORRELATION OF DIGITAL RECTAL EXAMINATION, PROSTATE SPECIFIC ANTIGEN LEVELS AND IMAGING WITH HISTOLOGY.

SES NG, FRCR , DES WONG, FRCR , SSS TAN, FRCR
C MOHAN, MBBS , HK BOEY, FRCR

ABSTRACT

Transrectal ultrasound (TRUS) followed, in the same sitting, by TRUS guided biopsy of the prostate was performed on 131 cases. Histological findings were prostatic carcinoma in 26 cases (19.8%), prostatitis in 11 cases (8.4%) and glandular atypia in 9 cases (6.9%).

The typical findings on digital rectal examination (DRE) were a hard, multinodular prostate for prostatic carcinoma and a hard, uninodular prostate for both prostatitis and glandular atypia. However its high false positive and false negative rates, 37.6% and 50% respectively, limits its role in predicting prostate pathology.

In terms of the Prostatic Specific Antigen (PSA), the mean levels for prostatic carcinoma, prostatitis and glandular atypia were 366, 17.5 and 7.2 ng/dl respectively.

On TRUS imaging, extracapsular and inhomogenicities in the peripheral zone (PZ) breach posted positive predictive values (PPV) of 100% and 71.4% for carcinoma respectively. Well defined solitary nodules were non specific and pointed move towards benign conditions such as prostatitis and atypia rather than carcinoma.

Patient acceptance of the procedure was high. Complications of the procedure were mild pain (23 cases), haematuria (12 cases), passing blood per rectum (4 cases) and fever (2 cases).

Key words: Transrectal ultrasound (TRUS) ; digital rectal examination (DRE); Prostatic Specific Antigen (PSA); prostatitis; glandular atypia.

Department of Diagnostic Imaging, TAN TOCK SENG Hospital, Singapore .

Correspondence: Dr. SAMUEL NG, Department of Diagnostic Imaging, TAN TOCK SENG Hospital, Moulmein Rd., Singapore 1130. Telephone : 065-3595354 Fax : 065-2553618

INTRODUCTION

The role of transrectal ultrasound (TRUS) in the evaluation of prostate pathology has been gaining considerable ground since its inception in 1971. In the early eighties, the introduction of spring driven biopsy mechanisms as well as sophisticated probes with needle guide capability made TRUS guided biopsy an accurate and relatively simple procedure (1). TRUS guided biopsy soon overtook trans-perineal biopsy as the method of choice in prostatic tissue sampling. As a consequence of this, there has been a flurry of reports co-relating endosonographic and histologic findings (2-5).

TRUS has played a critical role in establishing the commonest site of prostatic carcinoma as the peripheral zone (PZ). However, the debate concerning the acoustic properties of prostatic lesions is still on going (6).While investigators first thought of malignant lesions as echogenic (7), the currently accepted view is that a hypoechoic lesion in the peripheral zone is highly suggestive of malignancy (8). The utility of digital rectal examination (DRE) and serum Prostatic Specific Antigen (PSA) as predictors of prostatic carcinoma has yet to be ascertained, in spite of considerable study. Furthermore, although the use of TRUS guided transrectal biopsy is well reported in the West, the experience in South-East Asia is relatively limited. As such our prospective study was conducted to shed light on the current controversy and to recommend guidelines for TRUS guided biopsy. The role of both directed as well as random biopsies will also be discussed.

MATERIALS AND METHODS

Between January 1993 and August 1994, the Department of Diagnostic Imaging, Tan Tock Seng Hospital, Singapore, performed TRUS and TRUS guided biopsy on 131 consecutive cases. These were male patients, of age between 46 and 91 (mean=71) years. All had either symptoms suggestive of prostatomegaly, an abnormal DRE or a raised PSA level.

115 patients had PSA levels taken prior to TRUS. PSA measurement was made using a monoclonal antibody assay (Abbott Laboratories, Abbott Park, Illinois, USA).

All patients also received prophylactic antibiotics. The departmental regime comprised two tablets of Bactrim (Sulphamethoxazole 400 mg and Trimethoprim 80mg) twice daily for three days, commencing 24 hours before the examination. For cases of sulphur drug allergy, one capsule of Augmentin 375 mg thrice daily for three days was given. On the eve before the examination a laxative, to be taken orally, was given.

Informed consent was taken before the appointment for the procedure was given. On the appointed date, the radiologist would run through the procedure with the patient. A conscientious attempt was made to talk to the patient throughout the examination to reassure him.

The patient was placed in the left lateral decubitus, knee-chest position throughout the entire procedure. A pre-scan DRE was performed and all findings were documented, with a special emphasis on gland size, consistency and the presence of nodules (solitary or multiple).

TRUS was performed by three ultrasonologists (SN, DW and ST) familiar with the protocol using the Acuson 128 x P/10 console and 7.0 MHz transducers V714T and V714S. PSA levels were known to the ultrasonologists in some cases. Scanning was performed systematically, first in the transverse, and then in the sagittal plane. The TRUS examination was considered positive if a focal lesion, i.e.a nodule, was detected.

All patients were then subjected to a 4 quadrant transrectal biopsy under TRUS guidance. This biopsy was initiated by locating 4 anatomical sites from the upper and lower quadrant of each lobe of the prostate gland. A computer generated trajectory was then projected onto the monitor. If a focal lesion was demonstrated on TRUS, this lesion was brought into the trajectory by manipulating the transducer.

All biopsies were performed using an 18-gauge needle (Biopty-Cut; Bard Urological, Covington, Ga) with a spring-driven automatic firing device to obtain core biopsy samples, each of 1.7 cm in length, starting with the quadrants where a focal lesion is localized to. Random biopsies were then performed on each of the "uninvolved" quadrants.

Each specimen was placed separately in buffered formaldehyde (4%) solution.

No analgesics or anesthetics were used before, during, or after the biopsy. Patients were allowed to leave the department immediately after the biopsy. They were warned of possible complications and follow-up was carried out for a week post-biopsy.

RESULTS

TRUS guided biopsy performed on all 131 cases provided adequate tissue for histological analysis. Biopsy results were positive for malignancy in 26 cases (19.8%), prostatitis in 11 cases (8.4%) and glandular atypia in 9 cases (6.92%) (Table 1). Of the 26 cases of prostatic carcinoma, 24 were primary adenocarcinoma of the prostate, 1 was invasive transitional cell carcinoma of the bladder involving the prostate, and 1 was a case of disseminated gastric carcinoma with a peritoneal drop metastasis involving the prostate. Ages of these patients ranged from 53 to 83 (mean = 71) years of age.

DRE was considered abnormal if the prostate consistency was hard or if a nodule (or nodules) were felt. The incidence of abnormal DRE was 16 (62%), 3 (27.3%) and 4 (44.4%) for carcinoma, prostatitis and glandular atypia respectively. However, abnormal DRE was also recorded in 37.6% (32 of 85) of cases who were histologicaly normal.

The mean PSA levels for prostatic carcinoma, prostatitis and glandular atypia were 339.4, 17.7 and 10.1 ng/dl respectively (Table 1). All 18 cases with a PSA of more than 35ng/ml were positive for carcinoma irrespective of DRE or TRUS findings. (i.e. there were no cases of prostatitis or glandular atypia with PSA>35) (Table 2). 5 of 41 patients with a PSA range of 4 - 35 ng/ml had carcinoma. There were two cases of carcinoma with a normal PSA.

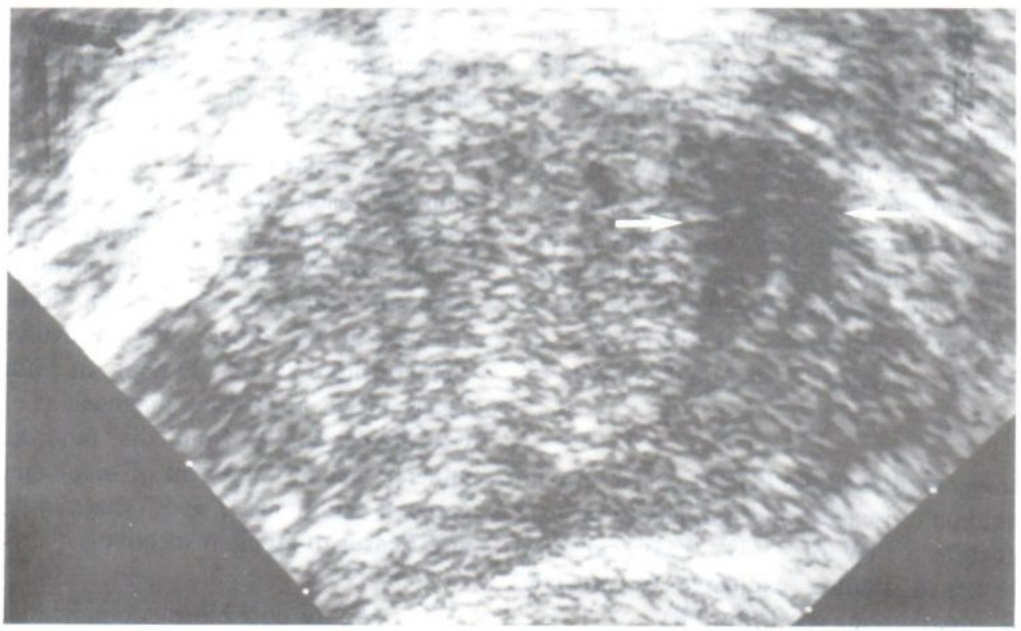

Fig. 1: Prostatitis. Axial TRUS scan

Shows well defined hypoechoic nodule (arrows) at junction of (L) PZ and transitional zone (TZ). Note curvilinear echoes within. This feature was only seen in cases of Prostatitis

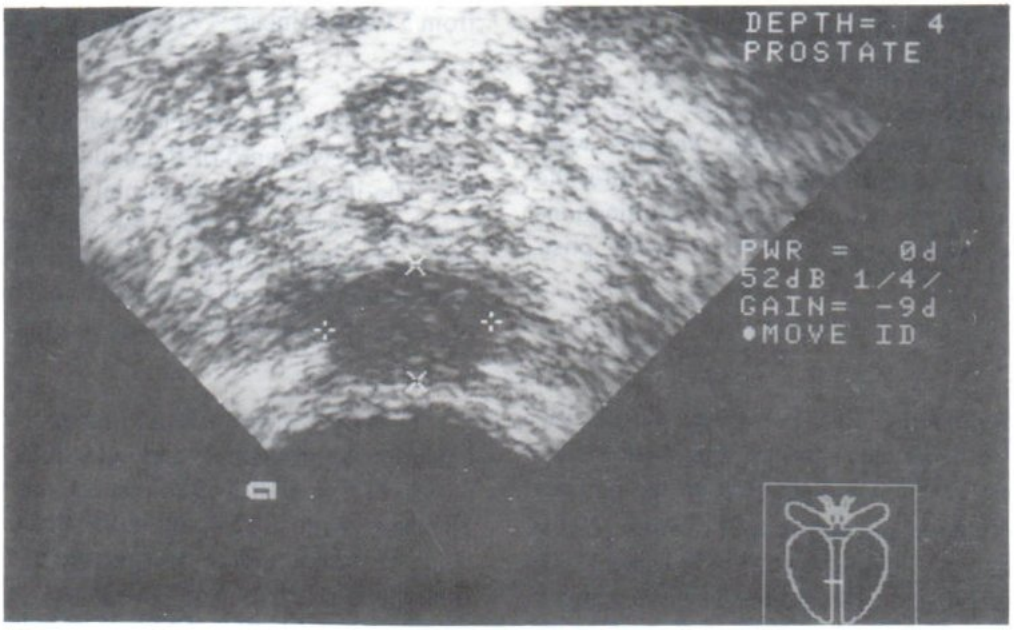

Fig. 2: Early Prostatic Carcinoma

Axial TRUS scan shows well defined hypoechoic nodule (cursors) in PZ.

The TRUS findings are summarized in Table 3. Hypoechoic nodules were generally discrete and well defined. They were not seen in association with hyperechoic nodules nor inhomogenicities in the PZ. They were noted in 8 cases of prostate carcinoma, but also in prostatitis (3 cases), atypia (2 cases) and normals (17 cases). This makes the PPV of this finding 43.3% and 26.7% for prostate disease and prostate carcinoma respectively. 2 cases of prostatitis showed curvilinear echoes within these nodules (Fig. 1). Well defined hyperechoic nodules were not a feature of prostate carcinoma, but were seen in prostatitis (3 cases), atypia (1 case) and normals (3 cases).

Inhomogenicities in the PZ were seen only in prostate carcinoma (15 cases) and normals (6 cases), giving this feature a PPV of 71.4%. Extra-capsular involvement was a finding exclusive to prostate carcinoma (9 cases), giving it a 100% PPV.

To correlate TRUS findings with extent of involvement and PSA levels the carcinoma group was further divided into 3 subgroups based on TRUS findings, i.e. Groups I (normal TRUS), II (well defined hypoechoic nodules) (Fig. 2) and III (poorly defined areas of mixed echogenicity) (Table 4). All 9 cases with extra-capsular involvement were in Group III (Fig. 3 and 4). The mean PSA levels in these subgroups were 168.4, 408 and 736 ng/ dl respectively. 5 cases posted PSA levels of greater than 999.9 ng/ dl. All 5 were found in Group III.

A total of 524 prostate quadrants were biopsied, each of the 131 patients receiving a 4 quadrant biopsy. The 69 biopsies directed at focal lesions seen on TRUS yielded positive results in 58 quadrants (84.1%) (Table 5). Random biopsies directed at the other 455 "uninvolved" quadrants were positive in 61 (13.4%). In terms of absolute cases, TRUS missed the diagnosis (i.e. the diagnosis was made solely from the random biopsy) and underestimated the extent of involvement in 4 and 7 cases of carcinoma, 2 and 5 cases of prostatitis and 6 and 7 cases of atypia respectively.

As for post biopsy complications, 23 patients (17.6%) felt mild pain during the procedure. 4(3%) experienced pain following the procedure. 2 patients (1.5%) developed a urinary tract infection after the biopsy. Both resolved with antibiotic treatment alone. 12 (9.1%) developed gross haematuria not requiring transfusion, of which 1 required catheterisation due to clot retention. All cases resolved spontaneously.

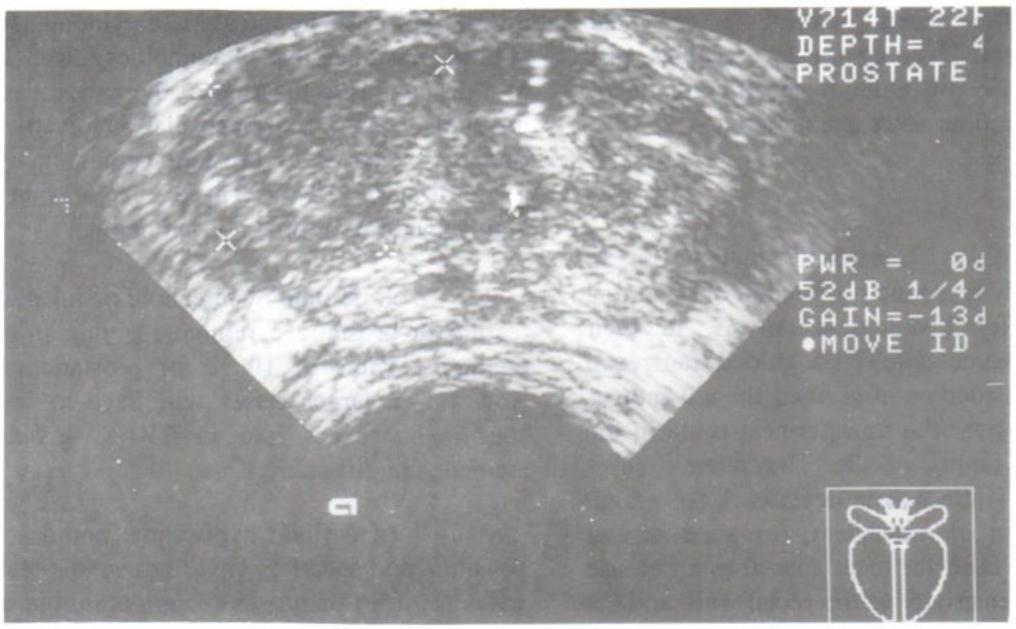

Fig. 3: Advanced Prostatic Carcinoma

Axial TRUS scan shows a poorly defined heterogeneous area (cursors) the (R) PZ, invading into the TZ anteromedially and distorting the prostatic capsule.

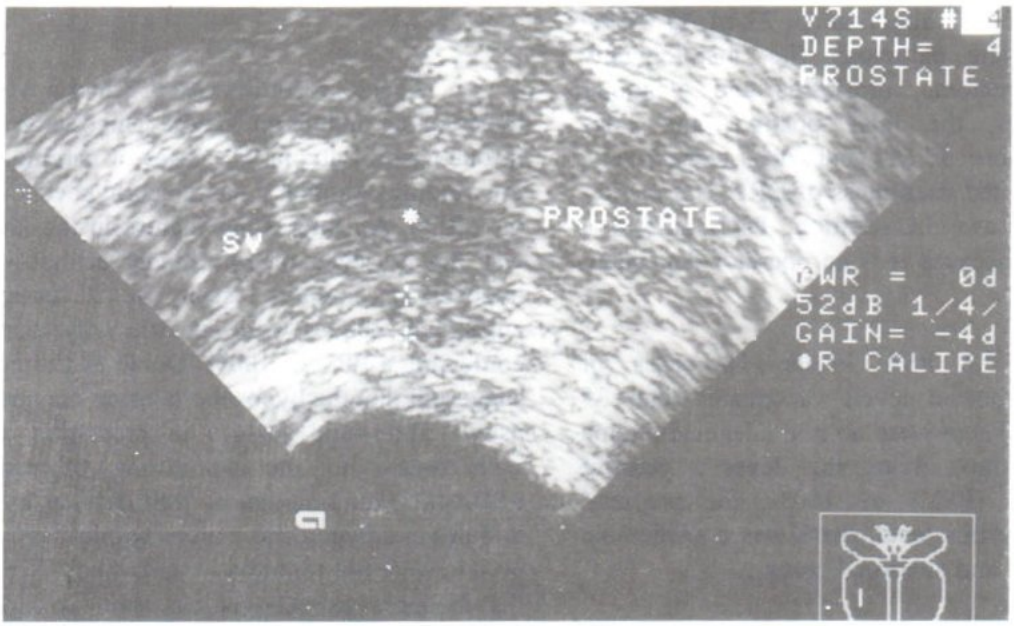

Fig. 4: Advanced Prostatic Carcinoma (same as patient as Fig 3).

Sagittal TRUS scan same area along the superior aspect of the PZ (asterisk), causing obliteration of the distal end of the seminal vesicles (cursors).

There was 1 case of haemospermia, also resolving spontaneously after several weeks. 1 case had continued per rectal bleeding for several days, also resolving spontaneously without specific treatment. No major complications were encountered.

DISCUSSION

TRUS guided transrectal biopsy is an accurate and highly reproducible method of obtaining prostatic tissue for histological anlysis. In their landmark article advocating TRUS guided transrectal biopsy (2), Torp-Pederson et al cited the advantages of the transrectal over the transperineal route in the placement of the biopsy needle. They were " (a) a short needle path (little needle deviation), (b) a high degree of freedom of movement, (c) good patient tolerance and no need for local anaesthesia because of the relative insensitivity of the rectal wall, and (d) a quick procedure (no skin preparation, no local anaesthetics)."

Our high success rate in obtaining adequate tissue sample reflects the efficacy of the procedure.

This increased availability of histological data in turn provided a gold standard by which we could correlate the DRE, PSA and TRUS findings.

The DRE was abnormal in 23 of 46 (50%) cases with prostate pathology (i.e. histologically proven adenocarcinoma, prostatitis and glandular atypia). However, the false positive and false negative rates were 37.6% and 50% respectively, reflecting the limited usefulness of DRE as a marker for prostatic disease. In addition, DRE suffers a major drawback because it is an operator dependent assessment.

As for the PSA levels, 18 cases of adenocarcinoma posted levels of greater than 35 ng/ml (Table 2). There were no non adenocarcinoma cases in this group, giving this level a positive predictive value (PPV) of 100% for prostatic carcinoma. Below this level, there was considerable overlap of normal and abnormal cases.

In terms of the TRUS findings of prostatic carcinoma, the PZ was the commonest site of involvement, all cases with positive TRUS findings having their lesions sited here (Table 3). Poorly defined inhomogenicities in the PZ was seen in 15 cases of prostatic carcinoma and 6 normals, yielding a PPV of 71.4% for prostatic carcinoma. Greenberg et al (9) postulate that this inhomogenicity is a result of a desmoplastic reaction of the native tissue to the invading cancer. Extra-capsular involvement was a finding exclusive to prostate carcinoma (9 cases), giving it a 100% PPV. These 3 features as such, are highly specific for prostatic carcinoma.

Well defined hyperechoic nodules were not a feature in prostatic carcinoma, giving it a negative predictive value of 100% for prostatic carcinoma. However, a larger series will have to be done to confirm its exact role in TRUS, given its low incidence in this study.

Well defined hypoechoic nodules were less sensitive and specific. This finding was featured in 8 cases (30.8%) of prostate carcinoma, but also in 20 normals (23.5%). However in the presence of a positive DRE and/ or a raised PSA, this finding is more indicative of early, rather than late, disease. This was confirmed when we compared all cases with this finding against those with poorly defined inhomogenicities in the PZ (Table 4), the former group (i.e. Group 2) having a lower mean PSA and quadrant involvement than Group 3. In addition, Group 2 cases did not post evidence of extra-capsular spread.

Of the prostatitis cases, 3 had a well defined hyperechoic nodule on TRUS. This feature was seen in one case of atypia. No cases of carcinoma posted this finding. Another 3 cases had hypoechoic nodules on TRUS. An interesting feature in the latter group was the presence of culvillinear echoes within the hypoechoic nodules, seen in 2 cases. These curvilinear echoes were specific only to prostatitis, conferring a PPV of 100%. Doble & Carter (10) had suggested that the hypoechoic lesion may be the most useful ultrasound feature in prostatitis, especially with regard to the monitoring of response to treatment. Our findings of well defined hyperechoic nodules and hyperechoic areas within the hypoechoic nodule were not reported in their study. We postulate that the increased echogenicity is due to early abscess formation in the former group, and to debris within a liquified abscess in the latter. While the number of such cases is small, we suspect that these findings will be a useful marker for prostatitis and will be reporting on this in a future article.

Our analysis of directed versus random biopsies show that directed biopsies provided the diagnosis in 34 cases (Table 5). Random biopsies provided the diagnosis in 12 cases. As such, these 12 cases would have been dismissed as negative had only directed biopsies been performed. Shinohara et al (11) postulate that any disease process that insinuates between normal prostate tissue can contain many echo-reflective interfaces and thus appear isoechoic on TRUS. These findings justify the need for random biopsies of benign looking quadrants (12).

No major complications were encountered. The 2 commonest were intraprocedural pain (17.6%) and mild haematuria (9.1%), findings which to those from other studies (4).

CONCLUSION

TRUS guided transrectal biopsy of the prostate is a safe procedure with a low complication rate, and high patient acceptance. It's utility in management is based on the patient's symptoms.

1. For those presenting with fever and/ or pain referable to the prostate, where prostatitis is the issue in question, the following is recommended:

(A) There is no need for transrectal biopsy in the first visit. If a focal lesion is detected, repeat TRUS should be performed after a course of antibiotics.

(B) Biopsy is recommended only if a focal lesion persists on follow up TRUS.

2. For those presenting with prostatism and/ or haematuria, where prostatic carcinoma is the issue in question, the following flow chart is recommended:

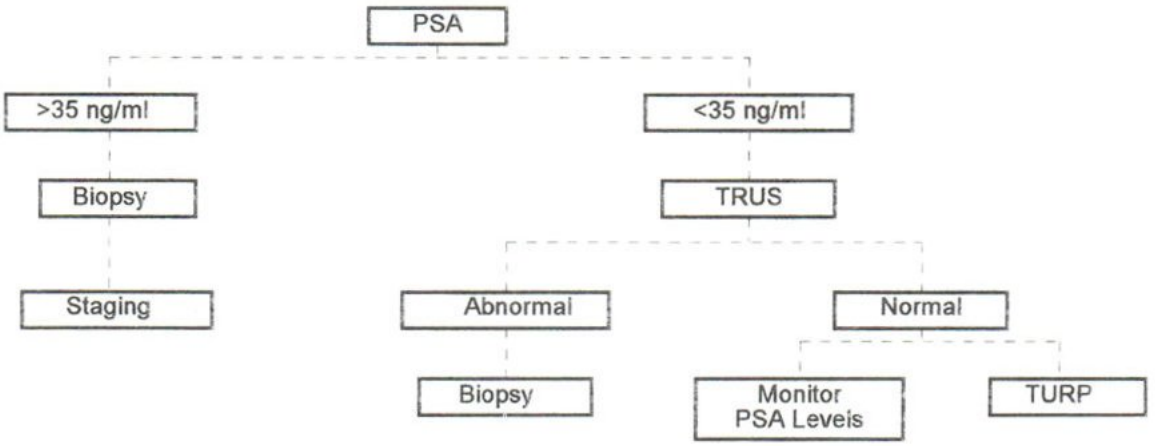

TABLE 1: DRE, PSA and TRUS Findings of the Different Histological Groups

Histology	No. of Cases (%)	AbN DRE (%)	PSA (ng/dl)	AbN TRUS (%)
Carcinoma	26 (19.8)	16 (62)	339.4	21 (80.8)
Prostatitis	11 (8.4)	3 (27)	17.7	6 (54.5)
Atypia	9 (6.9)	4 (44.4)	10.1	3 (33.3)

TABLE 2: Incidence of Cases Classified under PSA Range for Different Histological Groups

PSA Range	No. of Patients (n=115)	No. with Carcinoma (n=26)	No. with Prostatitis (n=8)	No. with Atypia (n=8)	Normals (n=73)
>35 ng/ml	18 (16%)	18 (69%)	0	0	0
4-35 ng/ml	53 (46%)	6 (23%)	7 (88%)	5 (63%)	35 (48%)
0-4 ng/ml (normal)	44 (38%)	2 (8%)	1 (12%)	3 (37%)	38 (52%)

TABLE 3: TRUS Findings and their incidence in the Different Histological Groups

TRUS FINDING	No. of Carcinoma Patients	No. of Prostatitis Patients	No. of Atypia Patients	No. of Normal Patients
Hypoechoic Nodule	8	3	2	17
Hyperechoic Nodule	0	3	1	3
Inhomogenicity in PZ	15	0	0	6
Extracapsular Breach	9	0	0	0

TABLE 4: TRUS and PSA Findings of Prostate Carcinoma Subgroups

Prostatic Carcinoma Subgroup	No. of Cases	TRUS Findings	Extracapsular Breach	Mean PSA (ng/ dl)
1	5	Normal	-	168.4
2	8	Well defined hypoechoic nodule	-	408
3	13	Poorly defined heterogenous areas	9	736

TABLE 5: Histological Diagnosis of Directed vs Random TRUS Guided Transrectal Biopsies Performed on 524 Quandrants

Biopsy	Nodule on TRUS	Histology				
		Carcinoma	Prostatitis	Atypia	Normal	Total No. of Quandrants
Directed	+	48	6	4	11	69
Random	-	33	21	7	394	455
Total		81	27	11	405	524

REFERENCES:

1. Lee F, Littrup P J, McLeary RD, et al. Needle aspiration and core biopsy of prostate cancer: comparative evaluation with bi-planar transrectal US guidance. Radiology 1987;163:515-520.
2. Torp-Pedersen S, Lee F, Littrup P J, et al. Transrectal Biopsy of the Prostate Guided with Transrectal US: Longitudinal and Multiplanar Scanning. Radiology 1989; 170:23-27.
3. Hodge K, McNeal J, Stamey T. Ultrasound Guided Transrectal Core Biopsies of the Palpably Abnormal Prostate. J Urology 1989;142:66-70.
4. Lee F, Torp-Pedersen S T, Siders D, Littrup P, McLeary R. Transrectal Ultrasound in the Diagnosis and Staging of Prostatic Carcinoma. Radiology 1989;170:609-615.
5. Lee F, Torp-Pedersen S, Littrup P J, et al: Ultrasound Guided Transrectal Prostatic biopsy. Hypoechoic Lesions of the Prostate: Clinical Relevance of Tumour Size, Digital Rectal Examination, and Prostate-specific Antigen. Radiology 1989;170:29-32.
6. Rifkin M D, Dahnert W, Kurtz A B. State or the Art: Endorectal Sonography of the Prostate Gland. A J R 1990;154:691-700.
7. Rifkin M D, Kurtz A, Choi H, Goldberg B. Endoscopic Ultrasonic Evaluation of the Prostate Using a Transrectal probe: Prospective Evaluation and Acoustic Characterization. Radiology 1983;149:265-271.
8. Clements R, Griffiths G J, Peeling W B. Staging Prostatic Cancer. Clinical Radiology 1992;46: 225-231.
9. Greenberg M, Neiman H L, Vogelzang R, Falkowski W. Ultrasonographic Features of Prostatic Carcinoma. Journal of Clinical Ultrasound 1982;10:307-312.
10. Doble A, Carter S. Ultrasonographic Findings in Prostatitis. Urol Clin North Am 1989;16(4):763-72.
11. Shinohara K, Wheeler T, Scardino P. The Appearance of Prostate Cancer on Transrectal Ultrasonography: Correlation of Imaging and Pathological Examinations. J Urology 1989;142: 76-82.
12. Dyke C H, Toi A, Sweet J M. Value of US-guided Transrectal Prostate Biopsy. Radiology 1990;176:345-349.

ACOUSTIC IMAGING
A Dornier Company

Presents...

HIGH PERFORMANCE, COST EFFECTIVE ULTRASOUND FOR:

- ABDOMINAL
- OBSTETRICS
- GYNECOLOGY
- VASCULAR
- PROSTATE
- MUSCULOSKELETAL
- SMALL PARTS
- MAMMOGRAPHY
- PEDIATRICS

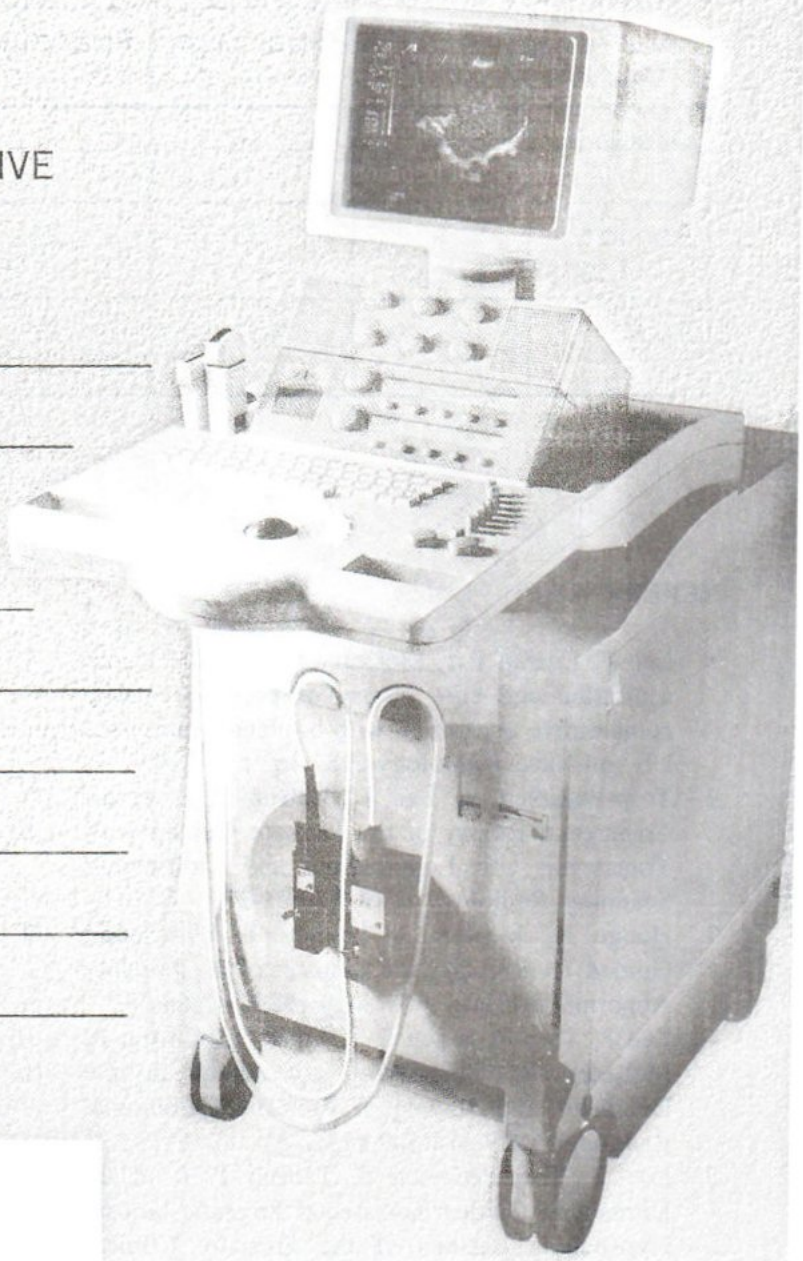

MEDICAL MEDIA PRODUCT CO., LTD.
บริษัท เมดิคอล มีเดีย โปรดักส์ จำกัด
633/14 ถนนสาธุประดิษฐ์ เขตยานนาวา กรุงเทพฯ 10120
โทร. (662) 2943364-8 โทรสาร : (662) 2943373

Performa™

High resolution ultrasound imaging scanner

A CASE REPORT : SPLENIC EPIDERMOID CYST.

Darunee BOONJUNWETWAT, M.D.
Bundit CHAOPRATHOMKUL M.D.

ABSTRACT

We reported a splenic epidermoid cyst who underwent a total splenectomy. The ultrasonography and computed tomography scans are the imaging tools to establish the diagnosis by demonstrating a cystic lesion with occasional septations, wall trabeculation and internal contents. There is no specific imaging characteristic to distinguish between the true and false cyst. The certained diagnosis should be made by histological prove. Anyhow, when the splenic cyst is found, the patient should be treated owing to the risk of rupture, or on top infection.

A CASE REPORT: SPLENIC EPIDERMOID CYST

Cystic lesions of the spleen can be divided into four cathegories: infectious cysts, post-traumatic cysts, primary congenital cysts and intrasplenic pancreatic pseudocysts [1] . Splenic cysts are commonly pseudocysts following old hematoma or infarcts. Less common cysts are primary congenital cysts such as epidermoid cysts or infectious cysts such as hydratid cysts. All types, but especially the latter two, may show marginal calcification [2] We described a case of splenic epidermoid cysts; an unusual form of the splenic cysts.

CASE REPORT

A 24 year-old Thai man presented with sudden onset of severe left upper quadrant pain referring to the left shoulder. He had no previous history of trauma in this area. He has suffered from this symptom on and off for one year. The blood laboratory findings including CBC, renal and liver function tests were normal. The spleen was palpated 4 cm. below costal margin. Abdominal sonography showed an echo free area with echo enhancement deep to the lesion occupying in the spleen, having smooth sharp border and oval shape about 12.2 x 8.7 cm^2 in size (fig. 1) . Normal liver, pancreas and both kidneys were noted. Computed tomography scan revealed a large cyst in the spleen with partial rim calcification (fig. 2). Explore lab was done after complete investigation with diagnosis of impending rupture of the splenic cyst. At operation, the huge spleen was found measuring 15 x 12 x 10 cm^3 in size occupied by a big cyst at its superior portion. Moderate degree of adhesion over posterior and hilar areas were noted. The patient underwent a total splenectomy. The pathological diagnosis was epidermal cyst of the spleen. Microscopic examination revealed the cyst wall lining by squamous epithelium with intercellular bridges and acidophilic amorphous material content.

DISCUSSION

The true cysts are rare found mainly in people under 20 years of age called epidermoid, epithelial or congenital cysts. False or pseudocysts usually occur after trauma, infarction or parasitic infection. Abdominal ultrasound and CT scan are very useful imaging tools to obtain the pre-operative diagnosis but the reliable radiologic distinction

Department of Radiology. Faculty of medicine, Chulalongkorn University, Bangkok, Thailand.

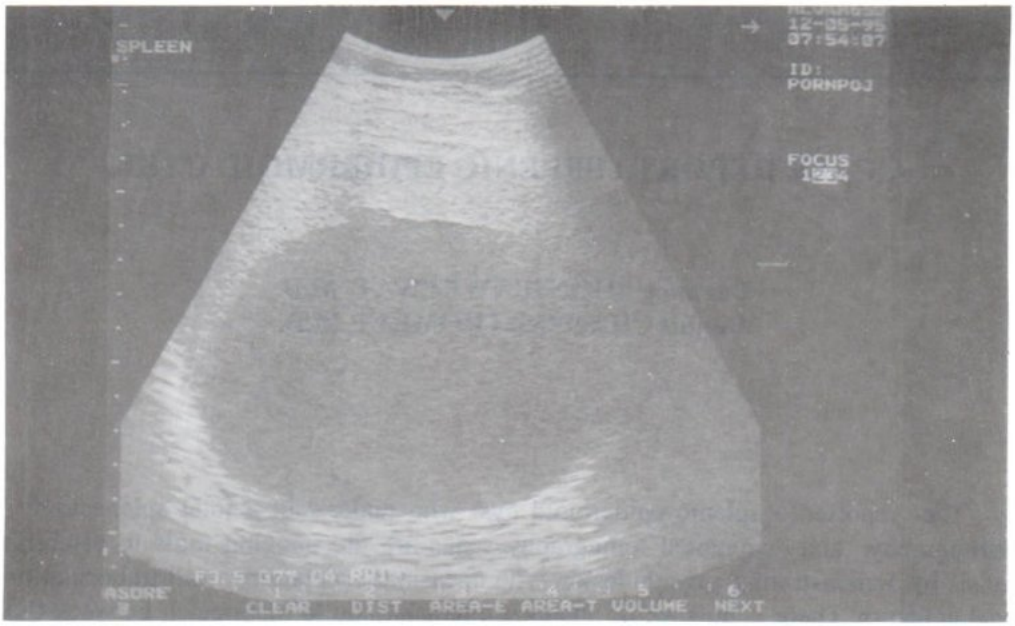

Fig. 1. Abdominal sonography showed an echo-free area with smooth, sharp border and enhancement of the echoes deep to the lesion occupying in the spleen about 12.2 x 8.7 cm^2.

between true and false splenic cyst does not seem possible [3]. The peak incidence of the splenic epidermoid cyst is in the second and third decades [4].

Basically true cysts containing an epithelial lining thought to originate from an abnormality in the development of the spleen during the seventh week of the embryological life when the spleen is close to the mesonephric tissue [5]. Others possible causes of true splenic cysts include infolding of peritioneal mesothelium after rupture of the splenic capsule, aggregation of peritioneal mesothelial cells trapped in splenic sulci or dilatation of normal lymphatic spaces.[6]

Abnormal findings on plain film may consist of splenomegaly with rim calcifications. On radionuclide studies the splenic cyst is seen as a well-defined photon-deficient area (cold lesion), but these findings are nonspecific, as an abscess or hematoma may assume a similar appearance [7]. Ultrasonography of the splenic cysts characteristically appear as echo-free areas with smooth, sharp borders and enhancement of the echoes deep to the lesions [1]. CT scan of the splenic cysts appear as thin-walled, unilocular, rounded, or oval intrasplenic masses of water density and typically display no contrast enhancement. Cyst wall trabeculation and septation may occur in either true or false cyst, but rim calcification is more common in false cysts. Debris or high-density material may be noted within either true or false cyst secondary to intracystic hemorrhage or in the case of false cyst residua of resolving hematoma [6]. MRI of the splenic cysts show the simple cyst as a low signal mass on T1-weighted scans that have a bright signal on T2-weighted scans.[8]

The differential diagnosis of non parasitic splenic cysts, which less common than traumatic pseudocysts, include hemangiomas, dermoids, lymphangiomas and, as in the present case, epidermoid variants [9]. The complication of the splenic epidermoid cysts are rupture and causing acute peritonitis [10,11]. The other is infection such as salmonella [11]. Epidermoid cyst in the intrapancreatic accessory spleen lined by squamous epithelium has been reported [12,13].

partial splenectomy is the treatment of choice of the splenic epidermoid cyst [14,15,16,17] or another benign cystic tumor because of the risk of post splenectomy sepsis. Another treatment procedures are drainage and deroofing [5], partial splenic decapsulation [18], percutaneous aspiration and tetracycline sclerosis [19], marsupialization [9].

REFERENCES

1. Mathieson R, Cooperberg PL. The spleen. In: Rumack CM, Willson SR, Charboneau JW, ed. Diagnostic ultrasound. Vol. 1. 1st ed. St. Louis: Mosby Year Book, 1991 :93.
2. Dick R. The liver and spleen. In: Sutton D, ed. Textbook of radiology and medical imaging. Vol. 2. 5th ed. New York: Churchill Livingstone, 1993:962.

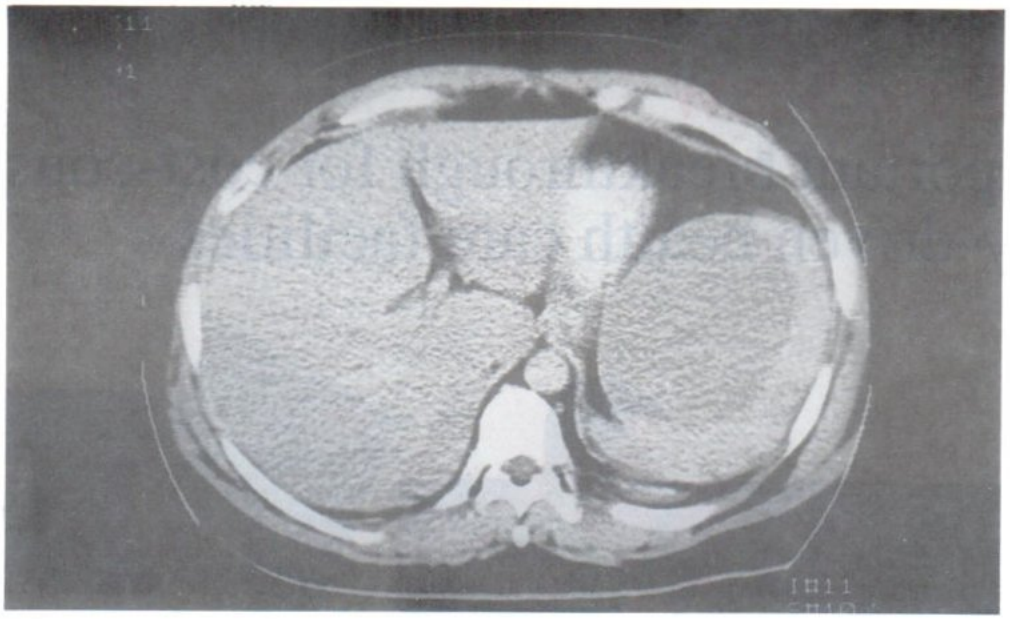

Fig. 2. Computed tomography scan revealed a large cyst in the spleen with partial rim calcification.

3. Dachman AH, Ros PR, Murari PJ, Olmsted WW, Lichtenstein JE. Nonparasitic splenic cyst: a case report of 52 cases with radiologic-pathologic correlation. AJR 1986;147:537-42.
4. Huang TY, Wylie RR, Thomas G, Gabedo J. Epidermoid cyst of the spleen: a clinico-pathologic correlation. Indiana Med 1990;83:326-8.
5. Carpenter G, Cotter PW, Davidson JR. Epidermoid cyst of the spleen. Aust N Z J Surg 1986;56:365-8
6. Grumbach K, McDowell R. The spleen. In: Haaga JR, Lanzieri CF, Sartoris DJ, Zerhouni EA, ed. Computed tomography and magnetic resonance imaging of the whole body. Vol. 2. 3rd ed. St. Louis: Mosby Year Book, 1994:1139-1140.
7. Chintapalli KN. Diseases of the spleen. In: Freeny PC, Stevenson GW, ed. Alimentary tract radiology. Vol. 2. 5th ed. St. Louis: Mosby Year Book, 1994:1774-1776.
8. Shirkhoda A. Spleen. In: Ros PR, Bidgood WD Jr, ed. Abdominal magnetic resonance imaging. 1 st ed. St. Louis: Mosby Year Book, 1993:289-291.
9. Sullivan CA, Konefal SH Jr. Epidermoid cyst of the spleen successfully treated by marsupialli-zation. Clin Pediatr 1987;26:203-5.
10. Vanhemelen G, Sebrechts R, Stroms P. Rupture mesothelial cyst of the spleen causing acute peritonitis. Acta Chir Belg 1994;94:210-1.
11. Panossian DH, Wang N, Reeves CD, Weeks DA. Epidermoid cyst of the spleen presenting as a generalized peritonitis. Am Surg 1990;56:295-8.
12. Tang X, Tanaka Y, Tsutsumi Y. Epithelial inclusion cysts in an intrapancreatic accessory spleen. Pathol Int 1994;44:652-4.
13. Morohoshi T, Hamamoto T, Kunimura T, Yoshida E, Kanda M, Fumo K, et al. Epidermoid cyst derived from an accessory spleen in the pancreas: a case report with literature survey. Acta Pathol Jpn 1991;41:916-21.
14. Khan AH, Bensoussan Al, Quimet A, Blanchard H, Grignon A, Ndaye M. Partial splenectomy for benign cystic lesions of the spleen. J Pediatr Surg 1986;21:749-52.
15. Brown MF, Ross AJ 3d, Bishop HC, Schnaufer L, Ziegler MM, Holcomb GW 3d. Partial splenectomy: the preferred alternative for the treatment of splenic cysts. J Pediatr Surg 1989;24:694-6.
16. Ehrlich P, Jamieson CG. Non parasitic splenic cysts: a case report and review. Can J Surg 1990;33:306-8.
17. Dillemans B, Mottrie A, Decoster M, Gruwez JA. Epidermoid cysts of the spleen. Acta Chir Belg 1993;93:265-7.
18. Touloukian RJ, Seashore JH. Partial splenic decapsulation: a simplified operation for splenic pseudocyst. J Pediatr Surg 1987;22:135-7.
19. Moir C, Guttman F, Jequier S, Sonnio R, Youssef S. Splenic cysts: aspiration, sclerosis, or resection. J Pediatr Surg 1989;24:646-8.

3M Dry View™

An important breakthrough for cost-conscious, quality-driven health care facilities

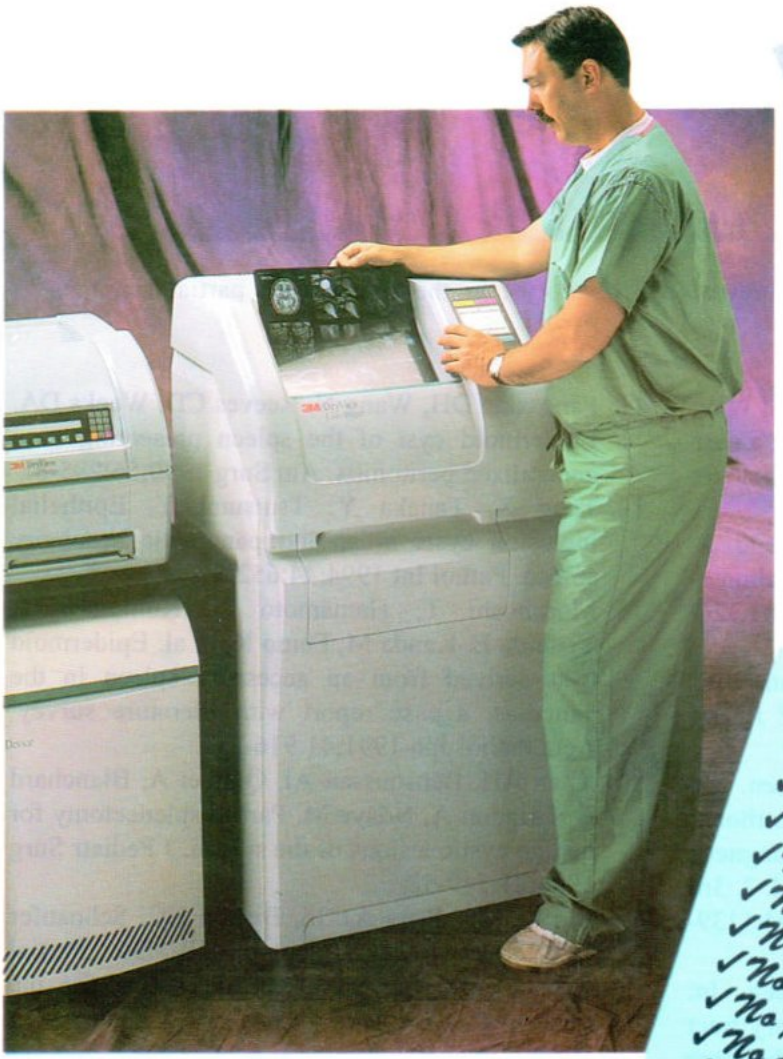

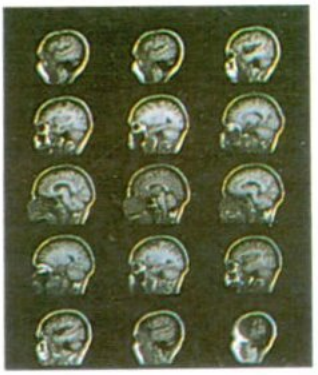

- ✓ No developer
- ✓ No fixer
- ✓ No wet processor
- ✓ No wet chemistry maintenance
- ✓ No wet processor downtime
- ✓ No wet chemistry purchase costs
- ✓ No processor/chemistry drift
- ✓ No plumbing for siting flexibility
- ✓ No darkroom
- ✓ No wet chemistry fumes
- ✓ No wet chemistry disposal costs

3M Medical Imagine Systems Division
3M Thailand Limited
Tel. 579-0023 Ext. 301
Fax 561-4052
Easy call 1500 - 130599

3M *Innovation*

ANGIOLYMPHOID HYPERPLASIA WITH EOSINOPHILIA OF THE ARM

Patchrin PEKANAN, Pimjai SIRIWONGPAIRAT, Wannanee MEUNNOOCH, Janjira CHATCHAVALA

ABSTRACT

A case of angiolymphoid hyperplasia with eosinophilia (ALHE) was shown in a 25-year-old female patient. The lesion was at the arm. CT scan showed a soft tissue mass with density 41-51 H.U. at the fat plane of the medial aspect of the lower one third of the arm. The lesion had infiltrated border with encasement of the vessels. Faint homogeneous enhancement was observed in the lesion. Peripheral eosinophil was mildly elevated. This is the first reported case of ALHE at the arm by CT scan

INTRODUCTION

Angiolymphoid hyperplasia with eosinophilia (ALHE) is a rare condition of uncertain etiology (1). It is thought by some to be a neoplasm of epithelioid endothelial cells (2). There are wide racial differences in presentation, with oriental patients being predominantly male and young in contrast to western cases which tend to occur in females and older patients (3). It causes papular or nodular angiomatous lesions in the dermis, subcutaneous tissues and adjacent lymph nodes, which average 1 cm in diameter (4). Distribution is almost entirely restricted to the head and neck (5) and there seems to be a predilection for area around the external ear and external auditory canal (6,7,8). There are reports involving the orbit (9), lacrimal gland (10), oral mucosa (11) and the arm (12).

We present a case of ALHE in a young female patient at her right arm. The images were of CT scan.

CASE REPORT

A 25-year-old single female patient from Nontaburi province had a mass at right arm for 1 year. The mass has increased size slowly and was not tender. The pain at the mass was observed only when she overused her right arm. There was no previous history of trauma. The soft tissue mass was palpated at the medial aspect of right upper arm, size 6 X 12 cm. The physical examination otherwise was normal. Complete white cell count showed total WBC 12.61 X 10^3/ul, Neu 59, Lym 29, Mono 5, Eos 7. CT scan at the mass showed a soft tissue mass, (density=41-51 H.U.) in the fat plane of lower medial part of the distal one third of the arm. The mass had irregular border. Faint and homogeneous enhancement in the mass was seen. Multiple linear soft tissue density was seen around the mass (Fig. 1).

At surgery, the mass with fibrofatty component, size 3 x 5 x 10 cm. was seen. The mass had ill defined border, infiltrating around the cephalic vein and sensory branch of the musculocutaneous nerve. The mass adhered to the brachial artery below and skin above. The CT scan also showed the vascular encasement (Fig. 2).

The mass was dissected with preservation of the vasculature. At pathology, section of the soft tissue of the arm revealed angiolymphoid hyperplasia with eosinophilia. Section of the lymph nodes of the arm showed angiolymphoid hyperplasia with mild eosinophilia, clusters of atypical lymphoid cells. Section of the skin revealed nonspecific perivascular lymphoid cells infiltration in the dermis.

[1] Department of Radiology, Ramathibodi Hospital, Rama 6 Street, Bangkok 10400, Thailand.

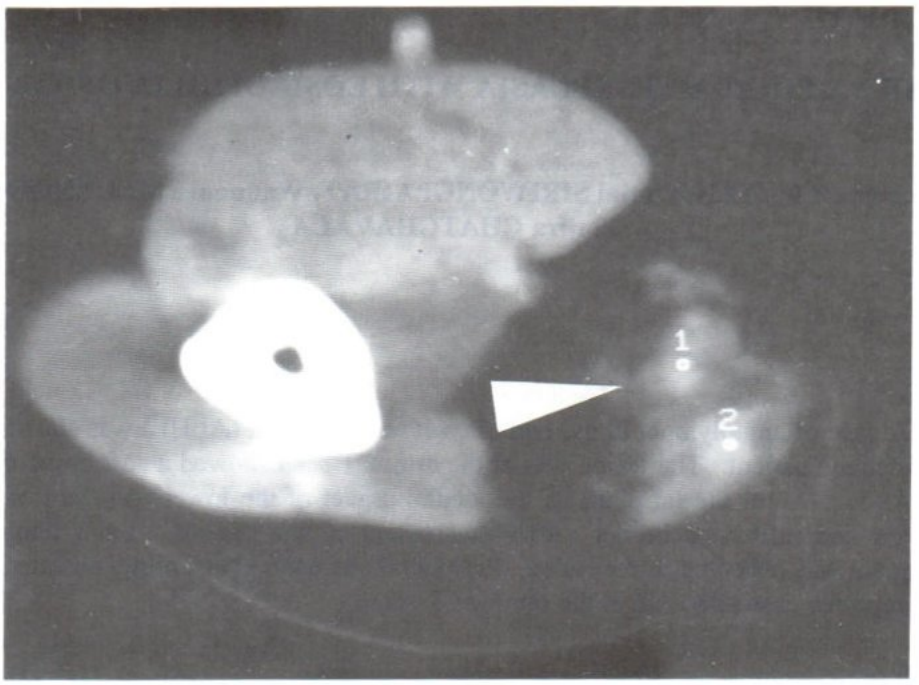

Fig. 1A. Non enhanced axial CT scan of the right arm showed an infiltrative border solid mass in the subcutaneous fat plane.

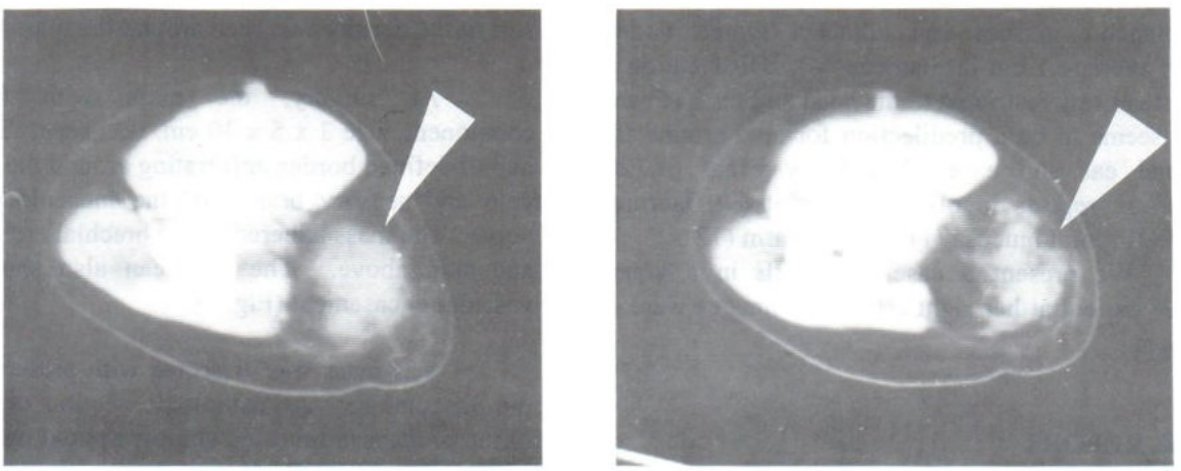

Fig. 1B Enhanced study showed faint homogenous enhancement in the lesion.

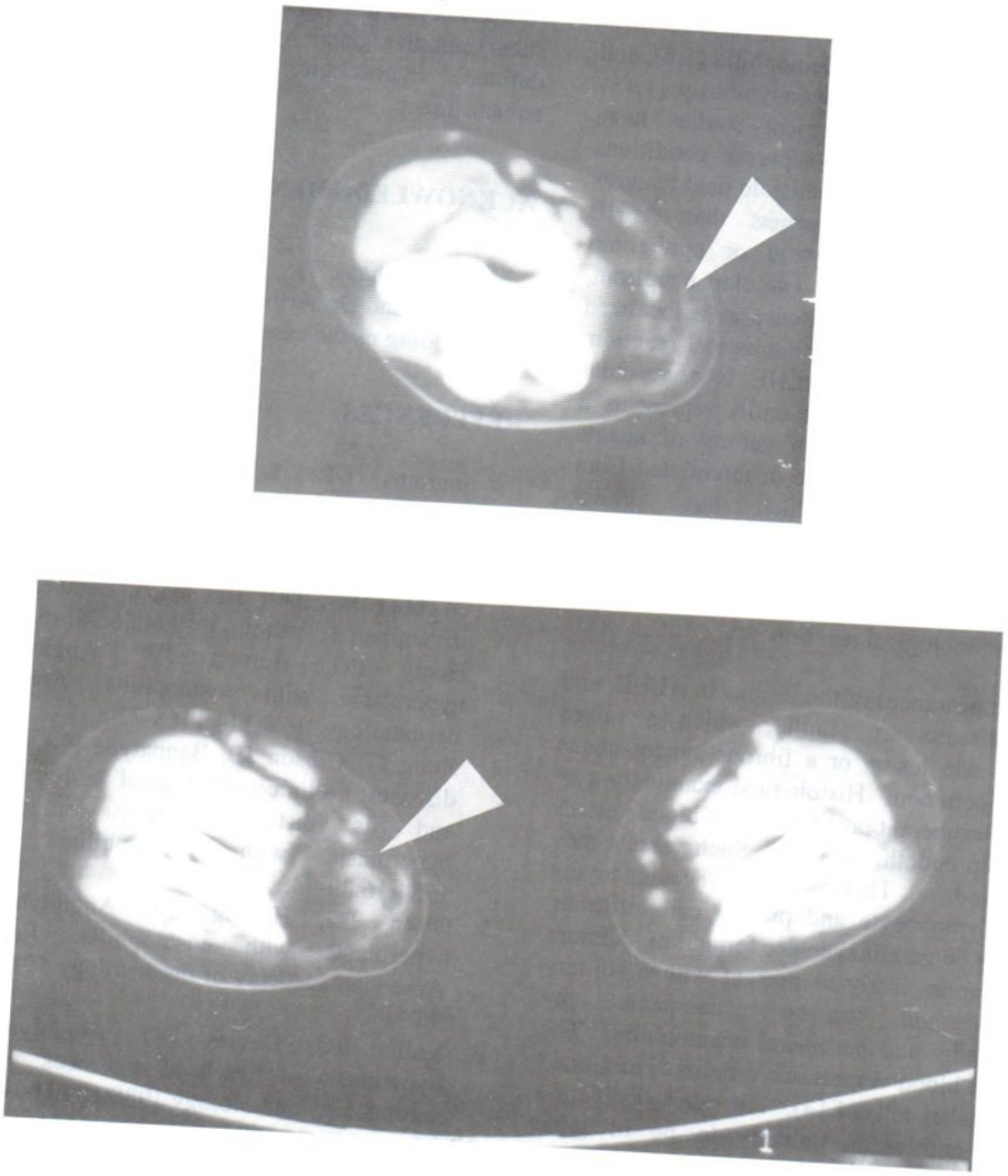

Fig. 2 Vascular encasement was also demonstrated by images, corresponding to the surgical findings.

DISCUSSION

Originally ALHE was thought to be equivalent to Kimura's diseases, a condition prevalent in Japan, China and South-east Asia which also causes angiomatous skin lesions, together with lymphadenopathy and marked eosinophilia (1,8), and the terms have often been used synonymously (1,15). However recent clinicopathological studies have suggested that these are two separate conditions which have different clinical and histological features (1,14,15). These authors suggest that ALHE represents a stage of histiocytoid or epithelioid hemangioma, which is a true vascular neoplasm, whereas they view Kimura's disease as a localized manifestation of a systemic immunological reaction. Other authors disagree that ALHE is a vascular neoplasm; they believe that the entity represents a localized atrophic reaction to a variety of agents (12,16). It therefore needs to be differentiated from epithelioid hemangioma, which has similar histological features to ALHE regarding endothelial cell morphology, but is without the eosinophilic infiltrate or formation of germinal centers which suggest an immunological reaction.

The appearances of the lesions in ALHE and Kimura's disease are similar, which a raised erythematous skin lesion or a fibrous subcutaneous nodule being common. Histological examination of ALHE shows exuberant proliferation of blood vessels lined by plump endothelial cells. Such vessels may be uncanalized. There is an accompanying perivascular lymphocyte and plasma cell infiltrate, and there may be germinal center formation. Kimura 's disease is more likely to present with a solitary larger mass and to be accompanied by lymphadenopathy and peripheral eosinophilia. The newly formed blood vessels are canalized, and lined by flat endothelial cells (4,14). The exact distinction of the two entities is unlikely to be of great importance, as these diseases probably represent a similar reactive process in the tissue, with the minor histological differences depending on whether the insult is localized or systemic.

ALHE is benign, and may regress spontaneously, but the majority of masses persist as slow growing tumours (17). There are no report of malignant change. The appearances of the lesion have led it to be mistaken for Kaposi's sarcoma, malignant lymphoma and angiosarcoma, as well as pyogenic granuloma, hemangioma and dermatofibroma (18,19).

Imaging study of ALHE was not reported before, according to our knowledge. Smith (20) reported CT of Kimura disease of the parotid gland. Ahuja (21) demonstrated Kimura's disease of the submandibular gland by ultrasonography as a well defined, hypoechoic, oval mass with distal enhancement.

ACKNOWLEDGMENTS

We thank Dr. Prawat Nitiyanan (Dept. of Pathology) and Dr. Arthit Kroewit (Dept. of Surgery) for providing us the case.

REFERENCES

1. Ingrams DR, Stafford ND, Creagh TM, Angiolymphoid hyperplasia with eosinophilia. The Journal of Laryngology and Otology 1995;109:262-4.
2. Webber JM. Test and teach, number seventy-seven, part 1. Pathology 1994;26:345-6.
3. Henry PG, Burnett JW. Angiolymphoid hyperplasia with eosinophilia. Archives of dermatology 1978;114:1168-72.
4. Kung IT, Gibson JB, Bannatyne PM. Kumura's diseases: a clinicopathological study of 21 cases and its distinction from angiolymphoid hyperplasia with eosinophilia. Pathology 1984;16:39-44.
5. Olsen TG, Helwig EB. Angiolymphoid hyperplasia with eosinophilia. Journal of American academy of dermatology 1985;12:781-96.
6. Vallis RC, Davies DG. Angiolymphoid hyperplasia of the head and neck. Journal of laryngology and otology 1988;102:100-01.
7. Murty GE, Cox HN. Angiolymphoid hyperplasia with eosinophilia: an uncommon tumour of the external auditory canal. Ear, Nose and Throat Journal 1990;69:012-103, 106-7.
8. Sharp JF, Rodgers MJC, Macgregor FB, Meehan CJ, McLaren K. Angiolymphoid hyperplasia with eosinophilia. Journal of laryngology and otology 1990;104: 977-9.
9. Smith DL, Kincaid MC, Nicolitz E. Angiolymphoid hyperplasia with eosinophilia (Kimura's disease) of the orbit. Archives of Ophthalmology 1988;106:793-5.

10. Cook HT, Stafford ND. Angiolymphoid hyperplasia with eosinophilia involving the lacrimal gland: case report. British Journal of Opthalmology 1988;72:710-12.
11. Buckerfield JB, Edwards MB. Angiolymphoid hyperplasia with eosinophils in oral mucosa. Oral Surgery, oral medicine and oral pathology 1979;47:539-44.
12. Akosa AB, Ali MH, Khoo CTK, Evans DM. Angiolymphoid hyperplasia with eosinophilia associated with tetanus toxoid vaccination. Histopathology 1990;16:589-93.
13. Kimura T, Yoshima S, Ishikawa E. Abnormal granulation combined with hyperplastic change of lymphoid tissue. Transactions of the Japanese pathological society 1948;37:179-80.
14. Sharp JF, Rodgers MJC, MacGregor FB, Meehand CJ, McLaren K. Angiolymphoid hyperplasia with eosinophilia. Journal of laryngology and otology 1990;104:977-9.
15. Smith DL, Kincaid MC, Nicolitz E. Angiolymphoid hyperplasia with eosinophilia (Kimura's disease) of the orbit. Archives of Ophthalmology 1988;106:793-5.
16. Henry PG, Burnett JW. Angiolymphoid hyperplasia with eosinophilia. Archives of dermatology 1978;114:1168-72.
17. Wells GC, Whimster IW. Subcutaneous angiolymphoid hyperplasia with eosinophilia. British Journal of dermatology 1969;81:1-15.
18. Barnes L, Koss W, Nieland ML. Angiolymphoid hyperplasia with eosinophilia:a disease that may be confused with malignancy. Head and neck surgery 1980;1:425-34.
19. Buckerfield JB, Edwards MB. Angiolymphoid hyperplasia with eosinophils in oral mucosa. Oral surgery, oral medicine and oral pathology. 1979;47:539-44.
20. Smith JRG, Hadgis C, Van Hasselt A, Metreweli C. CT of Kimura disease. AJNR 1989;10:534-6.
21. Ahuja AT, Loke RKL, Mok CO, Chow LTC, Metreweli C. Ultrasound of Kimura's disease. Clinical Radiology 1995;50:170-3.

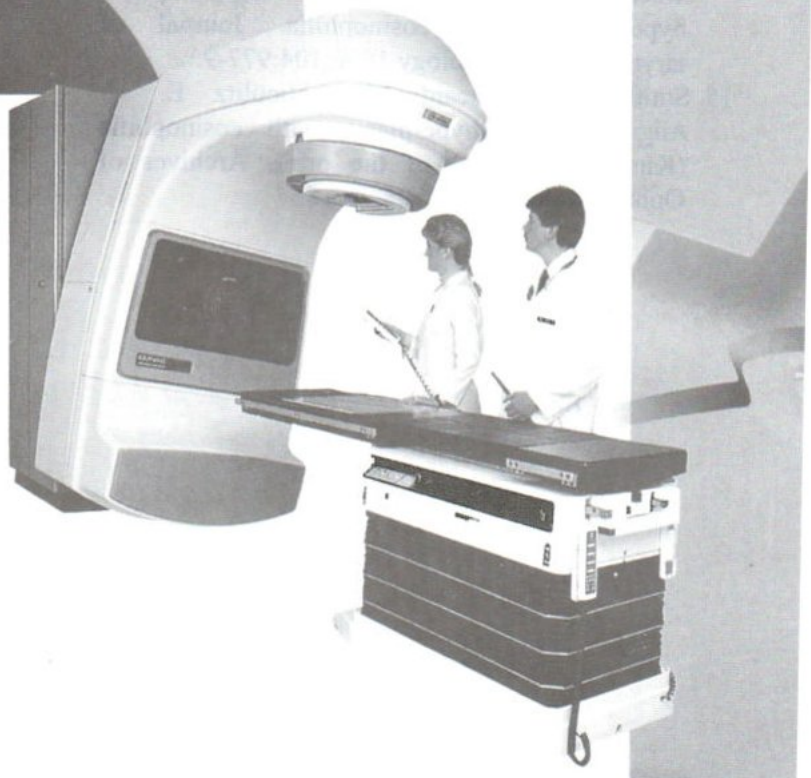

CLINAC 2100C

The standard in dual energy performance and operational efficiency.

The Clinac 2100C dual energy, standing-wave accelerator provides cost-effective, multi-modality treatments with a choice of x-ray energy combinations from 6 to 18 MV, literally two accelerators in one, and one of four electron combinations from 4 to 20 MeV.

The Clinac 2100C meets your unique clinical requirements with options like dual independent collimators, high dose-rate electrons, and electron arc therapy.

As with all the C-Series products, the Clinac 2100C can be linked to the RMS-2000 Radiotherapy Management System for efficient data entry and treatment verification.

CT AND ANGIOGRAPHY OF ESTHESIONEUROBLASTOMA

Patchrin PEKANAN[1], Sirintara PONGPECH[1], Wara VORRASUBIN[2], Pravit PRACHASILPCHAI[3], Chitchanok TANTIWIWAT[1].

ABSTRACT

A case report of Esthesioneuroblastoma in a 39-year-old female patient was presented. The mass was a slow growing one, when found it was quite extensive to be located in both nasal cavities, medial part of right maxillary sinus, both ethmoid sinuses, left sphenoid sinus, left orbital cavity, and epidural space of the anterior cranial fossa. Bowing pattern, bony erosion and tumoral calcification was shown by CT scan. The metastatic tumor to right parotid gland was already present. The tumor received blood supply from both maxillary arteries and left ophthalmic artery and the main feeder was left maxillary artery which indicated that the tumor originated from the left side of the nasal cavity.

INTRODUCTION

Esthesioneuroblastoma is a rare nasal neoplasm, arising from neuroepithelial elements in the olfactory membrane in the superior portion of the nasal cavity (1). It occurs in all ages, with a range of 3 to 79 years of age. The incidence shows a bimodal distribution with peaks in the second and sixth decades of life (2). The distribution between the sexes is roughly equal. The symptoms are non-specific and include epistaxis, anosmia, rhinorrhea and nasal obstruction. Due to this lack of symptoms, most patients are diagnosed late in the course of the disease (1). It usually appears as a red or fleshy mass in the nasal vault. Symptoms of local invasion, such as proptosis or headache, are usually evident at diagnosis.

The tumor was first described as 'L' esthesioneuroepitheliome olfactif' in 1924 by Berger (3). Numerous names have been used to describe this neoplasm including olfactory neuroblastoma, olfactory esthesioneuroma, esthesioneurocytoma and neuroendocrine carcinoma (4).

We present a case of this tumor by CT and angiographic imaging.

CASE REPORT

A 39-year-old female patient from Pracheenburi province, was referred to Rajvithi hospital due to the presence of the intranasal mass. She had the symptom of nasal congestion for 10 years and the left intranasal mass was palpated later. Another mass was palpated at right cheek for 8 months. Axial and coronal CT scan of the nasal cavities was performed and showed a 5.5X7X5.3 cm enhanced soft tissue density mass with an epicenter in the nasal cavities. The growth of the tumor was seen in both nasal cavities, medial part of right maxillary sinus, subcutaneous fat plane and skin of the nose, in both ethmoid sinuses, anterior part of left sphenoid sinus and medial part of left orbital cavity. Expanding appearance of the mass was appreciated at medial walls of both maxillary sinuses, in right ethmoid sinus and medial wall of ethmoid sinus. Dense calcification was shown in the central part of the mass. Small extension to epidural space of anterior cranial fossa was noted. Another tumor mass was seen at the superficial portion of right parotid gland, size 3 X 3.5 X 4 cm with well defined border. The cavernous sinuses were normal. Local

[1] Department of Radiology, Ramathibodi Hospital, Rama 6 Street, Bangkok 10400, Thailand.
[2] Department of ENT. Rajvithi Hospital, Bangkok.
[3] Department of Surgery, Rajvithi Hospital, Bangkok.

destruction of the hard palate was observed (Fig.1,2).

Biopsy from the mass in left nasal cavity revealed small round cell tumor. The study of immunohistochemical one led to the diagnosis of olfactory neuroblastoma by Dr. Arunluck Komindr, the pathologist of Rajvithi Hospital. Metastatic nodule at right parotid gland from esthesioneuroblastoma was also diagnosed from the biopsy by the same pathologist.

The patient was sent to Ramathibodi hospital for pre-surgical embolisation. Pre-embolized angiography revealed a hypervascular large nasal mass which received bloody supply from left maxillary artery (main feeder), right maxillary artery and left ophthalmic artery. Successful Ivalon and gelfoam embolization of both maxillary arteries was shown (Fig.3,4).

DISCUSSION

Because the normal distribution of olfactory epithelium may extend from the cribriform plate to the level of the middle turbinates, esthesioneuroblastoma may arise in the region of the nasal cavity anywhere throughout this distribution (4,5). Light microscopic study reveals features similar to classical childhood neuroblastoma. In an upper nasal neoplasm, the presence of a fibrillary intercellular background in conjunction with Homer-Wright pseudorosettes is considered to be diagnostic of olfactory neuroblastoma. However, these hallmarks are not always evident, and confusion with other primary tumors of the nasal cavity and paranasal sinuses, such as lymphoma, undifferen-tiated carcinoma, and extramedullary plasmacytoma is possible. Therefore, immunohisto-chemistry and electron microscopy are necessary for the histologic diagnosis (1).

Although slow growing, esthesioneuroblastomas are locally invasive and can metastasize to regional lymph nodes, lung or bone. No treatment had been convincingly (1,2,5,6). Survival is related to the stage of disease at initial diagnosis (2,4). Kadisch (6,7) proposed a staging classification of esthesioneuroblastoma based on extent of disease: stage A is involvement of the nasal cavity only; stage B is involvement of the nasal cavity and one or more paranasal sinus; and stage C is involvement outside the nasal cavity including orbit, base of the skull, intracranial cavity, cervical nodes, or distant metastases.

The CT features in 9 patients of this tumor studied by Hurst (4) demonstrate a fairly consistent pattern. All tumors were centered in the superior nasal cavity or ethmoids. Tumor density prior to enhancement was relatively homogeneous and was equal to or greater than the surrounding soft tissue. Contrast enhancement was usually moderate in intensity and homogeneous but, with one exception, was without cystic or hemorrhagic areas. Calcification has been reported. The location and size of the calcific densities often made it difficult to determine radiologically whether this represented tumoral calcification or bony fragments secondary to destruction by tumor. Bony erosion was often associated with bowing. Intracranial extension was seen in 20-57% and was very common is Stage C (4,8). All stage C cases demonstrated involvement of the orbit. Displacement of the medial rectus muscle by tumor mass was in present in 81%. The periorbital tissue is frequently acts as a barrier.

The MR features of the tumor are nonspecific and is variable (7). The tumor can have homogenous or heterogeneous signal characteristics. Compared with brain gray matter, the tumors are generally hypointense on T1WI and isointense to hyperintense on PD and T2WI. Contrast enhancement of the tumor is variable but always present. It often expands the nasal cavity, usually with concurrent destruction of the nasal septum turbinates, and ethmoid septa. Local extension with further bone destruction can occur.

Our patient should be classified as Stage C. The CT findings are similar to reported cases, including features of tumoral calcification, bony erosion and bowing pattern.

In the series of 26 patients, reported by Levine (9), an increased disease-free interval exists with the use of combined preoperative radiotherapy and craniofacial resection for stage A and B disease, and the addition of preoperative and postoperative vincristine and Cytoxan for stage C disease.

ACKNOWLEDGMENTS

We thank the department of Radiology of Rajvithi Hospital for the CT images.

REFERENCES

1. Sakato K, Aoki Y, Rarasawa K, Nakagawa K, et al. Esthesioneuroblastoma: A report of seven cases. Acta Oncological 1993;12:399-402.

2. Elkon D, Hightower SI, Lim ML, Cantrell RW, Constable WC. Esthesioneuroblastoma. Cancer 1979;44:1087-94.
3. Berger RL. L' esthesioneuroepitheliome olfactif. Bull Assoc Franc Pour L' Etude Cancer 1924;13:410-20.
4. Hurst RW, Erickson S, Cail WS, Newman SA, Levine PA, Burke J, Cantrell RW. Computed tomographic features of esthesioneuroblastoma. Neuroradiology 1989;31:253-57.
5. Shah JP, Feghali J. Esthesioneuroblastoma CA 1983;33:154-9.
6. Kadish S, Goodman M, Wang CC. Olfactory neuroblastoma: a clinical analysis of 17 cases. Cancer 1976;37:1571-6.
7. Shuster JJ, Phillips D, Levine PA. MR of esthesioneuroblastoma (Olfactory) (neuroblastoma) and appearance after craniofacial resection. AJNR 1994;15:1169-77.
8. Manelie C, Bonafe A, Fabre P, Pessey JJ. Computed tomography in olfactory neuroblastoma: One case of esthesioneuroepithelioma and four cases of esthesioneuroblastoma. J Comput Assist Tomogr 1978;2:412-20.
9. Levine PA, McLean WC, Cantrell RW, Charlottesville VA. Esthesioneuroblastoma: The university of Virginia: experience 1960-1985.Laryngoscope 1986;96:742-46.

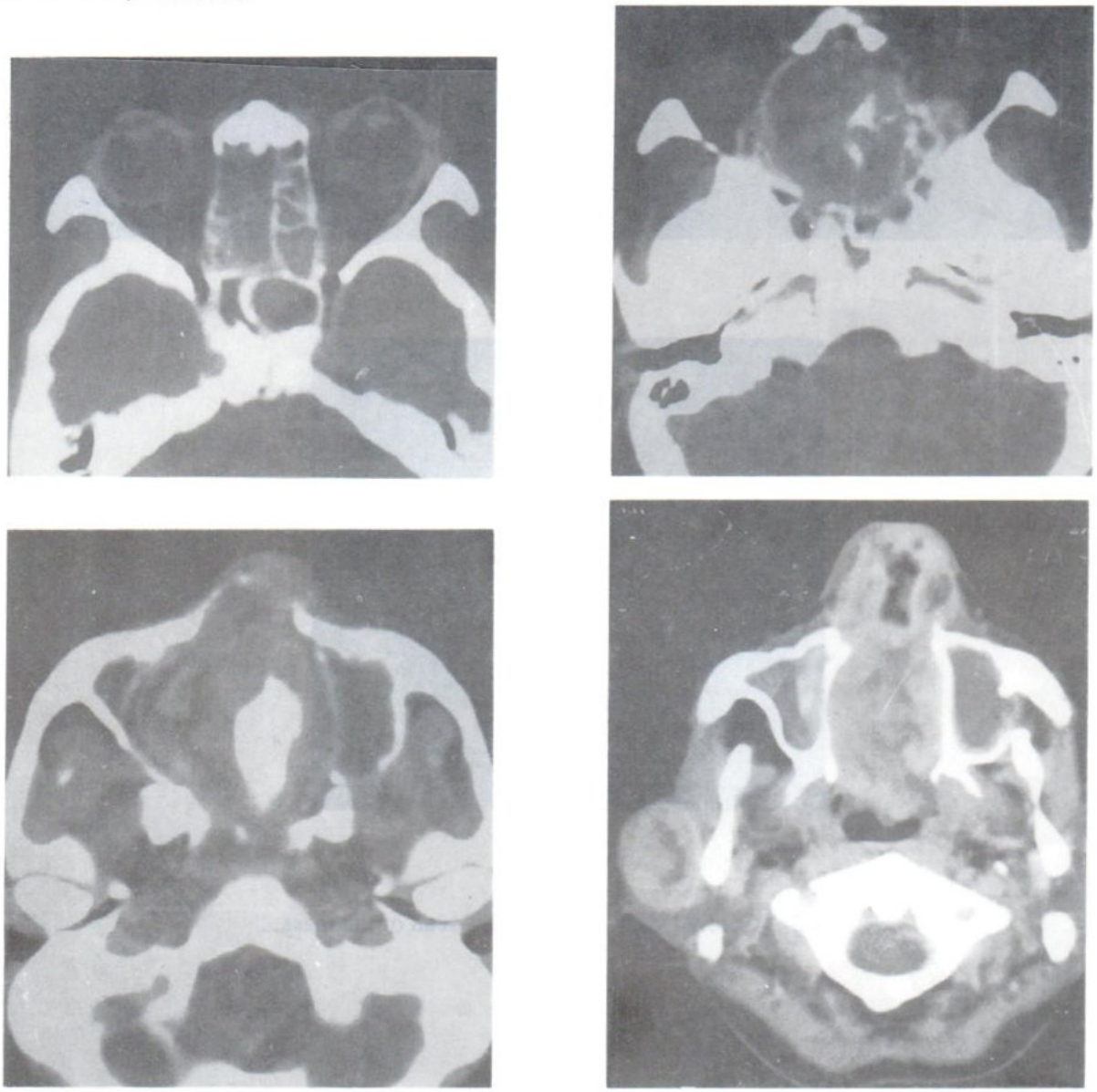

Fig.1 Axial view enhanced CT scan of the mass

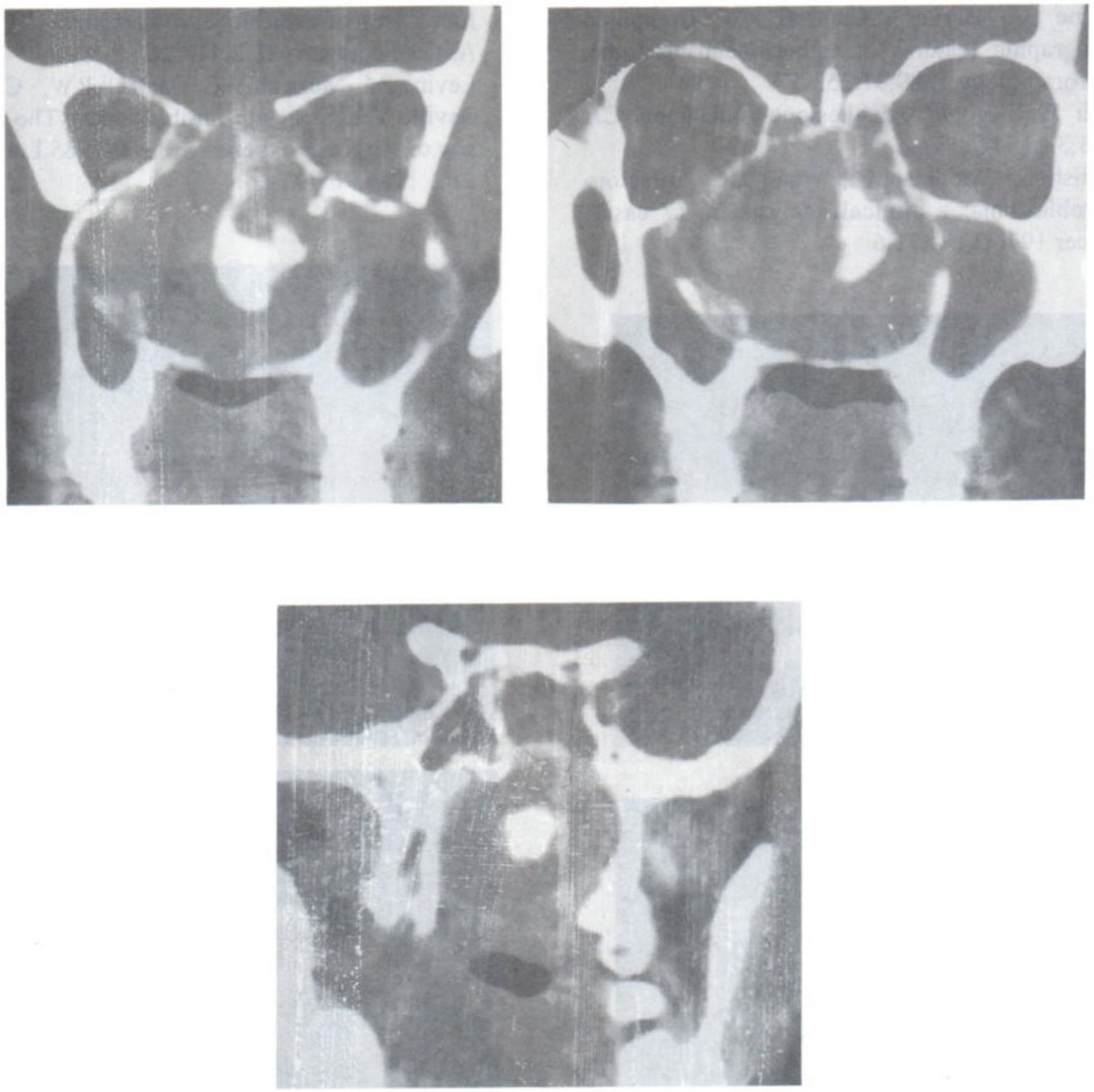

Fig.2 Coronal view enhanced CT scan of the mass .

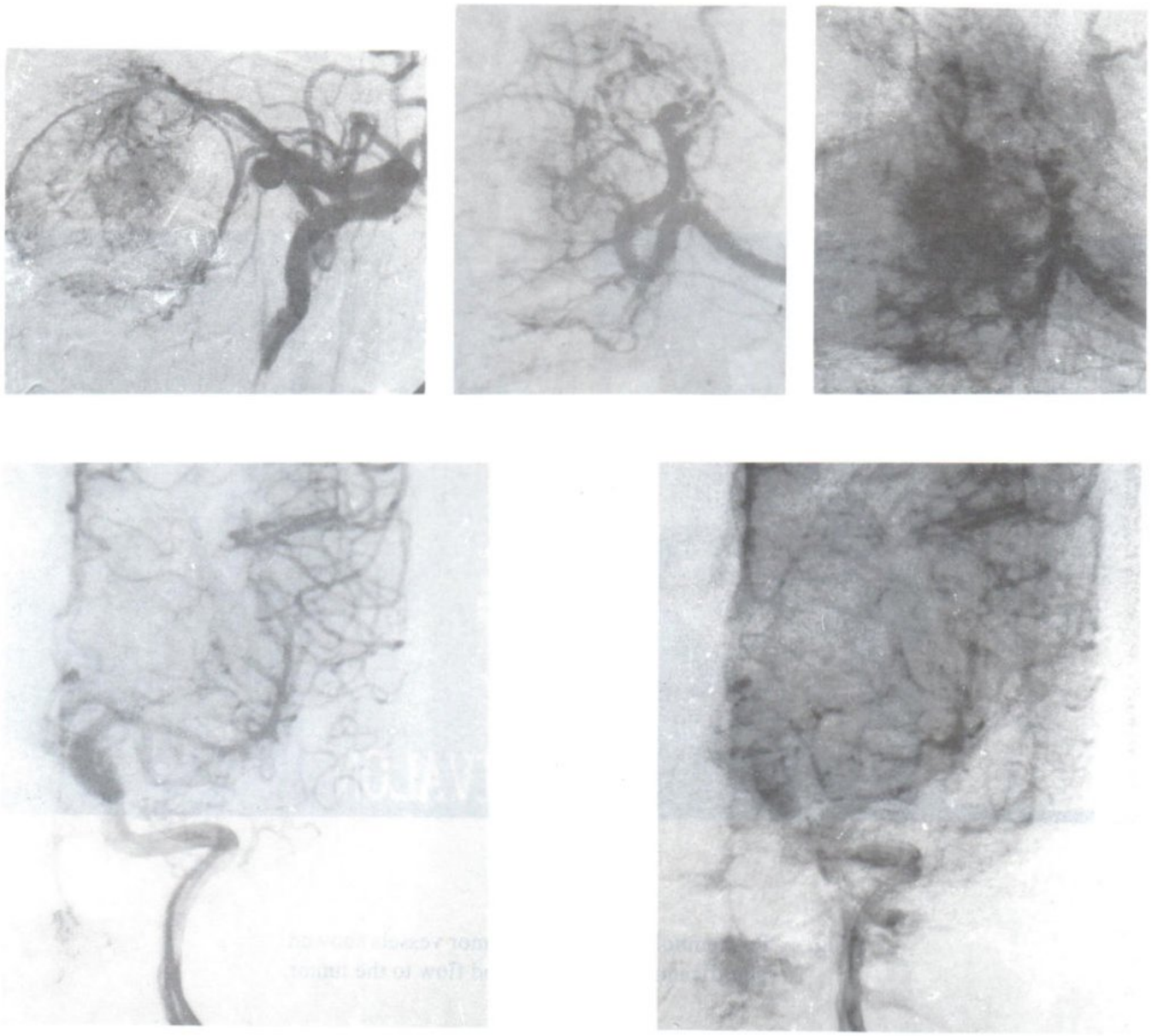

Fig.3 Preembolization angiography of the mass showed feeding arteries to the mass from both maxillary arteries and left ophthalmic artery.

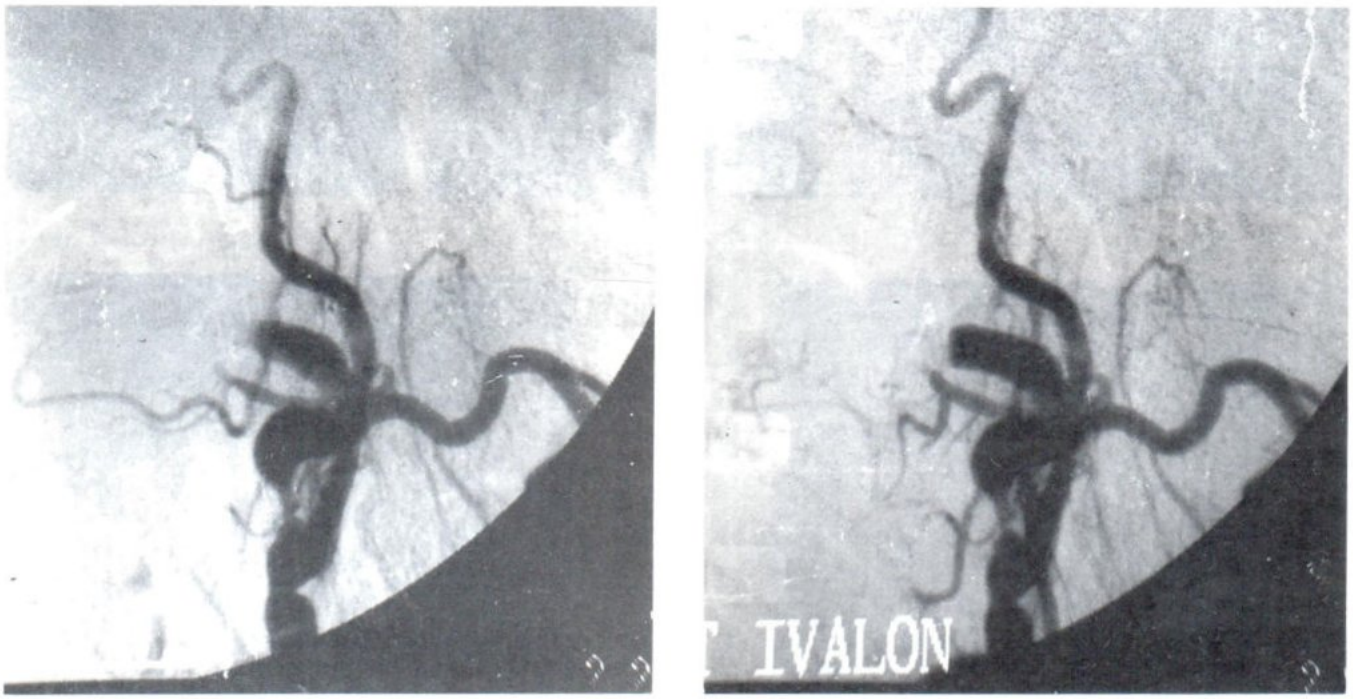

Fig. 4 Post embolization of the tumor vessels showed significantly decreased blood flow to the tumor.

CASE REPORT: SUBCLAVIAN VEIN THROMBOSIS TREATED BY PULSE-SPRAY THROMBOLYSIS USING A RETROGRADE APPROACH

DES Wong*, KH Leong,PH Feng**, TSG Chee***

ABSTRACT

We report a case of subclavian vein thrombosis in a 44 year old lady with SLE that was successfully treated with transcatheter thrombolytic techniques. The treatment was unusual in that a retrograde approach to the thrombosed vessel had to be employed due to the failure to canulate a distal peripheral vein. We also used the Pulse Spray technique to administer the thrombolytic drugs, the technique being originally described for thrombolysis in the arterial system. The patient has been followed up for 8 months with no recurrence of the problem.

INTRODUCTION

The axillary and subclavian veins is one area in the venous system in which local transcatheter low-dose fibrinolytic therapy is rapidly becoming the treatment of choice for thrombosis. We describe a case of acute axillary vein thrombosis that was successfully treated using a retrograde approach for pulse-spray thrombolysis.

CASE REPORT

A 44 year old Chinese lady with SLE of 12 years presented with a one day history of progressive swelling of the left upper limb. Distended veins were noted over her chest wall. Oedema was pitting and the arm not tender. Distal pulses were normal. In the past, she had biopsy proven Class IV nephritis, lupus gut and autoimmune hemolytic anemia. She also had pulmonary tuberculosis and steroid induced osteoporosis resulting in cough fractures. Prior to the current problem, she did not have livido reticularis, thrombocytopenia, miscarriages or clinical thrombotic events.

Diagnostic venography performed via an antecubital vein demonstrated an abrupt cut-off at the subclavian vein (Fig. 1) consistent with acute thrombosis. Unfortunately, the examining radiologist removed the venula after the procedure.

As no other suitable superficial veins for thrombolysis could be found in the left upper limb, a 5 French Head Hunter 1 catheter (Cook) was introduced into the subclavian vein via the right common femoral vein. Proximal venography (Fig 2) demonstrated the thrombus to be approximately 3cm in length. Due to the small thrombus load and a satisfactory respiratory reserve, we decided against prophylactically deploying a central caval filter in the SVC. A guide wire (0.035 inch curved hydrophilic Glidewire, Terumo) was negotiated through the thrombus and the catheter exchanged for a 5F, multi-sidehole Pulse Spray Catheter (Meditech, Boston Scientific) which was positioned across the thrombus. Using the Pulse Spray Technique described by Bookstein et al[1], 200,000 units of Urokinase (Ukidan, Serono) and 5000 IU of Heparin was administered over a period of 20 minutes. This

Departments of Diagnostic Imaging* and Rheumatology**, Tan Tock Seng Hospital,Moulmein Road,Singapore.

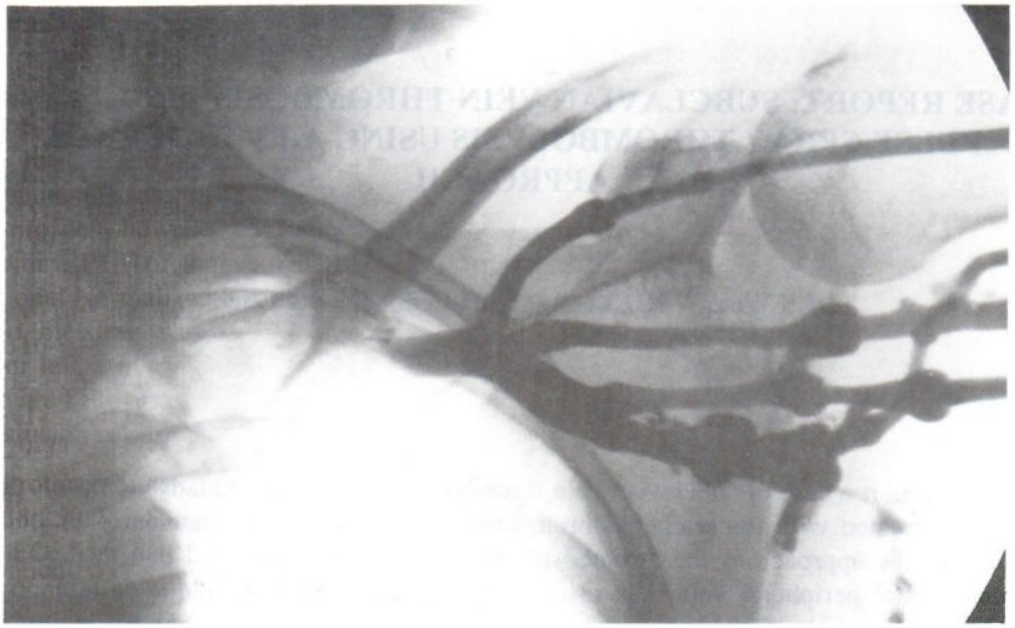

Fig. 1. Upper limb venography. Demonstrating thombosis of the subclavian vein.

was sufficient to reestablish blood flow through the thrombus. (Fig. 3) A further 300,000 units was infused over the next 15 hours (20,000 IU/hour) during which time the swelling of the arm gradually improved. The following day, a further 400,000 units was infused over 4 hours via a single end-hole catheter embedded in the distal portion of the clot, achieving complete lysis of the thrombus, and exposing a segment of underlying luminal irregularity (Fig. 4) During the entire treatment period, patient was maintained on 1000 units of Heparin per hour and thereafter for a further 24 hours. The swelling of the arm continued to improved and returned to normal 48 hours after commencement of thrombolysis. At no time during the procedure did patient experience any respiratory symptoms.

COMPLICATIONS

Perforation of the axillary vein distal to the thrombus occurred on the second day of thrombolysis during catheter manipulation. This was confirmed by contrast injection which outlined the fibers of pectoralis major. Patient did not experience any symptoms related to this and was unaware of the complication. The catheter was withdrawn back into the vessel without embolization of the false tract and

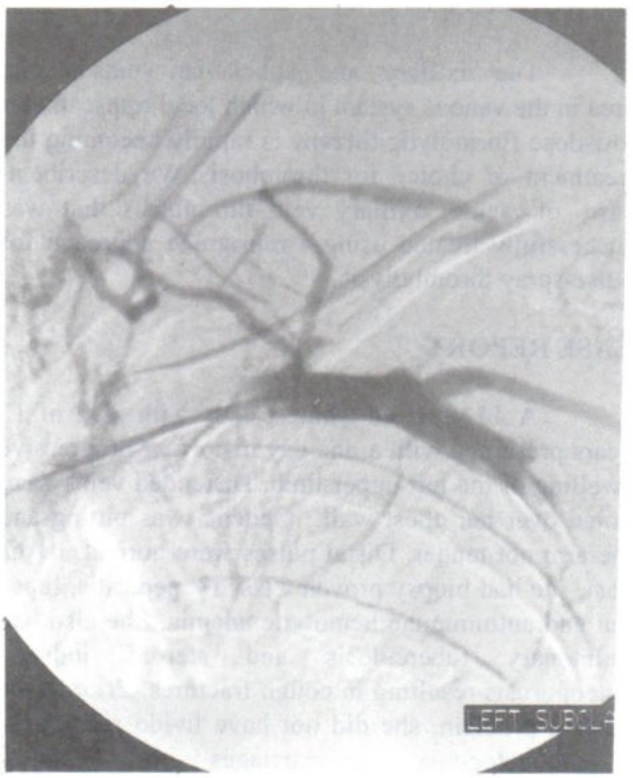

Fig. 2. Venography using a head hunter 1 catheter introduced retrogradely showing the length of thrombus to be about 3 cm., Drainage is via collaterals around the supra-clavicular fossa.

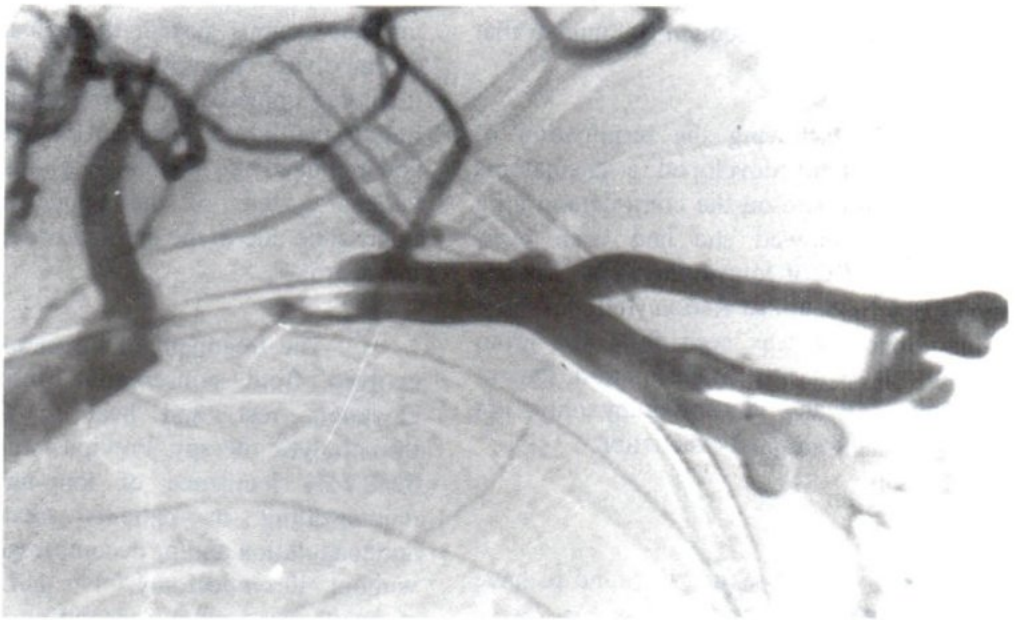

Fig. 3. After 200,000 units of urokinase and 5000 units of heparin. Note some contrast flowing around the catheter and better opacification of the innominate vein.

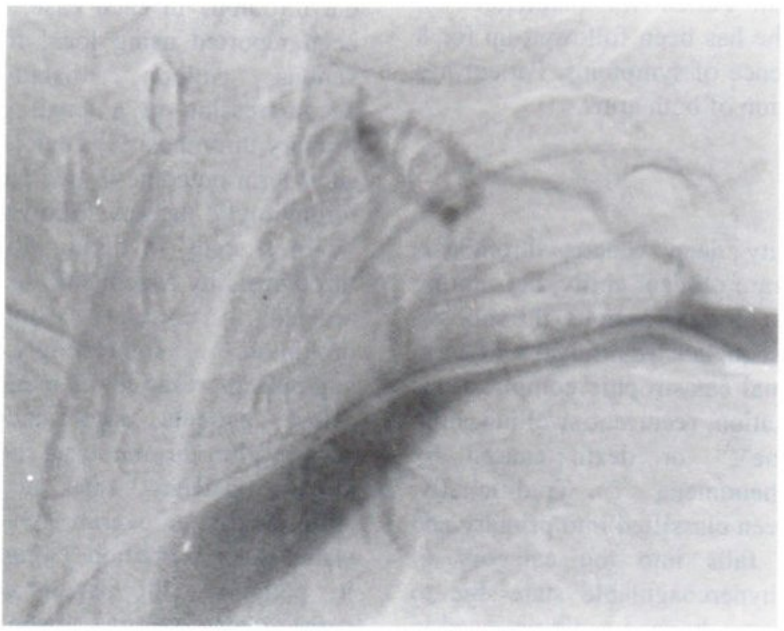

Fig. 4. After 900,000 units of urokinase showing no residual clot but some irregularity of the superior wall. Treatment was stopped at this stage.

thrombolysis continued. No evidence of bleeding or haematoma formation was subsequently found at that site.

On the day following the termination of thrombolysis, the patient developed a haematoma around a venepuncture site on the contralateral arm. Coagulation profile showed she had been over-heparinized with a PTT of longer than 120 seconds and a International Normalized Ration (INR) of more than 5.92. No bleeding was seen from the groin puncture site or left axillary vein perforation. Patient was treated with FFP and physiotherapy only, not requiring transfusion or surgical evacuation.

FOLLOW-UP

The patient was subsequently found to have secondary antiphospholipid syndrome with a raised Anti Cardiolipin Antibody of 33. A ventilation perfusion scan performed 10 days after the procedure demonstrated mismatched defects of the posterior basal segments of both lower lobes and the lateral aspect of the left upper lobe. Duplex studies of the deep venous system did not reveal any thrombosis in the lower limbs, IVC and renal veins, and the pulmonary emboli was assumed to have originated from the subclavian vein. Patient was maintained on Warfarin 5mg daily. She has been followed up for 8 months with no recurrence of symptoms. Patient has also regained full function of both arms.

DISCUSSION

Upper extremity deep venous thrombosis (DVT) is a relatively rare clinical entity, accounting for approximately 2% of total venous thrombosis, with potentially grave sequelae. Significant long-term morbidity and occasional catastrophic complications include venous claudication, recurrent swelling, limb loss due to gangrene[ii,iii] or death caused by pulmonary embolic phenomena[iv,v,vi]. Traditionally, upper limb DVT has been classified into primary and secondary. Our case falls into the category of secondary causes, a hypercoagulable state due to antiphospholipid syndrome, hence we did not need to exclude and treat for external compressive forces on the vein.

We chose to investigate our case by venography as this is the gold standard, doppler ultrasound having been shown to have a poorer sensitivity and specificity[vii,viii]. Having gained access into the venous system through a antecubital vein, thrombolytic therapy would ideally have been instituted immediately. Unfortunately, the examining radiologist did not consider this treatment possibility and removed the venula. Regaining access into the venous system of the upper limb then proved impossible due to the marked oedema already present in the arm.

The treatment of upper extremity DVT has evolved from conservative modalities including elevation, rest, and heat to the current local thrombolytic therapy. Previous studies documented a 50%-74% incidence of long-term morbidity, ie. pain/swelling in patients treated by systemic anticoagulation and/or decompressive surgery with or without thrombectomy.[ix,x,xi] D.L. Steed reported complete symptomatic resolution in 72% of patients with primary thrombosis. However, only 14.2% had complete resolution of thrombus on follow-up venography.[xii] Becker et al showed venous patency in four patients with primary thrombosis using local urokinase or streptokinase and achieved good short-term results in two patients that required decompressive surgery. As in our case, they also described an area of luminal irregularity at the site of the thrombus in each case.[xiii] Variable success has been reported using local fibrinolytic therapy with venous balloon dilatation and/or surgical decompression in a small group of patients with primary thrombosis.[XI] Taylor et al showed successful short-term outcome in two patients treated with local thrombolytic therapy followed by first rib resection.[xiv] In a study involving 50 patients with primary thrombosis by Machleder, long-term venous patency seemed to correlate with initial use of local urokinase. Interestingly, predecompressive angioplasty resulted in a high rate of reocclusion. Those patients who underwent decompressive surgery after thrombolysis showed a 64% versus 44% venous patency rate at 3 years follow-up. Additionally, an overall 93% and 64% asymptomatic status was reported on 3 years follow-up venography in patients with patent versus occluded veins, respectively.[xv] Hence upper extremity DVT is one area in which local thrombolytic therapy is now rapidly becoming the treatment of choice.

To our knowledge, there have been no previous reports on transcatheter thrombolysis administered through a retrograde route in the upper

limb using the pulse-spray technique. Gaining peripheral venous access in an oedematous limb is always difficult, but our case has shown that access via the femoral vein with retrograde catheterization of the subclavian-axillary is a viable alternative. This however lends itself to its own problems. Numerous valves are present along the axillary vein and catheter manipulation through these valves can sometimes be time consuming. Occasionally, prolonged manipulation can lead to perforation of the vein, as in our case, but this appears to be of no significant consequence. On the other hand, this technique allows a central caval filter to be deployed in the SVC without the need of a separate puncture. Also if clinically significant pulmonary embolism should occur, a pulmonary angiogram followed by suction, aspiration or fragmentation embolectomy of the pulmonary arteries can be performed immediately.

Whether a prophylactic caval filter should have been deployed in the SVC is also an issue of contention. It is the authors' belief that small emboli to the lungs are usually of no clinical significance. During the process of thrombolysis, contrast injections demonstrated several small fragments of clot becoming dislodged from the subclavian vein. The patient however, despite having active tuberculosis of the lungs, did not complain of any respiratory distress during the procedure and continuous oxymetry did not show any change in the oxygen saturation. However, it should be emphasized that if the thrombus load is large, or if respiratory reserve if small, it would be prudent to deploy a caval filter prophylactically before thrombolysis is undertaken.

REFERENCES

1. Bookstein JJ, Fellmeth B, Roberts A, Valji K, et al. Pulsed spray pharmacomechanical thrombolysis: preliminary clinical results. AJR 1989;152:1097-1100.
2. Geller MJ, Isner JM, Payne DD, et al: Limb loss due to transvenous endocardial pacemaker therapy. Am J Med 1985;78:351-354.
3. Smith BM, Shield MD, Riddle DH, et al: Venous gangrene of the upper extremity. Ann Surg 1985;201:511-519.
4. Kleinasser LJ:"Effort" thrombosis of axillary and subclavian veins. Arch Surg 1949;59:258-274.
5. Lindblad B, Tengborn L, Berggvist D: Deep venous thrombosis of the axillary-subclavian veins:Epidemiologic data, effects of different types of treatment and late sequelae. J Vase Surg 1988;2:161-165.
6. Tilney NR, Griffith MB, Edwards EA: Natural history of major venous thrombosis of the upper extremity. Arch Surg 1970;101:792-796.
7. Pollack EW, Walsch J: Subclavian - axillary vein thrombosis: Role of non-invasive diagnostic methods. South Med J 1980;73:1503-1506.
8. Knudson GJ, Wiedmeyer DA. Erickson SJ, et al: Color doppler sonographic imaging in the assessment of upper extremity deep venous thrombosis. AJR Am J Roentgenol 1990;154:399-403.
9. Donayre CE, White GH, Mehringer SN et al: Pathogenesis determines late morbidity of axillosubclavian vein thrombosis. Am J Surg 1986;152:179-184.
10. Lisse JR, Davis CP, Thurmond-Aderle M: Upper extremity deep venous thrombosis: Increased prevalence due to cocaine abuse. Am J Med 1989;87:457-460.
11. DeWeese JA, Adams JT, Gaiser DL: Subclavian venous thrombectomy. Circulation 1970:16:158-164.
12. Steed DL, Teodori M, Peitzman A, et al: Streptokinase in the treatment of subclavian vein thrombosis. Vasc Surg 1986;4:28-32.
13. Becker JB, Holder RW, Rabe FE, et al: Local thrombolytic therapy for subclavian and axillary vein thrombosis. Radiology 1983;149:419-453.
14. Taylor LM, McAllister, Dennis DL: Thrombolytic therapy followed by first rib resection for spontaneous ("effort") subclavian vein thrombosis. Am J Surg 1985;149:644-647.
15. Machleder HI:Evaluation of a new treatment strategy for Paget-Schroetter syndrome: Spontaneous thrombosis of the axillary/subclavian vein. J. Vasc. Surg. 1993;17:305-317.

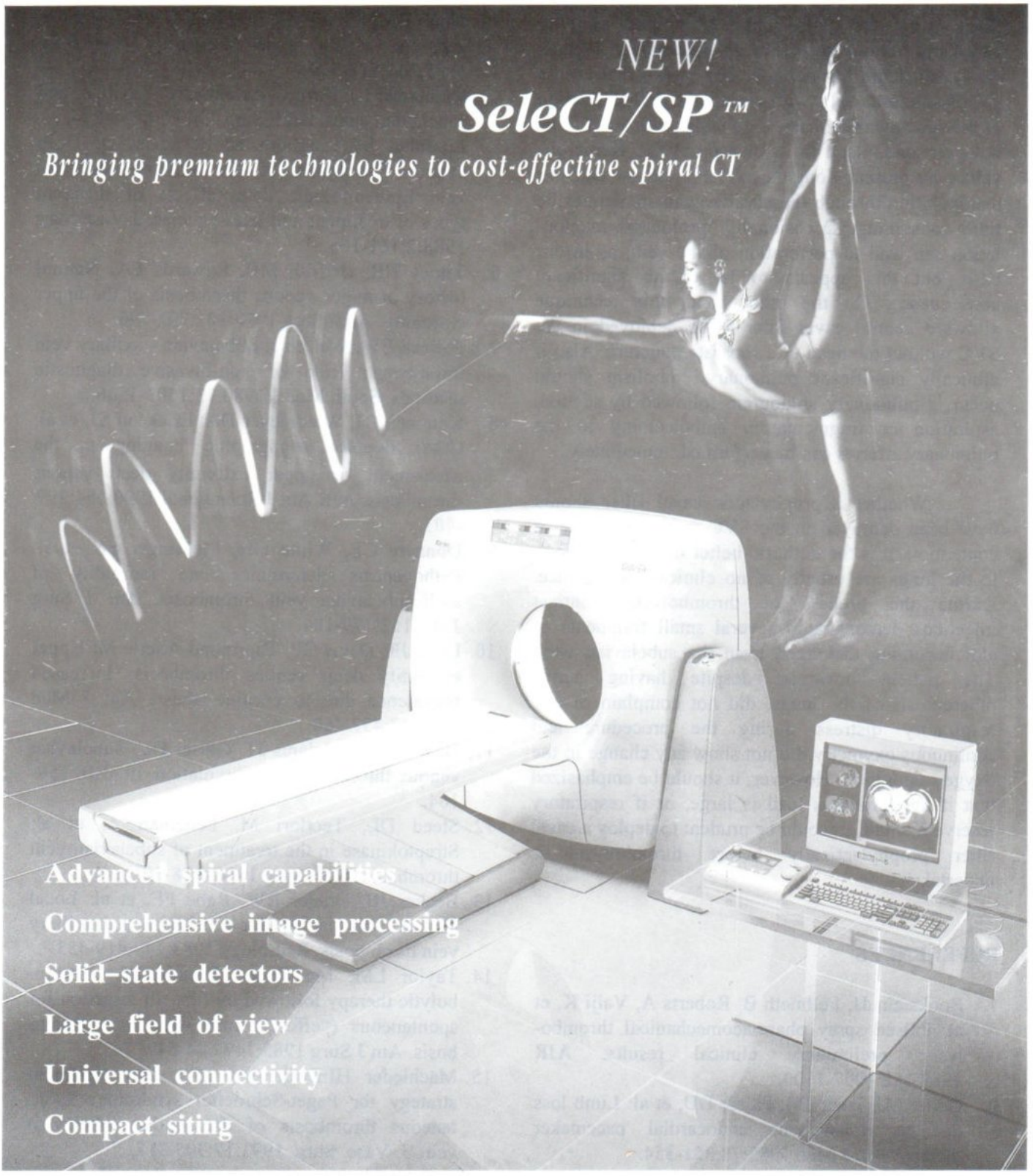

จำหน่าย และบริการโดย

supreme PRODUCTS CO.,LTD.

บริษัท สุพรีม โพรดักส์ จำกัด

163/81-82 ถ.พระปิ่นเกล้า แขวงบางยี่ขัน เขตบางพลัด กรุงเทพฯ 10700 แผนกขาย 434-0040,434-0050 แผนกบริการ 434-0060 โทรสาร 433-3971

MRI OF CONGENITAL SUB-GLOTTIC HEMANGIOMA : A CASE REPORT

Shashilekha BALACHANDRA, Patchrin PEKANAN, Ratanaporn PORNKUL

ABSTRACT

Sub-glottic hemangioma is generally a benign lesion which causes upper airway obstruction and dyspnea. We reported MRI findings in a case of sub-glottic hemangioma. A 2 month-old Thai girl presented with progressive dyspnea and upper airway obstruction secondary to a mass on the left side of the sub-glottic trachea. Conventional radiographs, CT scan of the neck and indirect laryngoscopy prior to MRI study failed to reveal the presence of the lesion. Repeated laryngoscopy after MRI scan showed a mass in the sub-glottic trachea corresponded to the MRI findings. Hemangioma was diagnosed because this child also had cutaneous hemangioma in the occipital region. The potential lethal nature of these lesions was emphasized.

INTRODUCTION

Congenital sub-glottic hemangioma is generally a benign lesion which causes progressive airway obstruction secondary to a mass of hemangioma involving the sub-glottic trachea (1-4). The airway obstruction may result in deaths in infants. The lesion usually can be seen on a lateral neck radiograph as narrowing of the trachea. Conventional roentgenogram of the neck in AP view may show asymmetrical narrowing of sub-glottic trachea but most of the times, the lesion will not be well appreciated by this modality of imaging. The lesions will not be readily demonstrated on CT scan (5-6). These patients require careful evaluation since smaller airway manifests a much greater potential for obstruction. The most common site of sub-glottic hemangioma is immediately below the true vocal cords. Differentiation from other tumors must be made during evaluation. Treatment is dependent on size, location, and degree of respiratory compromise.

CASE REPORT

The patient was a 2 month-old Thai girl who presented at Ramathibodi hospital in April 1995 with a 5 day history of progressive dyspnea. The child had no fever, stridor, dysphagia or trauma.

Physical examination was significant for an upper airway obstruction. Pertinent vital signs were a respiratory rate of 40 per minute and a temperature of 37.0°C. AP and lateral films of the neck, chest roentgenogram and barium swallowing showed no evidence of intra-luminal mass lesion in the trachea (Fig.1-3).

Indirect laryngoscopy revealed no evidence of intra-luminal mass lesion in the trachea. The child was intubated with a No. 3.5 endo-tracheal tube. Admission laboratory data revealed a WBC count of 6100 and admission cultures grew few colonies of normal flora. The child was given humidified oxygen by using an oxygen box. Adrenalin was also given but the symptoms were not improved.

Ultrafast computed tomography of the neck was performed using Imatron C-150. Axial scans were done with a 3 mm. slice thickness. The study demonstrated no intra-luminal mass lesion in the trachea (Fig. 4)

MRI was performed with a 1.5 Tesla superconducting magnet (GE Signa, MRS 2000), using a neck coil. The spin echo technique was used with a repetition time of 400 ms. and an echo time of 16 ms. (400/16) for T1-weighted images and gradient echo technique was used for T2-weighted images with the flip angle of 25° and 519/20 (TR/TE). Four signals were averaged for both T1

Department of Radiology, Ramathibodi Hospital, Rama VI Road, Bangkok 10400, Thailand.

and T2 weighted imaging. Axial T1WI were obtained with and without contrast agent (0.1 mmol/ml/kg Gd-DTPA) The study was done in coronal, sagittal and axial planes. The section thickness was 3 mm with 0.1 mm inter-section gap, and data were collected using a 256 X 192 matrix. The study demonstrated a 0.8 X 0.4 X 0.4 cm. oval shaped, nodule at left postero-lateral part of sub-glottic trachea with a markedly compromised airway (Fig. 5A - E). The lesion bulged locally into sub-glottic laryngeal lumen. It showed faint increased signal intensity when compared with the muscles on T1 weighted images, while on T2 weighted images it showed marked hyperintensity. Homogeneous contrast enhancement of the lesion is seen after gadolinium injection. The nature of this lesion is most likely a hemangioma because the child also had a cutaneous hemangioma at her occipital region (7). Findings corroborated the work of Rao et al. (8) and Hoh et al (9).

Repeated indirect laryngoscopy at this fime revealed a small red mass at left postero-lateral wall of sub-glottic trachea just below the true vocal cord. The child was treated with steroid and all the symptoms were gradually improved, and was symptom free at the last follow up in September 1995. There was no evidence of recurrence of symptoms nine months post steroid treatment.

DISCUSSION

Congenital sub-glottic hemangioma usually causes partial airway obstruction within the first six months to a year. They may go untreated if asymptomatic. Their incidence is unknown. The sub-glottic segment of the larynx is that portion bounded by the true vocal cords superiorly and the lower margin of the cricoid cartiliage inferiorly (10). Presenting symptoms vary with lesion size, age and extension into airway. Infants, because of their small tracheal lumen, may present with dyspnea and labored breathing, stridor or difficulty in feeding (11). Occasional complaints of hoarseness or other voice alterations are more commonly seen, but these symptoms were not present in our reported case, probably due to small sized lesion.

This case report typifies sub-glottic hemangioma. The lesion is not demonstrated by any imaging modality other than MRI in this case. MRI was performed to exclude intra-luminal tracheal mass lesion and/or determine the extent of the lower airway involvement(12-13). The diagnosis is supported by the presence of associated cutaneous hemangioma, presenting symptoms, physical examination and other radiological imaging. Presence of the lesion was confirmed by the repeated laryngoscopy. MRI is better than other imaging modalities due to its multiplanar capability (14). An awareness of the signal intensity from the lesion on MRI, the morphology and site of lesion as described may aid in recognition of these lesions. The differential diagnoses include laryngeal papilloma, adenoma, neurofibroma, rhabdomyoma and chondroma. Laryngeal papilloma usually arises at the vocal cord and multiple lesions are common. The tumor usually shows wart-like appearance with low signal intensity on T1WI and high signal intensity on T2WI. The adenoma will be a mass lesion similar to laryngeal carcinoma in the adult. Neurofibroma usually shows infiltrative abnormality involving the extra-laryngeal neck and paraglottic structures. Rhabdomyoma will appear as a mass lesion. Chondroma is usually found close to cartilagenous structures. Calcification is frequently found in chondroma and will be clearly seen on CT scan.

In 1995, Nozawa et al (15) reported the first case of MRI findings in sub-glottic hemangioma. Their case is similar to ours. To our knowledge, our case is the second case to be reported in the literature.

In the management of such a case, a tracheostomy may be necessary to maintain an adequate airway in some case but was not performed in our case due to small sized lesion. Decompression treatment of the mass was not done because there is a high risk of bleeding complication. We felt that removal with laryngeal instruments or laser surgery would have been time consuming and difficult because of the nature of the lesion and the risk of local bleeding. Radiation therapy was used in the past but is now rarely performed. However, the lesion is common to regress spontaneously.

For the line of investigation in children with an upper airway obstruction, the sequence of investigation presented in this case is quite appropriate. Although MRI was the only imaging modality that was able to demonstrate the intra-luminal lesion of sub-glottic trachea in our case; we should not begin the investigation with MRI in children with upper airway obstruction, because of the high cost of the study. Conventional AP film of

the neck with high KV technique and the use of a filter will readily demonstrate most of the tracheal lesion. However, in difficult cases, MRI would be very helpful as in our reported case (16-18).

REFERENCES

1. Jones SR, Myers EN, Barnes EL. Benign neoplasms of the larynx. In: Fried MP, ed, The larynx: a multidisplinary approach. Boston, Little Brown & Co, 1988:401-20.
2. Hugh D, Curtin. The larynx. In: Som PM and bergeron RT, eds, Head and neck imaging excluding the brain : St. Loius. The CV Mosby Co, 1991:593-692.
3. William N, Hanafee and Paul H Ward. Clinical correlation In : The head and neck volume 1. The larynx. Thieme Med Publi, Inc. 1990:1-81.
4. Lahoz - Zamarro - MT, Roya - Lopez - J, Valero - Ruiz -J, Camara - Gimenez - F, Urbiola - E. Cavernous hemangioma of the larynx in the adult. A propose of a case. Acta-Otorhinolaryngol - Esp. 1989;40(2):141-44.
5. Cohen EK, Kressel Hy, Perosio T. MR imaging of soft tissue hemangiomas: Correlation with pathologic findings. AJR 1988;150:1079-81.
6. Kassel EE, Keller MA, Kucharczy K. MRI of the floor of the mouth, tongue and orohypopharynx. Radio Clin North Am. 1989;27:131-351.
7. Maffee MF, Compos M, Raju S. Head and neck high field MRI versus CT. Otolaryngol Clin North Am. 1988;21:513-46.
8. Vijay M Rao, Adam E. Flanders, Barry M Tom. MRI and CT. Atlas of correlative imaging in otolaryngology. London, Martin Duvitz Ltd, 1992:127.
9. Hoh K, Nishimura K, Toyashi K. MR imaging of cavernous hemangioma of the face and neck. J Comput Assist Tomogr 1986;10(5):831-5.
10. Lawson W and Biller HF. Glottic and sub-glottic tumors. In: Thawley SE and Panje WR, eds, Comprehensive management of head and neck tumors. Philadelphia: WB Saunders Co, 1987:991-1015.
11. Lufkin BB, Lawson SG, Hanafee WN. Work in progress: NMR anatomy of the larynx and tongue base. Radiology 1983;148:173-5.
12. Lufkin R, Hanafee W, Wortham D. Magnetic resonance imaging of the larynx and hypopharynx using surface coils. Radiology 1986;158:747-54.
13. R. Nick Bryan, Charles W Mc Cluggage, Barry L. Horowitz, David Jenkins. The normal and abnormal neck. In: Richard E Latchaw, ed, MR and CT imaging of the head and neck and spine. St. Louis: Mosby. Year Book Inc, 1991:1035-67.
14. Louis M Teresi, Robert B Lufkin, Willam N Hanafee. Magnetic resonance imaging of the larynx. Radio Clin North Am. 1989;27:393-406.
15. K. Nozowa, T. Aihara, H. Takano. MR imaging of a sub-glottic hemangioma. Pedia Radio 1995;25:235-6.
16. Stephen F. Simoneaux, Estelle R. Bank, Joel B Webber, W. James Parks. MR imaging of the pediatric airway. Radiographics 1995;15(2):287- 9.
17. Griscom NT. Diseases of the trachea, bronchi and small airways. Radio Clin North Am 1993;31:605-15.
18. Hernandez RJ, Tucker CF. Congenital tracheal stenosis:role of CT and high KV films. Pedia Radio 1987;17:192-6.

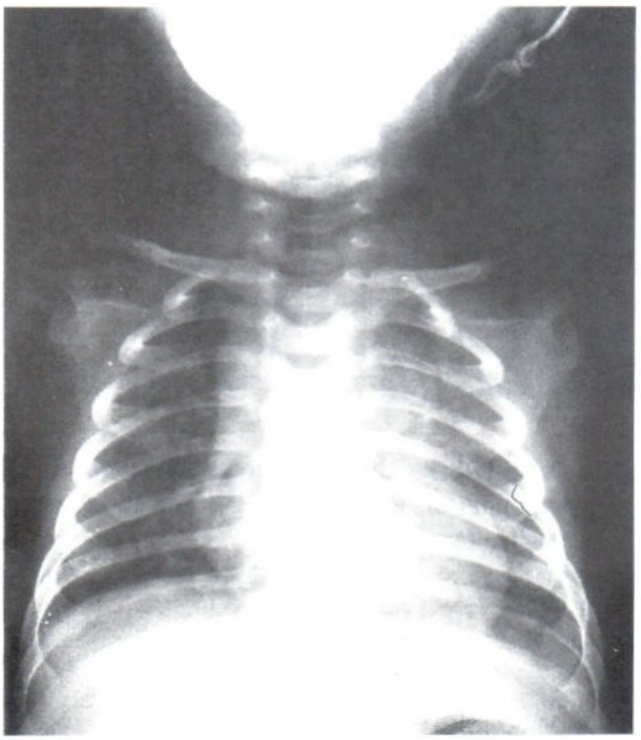

Fig.1 AP chest roentgenogram includes the neck showed no abnormalities.

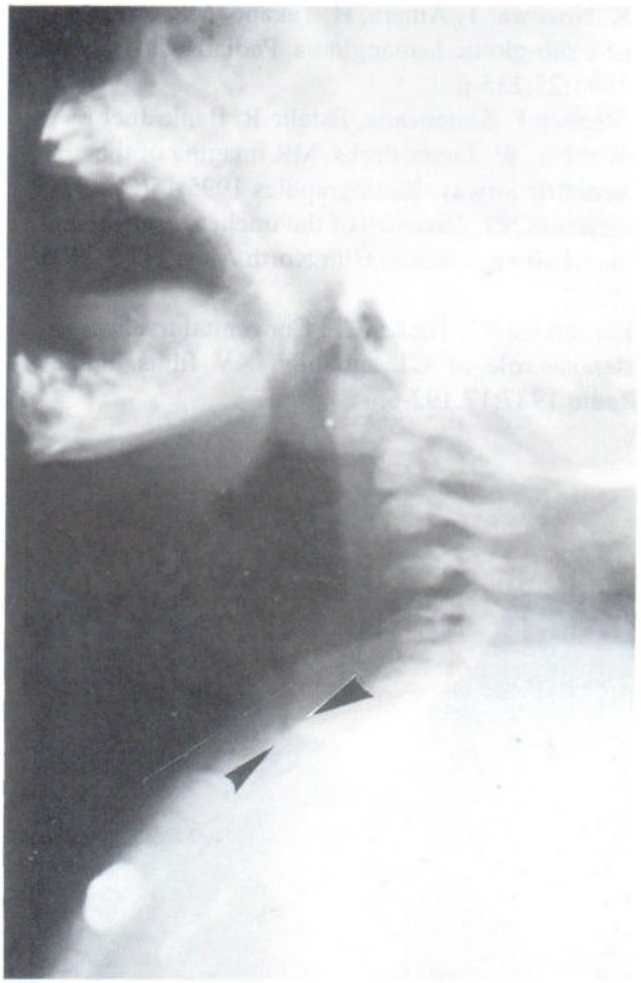

Fig. 2 Lateral neck radiograph shows distention of hypopharynx and narrowing of the sub-glottic trachea (arrow-heads).

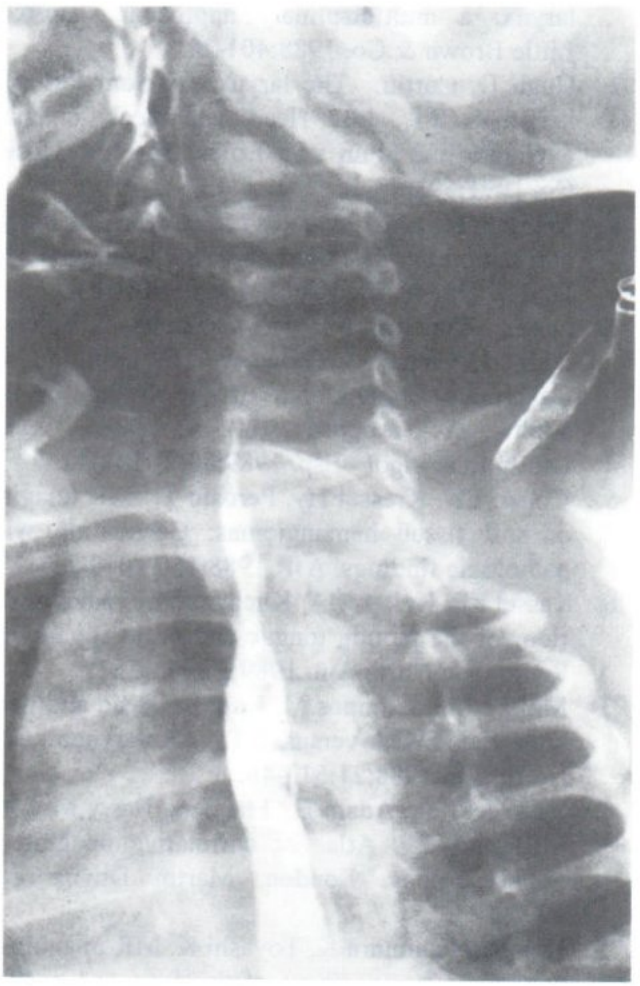

Fig. 3 Barium swallowing showed no abnormalities. No evidence of a vascular ring was demonstrated

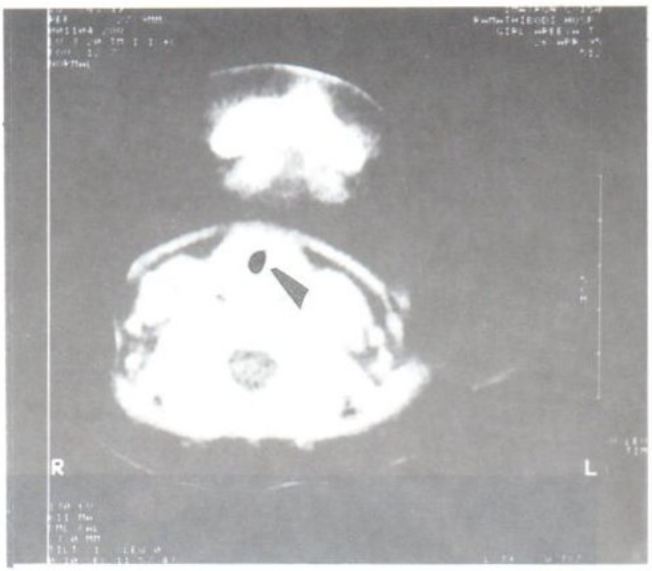

Fig. 4 Ultrafast CT scan at the level of sub-glottic trachea shows no intra-luminal mass lesion. Although asymmetry of sub-glottic trachea is seen (arrow-head).

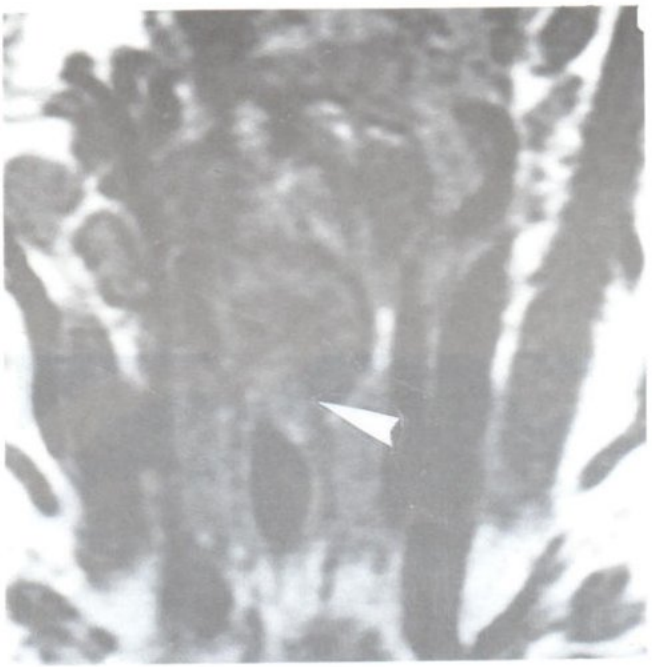

Fig. 5 A.

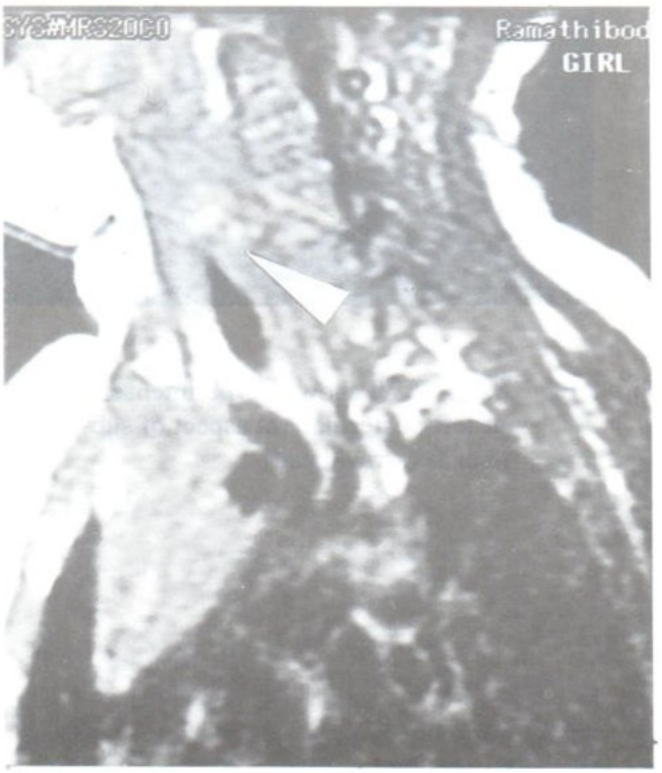

Fig. 5 B.

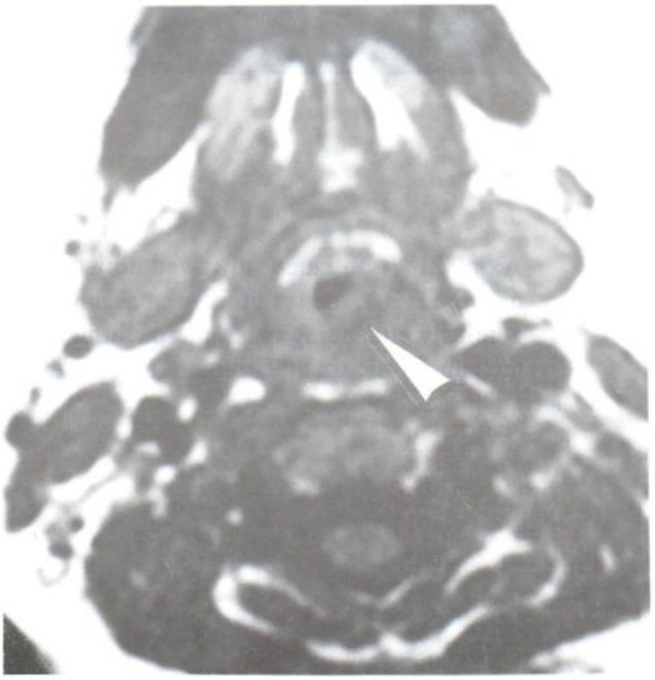

Fig. 5 C.

Fig. 5 A-C. MR imaging of the neck (A-C) in coronal, sagittal and axial T1WI showed an oval shaped, slightly hyperintense mass arising from left postero-lateral wall of sub-glottic trachea (arrow-heads).

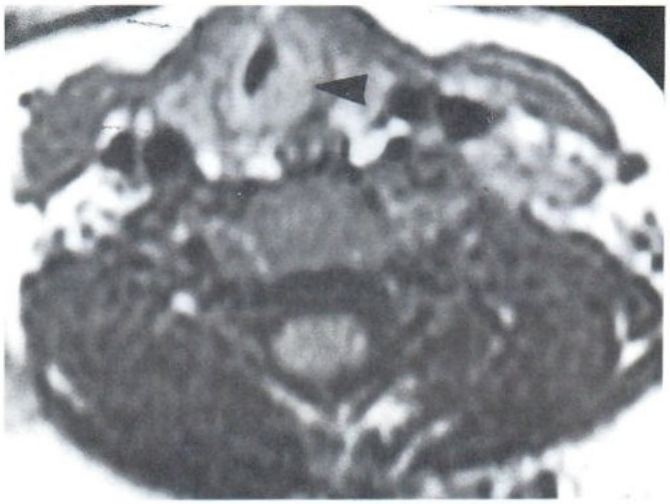

Fig. 5 D. Axial T1WI obtained after administration of GD-DTPA, the lesion is seen as a homogenously enhancing mass encroaching upon the sub-glottic tracheal lumen (arrow-head).

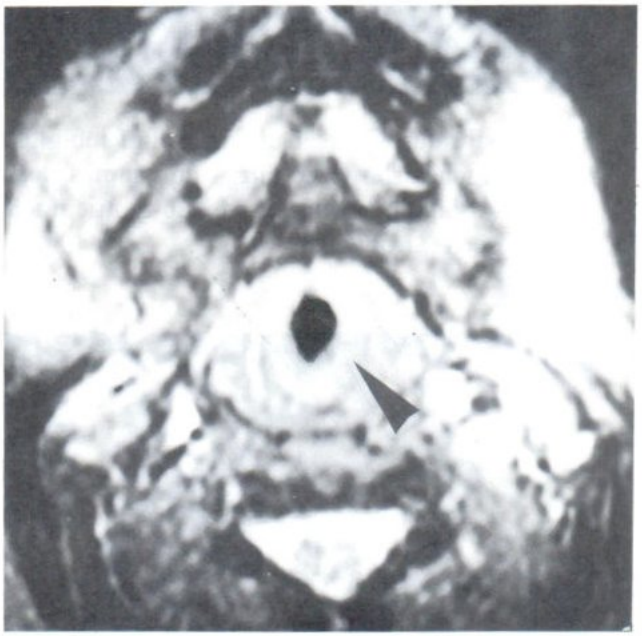

Fig. 5 E. Axial T2WI shows ahyperintense mass lesion at left posterolateral aspect of sub-glottic trachea (arrow-head).

RETROPERITONEAL LYMPHANGIOMA : SPIRAL CT IMAGES

Janjira JATCHAVALA[1], Patchrin PEKANAN[1], Sirintara PONGPECH[1], Kamolpong OSATHAVANICHVONGS[2].

ABSTRACT

A case of retroperitoneal lymphangioma was demonstrated by spiral CT scan. Sagittal and coronal reconstructions and spiral CT angiography were highly efficient in determination of the exact location and character of the tumor.

INTRODUCTION

Lymphangioma of the retroperitoneum is rare and usually found incidentally at surgery, autopsy or lymphography (1,2). When clinically significant, they may present as an abdominal mass or pressure effect to the adjacent organs (3.4). A correct preoperative diagnosis may be helpful in treatment planning. The radiologic features demonstrated by lymphography, ultrasonography, conventional CT and MRI had been previously reported (2-11). To our knowledge, the radiologic findings of retroperitoneal lymphangioma was not reported.

CASE REPORT

A 38-year-old man presented with recurrent epigastric pain. Physical examination revealed mild tenderness at epigastrium. The rest of the physical examination was normal. Routine laboratory values were within normal limits. Plain abdomen showed two faint tiny calcifications at left suprarenal region. Ultrasonography revealed a structureless cystic mass at the pancreatic tail and anterior aspect of left kidney (Fig. 1). Some septations were seen. Spiral CT scan with sagittal and coronal reconstruction showed a water-density mass with lobulated contour and small punctate calcifications, situated at left suprarenal region, measuring 3.5 X 4.6 X 9 cm. (Fig. 2). No significant enhancement was seen after contrast medium injection. The mass was not encapsulated and appeared to be soft and extended along anteromedial aspect of left kidney. The mass was anterior to left renal vein and artery. Spiral CT angiography demonstrated that the mass was hypovascular. Left renal arterial branches supplied the periphery of the mass (Fig. 3). There was an evidence of communication between the mass and the lymphatic chain at inferomedial aspect (Fig. 4). Left adrenal gland and pancreas were normal. The diagnosis of retroperitoneal lymphangioma was considered. At laparotomy, a multiloculated cystic mass, measuring 4 X 3 X 3 cm. was excised from the retroperitoneal space. The pathologic diagnosis was lymphangioma.

DISCUSSION

Lymphangiomas are the lymphatic analog of the hemangiomas of blood vessels (12). They are classified histologically into two groups, simple (capillary) and cavernous lymphangioma (cystic hygroma).

Simple (capillary) lymphangiomas are composed of a network of endothelium-lined lymph spaces. They tend to occur subcutaneously in the head, neck and axilla. Cavernous lymphangiomas (cystic hygroma) are made up of massively dilated

[1] Department of Radiology, Ramathibodi Hospital, Rama 6 Street, Bangkok 10400, Thailand.
[2] Medical software project and development, Mahidol University.

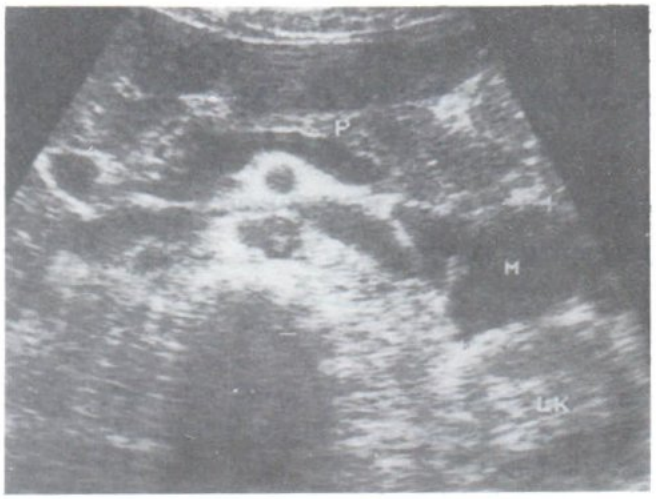

Fig.1A. Sonogram in trasverse plane showed a cystic mass with septations located at dorsal aspect of the pancreatic tail and anterior to left kidney.

cystic spaces lined by endothelial cells and separated by a scant intervening connective tissue stroma. This type of lymphangioma is analogous to the cavernous hemangioma.

The cause of lymphangioma of the retroperitoneum has not been clearly estabished (7,13). It is unlikely that it is either a true neoplasm or a hamartoma. Rather, it is now usually regarded as a developmental malformation resulting from failure of developing lymphatic tissue to establish normal communication with the remainder of the lymphatic system (10). They may be single or multiple, unilocular or multilocular, and may contain serous or chylous fluid (14). They can occur in patients of all ages (10) and no sex predilection. This tumor may cause no symptom or may cause symptoms by displacement or compression of adjacent structures (2-4) and some of the symptoms

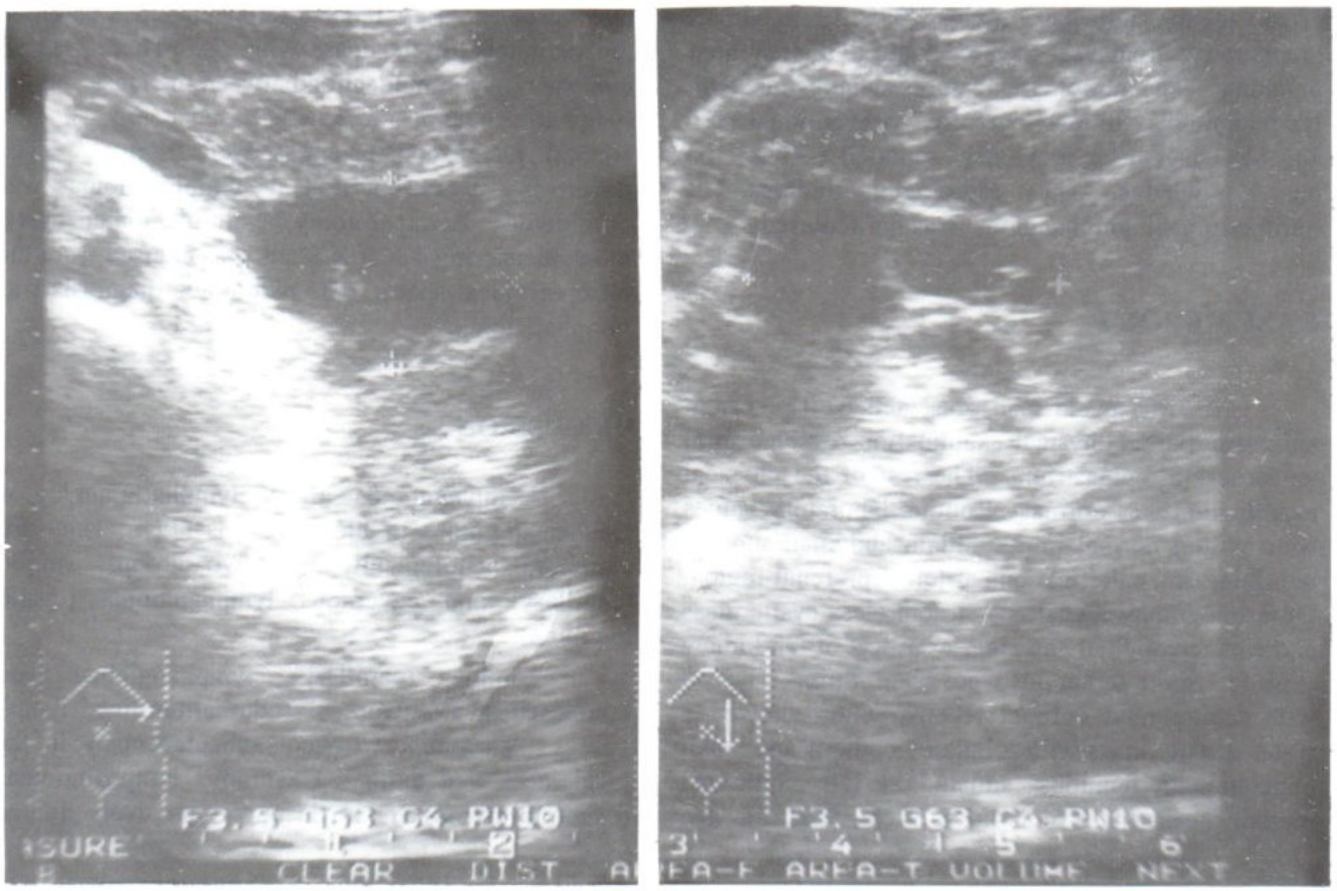

Fig. 1B Sonogram in transverse plane (left) and parasagittal plane (right) showed multiloculated cysts with elongated shape.

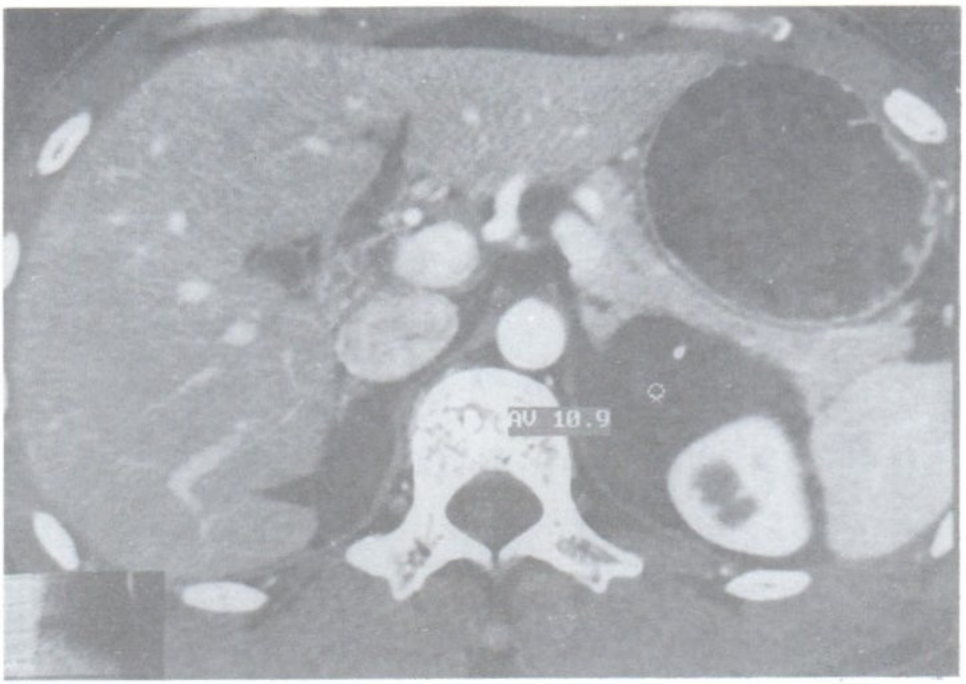

Fig.2B Post contrast study showed no enhancement of the mass.

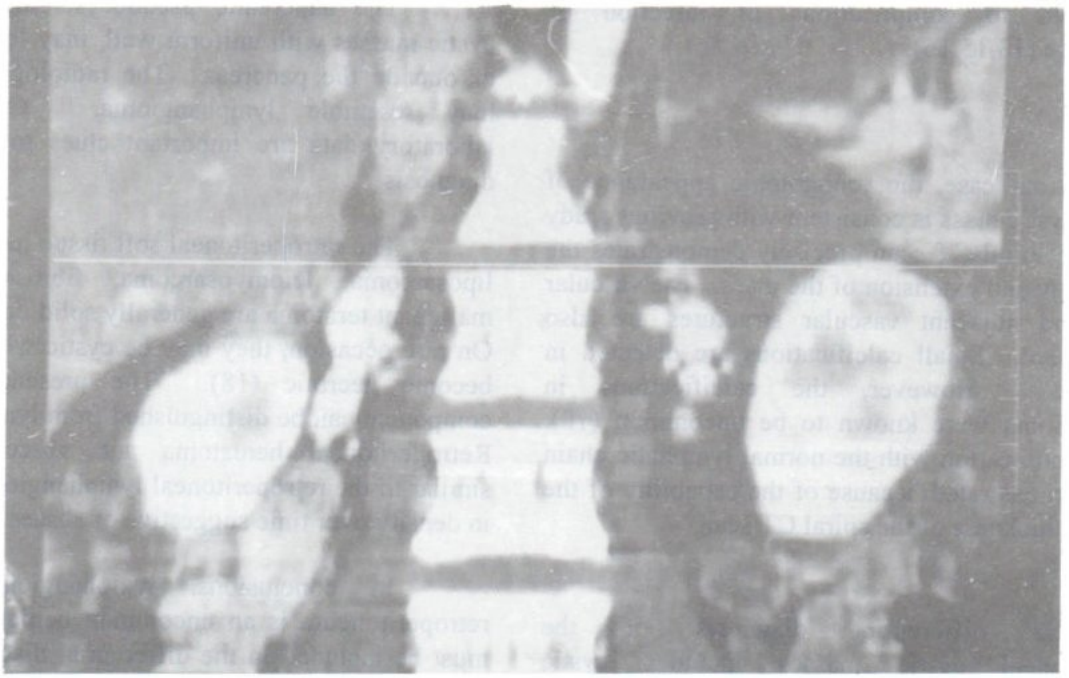

Fig.3 Spiral CT images
A. The mass has elongated shape, extending along the anteromedial aspect of left kidney.

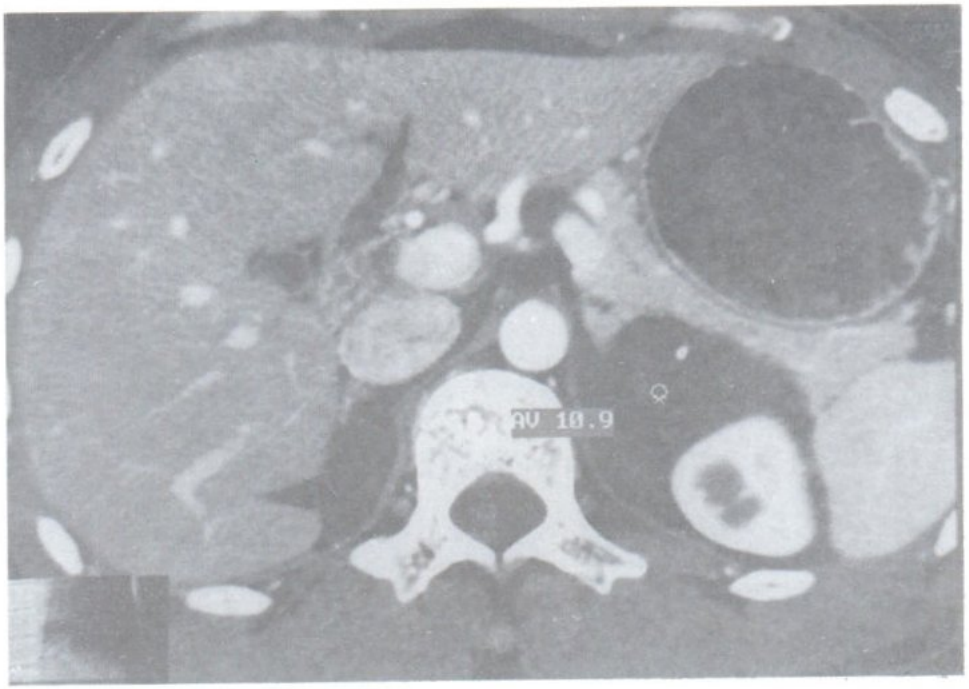

Fig.2B Post contrast study showed no enhancement of the mass.

Fig.3 Spiral CT images
A. The mass has elongated shape, extending along the anteromedial aspect of left kidney.

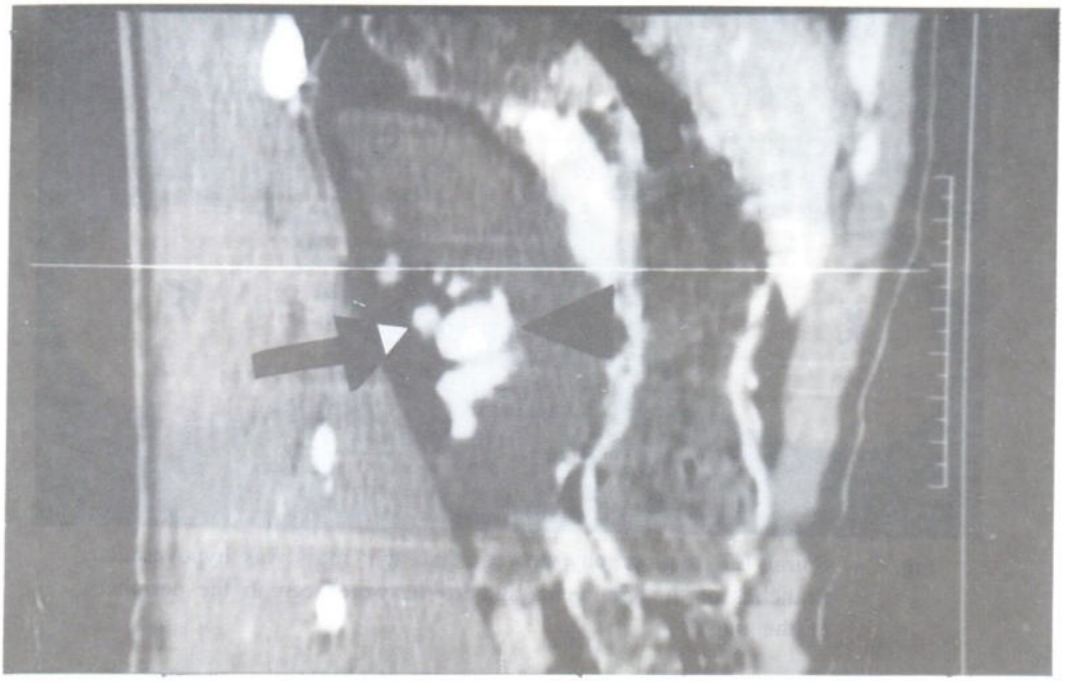

Fig.3B Left renal artery (arrow) and vein (arrowhead) are seen in the posterior aspect of the mass.

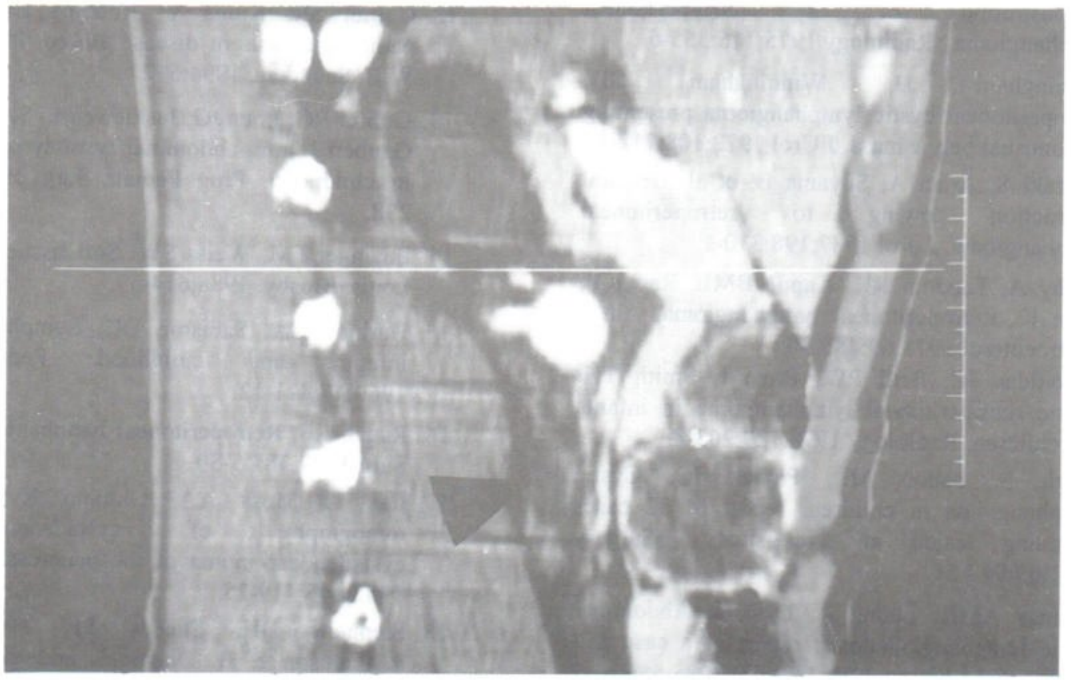

Fig.3C Communication of the mass to the normal lymphatic chain (arrowhead)

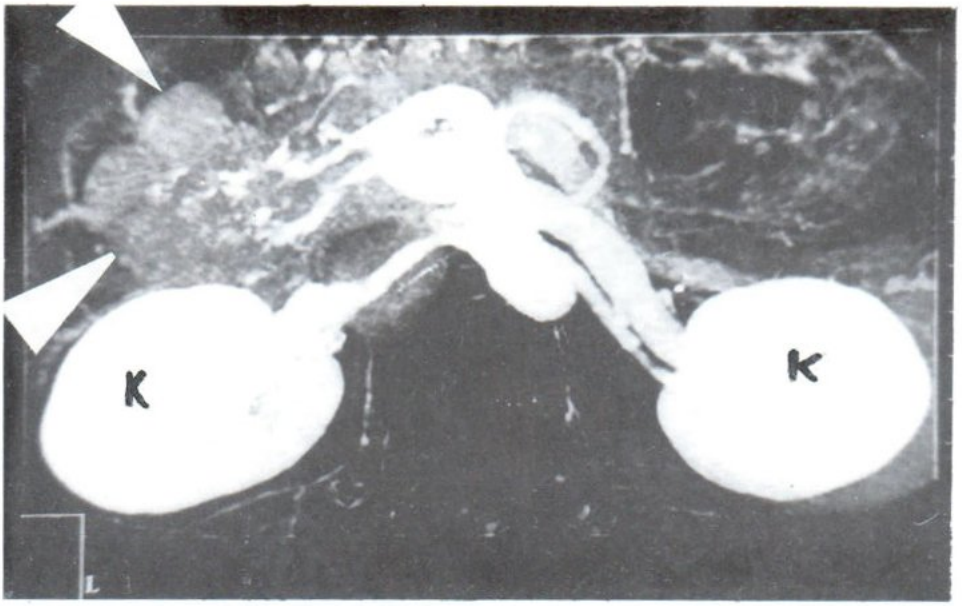

Fig. 4 Spiral CT angiography showed that the mass was hypovascular. Branches of the renal veins and arteries were seen in the periphery of the mass.

REFERENCE

1. Henzel JH, Pories WJ, Burget DE, et al. Intraabdominal lymphangioma. Arch Surg 1966;93:304-8.
2. Castellino RA, Finkelstein S. Lymphographic demonstration of a retro-peritoneal lymphangioma. Radiology 1975;115:355-6.
3. Cunningham JJ, Winningham GD. Retroperitoneal cystic lymphangioma presenting as a unusual pelvic mass. J Urol 1972;108:717-8.
4. Kanzaki S, Arata A, Suyama B, et al. Urethral obstruction owing to retroperitoneal lymphangioma. J urol 1987;198:370-1.
5. Koshy A, Tandom RK, Kapue BML, Rao KV, Joshi K. Retroperitoneal lymphangioma. Am J Gastroenterol 1978;69:485-90.
6. Lenonidas JC, Brill PW, Bhan I, Smith TH. Cystic retroperitoneal lymphangioma in infants and children. Radiology 1978;127:203-8.
7. Singh S, baboo ML, Pathak IC. Cystic lymphangioma in children: report of 32 cases including lesion at rare sites. Surgery 1971;69:947-51.
8. Thomas AMK, Leung A, Lynn J. Abdominal cystic lymphangiomatosis: report of a case and review of the literature.Br J Radiol 1985;58:467-9
9. Yunyonging Y, Tang CK, Bruce WG. Solitary cystic lymphangioma of retroperitoneum. J Urol 1977;118:388-9.
10. Davidson JA, Hartman SD. Lymphangioma of the retroperitoneum: CT and sonographic characteristics. Radiology 1990;175:507-10.
11. Cutillo PD, Swayne CL, Cucco J, Dougan H. CT and MR imaging in cystic abdominal lymphangiomatosis. J Comput Assist Tomogr 1989;13:534-6.
12. Cotran SR, Kuma V, Robbins LS. Robbins pathologic basis of disease 5th ed. Philadelphia: W.B. Saunders, 1994;512.
13. Galifer RG, Pous JG, Juskiewenski S, Pasquie M, Gaubert J. Intra-abdominal cystic lymphangiomas in childhood. Prog Pediatr Surg 1978;11:173-238.
14. Enzinger FM, Weiss SW. Soft tissue tumors. St Louis: Mosby, 1988;614-37.
15. Harkins GA, Sabiston DC. Lymphangioma in infancy and childhood. Pediatr Surg 1960;47:811-12.
16. Rauch RF. Retroperitoneal lymphangioma. Arch Surg 1959;78:45-50.
17. Itai Y, Moss AA, Ohtomo K. Computed tomography of cystadenoma and cystadenocarcinoma of the pancreas. Radiology 1982;145:419-25.
18. Stephens DH, Sheedy PF, Hattery RR, Williamson B Jr. Diagnosis and evaluation of retroperitoneal tumors by computed tomography. Am J Roentgenol 1977;129:395-402.
19. Munechika H, Honda M, Kushihashi T, Koizumi K, Gokan T. Computed tomography of retroperitoneal cystic lymphangiomas. J Comput Assist Tomogr 1987;11:116-9.

SPIRAL CT SCAN OF THE MYOSITIS OSSIFICANS TRAUMATICA

Patchrin PEKANAN[1,3], Kamolpong OSATHAVANICHVONGS[2,3]. Damrongrak PROEDPRING[3]

ABSTRACT

A demonstration of a case of myositis ossificans traumatica at right thigh by spiral CT scan was shown. The calcification at the muscle had a lacy pattern of peripheral calcification, more lucent center and there was a separation zone between the lesion and the adjacent bone. The lesion was 5 weeks old in a 9-year-old girl.

INTRODUCTION

Localized myositis ossificans is a tumor-like heterotopic formation of bone and cartilage in soft tissue, usually muscles, but also tendons, ligaments, fasciae, aponeuroses, and joint capsules (1,2,3). The mass may be doughy painful, and warm during its early development. With time, the lesion shrinks to a firm and definable mass attached to the adjacent soft tissues or bone (4). Growth of the mass occurs during this active proliferative phase and is self-limited (5). The proliferating tissue interdigitates with the muscle bundles. Eventually, the lesion develops into a mass of mature bone with a cortical shell surrounding central cancellous, less mature tissue (6).

We present a case of myositis ossificans traumatica, 5 weeks post trauma by spiral CT scan.

CASE REPORT

A 9-year-old girl was hit at her right thigh for 5 weeks. The mass has developed at right thigh at a later time. The mass was hard but not tender. Nodular fasciitis was first impressed. The mass did not increase is size but there was a progressive calcification in the soft tissue at the region of the mass on plain film.

Elscint spiral CT scan of the lesion was performed. The spiral scan used 2.5 mm beam width, 1.5 pitch, 26 seconds-total scan time, 430 mm-FOV, 120 -KV, 350 mAS/ slice. The image reconstruction was performed with 1.6 mm interval, using 512 X 512 matrix. The 3-D reconstruction technique was followings: 1) bony tissue of the femoral shaft, soft tissue of the thigh and calcified muscle were reconstructed separately using volume definition technique (the method to select tissue for 3-D surface rendering using connectivity algorithm by selecting seed pixel and setting range of Hounsfield unit to connect adjacent pixel of the same density range and compile to form a volume of tissue for rendering) 2) cut-3 D program was used to cut and displace 3-D surface rendering images and multiplanar CT images simultaneously in different cutting plane of the soft tissue, in axial, sagittal or oblique plane. The advantage of cut-3D images is the good demonstration of the relationship between the lesion and the adjacent structures in the three dimensional space.

Figure 1 showed calcification in the muscle plane, denser calcification at the peripheral portion and a calcium-free zone between the calcification and the cortex of the femur. Solid periosteal reaction is noted around the femoral cortex. Figure 2 showed 3-D reconstruction of the lesion, in relationship with the femur and the muscles.

[1] Department of Radiology, Ramathibodi Hospital, Rama 6 Street, Bangkok 10400, THAILAND.
[2] Institute of scientific research, development and technology, Mahidol University,Pinklao-Nakronchaisri Street, Bangkok.
[3] Urupong Medical Center, Theoddamri Street, Bangkok.

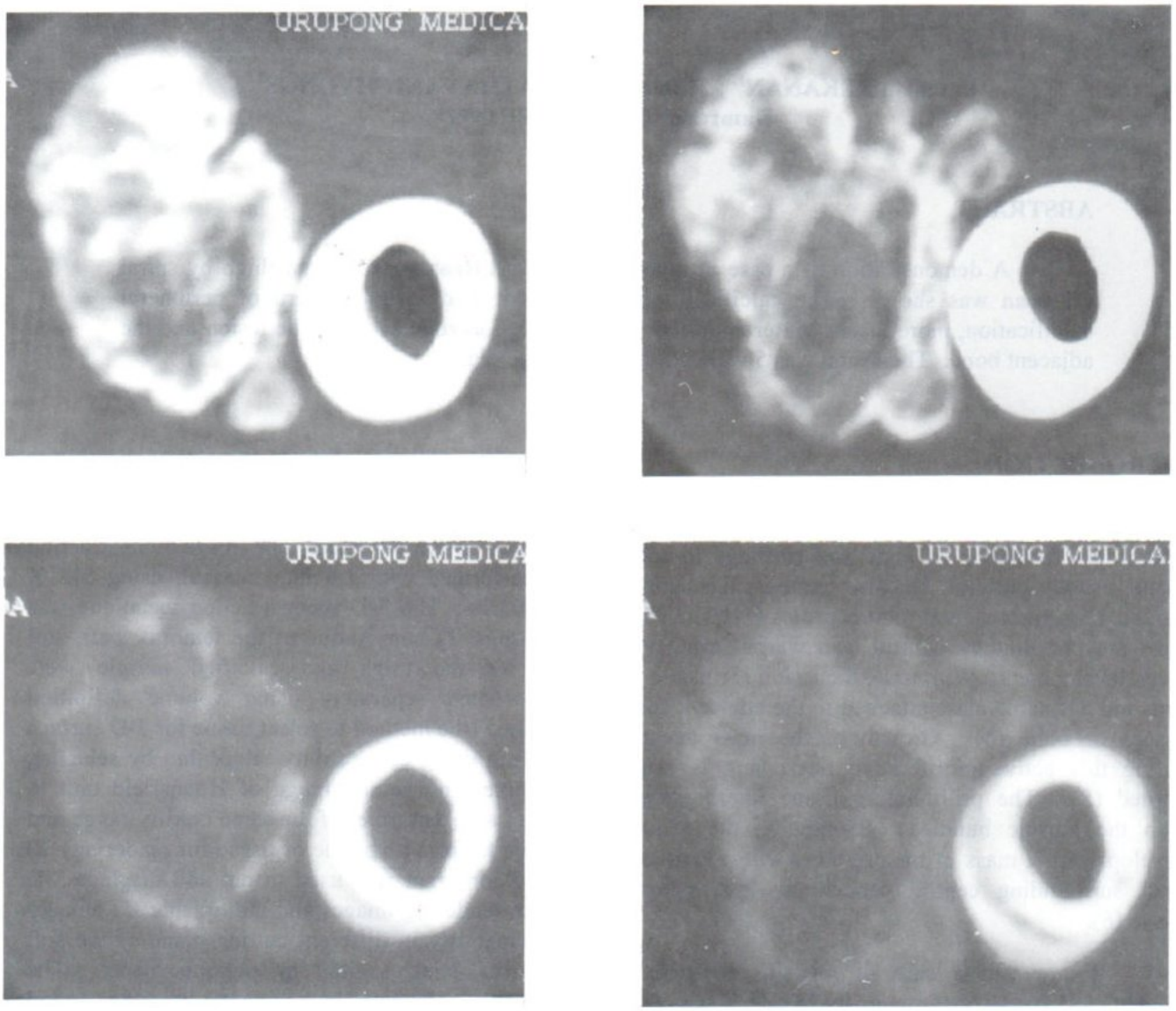

Fig. 1 Serial scans through a focus of myositis ossificans showed a well encapsulated lesion with a peripheral zone of ossification and a lucent center. The separation-zone between the lesion and the lunderlying bone was noted. Solid periosteal reaction at the adjacent femur was due to the simultaneous insult to the bone.

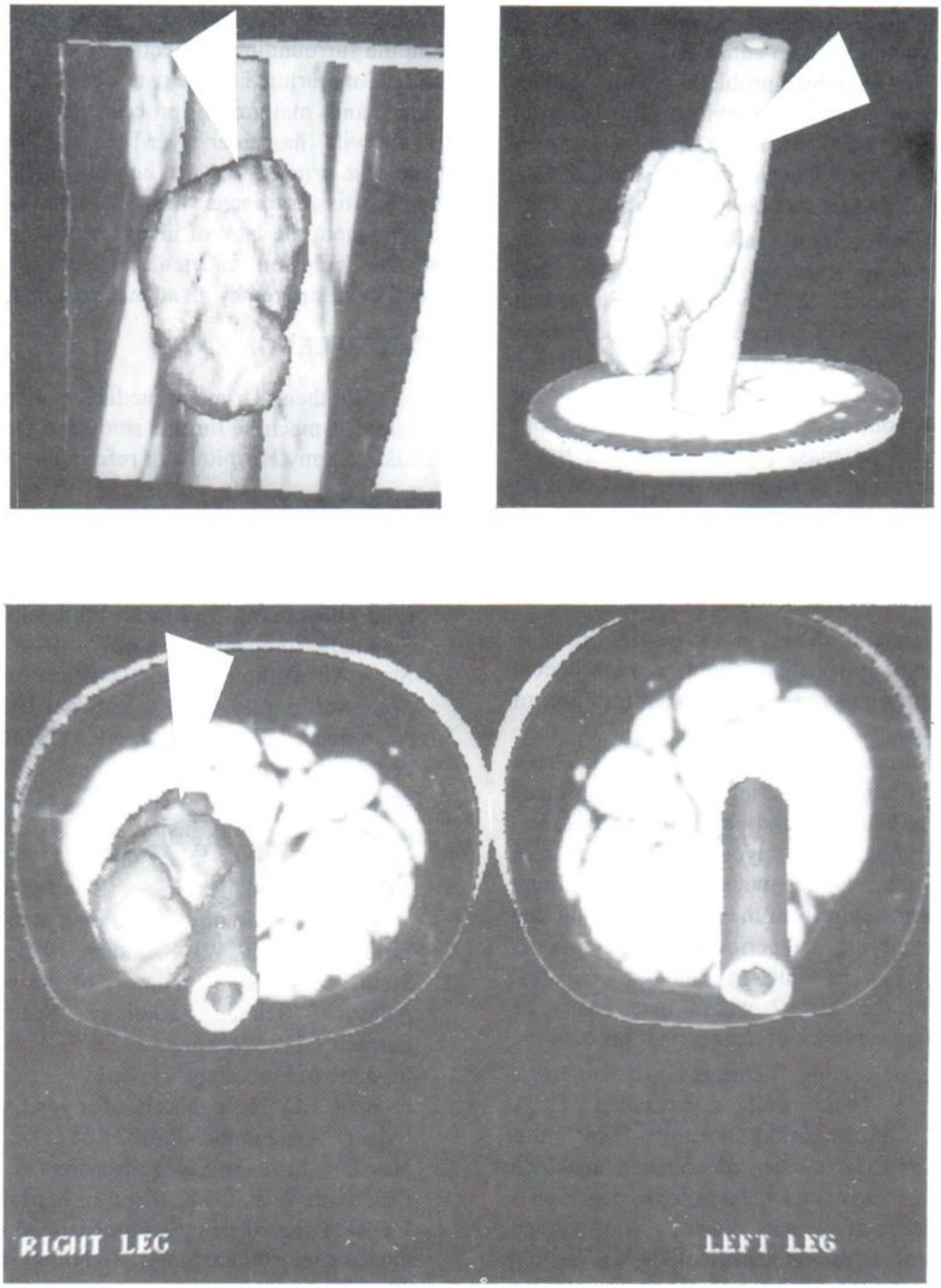

Fig. 2 3-D reconstruction of the lesion showed the relationship with the femur, muscle planes, compared with the normal leg.

DISCUSSION

Spiral CT is a potentially ideal acquisition method for three-dimensional imaging because it enables fast acquisition of an entire volume with high resolution. It obviates problems with patient movement and respiration. A previous study of spiral and standard CT has shown that spiral CT has a planar resolution equivalent to that of standard CT, lower noise, and a wider section profile (7,8).

Shortly after injury, a soft tissue mass or swelling becomes apparent, which may be associated with periosteal reaction in 7 to 10 days. Flocculent dense lesions arise in the mass from 11 days to 6 weeks after the trauma (1,9). The calcific dense areas gradually enlarge, and at 6 to 8 weeks a lacy pattern of new bone is sharply circumscribed about the periphery of the mass (1,10). The soft tissue central core occasionally becomes encysted, and an enlarging central cavity combined with peripheral calcification and ossification resembles an eggshell. Maturity is reached in 5 to 6 months, and the mass then shrinks.

The recognition of a peripheral rim of calcification and ossification about a more lucent center is an important radiographic manifestation of myositis ossificans. A radiolucent band or zone between the lesion and the subjacent cortex is also a very important finding, reflecting the lack of intimacy between the ossified mass and neighboring bone, and allowing differentiation of myositis ossificans from parosteal sarcoma. Direct damage to the cambium layer of the periosteum from the traumatic insult can lead to an ossifying subperiosteal hematoma or periosteoma (1,11), in which a sunburst periosteal reaction within the first 2 weeks may easily be misinterpreted as evidence of a malignant process.

The microscopic changes of myositis ossificans have been well documented (1,9). Mesenchymal proliferation results in the accumulation of focal masses of collagen in which calcium salts are deposited. Heterotopic osteoblasts appear, produce matrix, and create a well-defined lesion possessing a fibrous capsule. The developing lesion demonstrates three distinct zones, a phenomenon that allows differentiation from sarcomatous processes (1, 13,14). The center of the lesion contains rapidly proliferating fibroblasts with areas of hemorrhage and necrosis. A middle zone contains osteoblasts with island of immature bone. Biopsy of cellular inner and middle layers alone may result in an erroneous diagnosis of a sarcoma. It is the outer zone of the lesion that reveals the true benign nature of the process. In this region, mature trabeculae are discovered that are clearly demarcated from the surrounding connective tissue. A peripheral shell of maturing bone exists about a soft cellular center, and maturation proceeds in a centrifugal fashion with the center layer being the last to ossify. Pathologic criteria that are helpful in differentiation of myositis ossificans from sarcoma are a zone phenomenon, the lack of invasion of adjacent tissue, and the inclusion of viable muscle fibers, which would be destroyed by an advancing tumor (1,9).

ACKNOWLEDGMENTS

We thank Urupong medical center to provide us spiral CT machine for this study and Dr. Sahachart Pipitakul (Army Hospital) for refering us the case.

REFERENCES

1. Resnick D, Niwayama G. Soft tissues. In : Resnick & Niwayama, ed. Diagnosis of bone and joint disorders. 2nd ed. Philadelphia: W.B. Saunders Company, 1988:4274-54.
2. Stout AP. Pathology and classification of tumors of the soft tissue. Am J Roentgenol 1951;66:903.
3. Ackerman LV. Extra-osseous localized non-neoplastic bone and cartilage formation (so-called myositis ossificans) Clinical and pathological confusion with malignant neoplasms. J Bone Joint Surg (Am) 1958;40:279.
4. Aegerter E, Kirkpatrick JA Jr. Orthopedic Diseases: Physiology, Pathology, Radiology. 4th Ed. Philadelphia, WB Saunders, 1975, p271.
5. Stout AP, Lattes R. Tumors of the soft tissues. Atlas of Tumor Pathology. Second series, Fascicle 1, Washington DC, Armed Forces Institute of Pathology 1967,p11.
6. Johnson LC. Histogenesis of myositis ossificans (Abstr). Am J Pathol 1948;24:681.
7. Ney DR, Fishman EK, Kawashima A, Robertson DD, Scott WW. Comparison of helical and serial CT with regard to three-dimensional imaging of musculoskeletal anatomy. Radiology 1992; 185: 865-869.
8. Kalender WA, Polacin A. Physical performance characteristics of spiral CT scanning. Med Phys 1991;18:910-5.
9. Adams RD, Denny-Brown D, Pearson CM : Disease of muscle : A study in pathology, 2nd Ed. New York, Harper & Row, 1962.

10. Normal A, Dorfman HD. Juxtacortical circumscribed myositis ossificans : Evolution and radiographic features. Radiology 1970;96:301.
11. Gilmer WS Jr, Anderson LD. Reactions of soft somatic tissue which may progress to bone formation : Circumscribed (traumatic) myositis ossificans. South Med J 1959;52:1432.
12. Zadek I : Ossifying hematoma in the thigh. A case report. J Bone Joint Surg (AM) 1969;51: 386.
13. Ackerman LV. Extra-osseous localized non-neoplastic bone and cartilage formation (so-called myositis ossificans) : Clinical and pathological confusion with malignant neoplasms. J Bone Joint Surg (Am) 1958;40:279.
14. Johnson LC Histogenesis of myositis ossificans (Abstr.) Am J Pathol 1948;24:681.

SIEMENS

Make way for innovation!

150 years of Siemens

1997

The Siemens anniversary : 150 years - and always leading the way

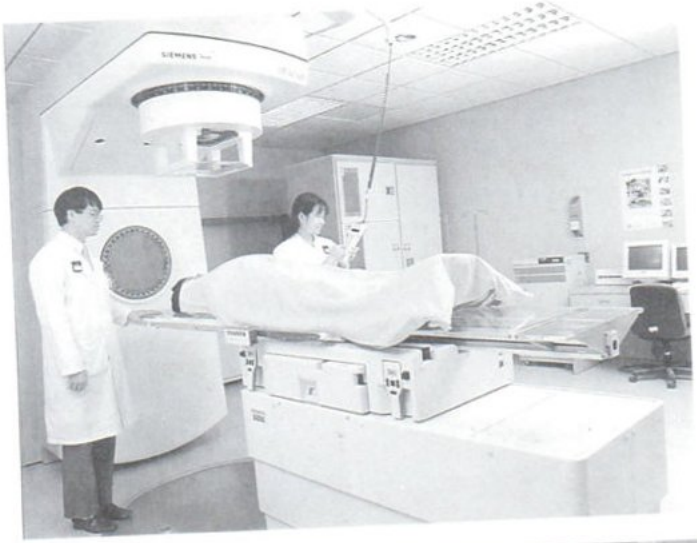

Siemens Limited
Medical Engineering Division

5th floor Dr.Gerhard Link Building,
33 Soi Lertnava, Krungthepkreetha Road,
Huamark, Bangkapi,
Bangkok 10240, Thailand.
Tel. (002) 379-4333, 379-4455
Fax. (002) 379-4470

RADIOSURGERY : A LITERATURE REVIEW

Sopol KAMPONPUNTH[1], Patchrin PEKANAN[1], Janjira CHATCHAVALA[1], Kamolpong OSATHAVANICHVONGS[2]

ABSTRACT

Radiosurgery will be performed in Thailand soon, both in the government and private section. A literature review, concerning general introduction, physics and indication was presented.

INTRODUCTION

In 1951, Leksell first described stereotactic radiosurgery (1,2). He took his 1949 first generation stereotactic guiding device and coupled it to an orthovoltage x-ray tube capable of being rotated into arc planes around a patient's head (1-3). He irradiated the gasserian ganglion of several patients with trigeminal neuralgia. These patients maintained long-term successful pain control without the need for further surgery. Lars Leksell was a professor of neurological surgery at the Karolinska institute in Stockholm.

In 1954, John Lawrence, working with the California Berkeley cyclotron initiated charged particle irradiation of the pituitary gland to suppress pain in patients with metastatic breast cancer (1,4). The first thirty patients were treated using the Bragg peak principle of the proton beam, but all patients thereafter were treated using the helium ion beam.

In 1959, Raymond Kjellberg initiated Bragg peak proton beam stereotactic irradiation at the Boston (Havard) cyclotron unit (4).

The technical and time-consuming aspects of proton irradiation proved frustrating. In 1967, Leksell and his colleagues completed the development of the first neurosurgical stereotactic radiosurgical tool, the Gamma Knife (1,5,6). This prototype 179 multisource cobalt-60 unit was designed intentionally to produce small, discoid-shaped lesions in deep-seated white matter tracts or brain nuclei. The first reported patient treated in 1967 had a craniopharyngioma (5). The application of Gamma Knife radiosurgery to destroy vascular malformations or small brain tumors began in the Karolinska hospital in the 1970's (6). Leksell completed the installation of a redesigned second-generation gamma unit in the same hospital. The collimators produced a more spherical irradiation field. Radiosurgery for carefully selected vascular malformations, acoustic neuromas, pituitary tumors, and craniopharyngiomas (1,6) was then performed. Leksell hesitated to advocate radiosurgery for malignant neoplasms because he was concerned that the biological behavior of such tumors was inherently so poor that radiosurgery might not offer great hope and the number of patients with benign tumors, vascular malformations or functional disorders was large and access to the device was limited.

The 1980 saw an explosive growth in the development of stereotactic radiosurgical techniques at many sites around the world. Fabrikant in Berkely (1980) began to use the helium ion beam technique for vascular malformation (1,7). In 1980, radiosurgery was performed at two U.S. cyclotron units (Boston and Berkeley), at two gamma units and at a number of medical cyclotrons units in the Soviet Union.

The photon destruction or inactivation of a small brain tumor or vascular malformation, using

[1] Department of Radiology, Ramathibodi Hospital, Rama 6 Street, Bangkok 10400, Thailand.
[2] Software and development project, Mahidol University, Bangkok.

newer generation stereotactic devices coupled with widely available medical linear accelerators, was pioneered by Betti and Derechninsky, working in Paris and Beunos Aires in 1982 (8), and by Columbo, working in Vicenza, Italy also in 1982 (9). Barcia-Salorio reported their modification of fractionated cobalt irradiation of carotid-cavernous fistulas (10). Winston and Lutz in Boston began to adapt their linear accelerator to a widely available stereotactic guiding device in 1987 (1,11).

In 1984, Bunge arranged for the construction in Switzerland of a newly designed third-generation gamma unit. It was subsequently installed in Buenos Aires. A fourth Gamma Knife was installed in Sheffield, England, in 1985 (12).

A commitment to undertake radiosurgery at a given center requires the dedication of time, personnel, resources, financing, and the expertise of a well-trained team (1). By mid-1992, more than 32 gamma units were in operation at a wide variety of medical centers in Europe, Asia, North America, and South America.

Stereotactic radiosurgery represents a merger of clinical disciplines (neurological surgery, radiation oncology, radiology, medical physics, and engineering).

RADIATION PHYSICS FOR RADIOSURGERY

Three general approaches to radiosurgery are employed today (1,13). The oldest utilizes positively charged particles like protons or helium ions from large accelerators that were originally built for nuclear physics research. The second approach, the Gamma Knife, makes use of the gamma radiation emitted from a fixed array of small cobalt-60 sources located within a large hemisphere that surrounds the patient's head. The third and most recent addition to radiosurgery techniques utilizes high energy x-ray radiation produced by the medical linear accerelator (LINAC) found in radiation oncology departments in most major hospitals.

Every radiosurgery system uses some type of sterotactic apparatus that is securely attached to the patient's head. This attached apparatus provides a coordinate system reference frame for determining the target location, a means of precise positioning for treatment, and a method of head immobilization during treatment.

Positively charged particle accelerators used for radiosurgery are generally either cyclotrons or synchrotrons. Both need the combined effects of electric and magnetic fields to produce beams of high-energy particles. Magnetic fields deflect charged particles and confine them to circular paths without changing their speed or energy. Once or twice in each orbit the charged particle passes through a strong electric field, which gives the particle a speed and energy boost.

The Gamma Knife utilizes 201 cobalt-60 sources distributed over the surface to a sphere 40 cm in radius. The sources, which emit gamma rays in all directions, are collimated and shielded, so that only the radiation directed toward the center of this spherical distribution of sources becomes the geometric focus of gamma rays from all 201 sources. The patient is positioned for treatment so that the center of the intracranial target and the center of the spherical distribution of sources coincide.

Cobalt-60 is an artifically made radioactive nuclide that is produced by exposing naturally occurring, stable cobalt-59 to neutrons in a nuclear reactor, where the cobalt-59 absorbs on neutron to become cobalt-60. The radioactive cobalt-60 decays to stable nickel-60 by emitting an electron from its nucleus followed by two relatively high-energy 1.2- and 1.3- Mev gamma rays (1 Mev=1 million electron volts and is a common unit of energy). The electron is absorbed within the source and plays no therapeutic role. Cobalt-60 has a half-life of 5.3 years. Gamma Knife unit therefore requires periodic replacement (i.e. every 5 to 10 years) of their radioactive sources.

High-energy-x-ray or photon beams produced by medical LINACs are available in virtually all radiation oncology departments. Production of these high energy x-rays, called bremsstrahlung radiation, by LINACs can be viewed as a two-step process. First electrons are accelerated to fixed high energy (e.g. 6 Mev) by strong electric fields generated by microwave power. This monoenergetic electron beam is focused onto a heavy metal (e.g. tungsten) target. The incident electrons are abruptly slowed down and stopped by collisions with the electrons and nuclei of the tungsten atoms in the target. During a collision with a nucleus, all or part of the incident electron's energy may be converted into a photon (called a bremsstrahlung x-ray). Most of the bremsstrahlung x-rays produced are directed nearly parallel to the original direction of the electron beam.

Collimation distal to the target determines the size of the treatment field.

The goal of radiosurgery is to deliver a high dose of radiation to the target while sharply minimizing the dose to the surrounding tissue. This is accomplished by firing multiple beams at the target that are incident from different directions. This strategy is most effective for small targets. As the targets, and treatment beams, increase in size, the dose fall-off immediately outside the target becomes more gradual. This is inescapable and applies to all radiosurgery techniques.

The concentration of dose within a radiosurgery target by the Gamma Knife is accomplished by directing 201 well-collimated individual cobalt-60 gamma ray beams toward a common point called the isocenter. These beams enter the head over an area covering approximately half of the upper hemisphere of the skull. Circular fields with four diameters are available: 4,8,14, and 18 mm. The shape of the isodose lines can be altered somewhat to provide better target coverage by selectively blocking some of the 201 beams. When all beams are used, the isodose surfaces are egg-shaped, elongated in the patient's superior-inferior direction. With the central one-third of the beams blocked, the isodose surfaces near the target become more spherical. Other isodense surface shapes may be produced by selective beam blocking. Beams may also be selectively blocked to minimize the dose delivered to critical structures that lie outside the target. For targets too large to be accomodated by the 18-mm beams or that are irregularly shaped, multiple isocenters are needed. Ideally, if one isocenter is to be used, the dimensions of the target should be slightly less than the diameter of the beam. In multiple-isocenter treatments, successive courses of radiation are directed to different points within the target. Up to 12 isocenters have been used. Large and irregularly shaped targets can be well covered this way. The potentially difficulty with this technique, apart from the increased treatment time, is that the individual sphere-like isodose surfaces do not stack together evenly, resulting in very nonuniforming dose deposition within the target.

For medical LINACs, the patient is supported supine on the treatment couch. By making use of two intersecting axes of rotation and by putting the center of the target at this intersection point, beam entry points over the entire upper hemisphere of the skull can be accessed. The turntable axis rotates the couch (patient and target), whereas the gantry axis rotates the x-ray beam. If x-rays are directed into the head while the gantry is rotating at each of four stationary couch positions, the central line of the beam might trace out paths. These paths and the radiation intensity along them can be altered to help the dose distribution conform better to the target and to reduce the dose to critical structures outside the target. This procedure is directly analogous to the blocking of beams in the Gamma Knife. Circular beams ranging from 10 to 50 mm in diameter have been in common use with LINAC radiosurgery. Because of the large field sizes available, multiple isocenters are used much less frequently than with Gamma Knife. Multiple isocenters are reserved primarily for irregularly shaped targets. Nonuniform dose deposition within the target is a natural consequence of multiple-isocenter use. On the other hand, using large diameter beams and a single isocenter to treat irregularly shaped targets will generally result in more normal tissue receiving higher doses than if well planned, multiple isocenters with smaller diameter are used. It is possible that the use of five or six individually shaped, fixed direction beams, similar to the charged partical strategy, will be the best way to treat relatively large, irregularly shaped targets.

Overview of treatment planning tasks and comparison between the different technique (1).

Task	Heavy Particles	Gamma Knife	LINAC
Imaging	CT, MRI, and angiography, PET, SPECT (mathematically correlated with spatially high-resolution images), and MEG for localization of functional abnormalities and metabolic activity.		
Fixation	Cranially fixated headframes: BRW, Leksell, Fischer, etc.		
	Cranial head frame or bite block		Repeat localization headframes and cranial markers
Patient positioning	Relative to markers or mechannically calibrated to headframe.	Mechanically calibrated positioning of focal or isocenter point to headframe	
Patient verification	X-ray verification of cranial landmarks or markers in treatment position	Patient position occluded by device treatment position	Port film or mechanical verification in treatment position
Beam alignment	Calibrated with respect to headframe		
Field shaping	Multiple static fields. Customized three-dimensional shaping to target volume possible	Multiple shots or targets positioned in target volume. Aperture size adjustable per treatment position. Treatment at a single position results in a nearly spherical treatment volume.	
Normalization	90-95%	50 %	80%
		Poor dose uniformity for multiple shots	
Software	Custom	Commercial/custom	
Entrance dose	Depends on number of static fields, $\leq$ 30%	Negligible except for superficial lesions	

Abbreviations: PET = positron emission tomography; SPECT = single photon emission computed tomography; MEG = magnetoencephalography.

Three-dimensional treatment planning for stereotactic radiosurgery: device properties (1)

Property	Heavy Particles	Gamma Knife	LINAC
Beam	Protons, π - mesons, or helium and neon ions	Photons	
Energy	70-250 MeV (range, 5-32 g/cm^2, protons)	Cobalt 60 (≈ 1.2 MeV)	4-to 20-MV photons.
Focusing	Multiple Bragg peaks superpositioned in target volume per beam. Multiple beams at different entry positions. Sharp distal fall-off beyond Bragg peak. Sharp lateral penumbra	201 fixed sources distributed over upper cranial hemisphere and focused at a single spot. Focal spot to source distance is 55 cm.	Gantry-based source sweeps out an are in a plane around the LINAC isocenter. Patient-plane intersection adjusted by pivoting patient treatment couch around isocenter. Dynamic, noncoplanar, treatments. Focal spot to source distance 100 cm.
Field sizes	Arbitrary shape and size.	Circular 4-18 mm.	Circular, 5-50 mm. Dynamic collimation devices.
		Treatment volume is spherical around a single target point. Field shaping accomplished through placement of multiple shots/targets inside the target volume and differential dose per target.	
Sparing	Small number of static beam portals geometrically chosen to avoid critical structures	Selective plugging of individual source apertures whose field of view includes critical structures. Standard patterns available	Customized gantry rotation intervals at specific couch angles.
Dose rate	Variable per beam portal. Arbitrary beam weighting.	Fixed source output. Dose rate inhomogenicity across target from individual sources, per shot weighting.	Variable per arc and target.

CLINICAL INDICATIONS AND RESULTS (14)

(datas from Gamma Knife radiosurgery)

1. Arteriovenous malformations

Gamma Knife surgery has proven highly effective in the treatment of AVMs. More than 8700 patients have been treated since 1971. The complete obliteration rate for AVMs is satisfactory (most of which were considered unsuitable for microsurgery). This success rate underscores the importance of Gamma Knife treatment as an alternative to microsurgery.

Multiple studies show that the clinical efficacy and the non-invasive procedure makes it advantageous for patients medically unable or unwilling to undergo conventional surgery. The non-invasive nature of the Gamma Knife treatment also helps when treating centrally located lesions and those close to critical structures such as the brain stem. In a recent study comparing hemorrhage in non-obliterated AVMs during the first two years following Gamma Knife surgery with the incidence in untreated patients, it was noted that the risk for permanent neurological deficit or death due to AVM rupture between the treatment and total nidus obliteration was less than 0.5% for small AVMs and 2-4 % for larger ones during the first two years. This compares to 4-6 % for an untreated AVM.

2. Acoustic neuromas

Several published studies indicate effective management of acoustic neuromas while still perserving cranial nerve function. According to a recent study, a permanent growth control rate after Gamma Knife surgery of 90-95 % was achieved with facial nerve function perservation of nearly 100 % and preservation of serviceable hearing of approximately 80 %. With enhanced diagnostic imaging technique, a growing number of previously undetected acoustic neuromas are being identified. In addition, noteworthy studies indicate that most of these tumors enlarge within 1 or 2 years. The challenge is to treat these tumors totally while preserving full cranial nerve function and hearing. Results in a study by the University of Pittsburgh comparing microsurgery with Gamma Knife surgery, indicate that microsurgery is associated with a greater

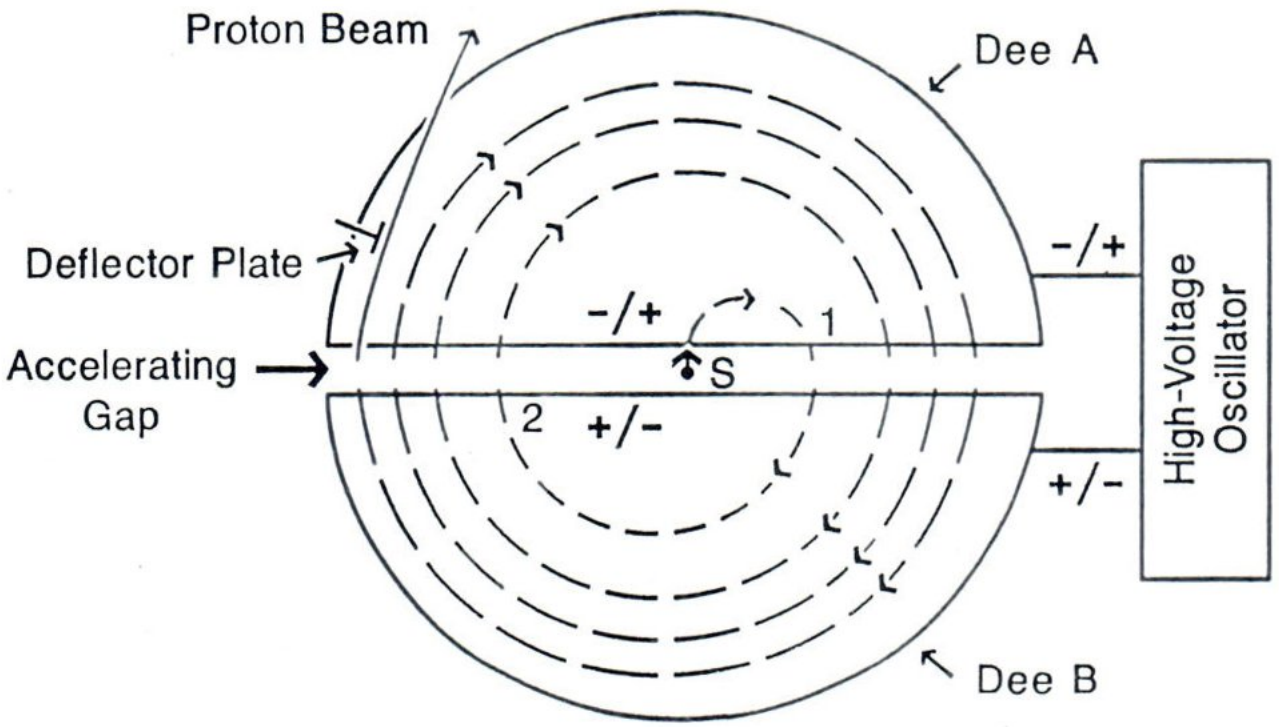

Fig 1 Schematic of the cyclotron, used primarily for the acceleration of protons.

incidence of peri-operative or delayed facial dysfunction and a decreased rate of preservation of the preoperative level of serviceable hearing. This further indicates the importance of Gamma Knife surgery for acoustic neuroma patients.

3. Mastastatic tumors

It is currently estimated that around 20-30 % of all patients harbouring malignant disease develop metastases to the brain. The established treatment modality for cerebral metastases has been craniotomy and whole brain radiation therapy. The convenience and efficacy of Gamma Knife procedures, however, has given rise to an increasing use of this treatment for both single and multiple metastases. Excellent results have been achieved with the Gamma Knife, even for such traditionally radioresistant tumors as melanoma.

4. Meningiomas

Although the accepted first line of treatment for meningiomas is microsurgical removal, Gamma Knife surgery is being increasingly used as a valuable adjunct, particularly in cases of subtotal tumor removal. Morbidity from intracavernous surgery may be markedly decreased by planning in advance for a less aggressive intracavernous surgical resection followed by delayed radiosurgery to the intracavernous tumor residual.

Additionally, Gamma Knife surgery can result in a significant reduction in recurrence rates and prevents reoperation in up to 87.5 % of patients with relatively low complication rates. This includes tumors close to important structures such as the brain stem and cranial nerves.

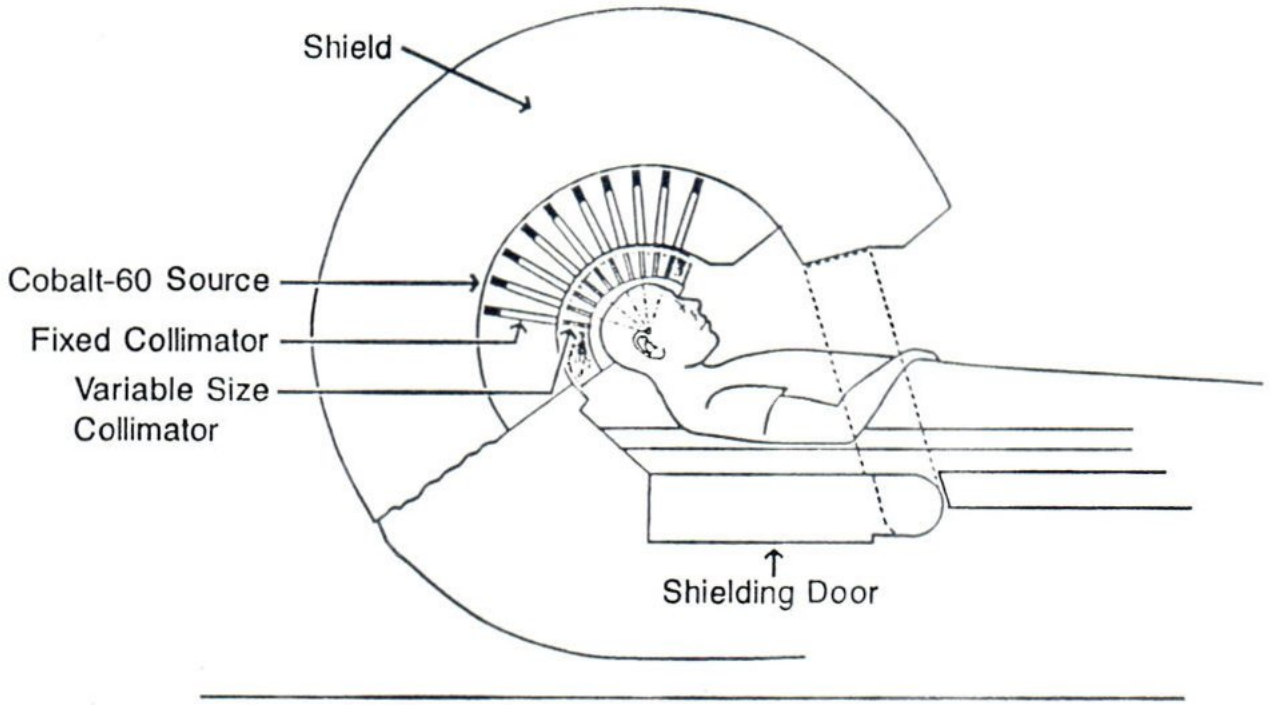

Fig. 2. A cross-sectional schematic of a Gamma Knife showing the location of the cobalt-60 sources, their collimators, and the point at which all gamma ray beams are aimed. The patient is positioned within the Gamma Knife so that the focal point of the beams and the center of the intracranial target coincide.

5. Chordoma and Chondrosarcoma of the cranial base

Kondziolka et al (15) attested to the value of stereotactic radiosurgery as an adjuvant or primary treatment for selected patients with chordoma or chondrosarcoma and demonstrated its potential advantages over standard fractionated irradiation.

6. Movement disorders, pain and psychological disorders (16)

Radiosurgery was applied to movement disorders, pain and psychological disorders such as obsessive compulsive neurosis. Disorders treated were tremor in Parkinson's disease, intractable pain with cancer, trigeminal neuralgia, and obsessive compulsive neurosis. Today, the Gamma Knife is used for making thalamotomies to arrest the tremor of Parkinson's disease, to ameliorate dyskinesia and rigidity of the same disease by pallidotomy, to stop intractable cancer pain by thalamotomy or hypophysectomy to eradicate the excruciating pain fo trigeminal neuralgia by radiation of the trigeminal root at its exit zone from the brain stem, and to make bilateral lesions of the anterior internal capsule for remedying obsessive compulsive disorder. Efforts have been made recently to use Gamma Knife surgery also as a treatment for focal epilepsy.

7. Other pathologic processes

The following conditions had been treated by radiosurgery; craniopharyngiomas (17,18), pituitary adenomas (19), pinealomas (20), primary glial tumors (21), hemangiopericytomas of the meninges (22), radiosurgery to the pituitary gland in Cushing's disease (23), refractory anxiety disorders (24), squamous cell carcinoma of the nasopharynx (25), Nelson's syndrome (26), human ACTH producing pituitary tumors (27), and eye melanoma (28).

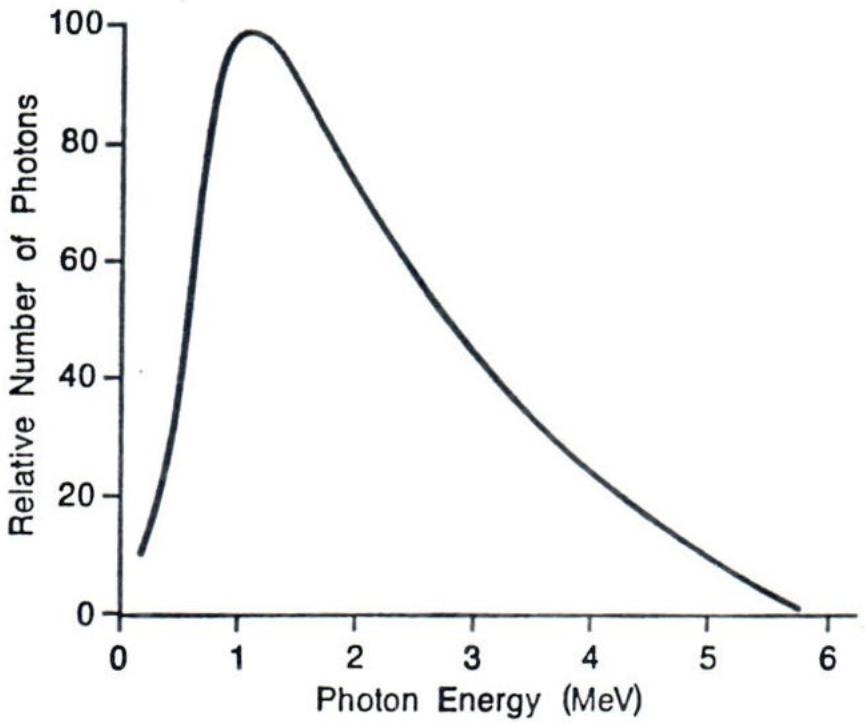

Fig. 3 The distribution of photons (bremsstrahlung x-rays) from a 6-MeV LINAC. The average energy of the x-rays produced is approximately 2 MeV, while the maximum energy is 6 MeV.

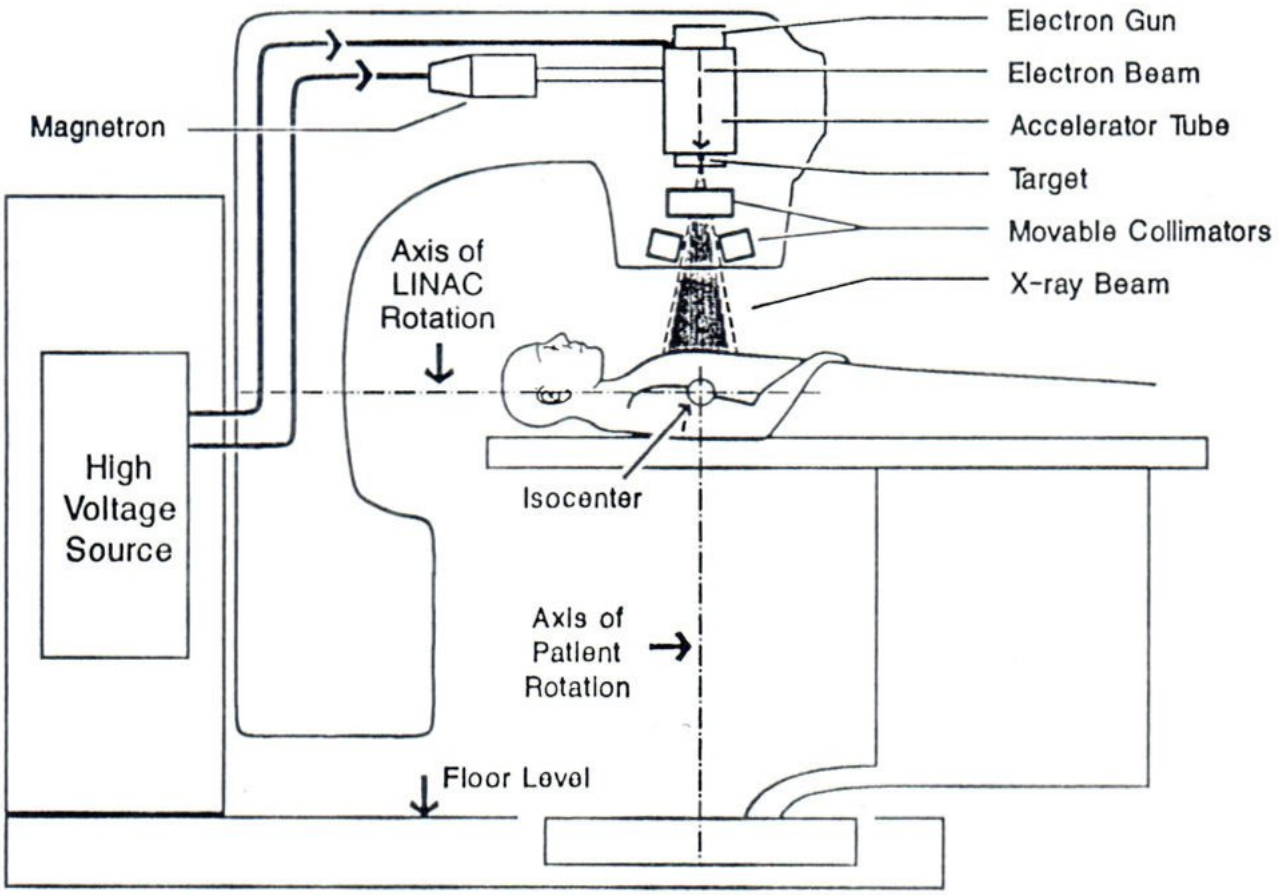

Fig. 4 Diagram of a common type of medical LINAC. The high-voltage source supplies high-voltage pulses simultaneously to both the electron gun and the magnetron, which converts them to microwave pulses. Thus a microwave pulse and electrons from the gun are simultaneously injected into the accelerator guide. The microwaves accelerate the electrons to high energy. The high-energy electrons strike a tungsten target, producing bremsstrahlung x-rays. The size of the x-ray beam is defined by two pairs of movable collimators. The entire x-ray producing unit can rotate about a horizontal axis passing through a point called the isocenter. The patient can be rotated about a vertical axis through the isocenter point. If the center of the larget to be treated is placed at the isocenter, then x-ray beams can be directed at the target from a variety of directions by utilizing different combinations of LINAC and patient rotations. When a LINAC is used for radiosurgery, it is fitted with a secondary collimator located downstream of the standard movable collimators.

REFERENCE

1. Altschuler E, Lunsford LD, Kondziolka D, Wu A, Maitz AH, Sclabassi R, Martinez J, Flickinger JC. In Lunsford LD (ed): Stereotactic Radiosurgery. Philadelphia: W.B Saunders Company, 1992.
2. Leksell L. The stereotaxic method and radiosurgery of the brain. Acta Chir Scand 1951;102:316-9.
3. Leksell L. A stereotactic apparatus for intracerebral surgery: Acta Chir Scand 1949;99:229-33.
4. Kirn TF. Proton radiotherapy:some perspectives. JAMA 1988;259:787-8.
5. Backlund EO. The history and development of radiosurgery, in Lunsford LS (ed), Stereotactic Radiosurgery Update. New York Elsevier, 1992, pp 3-9.
6. Leksell. Stereotactic radiosurgery. J Neurol Neurosurg Psych 1983;46:797-803.
7. Fabrikant JI, Lyman JT, Frankel KA. Heavy charged particle Bragg peak radiosurgey for intracranial vascular disorders. Radiat Res Suppl 1985;104:8244-58.
8. Betti OO, Derechinsky VE. Hyperselective encephalic irradiation with a linear accelerator. Acta Neurochir Suppl 1984;33:385-90.
9. Columbo F, Pozza F, Chierego G, et al. Linear accelerator surgery: current status and perspectives, in Lunsford LD (ed), Stereotactic Radiosurgery Update. New York, Elsevier, 1992, pp 37-46.
10. Barcia-Salorio JL, Hernandez G, Broseta J, et al Radiosurgical treatment of carotid-cavernous fistula, Appl Neurophysiol 1982;45:520-2.
11. Winston KR, Lutz W. Linear accelerator as a neurosurgical tool for stereotactic radiosurgery, Neurosurgery 1988;22:454-64.

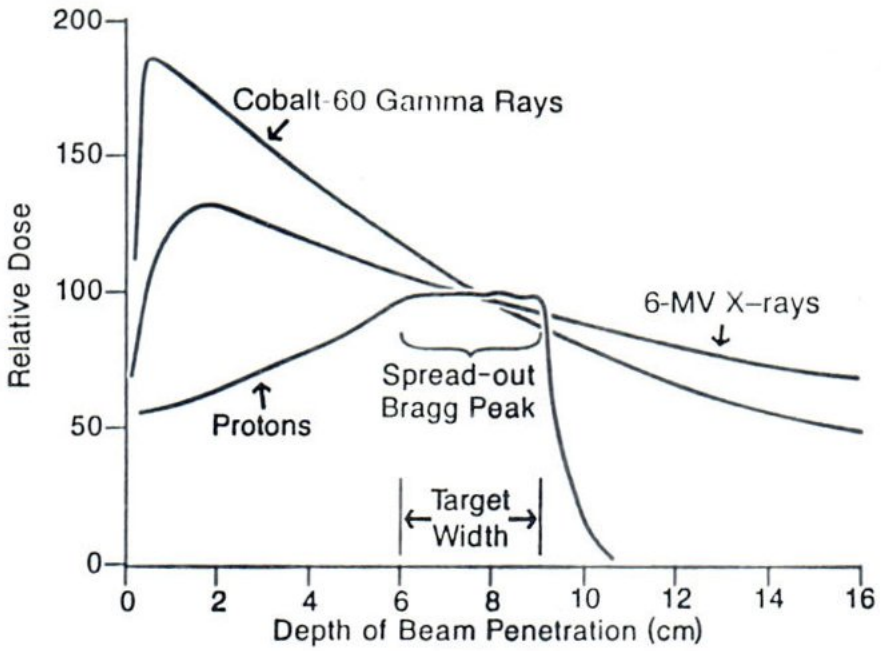

Fig. 5 Comparison of dose deposition for single beams of radiation measured from the head surface through the region of the target. In this example, the center of the target is 7.5 cm from the surface: If single beams were used for treatment, gamma rays and x-rays would be unsatisfactory because they deposit more dose outside the target than to the normal tissues along its entry path. The "single" proton beam is actually a composite beam.

12. Walton L, Banford CK, Ramsden D. The Sheffield stereotactic radiosurgery unit: physical characteristics and principles of operations. Br. J Radiol 1987;60:897-906.
13. Phillips M (ed) Physical aspects of stereotactic radiosurgery. New York, Plenum Press, in press.
14. Leksel Gamma Knife: A clinical perspective. A hand-out by Eleckta.
15. Kondziolka D, Lunsford D, Flickinger JC. The role of radiosurgery in the management of chordoma and chondrosarcoma of the cranial base. Neurosurgery 1991;29:38-46.
16. Lindquist C. Gamma Knife radiosurgery. Seminars in Radiation Oncology 1995;5:197-202.
17. Backlund Eo. Stereotactic treatment of craniophayngiomas, in Hamberger CA, Wersaell J (ed): Nobel symposium 10, Disorders of the skull base region. Stockholm: Almqvist & Wiksell, 1969, pp 237-44.
18. Backlund EO. Treatment of craniopharyngiomas. A ten year material (1196-1975), Proc 6th Int Congr Neurol Surg. Sap Paolo 1977.
19. Backlund EO, Bergstrand G, Hierton-Laurell U, Rosenborg M, Wajnot A, Werner S. Tumor changes after single dose irradiation by stereotactic radiosurgery in "nonactive" pituitary adenomas and prolactinomas. INSERM 1979;12:199-206.
20. Backlund EO, Raehn T, Sarby B. Treatment of pinealoma by stereotaxic radiation surgery. Acta Radiol (Ther Phys Biol) 1972;138:368-76.
21. Coffey RJ. Boost Gamma Knife radiosurgery in the treatment of primary glial tumors. Stereotact Funct Neurosurg 1993;61:59-64.
22. Coffey RJ, Cascino TL, Shaw EG. Radiosurgical treatment of recurrent hemangiopericytomas of the meninges: Priliminary results. J Neurosurg 1993;78: 903-8.

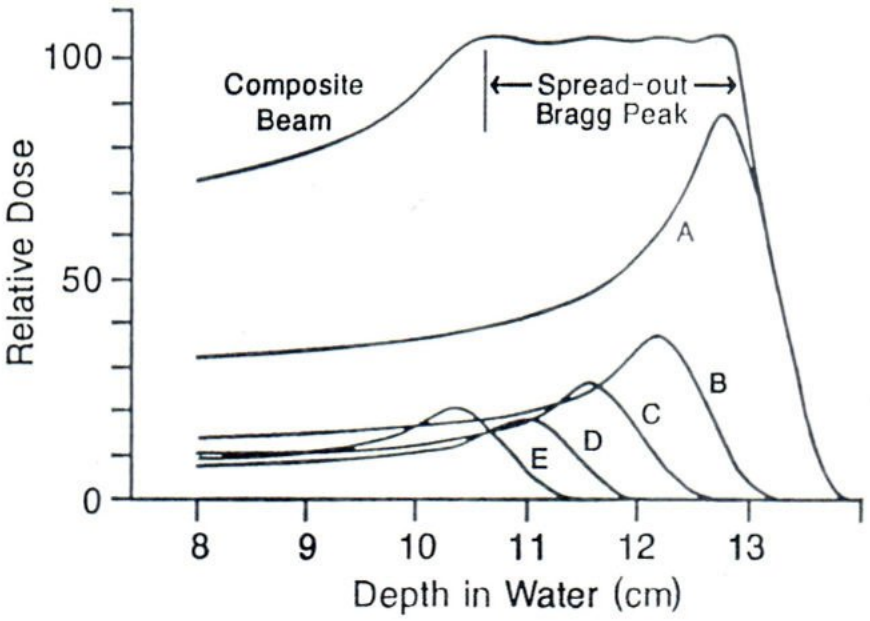

Fig. 6 The spread-out Bragg peak is formed by adding together beams of different penetrating ability (energy) and intensity (beams A,B,C,D and E) to form one composite beam. Beam A consists of 160-MeV protons. Beams B, C, D and E are various lower-energy beams formed from the 160 MeV beam by passing it through attenuators of different thicknesses. The high-dose, flat region of the composite beam is designed to have a width approximately equal to the width of the target in the beam direction. In this example, the flat region of the composite beam is approximately 2.5 cm.

23. Degerblad M, Raehn T, Bergstrand G, Thoren M. Long term results of stereotactic radiosurgery to the pituitary gland in Cushing's disease. Acta Endocrinol 1986;112:310-4.

24. Kihlstroem L, Guo W, Lindquist C, Mindus P. Radiobiology of radiosurgery for refractory anxiety disorders. Neurosurgery 1995;36:294-302.

25. Kondziolka D, Lunsford D. Stereotactic radiosurgery for squamous cell carcinoma of the nasopharynx. Laryngoscope 1991;101:519-22.

26. Raehn T, Arndt J, Thoren M, Backlund EO. Stereotactic radiosurgery in pituitary dependent Cushing's disease and Nelson's syndrome. Proc 6th Int Congr Neurol Surg. Sao Paolo 1977.

27. Raehn T, Thoren M, Anniko M. Gamma irradiation effects on human ACTH-producing pituitary tumors in organ culture. Arch Otorhinolaryngol 1983;238:209-15.

28. Rand RW, Khonsary A, Brown W, Winter J, Snow HD. Leksell stereotactic radiosurgery in the treatment of eye melanoma. Neuro Res 1987;9:142-6

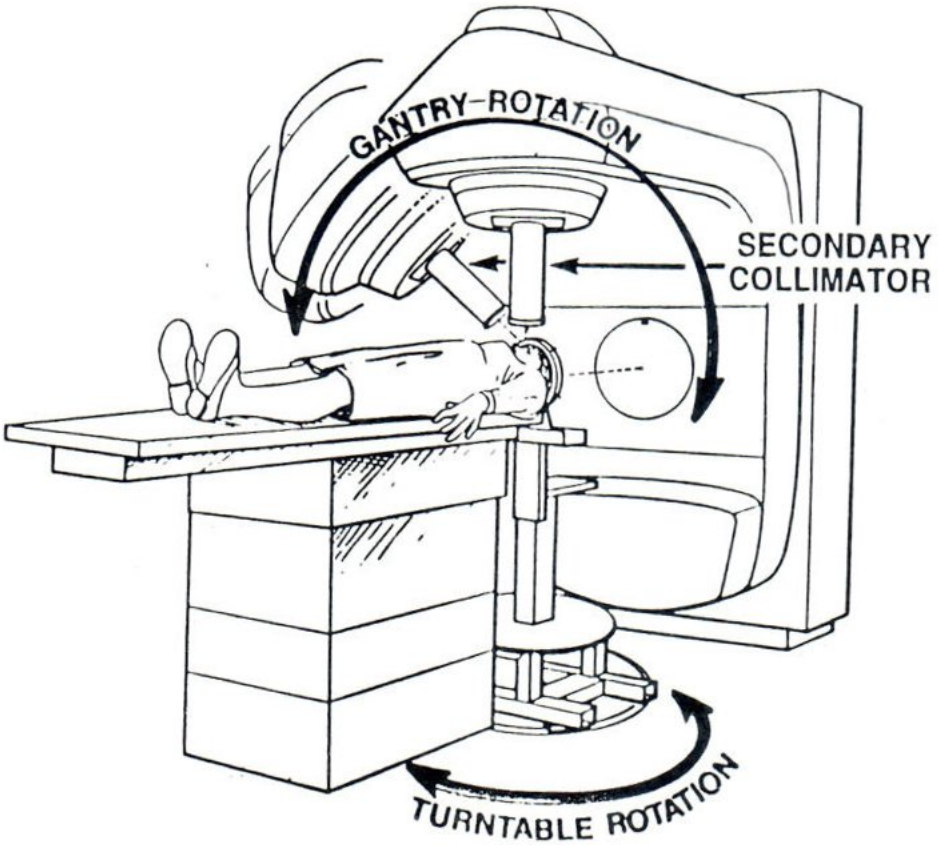

Fig. 7 Medical LINAC showing the two principal axes of rotation relevant for radiosurgery. Combinations of both rotations permit beams to be directed at an intracranial target from many different directions. A secondary collimator positioned close to the patient's head defines the shape of the x-ray beam.

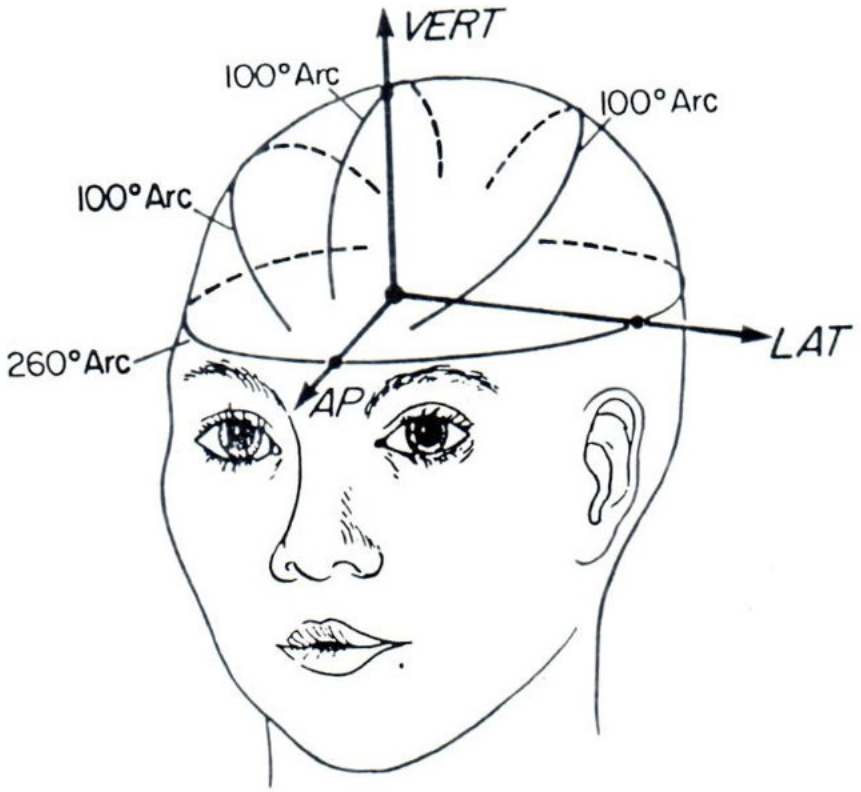

Fig. 8 Head schematic showing the paths traced by the central line of the x-ray beam on the surface of the head for a hypothetical treatment. Great flexibility exists in selecting these paths, or arcs, to optimize the dose distribution for a given patient's treatment.

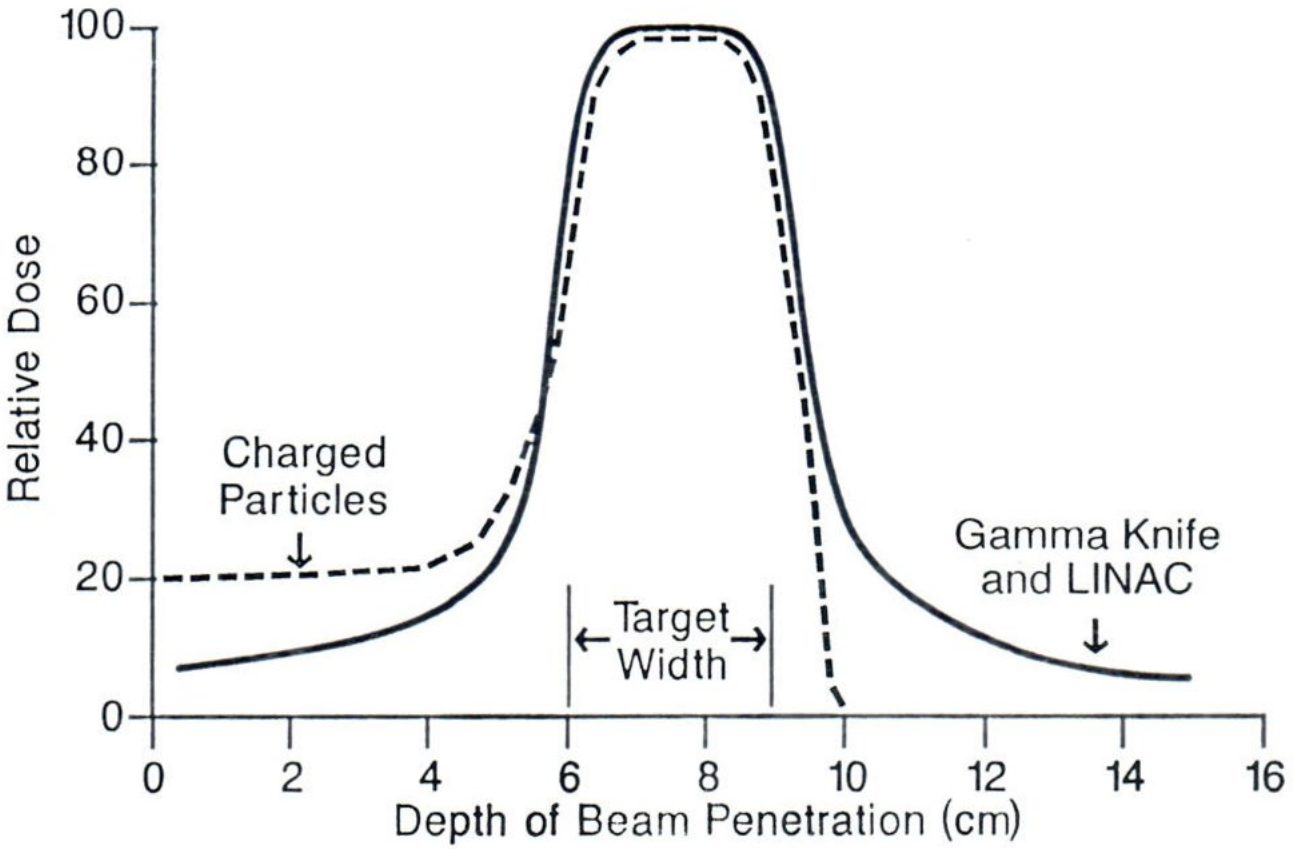

Fig. 9 Treatment dose measured along the center line of one beam from the head surface through the region of the target for a single isocenter. The dose values were generated by using a complete set of representative beams for each of the three treatment approaches. Each technique is capable of concentrating the dose within the target region. Entry doses appear to the left of the target and exit doses to the right. Note that charged particle beams have a finite range and hence deposit very little dose distal to the target. Entry and exit doses are essentially the same for both LINAC and Gamma Knife treatments. A charged particle treatment (e.g. four beams) deposits more dose (about 20 percent of the target dose) along each of its entry paths than the dose deposited along each entry path for either a LINAC (e.g., the four arcs or a Gamma Knife (201 beams) treatment. However, the typical charged particle treatment deposits dose to normal tissue only along four paths.

RADIOSURGERY BY X-KNIFE FOR RETROORBITAL METASTASIS FROM FIBROSARCOMA : A CASE REPORT

PATTARANUTAPORN. P.,MD.*
WANNISORN. J., MD.**
CHANSILPA. Y.,MD.*
KAKANAPORN J.,M.Sc.*
ONNOMDEE. K.,B.Sc.***
MUNGKUNG. N.,B.Sc.***

ABSTRACT

A case report of retroorbital metastasis fibrosarcoma patient who suffered from painful exopthalmos of left eye was treated with linac based stereotactic radiosurgery (X-knife), a technique that permits the precise delivery of a high dose of radiation from 6 MV linear acclerator to the target while sparing the normal tissue. The radiation dose was 20 Gy at the 75% isodose line encompassing the enhancing tumor. Four weeks after treatment, exophthalmos was almost disappeared and pain symptom was almost completely relieved. The CT scan showed marked regression of the tumor corresponding with clinical appearance, and almost disappeared at 10 weeks. The patient could tolerate well to the treatment procedure without any complications inherent to the technique.Radiosurgery with X-knife is an effective and safe therapy for single palliative treatment of lacalized lesion of head and neck tumor.

INTRODUCTION

Orbital metastasis is not an uncommon metastatic disease.[1-2] The sites of metastasis are choroid, retrobulbar soft tissue, eyelid or bony orbit.[3-6] Clinical symptoms and signs of ocular metastasis are exophthalmos, pain, ophthalmoplegia and diplopia, palpable mass, proptosis, periorbital swelling, and pseudo-inflammation.[2-3,5] Local treatment by radiotherapy for palliative treatment in single orbital metastasis could provide the fair result.The complete response were 25-50%, while the overall response rate was as high as 85%.[7-12] In cases of palliative treatment, simple technique of the short overall treatment period without adding complications should be used to have the best quality for the rest of one's life. The convenience and efficacy of radiosurgery procedure leading to an increasing use of this treatment for brain metastasis, and also in palliative treatment in other sites of tumor such as base of skull,head and neck region.[13-19]

This report describes the palliative radiation for orbital metastasis from fibrosarcoma by the linac based radiosurgery in term of accuracy and efficacy of the linear accelerator facility or X-knife.

CASE REPORT

A 56 years old female patient, known case of fibrosarcoma of left humerus post resection 4 years ago, developed bone and lung metastases 3 years later. She was treated with radiation for palliative

* Division of Radiation Oncology, Department of Radiology, Faculty of Medicine, Siriraj Hospital, Mahidol University.
** Division of Neurosurgery, Department of Surgery, Srisiam Hospital.
*** Department of Radiology, Srisiam Hospital.

bone pain but she refused systemic chemotherapy. Two months before attending our department, she suffered from the painful exopthalmos of left eye with diplopia and periorbital swelling. She refused conventional radiation therapy because of the long period of treatment. So the stereotactic radiosurgery technique with X-knife was offered.

RADIOSURGICAL TECHNIQUE

The technique was the same as we treated the intracranial lesion. The BRW stereotactic headframe was transversely fixed to the patient's head with local anaesthesia by neurosurgeon. The stereotactic images were done by computerized tomographic scan to get the spatial coordinates of the lesion. After stereotactic CT images were done, the data was transfered to the computerized planning system for X-knife treatment planning program. The external surface, the tumor and critical structures such as eyes, optic nerve, optic chiasma and brain stem were labeled in the CT images and reconstructed to be the three dimentional structures. The treatment planning was started by defining the isocenter with suitable collimator in the tumor and the multiple non-coplanar radiation beams were planned. The dose was prescribed at 75% isodose line to be 20 Gy which encompassed the area of enhancement. Before completion of the treatment planing, we have to ensure that the radiation field conforms precisely to the surgical target. Dose distribution is facilitated by 3-D visualization, dose volume histograms of the primary tumor and surrounding critical structures, especiallly optic nerve in this case. Radiation treatment set up proceeded by 2 radiation technologists under the supervision of the radiation oncologist.

RESULT

The radiosurgical procedure with X-knife was well succeeded without immediate complications. Four weeks later, the patient showed a very good response with improvement of exopthalmos and proptosis. Pain was almost completely relieved but diplopia was still exist. The CT scan showed marked decrease of tumor size as compared to the previous film.(Fig 2) There was no any skin reaction. Mild conjunctivitis occurred but subsided later without specific treatment. The quality of life was much improved.

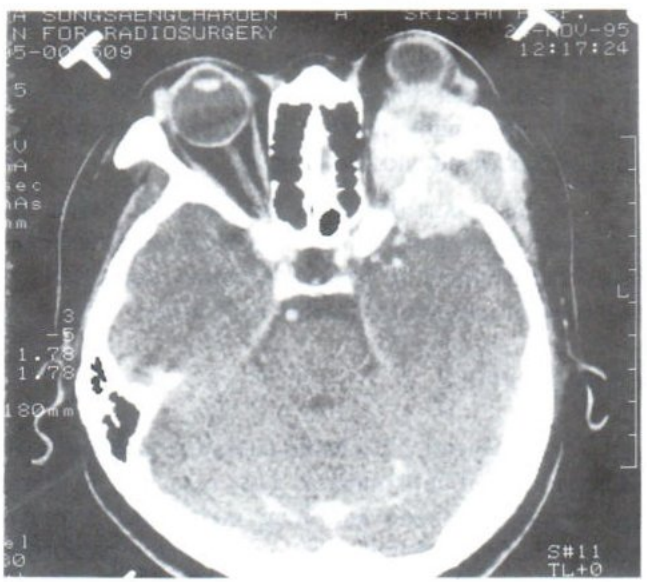

Fig.1 CT scan revealed ill defined mass at the superiolateral aspect of the left orbit forming an extraconal mass with exophthalmos and destruction of the surrounding bone.

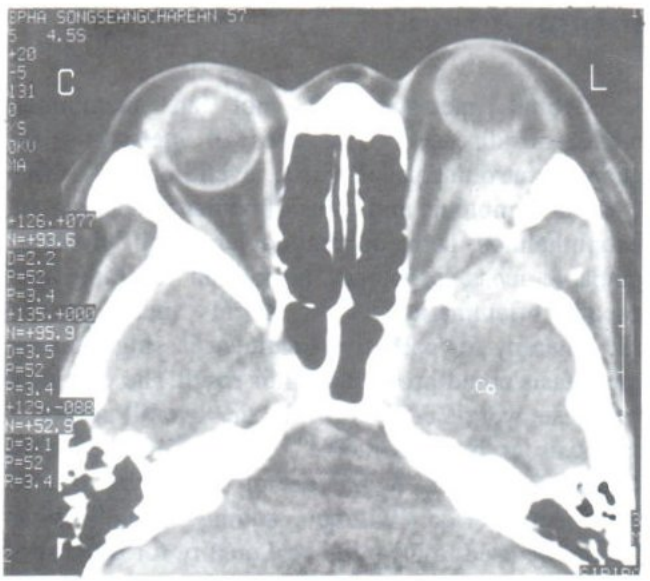

Fig 2. CT scan at 1 month after treatment shows decreasing in size of the tumor and the recovery of exopthalmos.

The tumor showed further shrinkage at the 10 weeks follow up.(fig.3)

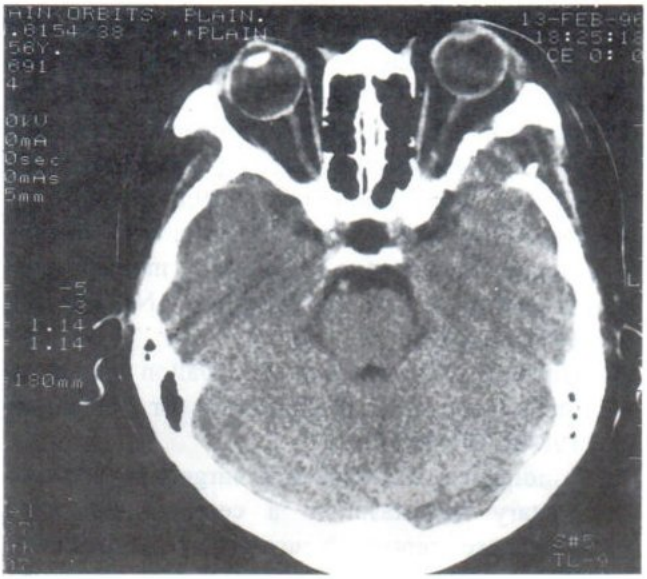

Fig 3. CT scan at 10 weeks showed the tumor almostly disappeared.

DISCUSSION

The most common metastatic site of fibrosarcoma is the lung.Orbital metastasis is a rare condition. [20-22] Surgery is the mainstay of therapy and radiation usually be the adjuvant or palliative treatment.In this case, the patient refused to be treated for the metastatic sites in the lungs but she asked for the treatment of pain in the orbital metastasis. Excellent result have been achieved eventhough it was a fibrosarcoma that was recognised as a radioresistant tumor . This result is the same as the good result of the focusing high radiation dose treated for the traditional radioresistant tumor like malignant melanoma[13-15, 23-27]

From the clinical symptom and follow up CT scan showed a very promising result, the exopthalmos almost disappeared without any complications, no skin reaction that normally appeared in conventional radiotherapy . The other distinct advantage is the short treatment period of only 1-2 days compared to one and a half month by conventional radiation.

CONCLUSION

Linac based radiosurgery or X-knife is a safe, effective and appropriate procedure for palliative treatment that provides good palliation of the symptoms with less complications and short treatment period. This technique can also be used in curative intent as a primary treatment, as booster in big tumor or in cases of having received previous radiation.

REFERENCES:

1. Glazer LC, Harris GJ, Simons KB. Orbital metastasis as the presenting sign of Ca. breast. Ophthal Plast Reconstr Surg 1991;7:252-255.
2. Stefanyszyn MA, DeVita EG, Flanagen JC. Breast carcinoma metastatic to the orbit. Ophthal Plast Reconstr Surg 1987;3:43-47.
3. Van Der Heijden A, Twijnstra A, Lamers WP, et al. An unusual cause of diplopia in a cancer patient. Eur J Cancer 1991;27: 1315-1316.
4. Burmeister BH, Benjamin CS, Childs WJ. The management of metastases to eye and orbit from carcinoma of the breast. Aust NZ J Ophthalmol 1990;18:187-190.
5. Motto-Lippa L, JaKobiec FA, Iwamoto T. Pseudoinflammatory metastatic breast carcinoma of the orbit and lids. Ophthalmology 1981;88:-575-580.
6. Hesselink JR, Davis KR, Weber AL, et al. Radiological evaluation of orbital metastases with emphasis on computed tomography. Radiology 1984;37:363-366.
7. Kagen AR. Radiation therapy in palliative cancer management.In:Perez CA, Brady AW. eds. Principles and Practice of Radiation Oncology. 2 nd ed. Philadelphia : JB Lippincott company, 1992:1498.
8. Dobrowsky W. Treatment of choroid metastasis. Br J Radiol 1988;61:140-142.
9. Sagerman RH. Radiation therapy for orbital tumor. In : Hornblass A ed. Tumor of the ocular adnexa and orbit. St.Louis : The CV Mosby, 1979:268.
10. Huh SH, Nisce LZ, Simpson LD, et al. Value of radiation therapy in the treatment of orbital metastasis. AJR 1974;120:589-594.
11. Panizzoni GA, Gasparini G, Dal Fior S, et al. Radiotherapeutic treatment for breast cancer choroidal metastasis. Tumori 1990;76:563-565.

12. Hoogenhout J, Brink HM, Verbuk AM, et al. Radiotherapy of choroidal metastasis. Strahlen-therapie and Onkologie 1989;165:375-379.
13. Alxander E 3rd, Moriarty TM, Davis RB, et al. Stereotactic radiosurgery for the definitive, non-invasive treatment of brain metastases. J Natl Cancer Inst 1995;87:34-40.
14. Flickinger JC, Konziolka D, Lundford LD, et al. A multi-institutional experience with stereotactic radiosurgery for solitary brain metastasis. Int J Radiat Oncol Biol Phys 1994;28:797-802.
15. Buatti JM, Friedman WA, BovaFJ, Mendenhall WM. Treatment selectiom factors for stereotactic radiosurgery of intracranial metastases. Int J Radiat Oncol Biol Phys 1995;32:1161-1166.
16. Voges J, Treuer H, Erdmann J, et al. Linac radiosurgery in brain metastases. Acta Neurochir suppl (Wien) 1994;62:72-76.
17. Martens F, Verbeke L. Stereotactic radiosurgery of cerebral metastases: Preliminary results. Acta Clin Belg 1993;48:228-233.
18. Kondziolka D, Lundford LD. Stereotactic Radiosurgery for Squamous cell carcinoma of the Nasopharynx. Laryngoscope 1991;101:519-522.
19. Kaplan ID, Adler JR, Hicks WL, et al. Radiosurgery for palliation of Base of Skull Recurrences from Head and Neck Cancers. Cancer 1992;70:1980-1984.
20. Jameel Ahmed M, Omar YT, Ali SM, Temmim L. Soft tiuue sarcoma in Kuwait : a review of 114 patients. Clin Radiol 1987;38:27-29
21. Vezeridis MP, Moore R, Karakousis CP. Metastatic patterns in soft-tissue sarcomas. Arch Surg 1983;118:915-918.
22. Rootman J, carvounis EP, Dolman CL, Dimmick JE. Congenital fibrosarcoma metastatic to the choroid. Am J Ophthalmol 1979;87:632-638.
23. Davey P, O'Brien P. Disposition of cerebral metastases from malignant melanoma : implication for radiosurgery. Neurosurgery 1991;28:8-15.
24. Hitchcock E, Kitchen G, Dalton E, et al. Stereotactic Linac Radiosurgery. Br J Neurosurg 1989;3:305-312.
25. Lindquist C. Gamma knife surgery for recurrent solitary metastasis of a cerebral hyperneph-roma:case report. Neurosurgery 1989;25:802-804.
26. Fedorssak I, Sipos L, Horvath a, et al. Multiple intracranial melanoma treated with surgery and radiosurgery with long term control. A case report. J Neurooncol 1993;16:173-176.
27. Somaza S, Kondziolka D, Lundford LD, et al. Stereotactic radiosurgery for cerebral metastatic melanoma. J Neurosurg 1993;79:661-666.

DOSE CALCULATION FOR THE HALF BLOCKED FIELDS DEFINED BY INDEPENDENT JAWS

Sivalee SURIYAPEE
Chotika JUMPANGERN
Chusak PUANGNAK

ABSTRACT

A system of dose calculation of a 6 MV photon beam from a Clinac 1800 linear acce -lerator for the half blocked fields defined by independent jaws was designed. The dose is computed as the product of the field size factors, the off axis ratios and the percentage depth dose which are determined from a data set of symmetric fields. The dosimetric measurements of these parameters for asymmetric fields were performed to evaluate the calculation method. The field size factors for asymmetric fields are within 1.1% compared to those for symmetric fields corrected for off axis ratios. Asymmetric field percent depth doses differ from those of symmetric field with maximum of 7.5% for field sizes range 4x4 to 20x20 cm. and depth down to 20 cm. The measured isodose curves of asymmetric fields show about 4% reduction of dose near the field edge closed to the flattening filter center. Calculation of the doses for half beam by this method have been checked by the measurement of the dosage at 1.5, 5 and 10 cm depth, the result shows an agreement within 1.3% which is acceptable.

key words : dose calculation, half blocked fields, independent jaws, asymmetric fields.

INTRPDUCTION

An asymmetric x-ray collimator of Varian Clinac 1800 has one collimating jaw that can be moved independently of the corresponding opposed jaw. By blocking off one half of the field at the central axis, beam divergence can be eliminated at the junction of two fields. This characteristic is useful in the treatment field that is matched to the other fields such as the supraclavicular field and tangential breast field or other techniques which need no divergence of beams.

The characterestic of asymmetrical beams should be evaluated before using the beams to treat the patient. In this work the dose measurements were performed to evaluate that dosimetric data from symmetric collimators could be used for asymmetric collimators. The study of asymmetric and symmetric field dosimetric data, i.e. output factor, percentage depth dose and isodose curves are included.

METHODS AND MATERIALS

The study was done for half blocked fields defined by independent jaw system of 6 MV x-rays from Clinac 1800. First, to evaluate whether the calculation of monitor unit using the off axis ratios, the field size factors and the percentage depth dose of symmetric beams is suitable. The output at the center of the beam as a function of field sizes both for the symmetric and the asymmetric collimation were measured in water phantom at the depth of maximum dose (1.5 cm.) and at the depth of 5 cm. to calculate

Division of Radiotherapy Department of Radiology Faculty of Medicine, Chulalongkorn University, Rama IV Road Bangkok 10330, Thailand.

the field size factors. For routine calculation of monitor unit in asymmetric beam, the field size factors were obtained from the measurement of the output at 5 cm. in the water phantom and converted to the dose at depth of maximum dose. So in this study the measurement were done both in 1.5 and 5 cm. depth to verify the difference of two techniques obtaining the field size factors. The dosemeter used is Nuclear Enterprise limited (NE) Ionex Dosemaster (model NE 2590 A) with 0.6 cc. ion chamber (model NE 2571).

Next, the measurement of percent depth dose and the set of beam profile at 1.5, 6.5, 11.5, 16.5 and 21.5 cm depth for each square field have been performed using a Therados BDS 3 - water scanner system with a silicon detector. The field sizes were ranging from 4x4 to 20x20 cm. These data were filled to the software dialogue of the GE target planning system which generated the isodose curves.

Then, the output measurements were performed to confirm the dose calculation using the symmetrical beam data. The measurements were done in water phantom at fixed SSD (100 cm.), the field sizes of half blocked fields were ranged from 5x5 to 20x20 cm.. Output reading were taken at 1.5, 5 and 10 cm. depths for each square field.

RESULTS AND DISCUSSION

A. Field size factors

The field size factor (FS) for asymmetric field (1) of size (r x r) and a lateral displacement of field center (x cm) from the true central axis is given by (see fig 1)

$$FS(r, x) = \frac{FS(r,o) \times OAR(x)}{FS(10 \times 10,0)} \quad \ldots\ldots\ldots\ldots \text{①}$$

where OAR (x) is the ratio of dose at off-axis points relative to dose at the true central axis of the beam measured at depth of maximum dose. Readings were taken in a profile of 40x40 cm. at depth of maximum dose relative to the dose at the center of beams. All dose measurements of the field were normalized to those measurements of the field of 10x10 cm. symmetric at 1.5 cm depth. Fig 2 shows the relative field size factors measured at the center of the beam both on the symmetric beam and asymmetric beam. The data plotted in Fig 2 indicates that field size factors for the half blocked fields generated by independent jaw closely approximate those for the symmetric fields of the same demension when each data point was corrected for the change in beam output for that off axis point. The data is shown in table 1 the maximum discrepancy is only 1.1%.

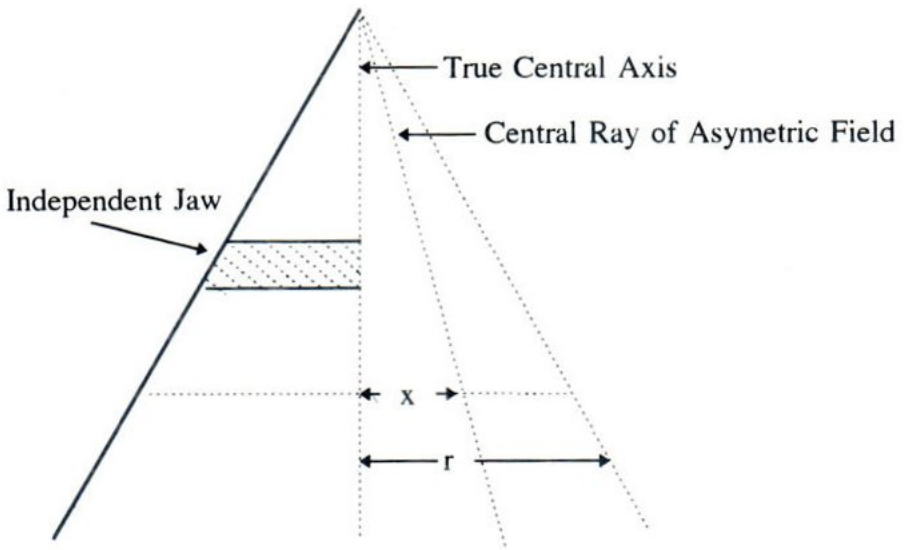

Fig 1. Geometry of half block field by an independent jaw

Table 1 Comparison between field size factor of symmetric fields and half blocked asymmetric fields.

Field size (cm)	5x5	8x8	10x10	16x16	20x20
Field size factor (FS) of symmetric fields	0.950	0.989	1.0	1.040	1.057
Off axis ratio (OAR) d_{max}	1.015	1.025	1.030	1.040	1.050
FS of symmetric fields x OAR	0.964	1.014	1.030	1.082	1.098
FS of asymmetric fields	0.960	1.013	1.041	1.094	1.107
$\frac{\text{FS sym x OAR}}{\text{FS Asym}}$	1.004	1.000	0.989	0.989	0.992

Table 2. Comparison between central axis percentage depth dose of symmetric fields and half blocked asymmetric fields.

Field size (cm.)	4x4			8x8			10x10			16x16			20x20		
Depth (cm.)	Sym (S)	Asym (A)	S/A	Sym (S)	Asym (A)	S/A	Sym (S)	Asym (A)	S/A	Sym (S)	Asym (A)	S/A	Sym (S)	Asym (A)	S/A
5	85.5	85.0	1.006	86.5	86.0	1.006	87.5	86.5	1.006	88.0	87.0	1.011	88.5	87.3	1.014
10	63.5	63.0	1.008	67.0	66.0	1.015	68.0	67.0	1.015	70.0	68.5	1.022	71.0	69.3	1.025
15	47.0	47.0	1.000	51.0	49.2	1.034	52.5	50.5	1.040	55.0	52.5	1.048	56.0	53.0	1.057
20	35.0	34.0	1.029	39.0	37.5	1.040	40.5	38.5	1.052	42.5	40.0	1.062	43.0	41.0	1.075

The field size factors measured at 1.5 cm in water are identical to field size factors obtained from the measurement at 5 cm. depth in water. The average discrepancy of field size factor by two methods is only 0.16%.

B. Percentage depth dose

The percentage depth dose along the central ray of the half blocked beams is expected to change due to significant change in beam quality at a point away from the true central ray (1,2,3). Percentage depth doses at 100 cm. SSD for field size 4x4 to 20 x20 cm. at 5, 10, 15, 20 cm depth are shown in table 2 both for symmetric and asymetric fields. The change in percentage depth doses for the depth less than 10 cm and field size smaller than 16x16 cm. is below 2.2%. The reduction in depth dose of asymmetric field is greater for larger field size and at greater depth. The percent depth dose of symmetric and asymmetric fields mostly differ by 7.5% as the field size is 20x20 cm and the depth is 20 cm. Beam quality is low when passing the thinner flattening filter comparing to beam passing the center of flattening filter (2). As field size get larger, the center of the field moves further from the flattening filter center. This causes the reduction of depth dose of asymmetric field compared to symmetric field. The effect is more when the depth is increased because the dose is contributed from primary and scattered interaction. At the superficial depths where the majority of dose is from primary interactions, these effects are small (2).

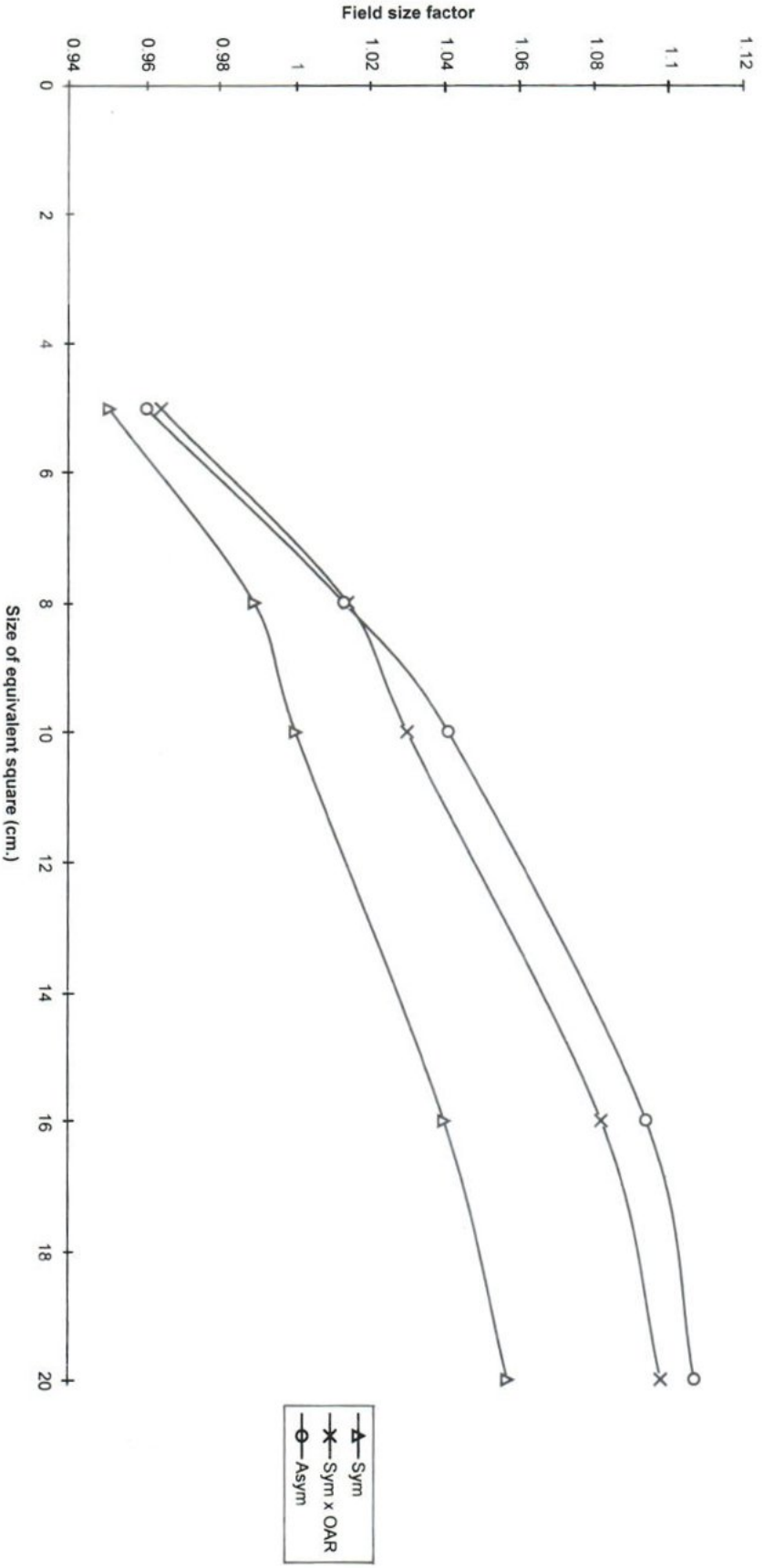

Fig 2. Field size factors measured on the center of symmetric and asymmetric beam

C. Dose distribution evaluation

Fig 3 shows the isodose distribution of 10x10 cm symmetric field "A" compared to 10x10 cm half blocked field "B" (5 cm off axis).

The shape of the isodose lines is altered by the asymmetric collimation. The shallower depth dose are shown on the left hand side of the field that is closer to the center of flattening filter. This is due to the attenuation by the flattening filter. Without the full scatter dose that would normally occur in this area of the field (2). The maximum decreasing of dose is 4%. Increasing depth diminized the reducing of isodose curves.

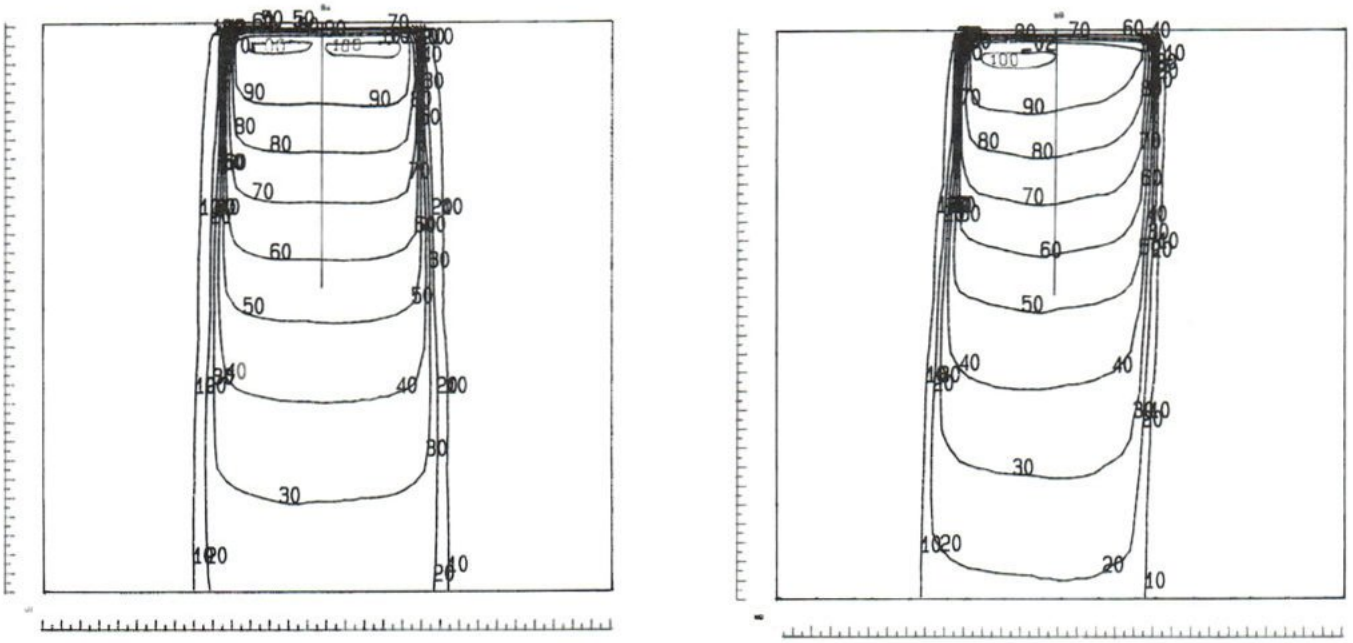

Fig 3. Comparison of 10x10 cm. symmetric field (A) and half blocked field (B).

D. Dose to a point on the center of half blocked fields

Measurement of the dosage in a water phantom along the central ray of asymmetric fields at the reference depth (1.5 cm) verified the following equation (3).

$$D(d_m, x, r) = k\ MU\ FS(r, o)\ OAR_{dm}(x) \quad \text{..... ②}$$

where MU is the number of monitor unit and k is the dose per MU, which is 1 cGy per1 MU at the calibration point (at depth d_m) on the central axis of a symmetrical 10x10 cm. field. $OAR_{dm}(x)$ is the off oxis ratio at depth of maximum dose.

Similarly the dose to a point x at depth d on the central ray of a half blocked field is

$$D(d, x, r) = k\ MU\ FS(r, o)\ P(d, o, r)\ OAR_d(x) \quad \text{....③}$$

where $OAR_d(x)$ is the off axis ratio at depth d of symmetric field. For isocentric techniques

$$D(d, x, r) = k\ MU\ FS(r, o)\ TMR(d, o, r_d)\ OAR_d(x) \left(\frac{SCD}{SAD}\right)^2 \quad \text{..... ④}$$

Where SCD is the source to calibration point distance and SAD is the source to axis distance.

The doses measured at depth of 1.5, 5 and 10 cm. using 100 MU. were then compared to the calculated values from eq ② and ③, their results show in Table 3.The calculated and measured values show good correlation. The maximum difference between calculated values and measured values is 1.3%

Table 3. Comparison of measured dose and calculated dose for half blocked asymmetric fields

Depth in water (cm)	Measured dose / calculated dose				
	5x5 cm.	8x8 cm.	10x10 cm.	16x16 cm.	20x20 cm.
1.5	0.997	1.001	1.012	1.013	1.001
5.0	1.007	1.010	1.013	1.013	1.000
10.0	1.008	1.001	1.009	1.006	0.990

SUMMARY

The half blocked beam defined by asymmetric collimator causes certain dosimetric effects. Off axis factors can be used to calculate the monitor unit giving to the patient. The present of flattening filter causes the quality change of photon beam. Reduction in beam quality occurs because the thinner flattening filter allows lower energy photons to penetrate, reducing the percentage depth dose as off axis distance increases.

The agreement of dose calculation using off axis ratio, field size factor and symmetric percentage depth dose verifies that the data from symmetric beam can be used for the asymmetric beam. Correction for percentage depth dose is not neccessary unless the treatment field is at the depth greater than 10 cm. and field size greater than 16x16 cm.

For treatment planning system, the new set of isodose lines of asymmetric beam should be installed. Some commercial treatment planning system does not correct for off axis energy change. Therefore the error will be occurred and produce the misunderstood plan. However, the accurate isodose distribution by commercial treatment planning systems requires special dose calculation algorithms.

REFERENCES

1. Palta JR, Ayyangar KM, Suntharalingam N. Dosimetric characteristics of a 6 MVphoton beam from a linear accelerator with asymmetric collimator jaws. Int J Radiation Oncology Biol Phys 1988; 14 (2): 383-387.
2. Slessinger ED, Gerber RL, Harms WB, et al. Independent collimator dosimetry for a dual photon energy linear accelerator. Int J Radiation Oncology Biol Phys 1993; 27 (3): 681-687.
3. Khan FM, Gerbi BJ, Deibel FC. Dosimetry of asymmetric x-ray collimators. Med Phys 1986; 13 (6): 936-941.

DOSE DISTRIBUTION IN TOTAL BODY PHOTON IRRADIATION

R. PIRABUL, T. LAYANGKUL,
C. TANNANONTA, P.SUWANNAKORN,
P. KRAIPHIBUL

ABSTRACT

In the total body photon irradiation (TBI) of leukemic and lymphoma patients prior to bone marrow transplantation, bilateral opposing beams of the fully opened collimator produced by a 6 MV Clinac 2100C with perspex beam spoiler of 1 cm thick were used to irradiated the Randophantom at a large target surface distance (TSD). The measurements of the radiation doses at the surface and inside the phantom were performed using LiF Thermoluminescent dosemeters. The dose at the center of the abdomen at the umbilicus level was taken as a reference dose.

The first study without bolus and shieldings showed the high surface doses of 125 % and 128 % at the right and left lateral neck respectively. The rest of them were not more than 17 % higher than the reference dose. The largest different doses from the reference for various organs inside the phantom were 33 % at the larynx and 29 % at the cervical cord. The doses at the brain, right lung and left lung were 12 %, 16 % and 18 % higher than the reference dose respectively.

In the second study, the bolus was added to the neck region for uniformity of dose distribution and one half value thickness of shielding blocks were used for both lungs and brain. The surface doses at right and left lateral neck were reduced to 109 % and 104 % respectively. The doses at larynx and cervical cord were 5 % and 2 % higher than the reference dose. The doses variations within ± 10 % were obtained at the surface and inside the phantom while the dose in the shielding region were reduced to approximately 50 %

1. INTRODUCTION

High dose total body irradiation with megavoltage photon beams is used to destroy the bone marrow and malignant cells, and also immunosuppress the patient prior to receiving a bone marrow transplant [1, 2, 3]. Before instituting the TBI procedure, medical physicists have to establish the available and approriate irradiation method that patients should receive most uniform dose distribution without over tolerance dose to critical organs. AAPM report no.17 recommends AP/PA parallel opposed fields although under some conditions (e.g. pediatric cases, higher energies), a ± 10 % uniformity can be acheived with bilateral fields [1]. Due to the complex geometry of the human body, in total, a degree uniformity of ± 10 % is desired [2,4]. The possibility technique performing in our department is bilateral fields with the patient in supine position.

Department of Radiology, Ramathibodi Hospital, Bangkok, Thailand

2. EXPERIMENTAL DESIGN

The experiments are devided into 2 parts.

part I : Determination of the surface dose and the dose inside the phantom without any bolus and shielding block.

part II : The dose determination are the same as part I but the bolus will be employed to improve the dose homogeneity and the shielding blocks will be provided to reduce the dose in some critical organs.

Part I The Clinac 2100C is the equiptment used for delivering 6 MV photon to patients. Due to the limitation of the size of the treatment room and the difficulty in the shielding of certain organs, the possibility TBI technique has to be bilateral fields with the patient in supine position on the special couch close to the wall. The irradiated beam size is 140 x 140 cm_2 in diagonal shape at 350 cm target surface distance as shown in Fig. 1. The Randophantom was used to represent the patient. Due to the effect of low dose in the build up region of 6 MV photon, a perspex beam spoiler with 1.0 cm thick was placed at 15 cm apart from the skin surface for increasing the dose in this region. The mid point of the level at the umbilicus is selected to represent the point of the reference dose [1,4]. The surface dose and the absorbed dose of various organs inside the Randophantom were measured by the LiF dosemeters as Fig. 1.

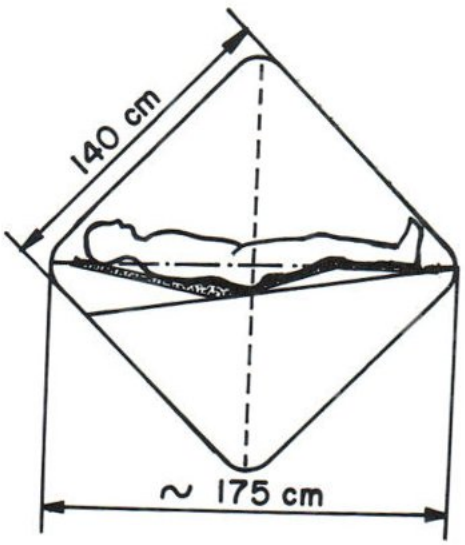

Fig 1. Field size at TSD 350 cm.

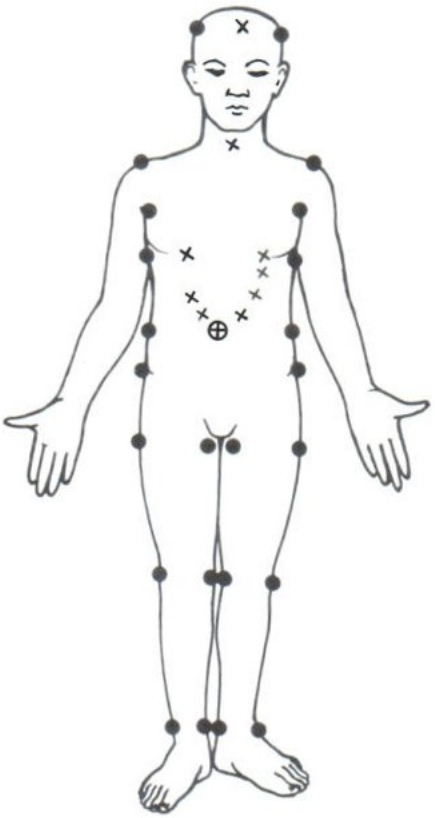

Fig 2. Position of TLD dosemeters for surface doses and doses of the organs inside the phantom.

Part II The blocks with one half value thickness (HVT) were used to reduce the doses of both lungs and brain to be a half of prescribed dose (which is the technique used at Ramathibodi Hospital) to decrease the pulmonary fibrosis and leukoencephalopathy [2]. The small rice bags were used as the bolus for missing tissue at the neck region.

3. DOSE CALIBRATION

A 0.6 cc cylindrical chamber with Ionex Dosemaster electrometer were used for dose calibration in a water phantom at 5 cm depth, 140 x 140 cm_2 in diagonal shape, 350 cm TSD. The percent depth dose along the central ray were measured under the same geometry by the silicon diode detector with RFA-300 scanning system of Scanditronix. The perspex beam spoiler with 1.0 cm thick was also placed at a distance 15 cm from the water phantom surface to produce the scattered radiation to the phantom surface. Fig. 3 shows the plot of the depth dose along the central axis.

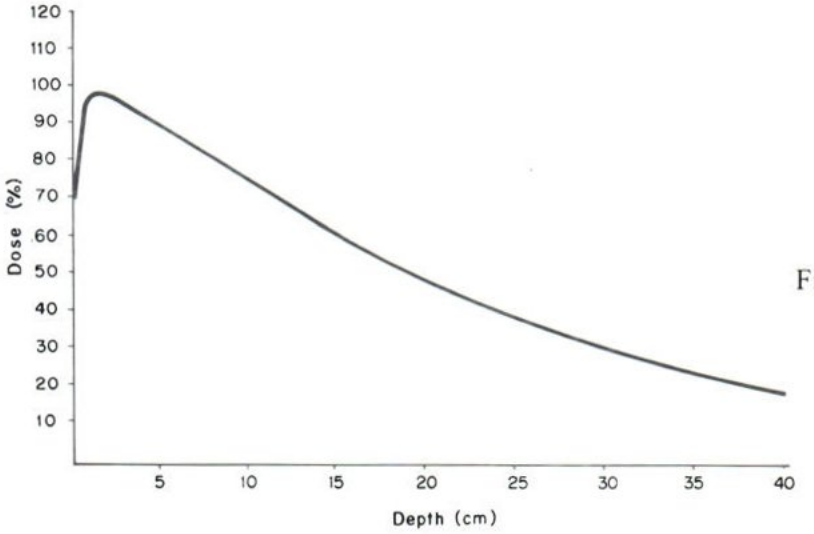

Fig 3. Central axis percent depth dose for 6 MV photon in a water phantom with a perspex beam spoiler of 1 cm thick 15 cm apart from the surface. field size 140 x 140 cm^2 , 350 cm TSD, diagonal setting.

4. RESULTS

4.1 Part 1 experiment

Table IA illustrates the higher doses at the surface of the head, neck and chest than the dose at the reference point for 9, 25 and 16 % respectively. The doses inside the phantom at the brain, the larynx, cervical cord, heart and both lungs in Table IB were more than 10 % higher than the reference dose.

Table I Doses at various points as the percents of the reference at the mid point of umbilical level, without bolus and blocks.

A : Surface doses

Organ	Surface dose (%)	
	Right	Left
head	110	109
neck	125	128
shoulder	90	99
axilla	116	116
chest	117	116
waist	103	102
hip	94	95
thigh	94	95
wax phantom -		
lateral knee	106	101
medial knee	97	98
lateral ankle	107	111
medial ankle	110	106

B : Organ doses

Organ	Organ dose (%)
brain	113
larynx	133
cervical cord	129
heart	112
lung (Rt, Lt)	116 , 118
liver	114
spleen	110
kidneys (Rt, Lt)	87 , 90
mid point at the level of umbilicus	100
ovary (Rt, Lt)	89 , 90

4.2 Part II experiment

The doses at the neck surface from the experiment in part I were reduced by placing the rice bags as the bolus for the missing tissue at the neck region (Table IIA). The doses in the brain and both lungs were reduced about 50 % due to the 1 HVL of MCP 96 were used as the shielding blocks (Table IIB). The doses were remarkly reduced 27 % at the cervical cord and 52 % at the heart due to the bolus at the neck region and the 1 HVL lung blocks (Table IIB).

Table II Doses at various points as the percents of the reference at the mid point of umbilical level, with bolus and blocks.

A : Surface doses

Organ	Surface dose (%)	
	Right	Left
head	52	50
neck	66	96
shoulder	99	102
axilla	60	79
chest	59	58
waist	107	106
hip	95	97
thigh	94	96
lateral knee	104	100
medial knee	102	100
lateral ankle	108	103
medial ankle	110	109

B : Organ doses

Organ	Organ dose (%)
brain	53
larynx	105
cervical cord	102
lung Rt, Lt	62 , 62
heart	60
liver	61
spleen	59
kidney Rt, Lt	67 , 66
mid point at the level of umbilicus	100
ovary Rt, Lt	84 , 93

5. DISCUSSION

The bilateral fields TBI with the patient in supine position can undergo irradiation without discomfort and distortion of some organs. The surface and inside organ doses excluded the shielding organs achieved the uniformity within ± 10 %. The dose at the neck with bolus was 9 % higher than the reference dose because of the thickness of the bolus used was not enough to compensate the missing tissue. So the appropriate bolus thickness should be placed carefully at the neck and should not enlarge to cover the shoulder. The size of the brain and lung blocks should be individualized and have to be located at the correct position that will not protect the irradiated organs.

Before treating the patient, the multiplication of correction factors [1] for adjusting the absolute dose in the patient that is different from that in the phantom due to the larger treatment field size than the patient, should be done.

6. REFERENCES

1. Van Dyk J. galvin JM, Glasgow GP, Podgorsak EB. The physical aspects of total and half body photon irradiation. AAPM Report No.17. New York: The American Institute of Physics, Inc., 1986
2. Goolden, AWG et al. Fractionation of whole body irradiation before bone marrow transplantation for patient with leukemia. Br J Radiol 1983,56: 245-250.
3. Kein TH, Khan FM, Galvin JM. A report of the work party : Comparison of total body irradiation techniques for bone marrow transplantation. Int J Radiol Oncol Biol Phys 1980, 6: 779 - 784.
4. Van Dyk J. Whole and partial body radiotherapy. In: Wright AE, Boyer AL. Advances in radiation treatment Planning: American Association of Physicists in Medicine, Medical Physics Monograph No. 9. New York : The American Institute of Physics, Inc., 1983: 403-426.